DIVISION DE EDUCACION CONTINUA
FACULTAD DE INGENIERIA U.N.A.M.

CURSOS DE INGENIERIA CIVIL EN EL PROYECTO

DE PLANTAS HIDROELECTRICAS

INGENIERIA SISMICA

Dinámica Estructural

Dr. Octavio Rascón Chávez

Mayo 1981

DINAMICA ESTRUCTURAL

DR. OCTAVIO A. RASCON CH.

DEFINICION.

GRADOS DE LIBERTAD = NUMERO DE COORDENADAS GENERALIZADAS (DESPLAZAMIENTOS O GIROS) QUE SE REQUIEREN PARA DEFINIR LA POSICION DEL SISTEMA EN CUALQUIER INSTANTE.

EJEMPLOS

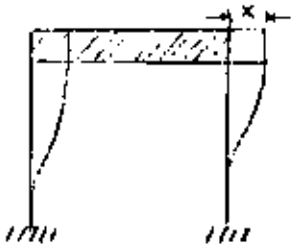

UN GRADO DE LIBERTAD

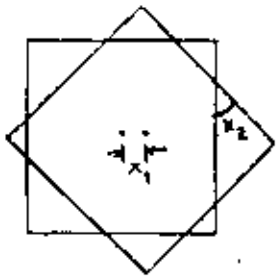

DOS GRADOS DE LIBERTAD

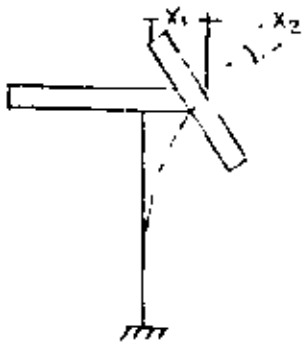

DOS GRADOS DE LIBERTAD

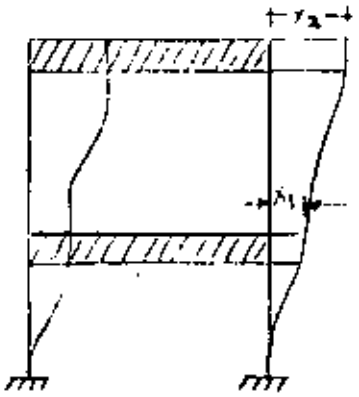

DOS GRADOS DE LIBERTAD

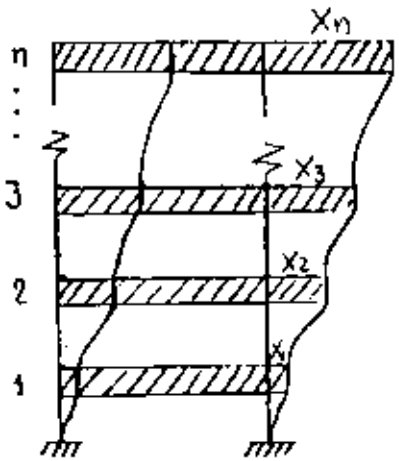

n GRADOS DE LIBERTAD

INFINITO NUMERO DE GRADOS DE LIBERTAD

UC. 2

METODOS DE DISCRETIZACION DE SISTEMAS CONTINUOS

1. POR CONCENTRACION DE MASAS

MASA POR UNIDAD
DE LONGITUD = m

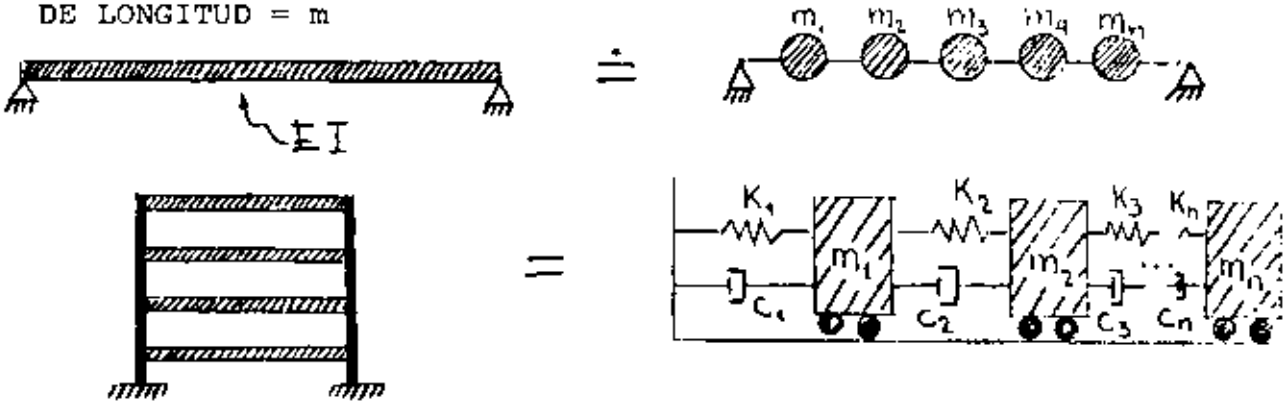

2. EXPRESANDO LA CONFIGURACION DE VIBRACION DE LA ESTRUCTURA COMO UNA SERIE DE FUNCIONES ESPECIFICADAS. POR EJEMPLO, SI ESTAS FUNCIONES SON ARMONICAS:

$$z(x,t) = \sum_{i=1}^{N} b_i \operatorname{sen} \frac{i\pi x}{L}$$

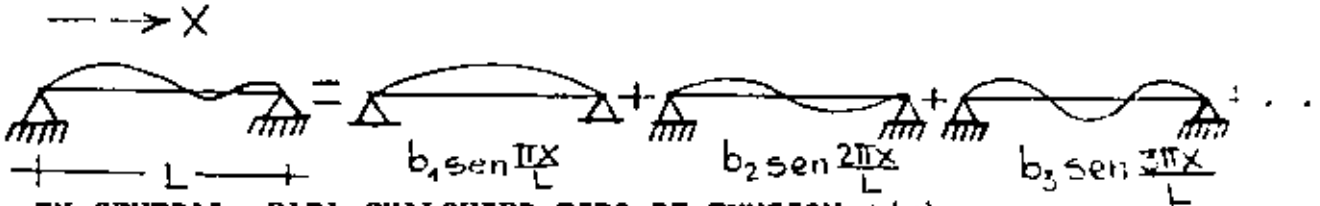

EN GENERAL, PARA CUALQUIER TIPO DE FUNCION $\psi(x)$:

$$z(x,t) = \sum_{i=1}^{N} z_i(t)\psi_i(x)$$

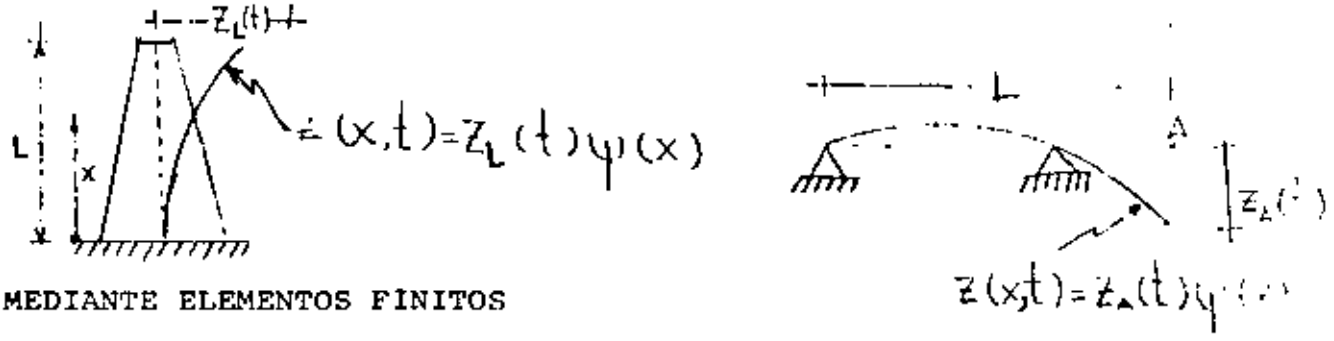

3. MEDIANTE ELEMENTOS FINITOS

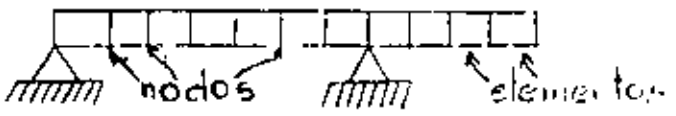

AL PLANTEAR LAS ECUACIONES DE EQUILIBRIO DE CUERPOS RIGIDOS ES A MENUDO NECESARIO CONOCER LOS MOMENTOS DE INERCIA DE MASA. A CONTINUACION SE PRESENTAN ALGUNOS CASOS:

$\bar{m}$ = MASA POR UNIDAD DE LONGITUD

γ = MASA POR UNIDAD DE AREA

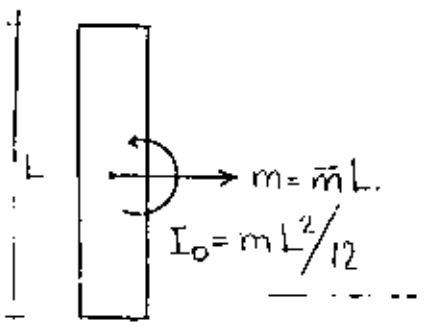

BARRA UNIFORME

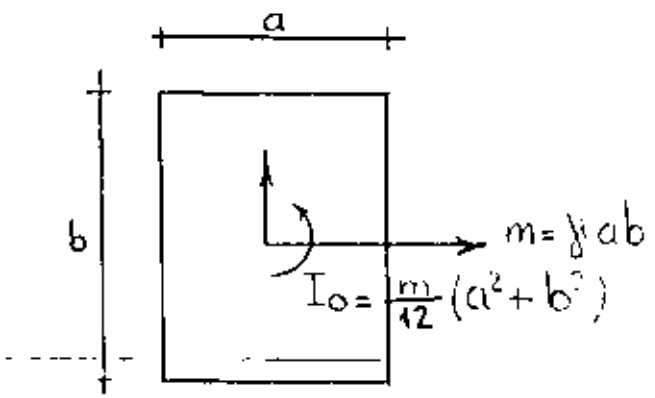

PLACA UNIFORME RECTANGULAR

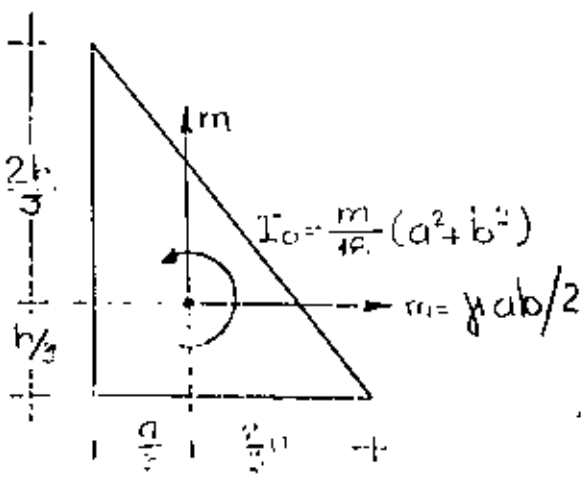

PLACA UNIFORME TRIANGULAR

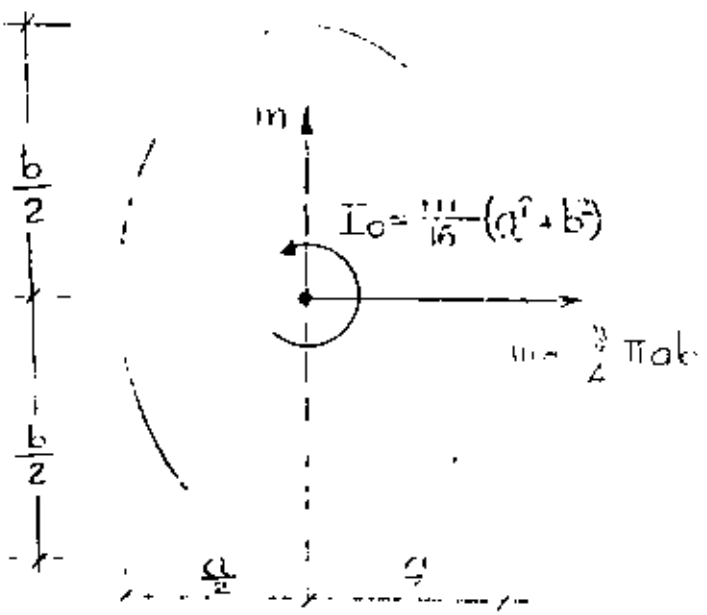

PLACA UNIFORME ELIPTICA

GE. 4

RESPUESTA DINAMICA DE SISTEMAS ELASTICOS LINEALES DE UN GRADO DE LIBERTAD CON AMORTIGUAMIENTO VISCOSO

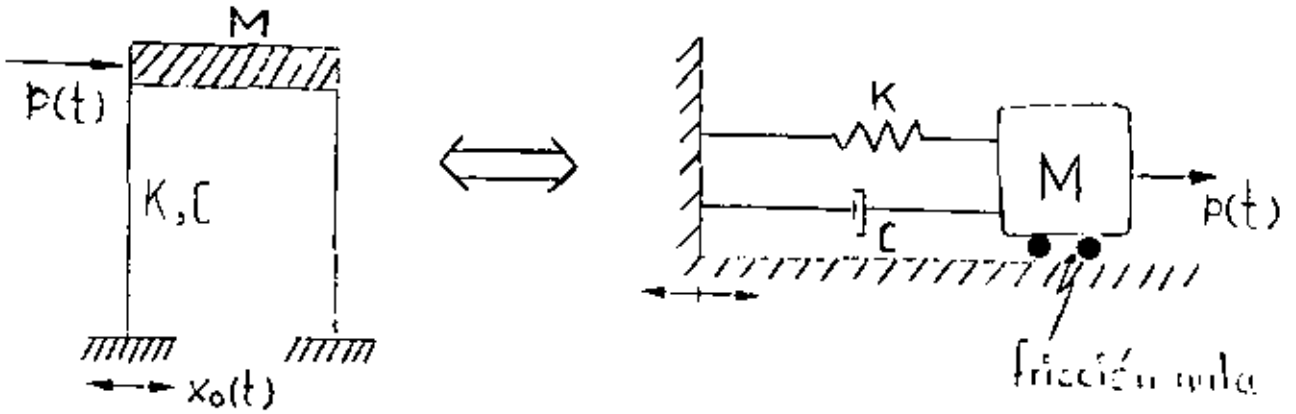

t = TIEMPO

M = MASA

K = RIGIDEZ

C = AMORTIGUAMIENTO

f(t) = FUERZA EXTERNA

$X_o(t)$ = DESPLAZAMIENTO DEL SUELO

EL AMORTIGUAMIENTO VISCOSO ES TAL QUE PRODUCE UNA FUERZA DE RESTAURACION PROPORCIONAL A LA VELOCIDAD RELATIVA DE LA MASA RESPECTO AL SUELO.

EL AMORTIGUAMIENTO SE DEBE PRINCIPALMENTE A LA FRICCION INTERNA ENTRE LOS GRANOS O PARTICULAS DEL MATERIAL DE LA ESTRUCTURA, Y A FRICCION EN LAS JUNTAS Y CONEXIONES DE LA MISMA. ES EL ELEMENTO DEL SISTEMA QUE DISCIPA ENERGIA.

2a. LEY DE NEWTON:

"LA RAPIDEZ DE CAMBIO DEL MOMENTUM DE CUALQUIER MASA, m, ES IGUAL A LA FUERZA QUE ACTUA SOBRE ELLA"

$$p(t) = \frac{d}{dt}\left(m\frac{dx}{dt}\right) = \frac{d}{dt}(m\dot{x})$$

$p(t)$ = FUERZA ACTUANTE

x = DESPLAZAMIENTO

t = TIEMPO

SI m ES CONSTANTE: $p(t) = m\ddot{x}$

PRINCIPIO DE D'ALAMBERT

SI LA 2a. LEY DE NEWTON LA ESCRIBIMOS COMO

$$p(t) - m\ddot{x} = 0$$

AL SEGUNDO TERMINO DE LA ECUACION SE LE CONOCE COMO *FUERZA DE INERCIA*; EL CONCEPTO DE QUE UNA MASA DESARROLLA UNA FUERZA DE INERCIA PROPORCIONAL A SU ACELERACION Y QUE SE OPONE A ELLA SE CONOCE COMO PRINCIPIO DE D'ALAMBERT, Y PERMITE QUE LAS ECUACIONES DE MOVIMIENTO SE EXPRESEN COMO ECUACIONES DE *EQUILIBRIO DINAMICO*.

ECUACION DE EQUILIBRIO

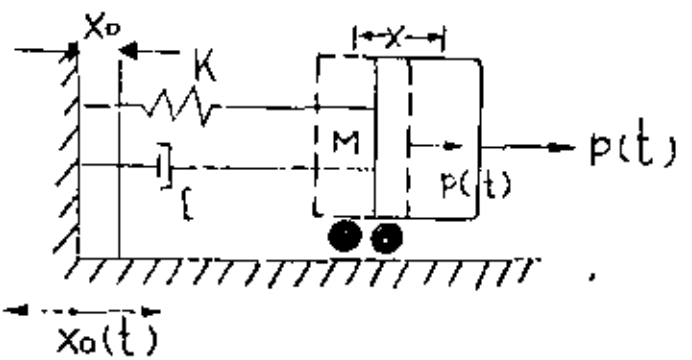

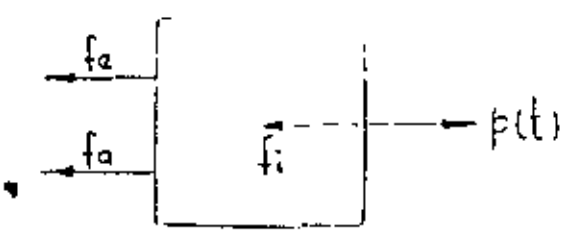

DIAGRAMA DE CUERPO LIBRE

EQUILIBRIO: $f_e + f_a + f_i = p(t)$ (1)

PARA UN SISTEMA ELASTICO: $f_e = K(x - x_o) = ky$

PARA AMORTIGUAMIENTO VISCOSO: $f_a = c(\dot{x} - \dot{x}_o) = C\dot{y}$ (2)

POR EL PRINCIPIO DE D'ALAMBERT: $f_i = m\ddot{x} = m(\ddot{y} + \ddot{x}_o)$

SUSTITUYENDO LAS ECS. 2 EN LA EC. 1 SE OBTIENE:

$$m(\ddot{y} + \ddot{x}_o) + c\dot{y} + k\dot{y} = p(t)$$

DE DONDE

$$\boxed{M\ddot{y} + c\dot{y} + Ky = p(t) - M\ddot{x}_o} \qquad (3)$$

DIVIDIENDO ENTRE M AMBOS MIEMBROS DE LA EC. 3:

$$\ddot{y} + \frac{C}{M}\dot{y} + \frac{K}{M}y = \frac{p(t)}{M} - \ddot{x}_o$$

SI $\frac{C}{M} = 2h$, y $\frac{K}{M} = \omega^2$, DONDE ω = FRECUENCIA CIRCULAR NATURAL, EN RAD/SEG:

$$\boxed{\ddot{y} + 2h\dot{y} + \omega^2 y = \frac{p(t)}{M} - \ddot{x}_o} \qquad (4)$$

CUANDO SE TIENEN EXCITACIONES EN EL SISTEMA SE TRATA DE UN PROBLEMA DE VIBRACIONES FORZADAS; EN CASO CONTRARIO EL PROBLEMA ES DE VIBRACIONES LIBRES.

VIBRACIONES LIBRES

EN ESTE CASO LA ECUACION DIFERENCIAL DE EQUILIBRIO RESULTA SER

$$\ddot{y} + 2h\dot{y} + \omega^2 y = 0$$

CUYA SOLUCION ES

$$y(t) = e^{-ht}(C_1 \text{ sen } \omega' t + C_2 \cos \omega' t) \qquad (5)$$

DONDE $\omega' = \sqrt{\omega^2 - h^2}$ = FRECUENCIA CIRCULAR NATURAL AMORTIGUADA

Y C_1 Y C_2 SON CONSTANTES QUE DEPENDEN DE LAS CONDICIONES INICIALES

(EN t=0) DE DESPLAZAMIENTO Y VELOCIDAD QUE TENGA LA MASA DEL SISTEMA.

ESTAS RESULTAN SER

$$\left[C_1 = \frac{\dot{y}(0) + hy(0)}{\omega'} \right] Y \left[C_2 = y(0) \right] \qquad (6)$$

LA EC (5) SE PUEDE ESCRIBIR TAMBIEN COMO:

$$y(t) = Ae^{-ht} \cos(\omega' t - \theta) \qquad (7)$$

DONDE $A = \sqrt{C_1^2 + C_2^2}$ Y $\theta = \tan^{-1} \frac{C_1}{C_2}$ = ANGULO DE FASE

LA GRAFICA DE LA EC (7) ES

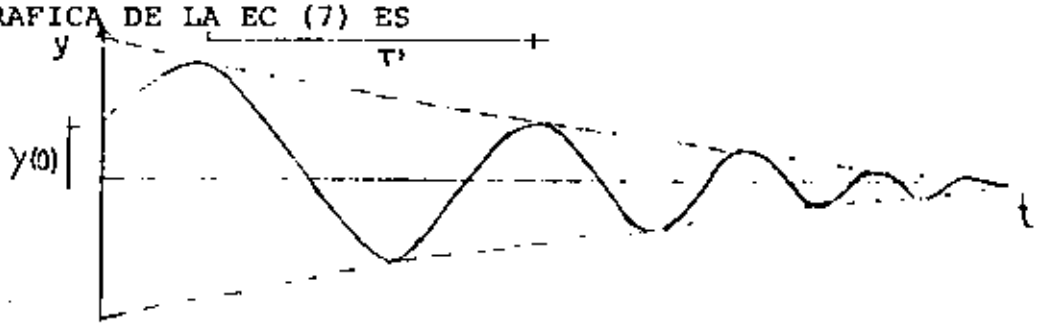

$T' = \frac{2\pi}{\omega'}$ = PERIODO NATURAL AMORTIGUADO, SEG

$f' = \frac{1}{T'}$ = FRECUENCIA NATURAL AMORTIGUADA, cps

VEAMOS EL CASO ESPECIAL DE LA EC. (5) EN QUE $h \to \omega$. EN TAL CASO, $\omega' = \sqrt{\omega^2 - h^2} \to 0$, $\cos \omega' t \to 1$ Y $\text{sen } \omega' t \to \omega' t$, CON LO CUAL LA EC. (5) SE REDUCE A

$$y(t) = e^{-\omega t} \{ [(\dot{y}(0) + hy(0))/\omega'](\omega' t) + y(0) \}$$

$$= e^{-\omega t} [\dot{y}(0) t + (1 + \omega t) y(0)]$$

LA GRAFICA DE ESTA ECUACION ES

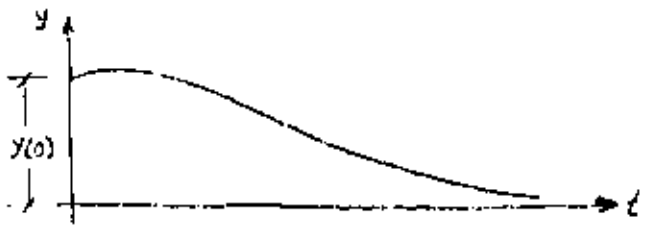

Y OBVIAMENTE NO REPRESENTA UN MOVIMIENTO OSCILATORIO, POR LO CUAL SI $h = \omega$ SE DICE QUE SE TIENE AMORTIGUAMIENTO CRITICO. EN TAL CASO:

$$h_{cr} = \omega = \frac{C_{cr}}{2M} = \sqrt{\frac{K}{M}}$$

DE DONDE $C_{cr} = 2\sqrt{KM}$. (8)

A LA RELACION $\zeta = C/C_{cr}$ SE LE LLAMA FRACCION DEL AMORTIGUAMIENTO CRITICO.

DESPEJANDO A M DE LA EC. (9) Y SUSTITUYENDOLA EN LA EC. $h = C/(2M)$ SE OBTIENE:

$$h = \frac{C}{2\frac{C_{cr}^2}{4K}} = \frac{C}{C_{cr}}\,\frac{2K}{2\sqrt{KM}} = \zeta\sqrt{\frac{K}{M}} = \zeta\omega$$

ADEMAS:

$$\omega' = \sqrt{\omega^2 - h^2} = \sqrt{\omega^2 - \omega^2\zeta^2} = \omega\sqrt{1-\zeta^2}$$

$$\omega' = \omega\sqrt{1 - \zeta^2} \qquad (9)$$

LOS VALORES USUALES EN ESTRUCTURAS QUE ASUME ζ VARIAN ENTRE 2 Y 5%. EN ESTE INTERVALO ω' Y ω SON CASI IGUALES; VEAMOS, POR EJEMPLO, EL CASO EN QUE $\zeta = 0.1$

$$\omega' = \omega\sqrt{1 - 0.01} = 0.995\omega$$

OTRA FORMA DE MEDIR EL GRADO DE AMORTIGUAMIENTO QUE TIENE UNA ESTRUCTURA ES MEDIANTE EL DECREMENTO LOGARITMICO, EL CUAL SE DEFINE COMO EL LOGARITMO DEL COCIENTE DE DOS AMPLITUDES CONSECUTIVAS

$$L = \ln \frac{y(t)}{y(t+T')} = \ln \frac{Ae^{-ht}\cos(\omega' t-\theta)}{Ae^{-h(t+T')}\cos[\omega'(t+T')-\theta]}$$

$$= \ln\{\frac{e^{-ht}}{e^{-h(t+T')}} \frac{\cos(\omega' t - \theta)}{\cos(\omega' t + \omega' T' - \theta)}\}$$

$$= \ln\{\frac{e^{-ht}}{e^{-ht}\, e^{-hT'}} \frac{\cos(\omega' t - \theta)}{\cos(\omega' t - \theta + 2\pi)}\}$$

$$= \ln e^{+hT'} = hT' = \zeta\omega T' = \zeta\omega \frac{2\pi}{\omega\sqrt{1-\zeta^2}}$$

$$\boxed{L = \frac{2\pi\zeta}{\sqrt{1-\zeta^2}}} \qquad (10)$$

SI ζ ES PEQUEÑO,

$$\boxed{L \doteq 2\pi\zeta} \qquad (11)$$

ECUACION DE MOVIMIENTO GENERALIZADA.

HAY PROBLEMAS QUE APARENTEMENTE CORRESPONDE A VIBRACIONES DE SISTEMAS DE VARIOS GRADOS DE LIBERTAD PERO QUE EN REALIDAD SON DE UN GRADO SOLAMENTE.

EJEMPLO

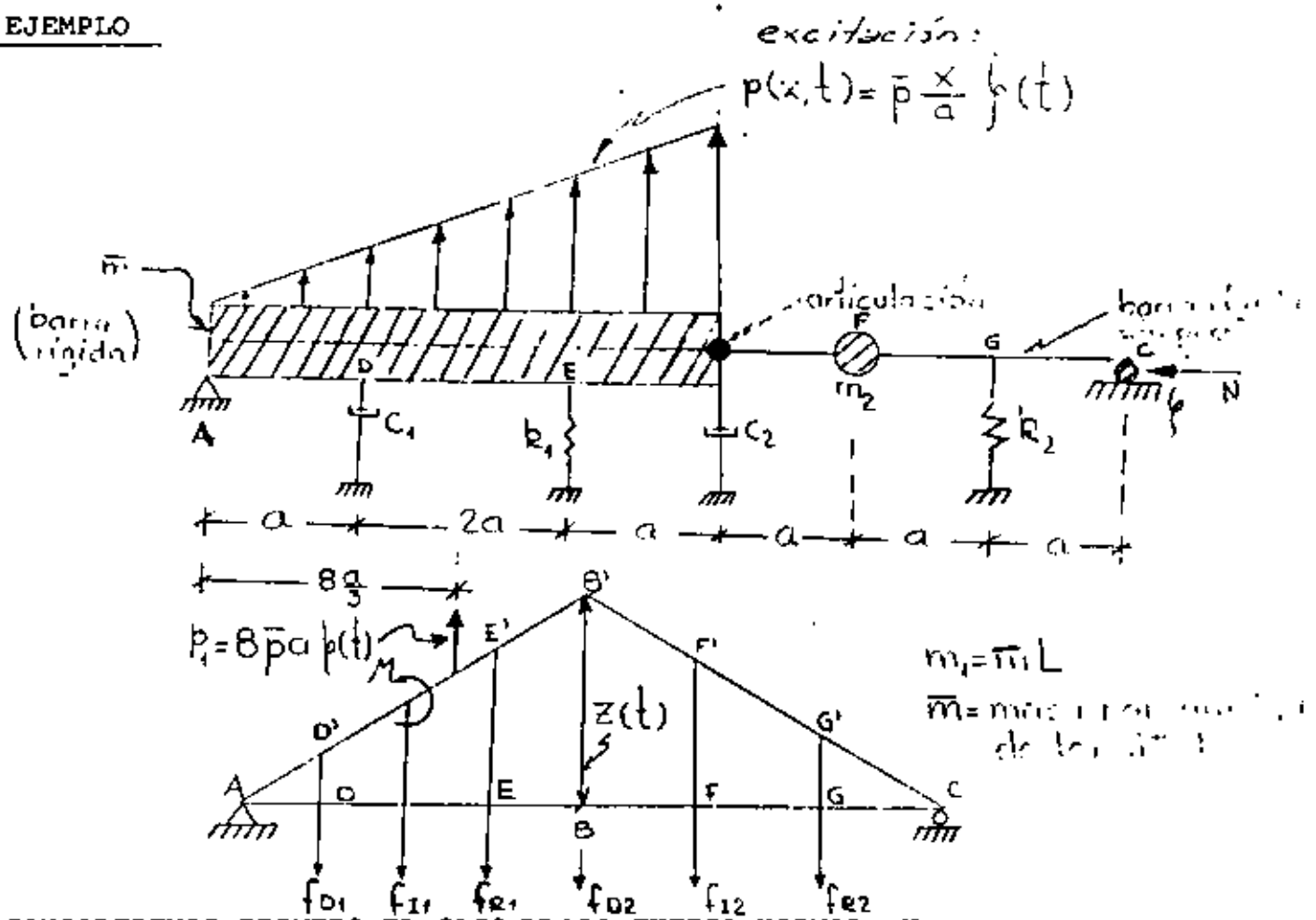

CONSIDEREMOS PRIMERO EL CASO SIN LA FUERZA NORMAL, N.

TOMANDO COMO COORDENADA GENERALIZADA A Z(t):

$$f_{R1} = k_1(EE') = k_1\frac{3}{4}z(t) \; ; \quad f_{R2} = k_2(GG') = K_2\,\frac{1}{3}\,z(t)$$

$$f_{D1} = C_1\,(\frac{d}{dt}DD') = C_1\,\frac{1}{4}\,\dot{z}(t); \quad f_{D2} = C_2\dot{z}(t)$$

$$f_{I1} = m_1\,\frac{1}{2}\,\ddot{z}(t) = \bar{m}L\,\frac{1}{2}\,\ddot{z}(t) = 2a\bar{m}\ddot{z}\,(t)$$

$$f_{I2} = m_2\,\frac{2}{3}\,\ddot{z}\,(t)$$

$$M = I_0 \frac{1}{4a} \ddot{z}(t) = \frac{\bar{m}L}{4a} \frac{L^2}{3} \ddot{z}(t) = \frac{4}{3} a^2 \bar{m} \ddot{z}(t)$$

$$p_1 = 8\bar{p}a\zeta(t)$$

LA ECUACION DE MOVIMIENTO DEL SISTEMA SE PUEDE ESTABLECER IGUALANDO A CERO EL TRABAJO VIRTUAL REALIZADO POR TODAS LAS FUERZAS AL DARLE AL SISTEMA UN DESPLAZAMIENTO VIRTUAL EN EL PUNTO B IGUAL A δZ. EN TAL CASO

$$\delta W = -k_1 \frac{3}{4} z(t)(\frac{3}{4}\delta Z) - K_2 \frac{1}{3} z(t)(\frac{1}{3}\delta Z) - C_1 \frac{\dot{z}(t)}{4} (\frac{\delta Z}{4}) -$$

$$- C_2 \dot{z}(t)(\delta Z) - 2a\bar{m} \ddot{z}(t)(\frac{\delta Z}{2}) - m_2 \frac{2\ddot{z}(t)}{3}(\frac{2}{3}\delta Z) -$$

$$- \frac{4}{3} a^2 \bar{m} \ddot{z}(t)(\frac{\delta Z}{4a}) + 8\bar{p}a\zeta(t)(\frac{2}{3}\delta Z) = 0$$

SIMPLIFICANDO SE OBTIENE

$$\left[(a\bar{m} + \frac{a\bar{m}}{3} + \frac{4m_2}{9}) \ddot{z}(t) + (\frac{C_1}{16} + C_2) \dot{z}(t) + (\frac{9}{16} k_1 + \frac{k_2}{9}) z(t) - \right.$$

$$\left. - \frac{16}{3} \bar{p}a\zeta(t)\right] \delta Z = 0 \qquad (A)$$

COMO EL DESPLAZAMIENTO VIRTUAL δZ NO ES CERO, SE DEBE CUMPLIR QUE EL TERMINO ENTRE PARENTESIS ES CERO. EN TAL CASO:

$$\boxed{\tilde{m} \ddot{z}(t) + \tilde{C} \dot{z}(t) + \tilde{k} z(t) = \tilde{p}(t)}$$

EN DONDE

$$\tilde{m} = \frac{4}{3}\ \bar{m}a + \frac{4}{9}\ m_2 \quad ; \quad \tilde{c} = \frac{c_1}{16} + c_2$$

$$\tilde{k} = \frac{9}{16}\ k_1 + \frac{k_2}{9} \quad ; \quad \tilde{p}(t) = \frac{16}{3}\ \bar{p}a_\zeta(t)$$

ESTOS PARAMETROS SE DENOMINAN MASA, AMORTIGUAMIENTO, RIGIDEZ Y FUERZA GENERALIZADAS, RESPECTIVAMENTE.

CONSIDEREMOS AHORA EL CASO DE LA FUERZA NORMAL N SOLAMENTE:

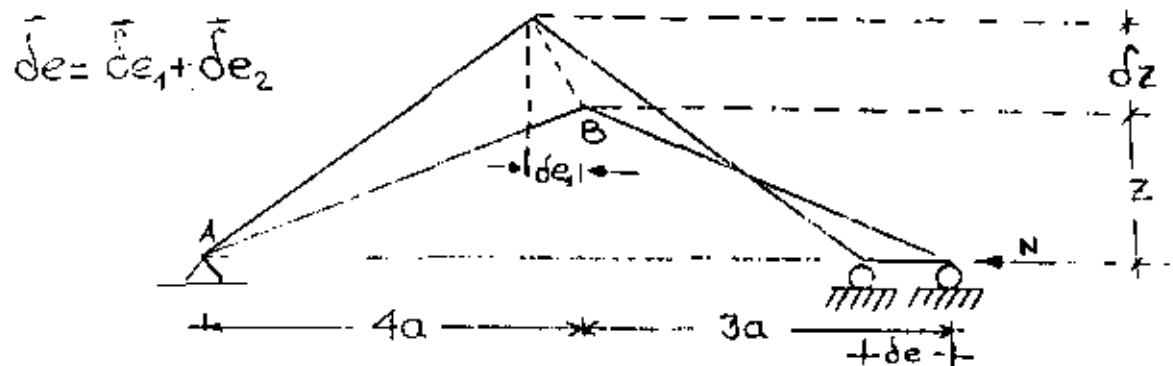

δ_{e_i} = DESPLAZAMIENTO HORIZONTAL DEBIDO AL GIRO DE LA BARRA i

$$\delta e_1 = \frac{Z}{4a}\ \delta Z \ ; \ \delta e_2 = \frac{Z}{3a}\ \delta Z$$

$$\therefore \quad \delta e = \frac{7}{12}\ \frac{Z}{a}\ \delta Z$$

EL TRABAJO VIRTUAL ES:

$$\delta W = N\delta e = \frac{7}{12}\ \frac{NZ}{a}\ (\delta Z)$$

COMO EL SISTEMA ES LINEAL SE PUEDE SUMAR ESTE TRABAJO VIRTUAL AL DE LA ECUACION (A), CON LO CUAL LA RIGIDEZ GENERALIZADA SE MODIFICA, QUEDANDO EN LA FORMA:

$$\tilde{k} = \frac{9}{16} k_1 + \frac{1}{9} k_2 \quad \boxed{\frac{7}{12} \frac{N}{a}}$$

DE ESTA RIGIDEZ SE PUEDE SACAR, DE PASO, LA CARGA CRITICA DE PANDEO HACIENDO $\tilde{k} = 0$:

$$N_{cr} = \left(\frac{27}{28} k_1 + \frac{4}{21} k_2\right) a$$

DETERMINACION EXPERIMENTAL DE ζ EN ESTRUCTURAS REALES O EN MODELOS

SI SE REALIZA UN EXPERIMENTO EN EL CUAL SE SACA A LA ESTRUCTURA DE SU POSICION SE SACA A LA ESTRUCTURA DE SU POSICION DE EQUILIBRIO ESTATICO Y SE DEJA VIBRANDO LIBREMENTE, EL REGISTRO DE LAS ACELERACIONES QUE SE REGISTREN EN LA MASA TENDRA LA MISMA FORMA QUE LA GRAFICA DE LA EC. 7.

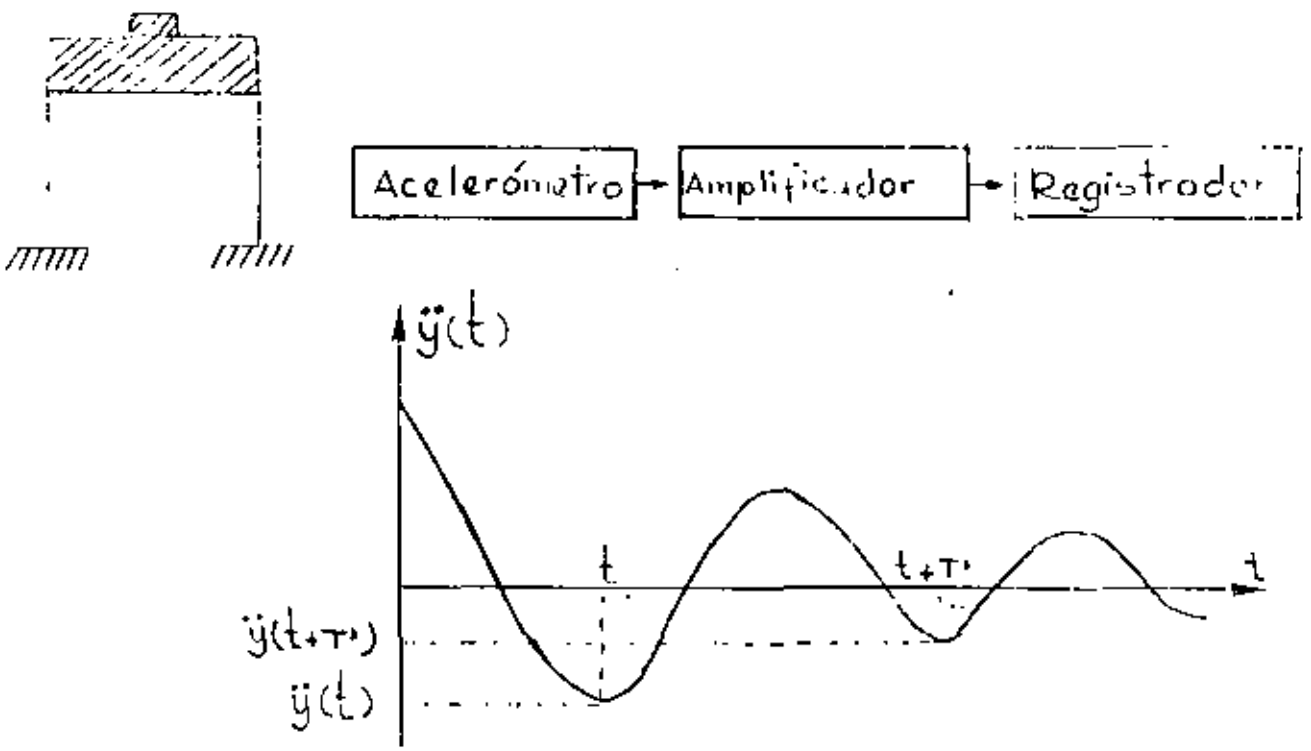

SI DE DICHO REGISTRO SE MIDEN $\ddot{y}(t + T')$ y $\ddot{y}(t)$ SE PUEDE OBTENER L Y, DE LA EC. (11), DESPEJAR A ζ

$$\zeta = \frac{L}{2\pi}$$

Ejemplo

Calcular el periodo natural de vibración de la estructura mostrada en la siguiente figura:

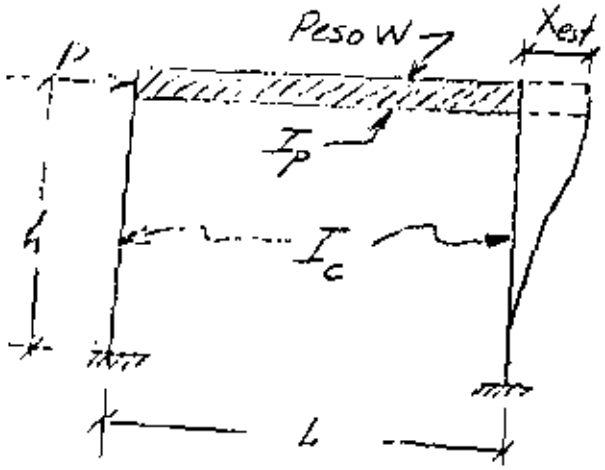

$$K = \frac{P}{X_{est}}$$

P = carga estática

X_{est} = desplazamiento producido por P

I_c = Momento de inercia de las columnas

I_p = Momento de inercia del sistema de piso

Mediante el análisis estático del marco se encuentra que

$$X_{est} = \frac{Ph^3}{6EI_c} \frac{\frac{3}{2} + \frac{I_c}{I_p}\frac{L}{h}}{6 + \frac{I_c}{I_p}\frac{L}{h}} \Rightarrow K = \frac{6EI}{h^3} \frac{6 + \frac{I_c}{I_p}\frac{L}{h}}{\frac{3}{2} + \frac{I_c}{I_p}\frac{L}{h}}$$

$$\text{Periodo natural} = T = \frac{2\pi}{\omega} = \frac{2\pi}{\sqrt{\frac{K}{m}}} = 2\pi\sqrt{\frac{W}{gK}}$$

$$T = 2\pi\sqrt{\frac{Wh^3}{g6EI} \frac{\frac{3}{2} + \frac{I_c}{I_p}\frac{L}{h}}{6 + \frac{I_c}{I_p}\frac{L}{h}}}, \text{ en seg}$$

$\therefore$ si $I_p \gg I_c$ $\quad (I_p \to \infty)$, $\quad K = \frac{12EI}{h^3}$

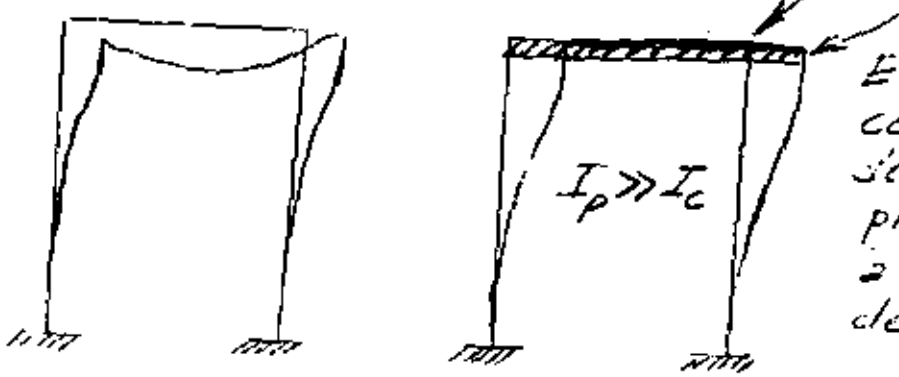

Estructura de CORTANTE: Cuando las deformaciones ocurren principalmente debidas a la fuerza cortante de entrepiso.

EJEMPLO

A UNA ESTRUCTURA DE UN PISO SE LE APLICA UNA CARGA HORIZONTAL DE 20 TON EN SU MASA, OBSERVANDOSE UN DESPLAZAMIENTO ESTATICO DE 0.2 CM. AL SOLTAR SUBITAMENTE LA FUERZA SE REGISTRA UN PERIODO DE OSCILACION DE 0.2 SEG, Y QUE LA AMPLITUD EN EL SEGUNDO CICLO ES DE 0.14 CM.

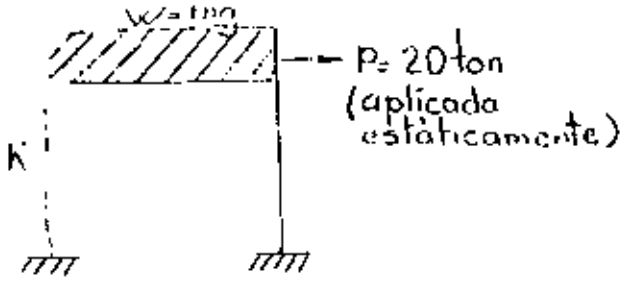

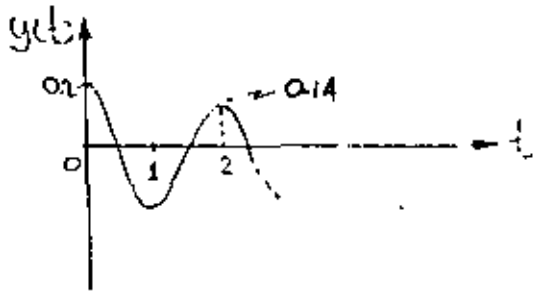

CALCULAR ω, ω', f', L y ζ

1. DE $T' \doteq \frac{2\pi}{\omega} = \frac{\pi 2}{\sqrt{\frac{K}{M}}} = \frac{2\pi\sqrt{W}}{\sqrt{Kg}} = 0.2$ Y $K = \frac{2.0}{0.2} = 100 \frac{TON}{CM}$

SE OBTIENE

$$W \doteq T'^2 \, Kg/4\pi^2 = (0.2)^2 \times 100 \times 981/4\pi^2 = \frac{0.04 \times 100 \times 981}{4 \quad 9.87}$$

$W \doteq 99.4$ TON

2. $\omega' = \frac{2\pi}{T'} = \frac{2\pi}{0.2} = 10\pi \frac{RAD}{SEG}$; $f' = \frac{1}{T'} = \frac{1}{0.2} = 5$ cps

3. $L = \ln \frac{0.2}{0.14} = \ln 1.43 = 0.357$

$$\zeta \doteq \frac{L}{2\pi} = \frac{0.357}{2\pi} = 0.0568 \quad \text{o} \quad \zeta = 5.68\ \%$$

$$C = \zeta C_{cr} = \zeta 2\sqrt{KM} = 0.1132 \sqrt{100 \times 99.4/981}$$

$$= 1.132 \times 0.318 = 0.36 \quad \text{TON SEG/CM}$$

EJEMPLO

CALCULAR LA RESPUESTA DE UN SISTEMA DE UN GRADO DE LIBERTAD SUJETO A LA SIGUIENTE EXCITACION:

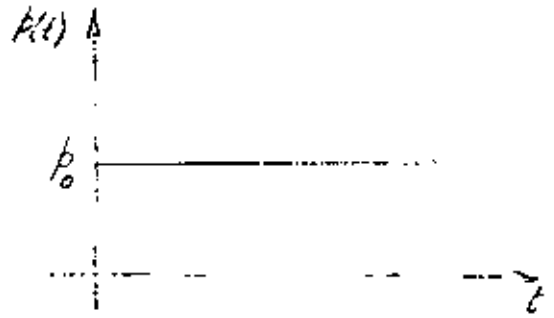

CON $C = 0$

$$m\ddot{x} + kx = p_o$$

$$x = C_1 \operatorname{sen}\omega t + C_2 \cos\omega t + p_o/k$$

SI EN $t = 0$, $x = 0$ Y $\dot{x} = 0$:

$$C_2 = -F_o/k \quad Y \quad C_1 = 0$$

$$\therefore \quad x = \frac{p_o}{k}(1 - \cos\omega t);$$

B = FACTOR DE AMPLIFICACION DINAMICA $= \dfrac{x}{\left(\frac{p_o}{k}\right)} = (1 - \cos\omega t)$

$B_{MAX} = 2$, EN $t = T/2, 3T/2 \ldots$

AHORA, SI LA EXCITACION ES DE DURACION t_o:

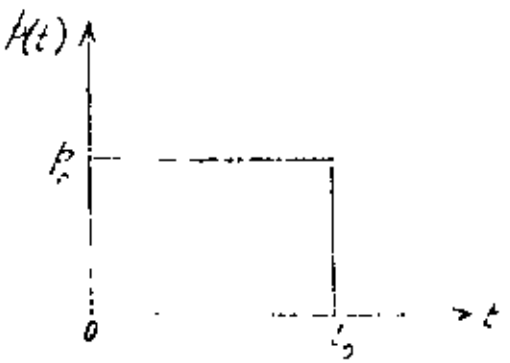

SI $t < t_o$:

$$x = \frac{p_o}{k}(1 - \cos\omega t)$$

$$\dot{x}(t) = \frac{\omega p_o}{k} \operatorname{sen}\omega t$$

EN $t = t_o$:

$$x(t_o) = \frac{p_o}{k}(1 - \cos\omega t_o)$$

$$\dot{x}(t_o) = \frac{\omega p_o}{k} \operatorname{sen}\omega t_o$$

} CONDICIONES INICIALES PARA $t > t_o$

SI $t>t_o$, $x = A\cos\omega t' + B\,\mathrm{sen}\omega t'$, CON $t' = t - t_o$

EN $t' = 0$ ($t = t_o$), SE DEBEN CUMPLIR LAS CONDICIONES INICIALES ANTERIORES, LO CUAL CONDUCE A

$$A = \frac{p_o}{k}(1 - \cos\omega t_o) \quad Y \quad B = \frac{p_o}{k}\,\mathrm{sen}\omega t_o$$

POR LO QUE $x = \frac{p_o}{k}(1 - \cos\omega t_o)\cos\omega t' + \frac{p_o}{k}\,\mathrm{sen}\omega t_o\,\mathrm{sen}\omega t'$

$$= \frac{p_o}{k}\sqrt{(1 - \cos\omega t_o)^2 + \mathrm{sen}^2\omega t_o}\;\;\mathrm{sen}(\omega t' - \theta)$$

O

$$x = \frac{p_o}{k}\sqrt{2(1 - \cos t_o)}\;\;\mathrm{sen}(\omega t' - \theta)$$

$$= \frac{p_o}{k}\;\underbrace{(2\,\mathrm{sen}\frac{\omega t_o}{2})\,\mathrm{sen}(\omega t' - \theta)}$$

B= FACTOR DE AMPLIFICACION

$$B_{MAX} = 2\,\mathrm{sen}\frac{\omega t_o}{2} = 2\,\mathrm{sen}(\pi\frac{t_o}{T})$$

CUANDO $\frac{\pi t_o}{T} = \frac{\pi}{2}$, $B_{MAX} = 2$

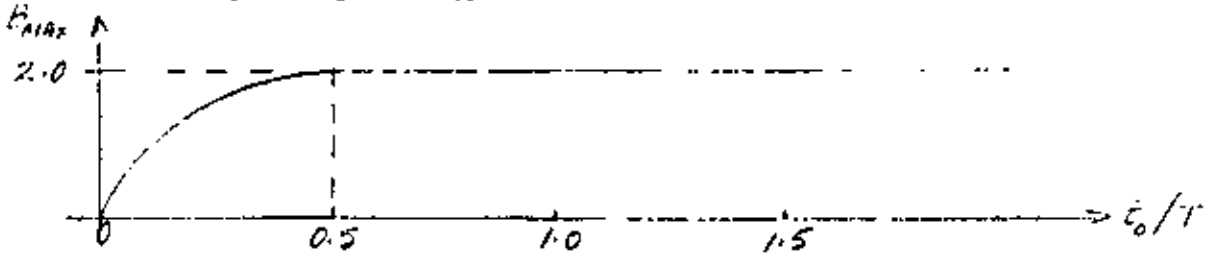

EL MAXIMO OCURRE DESPUES DE LA EXCITACION

EL MAXIMO OCURRE DURANTE LA EXCITACION

SI t_o/T ES MUY PEQUEÑO, $\mathrm{sen}\frac{\pi t_o}{T} = \pi t_o/T$

$$Y\ x_{MAX} = \frac{2p_o}{k}\frac{\pi t_o}{T} = \frac{2p_o}{m\frac{k}{m}}\frac{\omega t_o}{2} = \frac{p_o t_o}{m\omega} = \frac{I}{m\omega}$$

EN DONDE $i = p_o t_o$ = AREA BAJO LA EXCITACION

EJEMPLO: EXCITACION DADA POR UN IMPULSO, SEA UN IMPULSO APLICADO DURANTE UN INTERVALO DE TIEMPO Δt MUY PEQUEÑO, TAL QUE $\Delta t/T << 1$:

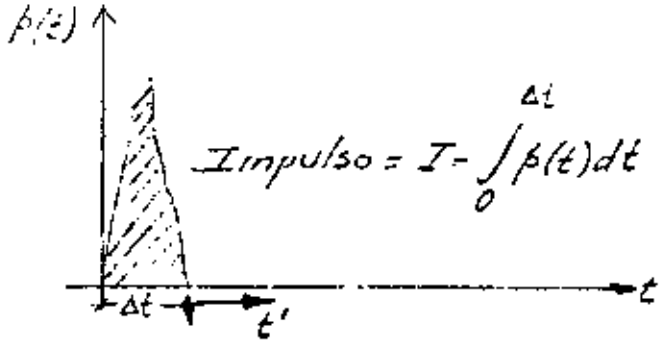

POR EL PRINCIPIO IMPULSO - MOMENTO SE TIENE QUE

$$I = \int_0^{\Delta t} p(t)dt = m\dot{x}$$

EN DONDE $\dot{x}$ ES LA VELOCIDAD QUE EL IMPULSO LE IMPRIME A LA MASA DEL SISTEMA. DESPUES DE Δt EL SISTEMA QUEDA VIBRANDO LIBREMENTE CON VELOCIDAD INICIAL $\dot{x}(0) = \frac{I}{m}$, MIDIENDO EL TIEMPO EN LA ESCALA DE t', Y CON DESPLAZAMIENTO INICIAL QUE PUEDE CONSIDERARSE NULO, DEBIDO A QUE EN EL CORTO INTERVALO DE TIEMPO Δt LA MASA ADQUIERE UN DESPLAZAMIENTO DE MAGNITUD DESPRECIABLE. EN TAL CASO LA RESPUESTA RESULTA SER

$$x(t') = \frac{\dot{x}(o)}{\omega}\,\text{sen}\omega t' = \frac{I}{m\omega}\text{sen}\omega t'$$

SI EL SISTEMA TIENE AMORTIGUAMIENTO,

$$x(t') = \frac{I}{m\omega}\ e^{-\zeta\omega t'}\ \text{sen}\omega' t'$$

PRINCIPIO DE HAMILTON

$$\int_{t_1}^{t_2} \delta(T-V)dt + \int_{t_1}^{t_2} \delta W_{nc}\,dt = 0$$

DONDE

T = ENERGIA CINETICA TOTAL

V= ENERGIA POTENCIAL TOTAL, INCLUYENDO ENERGIA DE DEFORMACION Y ENERGIA POTENCIAL DE LAS FUERZAS CONSERVATIVAS

W_{nc} = TRABAJO REALIZADO POR LAS FUERZAS NO CONSERVATIVAS (TALES COMO LAS DE AMORTIGUAMIENTO)

δ= VARIACION TOMADA DURANTE EL INTERVALO DE TIEMPO DE t_1 A t_2

EN ESTE PRINCIPIO SE ASUME QUE LA VARIACION, δx, DEL DESPLAZAMIENTO EN LOS INSTANTES t_1 Y t_2 ES NULO.

EJEMPLO

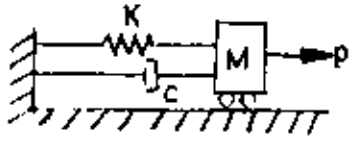

$T = \frac{1}{2} m\dot{x}^2$; $V = \frac{1}{2} kx^2$ (ES LA ENERGIA DE DEFORMACION, UNICAMENTE)

$$\delta W_{nc} = p(t)\delta x - c\dot{x}\delta x$$

$$\int_{t_1}^{t_2} \delta(\tfrac{1}{2} m\dot{x}^2 - \tfrac{1}{2}kx^2)dt + \int_{t_1}^{t_2} (p(t)\delta x - c\dot{x}\delta x)dt$$

$$\int_{t_1}^{t_2} (m\dot{x}\delta\dot{x} - kx\delta x)dt + \int_{t_1}^{t_2} (p(t) - c\dot{x})\delta x\,dt = 0$$

$$\int_{t_1}^{t_2} [m\dot{x}\delta\dot{x} - (c\dot{x} + kx - p(t))\delta x]dt = 0$$

INTEGRANDO POR PARTES EL PRIMER TERMINO DE ESTA INTEGRAL;

$$\int_{t_1}^{t_2} m\ddot{x}\delta x\, dt = m\dot{x}\delta x\Big]_{t_1}^{t_2} - \int_{t_1}^{t_2} m\dot{x}\,\delta\dot{x}\, dt$$

$$= -\int_{t_1}^{t_2} m\dot{x}\delta\dot{x}\, dt$$

POR LO QUE

$$\int_{t_1}^{t_2} [-m\ddot{x} - c\dot{x} - kx + p(t)]\delta x\, dt = 0$$

PUESTO QUE δx ES ARBITRARIA, LA ECUACION ANTERIOR SE SATISFACE EN GENERAL SOLO SI

$$m\ddot{x} + c\dot{x} + kx - p(t) = 0$$

EJEMPLO

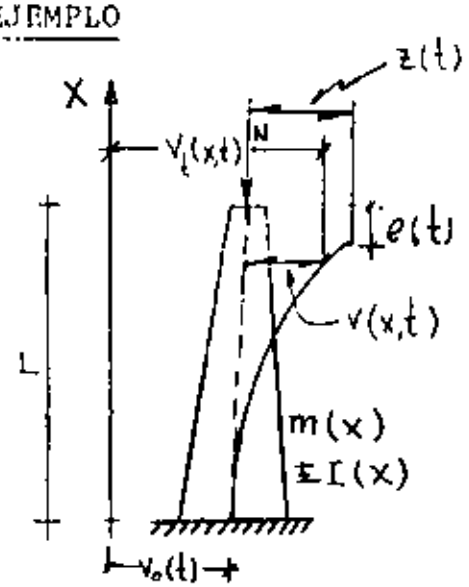

$$v(x,t) = \psi(x)z(t)$$

APLICANDO EL PRINCIPIO DE HAMILTON:

$$T = \frac{1}{2}\int_0^L m(x)(\dot{v}_t(x,t))^2 dx$$

ENERGIA POTENCIAL POR DEFORMACION:

$$V = \frac{1}{2}\int_0^L EI(x)(v''(x,t))^2 dx$$

$$e(t) = \frac{1}{2}\int_0^L [v'(x,t)]^2 dx$$

ENERGIA POTENCIAL DEBIDA A LA FUERZA NORMAL:

$$V_N = -\frac{N}{2}\int_0^L [v'(x,t)]^2 dt$$

EN ESTAS ECUACIONES: $\dot{v} = dv/dt$; $v' = dv/dx$

$$v'' = d^2v/dx^2$$

PUESTO QUE NO HAY FUERZAS DINAMICAS EXTERNAS, Y SI CONSIDERAMOS AMORTIGUAMIENTO NULO, ENTONCES $\delta W_{nc} = 0$, POR LO QUE

$$\int_{t_1}^{t_2} \delta(T-V)dt = 0 \qquad o$$

$$\int_{t_1}^{t_2} \left[\int_o^L m(x)\dot{v}_t(x,t)\ \delta\dot{v}_t dx - \int_o^L EI(x)v''(x,t)\ \delta v'' dx + \right.$$

$$\left. + N \int_o^L v'(x,t)\ \delta v' dx \right] = 0$$

TOMANDO EN CUENTA QUE

$$\dot{v}_t = \dot{v} + \dot{v}_o \ , \ v'' = \phi'' Z, \ v' = \psi' Z \quad \dot{v} = \psi \dot{Z}$$

$$\delta\dot{v}_t = \delta\dot{v} \ , \ \delta v'' = \phi''\delta Z, \ \delta v' = \phi'\delta z, \ \delta\dot{v} = \psi\delta\dot{z}$$

SE OBTIENE

$$\int_{t_1}^{t_2} \left[\ddot{z}\delta z \int_o^L m(x)\ \psi^2 \delta x \ + \delta z \ddot{v}_o(t) \int_o^L m(x)\psi\delta x - \right.$$

$$\left. - z\delta z \int_o^L EI(x)(\psi'')^2 \delta x + Nz\delta z \int_o^L (\psi'')^2 \delta x \right] dt = 0$$

INTEGRANDO POR PARTES LAS PRIMERAS DOS INTEGRALES Y HACIENDO

$$\tilde{m} = \int_o^L m(x)\psi^2\, dx = \text{MASA GENERALIZADA}$$

$$\tilde{K} = \int_0^L EI(x)(\psi'')^2 dx = \text{RIGIDEZ GENERALIZADA SIN CONSIDERAR FUERZA NORMAL}$$

o

$$\tilde{K} = \int_0^L EI(x)(\psi'')^2 dx - N\int_0^L (\psi')^2 dx = \text{RIGIDEZ GENERALIZADA CON N}$$

$$\tilde{p}(t) = \text{FUERZA GENERALIZADA EFECTIVA} = -\ddot{v}_o \int_0^L m(x)\psi\delta x$$

SE OBTIENE LA ECUACION

$$\int_{t_1}^{t_2} [\tilde{m}\ddot{z} + \tilde{k}z - \tilde{p}(t)]\delta z \, dt = 0$$

POR LO QUE

$$\tilde{m}\ddot{z} + \tilde{k}z = \tilde{p}(t)$$

<u>CASO PARTICULAR</u>. CONSIDEREMOS EI=cte Y m=cte = $\bar{m}$

SEA $\psi(x) = 1 - \cos\frac{\pi x}{2L}$; EN TAL CASO:

$$\tilde{m} = \int_0^L \bar{m}(\psi)^2 dx = \bar{m}\int_0^L (1 - \cos\tfrac{\pi x}{2L})^2 dx = 0.228\ \bar{m}L$$

<u>SI N=0:</u>

$$\tilde{k} = \int_0^L EI(\psi'')^2 dx = EI\int_0^L (\tfrac{\pi^2}{4L^2}\cos\tfrac{\pi x}{2L})^2 dx = \tfrac{\pi^4}{32}\tfrac{EI}{L^3}$$

$$\tilde{p}(t) = -\ddot{v}_o(t)\int_0^L \bar{m}\psi\, dx = -\bar{m}\ddot{v}_o(t)\int_0^L (1 - \cos\tfrac{\pi x}{2L})\, dx = -0.364\,\tilde{m}L\ddot{v}_o(t)$$

<u>SI N≠0:</u>

$$\tilde{k} = \tfrac{\pi^4}{32}\tfrac{EI}{L^3} - N\int_0^L (\psi')^2 dx = N\int_0^L (\tfrac{\pi}{2L}\,\mathrm{sen}\tfrac{\pi x}{2L})^2 dx$$

$$\bar{k} = \frac{\pi^4}{32}\frac{EI}{L^3} - \frac{N\pi^2}{8L}$$

PARA CARGA DE PANDEO: $\frac{\pi^4}{32}\frac{EI}{L^3} - \frac{N_{cr}\pi^2}{8L} = 0 \Rightarrow N_{cr} = \frac{\pi^2}{4}\frac{EI}{L^2}$

CON LO QUE $\bar{K} = \frac{\pi^4 EI}{32L^3}\left(1 - \frac{N}{N_{cr}}\right)$ Y LA ECUACION DE EQUILIBRIO

QUEDA EN LA FORMA:

$$0.228\,\bar{m}L\ddot{z}(t) + \frac{\pi^4 EI}{32L^3}\left(1 - \frac{N}{N_{cr}}\right) z(t) = 0.364\bar{m}L\ddot{v}_o(t)$$

LA FRECUENCIA CIRCULAR NATURAL CORRESPONDIENTE ES

$$\omega = \sqrt{\frac{\pi^4 EI\left(1-\frac{N}{N_{cr}}\right)}{7.296\,\bar{m}L^4}}$$

SOLUCION AL PROBLEMA DE VIBRACIONES FORZADAS

A. FUERZA EXTERNA

VEAMOS PRIMERO EL CASO EN QUE EXISTE p(t) Y QUE $\ddot{x}_o(t) = 0$, SIENDO p(t) ARBITRARIA

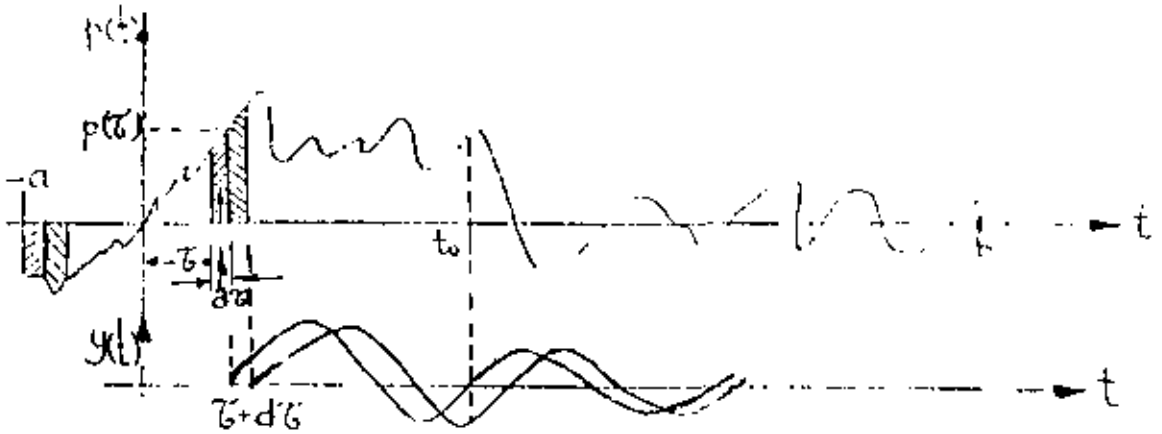

PUESTO QUE $d\tau \ll T$, LA FUERZA APLICADA EN $t=\tau$ PRODUCIRA UN INCREMENTO INSTANTANEO EN LA VELOCIDAD DE LA MASA IGUAL A

$$\dot{y} = \frac{p(\tau)d\tau}{M}$$

Y UN INCREMENTO INSTANTANEO NULO EN EL DESPLAZAMIENTO, ES DECIR, y=0. TOMANDO ESTOS INCREMENTOS COMO CONDICIONES INICIALES EN $t=\tau$, LA EC. 5 DA COMO RESULTADO

$$y(t) = \frac{p(\tau)d\tau}{M\omega'} \text{ sen } \omega'(t-\tau)\, e^{-h(t-\tau)} \quad ; \quad t \geq \tau$$

PUESTO QUE EL SISTEMA ES LINEAL ES POSIBLE SUPERPONER LOS EFECTOS OCASIONADOS POR LOS IMPULSOS APLICADOS EN CADA τ QUE HAYAN OCURRIDO ANTES DEL INSTANTE t DE INTERES; ES DECIR,

$$y(t) = \frac{1}{M\omega'} \int_{-\infty}^{t} p(\tau) e^{-h(t-\tau)} \operatorname{sen}\omega'(t-\tau)\, d\tau \qquad (12)$$

LA FUNCION $\frac{1}{M\omega'} e^{-h(t-\tau)} \operatorname{sen}\omega'(t-\tau)$, QUE ES LA RESPUESTA A UN IMPULSO INSTANTANEO UNITARIO DE FUERZA, SE LE CONOCE COMO *FUNCION DE TRANSFERENCIA DEL SISTEMA.*

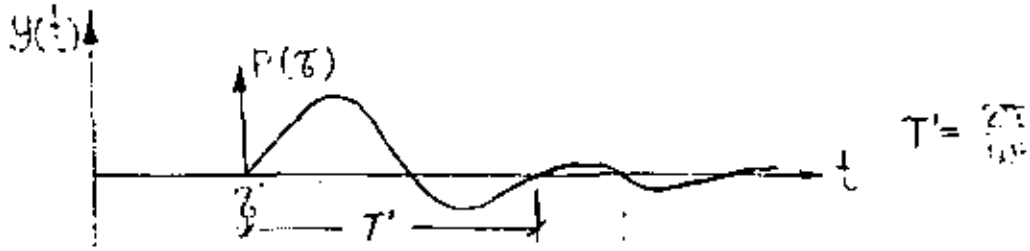

LA SOLUCION DADA EN LA EC. (12) SE DENOMINA INTEGRAL DE DUHAMEL. ESTA CONSTITUYE LA SOLUCION PARTICULAR DE LA ECUACION DIFERENCIAL DE EQUILIBRIO; LA SOLUCION GENERAL ES:

$$y(t) = Ae^{-ht} \cos(\omega' t - \theta) + \frac{1}{M\omega'} \int_{-\infty}^{t} p(\tau) e^{-h(t-\tau)} \operatorname{sen}\omega'(t-\tau)\, d\tau ,$$

EN DONDE A y θ DEPENDEN DE LAS CONDICIONES INICIALES DE DESPLAZAMIENTO Y VELOCIDAD, $y(0)$ Y $\dot{y}(0)$, RESPECTIVAMENTE. EN GENERAL LA PARTE DE LA RESPUESTA DADA POR LA SOLUCION PARTICULAR ES LA MAS IMPORTANTE, YA QUE LA OTRA PARTE SE AMORTIGUA RAPIDAMENTE.

B. MOVIMIENTO DEL SUELO

PARA ESCRIBIR LA SOLUCION PARTICULAR DE LA ECUACION DIFERENCIAL DE EQUILIBRIO PARA EL CASO DE VIBRACION FORZADA POR MOVIMIENTO DE LA BASE DE LA ESTRUCTURA, BASTA CAMBIAR $p(\tau)/M$ DE LA EC. (12) POR $-\ddot{x}_o$, YA QUE EN DICHA ECUACION APARECE EN EL MIEMBRO DERECHO $p(t)/M$ CUANDO LA EXCITACION ES $P(t)$ Y APARECE $-\ddot{x}_o$ CUANDO LA EXCITACION ES POR MOVIMIENTO DEL SUELO. EN ESTE CASO

LA SOLUCION PARTICULAR ES, ENTONCES

$$y(t) = \frac{-1}{\omega'} \int_{-\infty}^{t} \ddot{x}_o(\tau) e^{-h(t-\tau)} \operatorname{sen}\omega'(t-\tau)\,d\tau \qquad (14)$$

EJEMPLO

CALCULAR LA RESPUESTA DE UN SISTEMA DE UN GRADO DE LIBERTAD CON AMORTIGUAMIENTO NULO, CUANDO LA EXCITACION ES LA SIGUIENTE:

$$\zeta = 0$$

$$\ddot{x}_o(t) = a, \quad SI \quad 0 \leq t \leq t_o$$

$$\ddot{x}_o(t) = 0, \quad SI \quad t < 0 \ \acute{o} \ t > t_o$$

CONSIDERESE QUE $y(0)=0$ Y $\dot{y}(0)=0$. PUESTO QUE LAS CONDICIONES INICIALES SON NULAS SE TIENE QUE $A=0$ (UTILIZANDO LA EC. (13) Y LA SOLUCION PARTICULAR QUE SIGUE, EC. (A)):

$$y(t) = \frac{-1}{\omega} \int_{-\infty}^{t} a \operatorname{sen}\omega(t-\tau)\,d\tau = \frac{-a}{\omega} \int_{0}^{t} \operatorname{sen}\,\omega(t-\tau)\,d\tau$$

$$= \frac{-a}{\omega^2} (1 - \cos\omega t) \qquad SI \quad 0 \leq t \leq t_o \qquad (A)$$

PARA FINES DE DISEÑO ESTRUCTURAL ES IMPORTANTE CONOCER LA RESPUESTA MAXIMA; ESTA OCURRE CUANDO $\cos\omega t = -1$, O SEA, CUANDO

$$\omega t = \pi \quad O \quad t = \frac{\pi}{\omega} = \frac{\pi}{\frac{2\pi}{T}} = \frac{T}{2}$$

Y VALE

$$\text{MAX}\{|y(t)|\} = \frac{2a}{\omega^2} = \frac{a}{2\pi^2}T^2, \text{ SI } 0 \leq \frac{T}{2} \leq t_o \text{ O } 0 \leq T \leq 2t_o$$

PARA $t>t_o$, O SEA, PARA $T/2>t_o$ ES NECESARIO OBTENER LA RESPUESTA EN VIBRACION LIBRE CON LAS CONDICIONES INICIALES DE VELOCIDAD Y DESPLAZAMIENTO CORRESPONDIENTES A $t=t_o$:

$$y(t_o) = \frac{-a}{\omega^2}(1 - \cos\omega t_o) \; ; \quad \dot{y}(t_o) = \frac{-a}{\omega}\operatorname{sen}\omega t_o$$

APLICANDO LAS ECS. (5) Y (6) OBTENEMOS:

$$y(t) = \frac{-a}{\omega^2}\left[\operatorname{sen}\omega t_o \operatorname{sen}\omega t' - (1 - \cos\omega t_o)\cos\omega t'\right]$$

$$= \frac{-a}{\omega^2}\sqrt{\operatorname{sen}^2\omega t_o + (1 - \cos\omega t_o)^2}\,\operatorname{sen}(\omega t' - \phi)$$

$$y(t) = \frac{-2a}{\omega^2}\operatorname{sen}\frac{\omega t_o}{2}\operatorname{sen}(\omega t' - \phi)$$

DONDE $t' = t - t_o$ Y $\phi = \tan^{-1}\left(\frac{1-\cos\omega t_o}{\operatorname{sen}\omega t_o}\right)$

EL VALOR MAXIMO DE LA RESPUESTA EN ESTE INTERVALO ES

$$\text{MAX}\{|y(t)|\} = \frac{2a}{\omega^2}\left|\operatorname{sen}\frac{\omega t_o}{2}\right|, \quad \text{SI } t>t_o \text{ O } T>2t_o$$

EXCITACION ARMONICA

CONSIDEREMOS AHORA EL CASO EN QUE LA ESTRUCTURA ES EXCITADA POR LA FUERZA ARMONICA

$$p(t) = p_o \operatorname{sen}\Omega t$$

DE DURACION INDEFINIDA.

LA SOLUCION DE ESTE PROBLEMA SE PUEDE ENCONTRAR SUSTITUYENDO A $p(t) = p_o \operatorname{sen}\Omega t$ EN LA INTEGRAL DE DUHAMEL Y OBTENIENDO SU SOLUCION. SIN EMBARGO, EL RESULTADO LO OBTENDREMOS DE LA CONSIDERACION DE QUE PARA QUE EL MIEMBRO DERECHO DE LA ECUACION DIFERENCIAL DE EQUILIBRIO APAREZCA UN TERMINO ARMONICO ES NECESARIO QUE EN EL IZQUIERDO SE TENGAN COMBINACIONES DE TERMINOS TAMBIEN ARMONICOS. CONSIDEREMOS, POR LO TANTO, LA SOLUCION

$$y(t) = A \operatorname{sen}\Omega t + B \cos\Omega t \qquad (14)$$

Y DETERMINEMOS LOS VALORES QUE DEBEN TENER A Y B PARA SATISFACER LA ECUACION DIFERENCIAL DE EQUILIBRIO, PARA LO CUAL HAY QUE SUSTITUIR A $y(t)$, $\dot{y}(t)$ Y $\ddot{y}(t)$ EN LA ECUACION DIFERENCIAL. HACIENDO ESTO Y FACTORIZANDO:

$$(-A\Omega^2 - 2h\Omega B + \omega^2 A) \operatorname{sen}\Omega t +$$

$$(-B\Omega^2 + 2hA\Omega + \omega^2 B) \cos\Omega t = \frac{p_o}{M} \operatorname{sen}\Omega t + 0 \times \cos\Omega t$$

PARA QUE ESTA IGUALDAD SE CUMPLA SE REQUIERE QUE

$$-A\Omega^2 - 2h\Omega B + \omega^2 A = \frac{p_o}{M}$$

$$-B\Omega^2 + 2h\Omega A + \omega^2 B = 0$$

RESOLVIENDO ESTE SISTEMA DE ECUACIONES SE OBTIENE:

$$A = \frac{\frac{P_o}{M}\ (\Omega^2 - \omega^2)}{(\omega^2 - \Omega^2)^2 + 4h^2\Omega^2}$$

$$B = \frac{-2h\Omega\ \frac{P_o}{M}}{(\omega^2 - \Omega^2)^2 + 4h^2\Omega^2}$$

SUSTITUYENDO A Y B EN LA EC. (14'):

$$y(t) = \frac{\frac{P_o}{M}}{(\omega^2 - \Omega^2)^2 + 4h^2\Omega^2}\left[(\Omega^2 - \omega^2)\ \text{sen}\Omega t - 2h\Omega\ \cos\Omega t\right] \qquad (15)$$

O, TAMBIEN

$$y(t) = \frac{\frac{P_o}{M}}{\sqrt{(\omega^2 - \Omega^2)^2 + 4h^2\Omega^2}}\ \text{sen}(\Omega t - \phi) \qquad (16)$$

EN DONDE $\phi = \text{ANG TAN}\left(\frac{-B}{A}\right) = \text{TAN}^{-1}\ \frac{2h\Omega}{\omega^2 - \Omega^2}$ = ANGULO DE FASE (17)

DIVIDIENDO NUMERADOR Y DENOMINADOR DE LAS ECS. (16) Y (17) ENTRE ω^2

SE OBTIENE:

$$y(t) = \frac{\frac{P_o}{k}}{\sqrt{\left(1 - \frac{\Omega^2}{\omega 2}\right) + (2\zeta -)^2}}\ \text{sen}(\Omega t - \phi) \qquad (18)$$

$$\phi = \text{TAN}^{-1}\ \frac{2\zeta\frac{\Omega}{\omega}}{1 - \frac{\Omega^2}{\omega^2}} \qquad (19)$$

SI SE TIENE EXCITACION ARMONICA EN LA BASE DE LA ESTRUCTURA $x_o(t) = a\,\mathrm{sen}\Omega t$, O SEA, $\ddot{x}_o = a\Omega^2 \mathrm{sen}\Omega t$, BASTA CAMBIAR A p_o/M EN LA EC. (16) POR $-a\Omega^2$; HACIENDO ESTO SE OBTIENE

$$y(t) = \frac{(\Omega/\omega)^2}{\sqrt{(1 - \frac{\Omega^2}{\omega^2})^2 + (2\zeta\frac{\Omega}{\omega})^2}}\, a\, \mathrm{sen}(\Omega t - \phi) \qquad (20)$$

FACTOR DE AMPLIFICACION DINAMICA DE DESPL. = $B_d = \mathrm{MAX}\left|\frac{y(t)}{a}\right|$

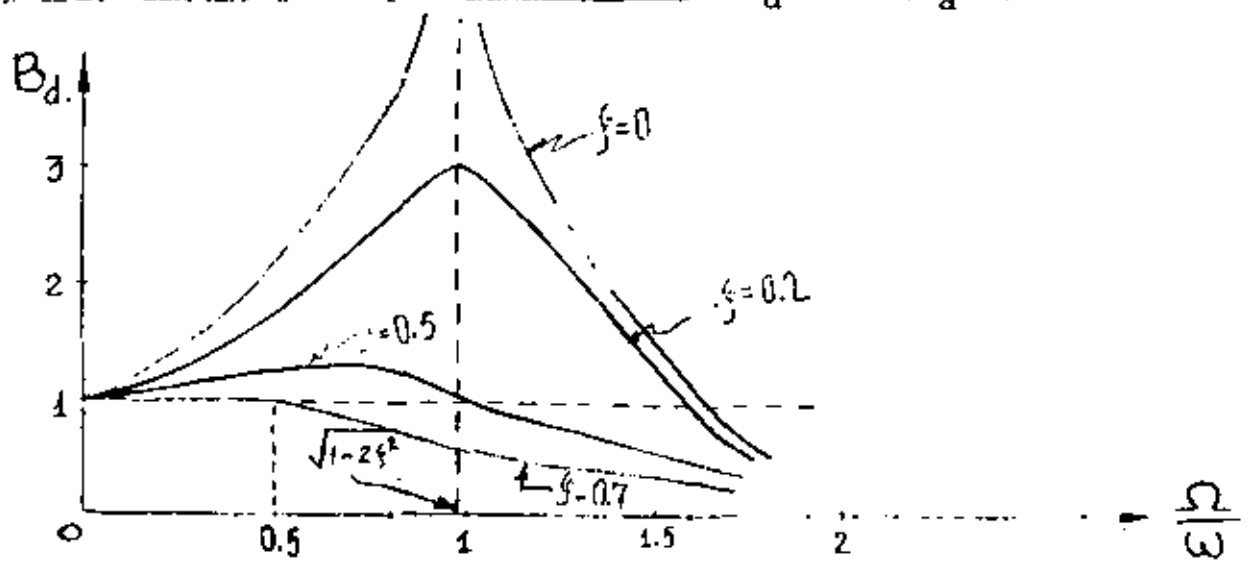

FIG. 1. CURVAS DE AMPLIFICACION DINAMICA PARA EL CASO DE FUERZA EXTERNA

$$B_d = \frac{1}{\sqrt{(1 - \frac{\Omega^2}{\omega^2})^2 + (2\zeta\frac{\Omega}{\omega})^2}} \qquad (21)$$

LOS FACTORES DE AMPLIFICACION DINAMICA DE VELOCIDAD Y ACELERACION SE SE PUEDEN OBTENER DERIVANDO RESPECTO A t LA EC. (16) O LA (20), SEGUN SEA EL CASO. LOS RESULTADOS SON, RESPECTIVAMENTE,

$$\mathrm{MAX}\left|\frac{\dot{y}(t)}{a\omega}\right| = B_v = \frac{\Omega}{\omega} B_d \quad \text{Y} \quad B_a = (\frac{\Omega}{\omega})^2 B_d = \mathrm{MAX}\left|\frac{\ddot{y}(t)}{a\omega^2}\right| \qquad (22)$$

EJEMPLO

CON UNA MAQUINA VIBRATORIA PORTATIL QUE PRODUCE FUERZAS ARMONICAS SE PROBO UNA ESTRUCTURA, AJUSTANDO LA MAQUINA EN LAS FRECUENCIAS $\Omega_1 = 16 \frac{RAD}{SEG}$ Y $\Omega_2 = 25 \frac{RAD}{SEG}$, CON UNA FUERZA MAXIMA DE 500 LB EN CADA CASO. LAS AMPLITUDES Y ANGULOS DE FASE DE LA RESPUESTA QUE SE MIDIERON FUERON:

$$\rho_1 = 7.2 \times 10^{-3} \text{in}, \ \phi_1 = 15^\circ \ (\cos\phi_1 = 0.966 \ ; \ \text{sen}\phi_1 = 0.259)$$

$$\rho_2 = 14.5 \times 10^{-3} \text{in}, \ \phi_2 = 55^\circ (\cos\phi_2 = 0.574; \ \text{sen}\phi_2 = 0.819)$$

EVALUAR LAS PROPIEDADES DINAMICAS DEL SISTEMA.

HACIENDO:

$$\rho_i = \frac{p_o}{k} B_{d_i} = \frac{p_o}{k} \frac{1}{1-\beta^2} \underbrace{\left(\frac{1}{1+[2\zeta\beta/(1-\beta^2)]^2}\right)_i^{1/2}}_{\cos\phi_i}$$

$$\rho_i = \frac{p_o}{k} \frac{\cos\phi_i}{1-\beta^2} \ ; \ \beta = \Omega/\omega$$

O

$$k - k\beta^2 = \frac{p_o \cos\phi_i}{\rho_i} = k - \Omega^2 m \qquad (23)$$

SUSTITUYENDO LOS VALORES EXPERIMENTALES DE LAS DOS PRUEBAS:

$$k - (16)^2 m = \frac{500\ (0.966)}{7.2 \times 10^{-3}}$$

$$k - (25)^2 m = \frac{500\ (0.574)}{14.5 \times 10^{-3}}$$

$$k = 100\ 000 \ \frac{lb}{in}$$

$$m = 128.5 \ \frac{lb\ SEG^2}{in}$$

$$\omega = \sqrt{\frac{k}{m}} = 27.9 \ \frac{RAD}{SEG}$$

USANDO LAS ECS. (17) Y (23) SE OBTIENE:

$$\zeta = \frac{p_o \operatorname{sen}\phi_i}{2\beta_i k\rho_i} \text{ ; DE DONDE } \zeta \frac{500\ (0.259)}{2\frac{16}{27.9}\ 100\ 000(7.2 \times 10^{-3})} = 15.7\%$$

RESONANCIA

CUANDO LA EXCITACION TIENE FRECUENCIA IGUAL A LA NATURAL DEL SISTEMA, SE DICE QUE SE PRESENTA EL CASO DE RESONANCIA. DE LA EC.(20) ES EVIDENTE QUE SI $\beta=\Omega/\omega=1$ SE TIENE

$$y(t) = \underbrace{\frac{1}{2\zeta}}_{B_d} a\ \operatorname{sen}(\Omega t-\phi)$$

$O(B_d)_{res} = \frac{1}{2\zeta}$ EN CASO DE MOVIMIENTO DEL SUELO Y DE FUERZA EXTERNA

SIN EMBARGO, AUNQUE ESTA RESPUESTA ES CASI IGUAL A LA MAXIMA, ESTA OCURRE CUANDO $\Omega = \omega\sqrt{1-2\zeta^2}$. EN EL CASO DE $\dot{y}(t)$ Y $\ddot{y}(t)$, EL MAXIMO OCURRE, RESPECTIVAMENTE, CUANDO

$\Omega = \omega$ Y $\Omega = \frac{\omega}{\sqrt{1-2\zeta^2}}$. SI $\zeta \leq 20\%$, LOS VALORES DE ESTAS Ω NO DIFIEREN EN MAS DE 2%.

EL MAXIMO VALOR DE B_d (PARA $\Omega = \omega\sqrt{1-2\zeta^2}$) ES

$$(B_d)_{MAX} = \frac{1}{2\zeta\sqrt{1-\zeta^2}} \quad O \quad (B_d)_{MAX} = \frac{(\Omega/\omega)^2}{2\zeta\sqrt{1-\zeta^2}}$$

SI SE TIENE FUERZA EXTERNA O MOVIMIENTO DEL SUELO, RESPECTIVAMENTE.

SE OBSERVA EN ESTAS ECUACIONES QUE SI $\zeta=0$, $(B_d)_{MAX} = \infty$.

SI SE ANALIZA LA SOLUCION GENERAL DE LA ECUACION DIFERENCIAL DE MOVIMIENTO PARA EL CASO DE CONDICIONES INICIALES NULAS Y $\beta=1$ SE TIENE QUE:

$$y(t) = e^{-ht}(A \operatorname{sen} \omega' t + B \cos \omega' t) - \frac{P_o}{k} \frac{\cos\omega t}{2\zeta}$$

$$y(0) = B - p_o/(2\zeta k) = 0$$

DE DONDE, HACIENDO $y(0)=0$ Y $\dot{y}(0)=0$, SE OBTIENEN:

$$A = \frac{P_o}{k} \frac{\omega}{2\omega'} = \frac{P_o}{k} \frac{1}{2\sqrt{1-\zeta^2}} \quad ; \quad B = \frac{P_o}{k} \frac{1}{2\zeta}$$

POR LO QUE

$$y(t) = \frac{1}{2\zeta} \frac{P_o}{k} \left[e^{-ht} \left(\frac{\zeta}{\sqrt{1-\zeta^2}} \operatorname{sen}\omega' t + \cos\omega' t\right) - \cos\omega t\right]$$

PARA AMORTIGUAMIENTOS PEQUEÑOS:

$$\frac{y(t)}{p_o/k} \doteq \frac{1}{2\zeta} (e^{-ht} - 1)\cos\omega t$$

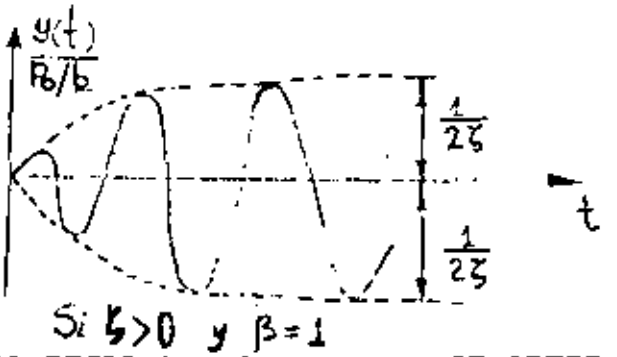

Si $\zeta>0$ y $\beta=1$

SI $\zeta=0$, APLICANDO LA REGLA DE L'HOSPITAL, SE OBTIENE:

$$\frac{y(t)}{p_o/k} = \frac{1}{2} (\operatorname{sen}\omega t - \omega t \cos\omega t)$$

O SEA, EL MAXIMO DE LA RESPUESTA TIENDE A INFINITO GRADUALMENTE.

DE LAS ECS. (I) Y (II) SE CONCLUYE QUE EL FACTOR DE AMORTIGUAMIENTO VISCOSO ES FUNCION DE LA FRECUENCIA, ω.

EXISTE OTRO TIPO DE AMORTIGUAMIENTO QUE ES INDEPENDIENTE DE LA FRECUENCIA, QUE SE CONOCE COMO AMORTIGUAMIENTO HISTERETICO, EL CUAL PRODUCE UNA FUERZA EN FASE CON LA VELOCIDAD RELATIVA DE LA MASA, PERO PROPORCIONAL AL DESPLAZAMIENTO, ES DECIR

$$f_a = \eta k |y(t)| \frac{\dot{y}(t)}{|\dot{y}(t)|} \qquad \text{(III)}$$

DONDE η ES EL COEFICIENTE DE AMORTIGUAMIENTO HISTERETICO. EL DIAGRAMA DE f_a DURANTE UN CICLO ES

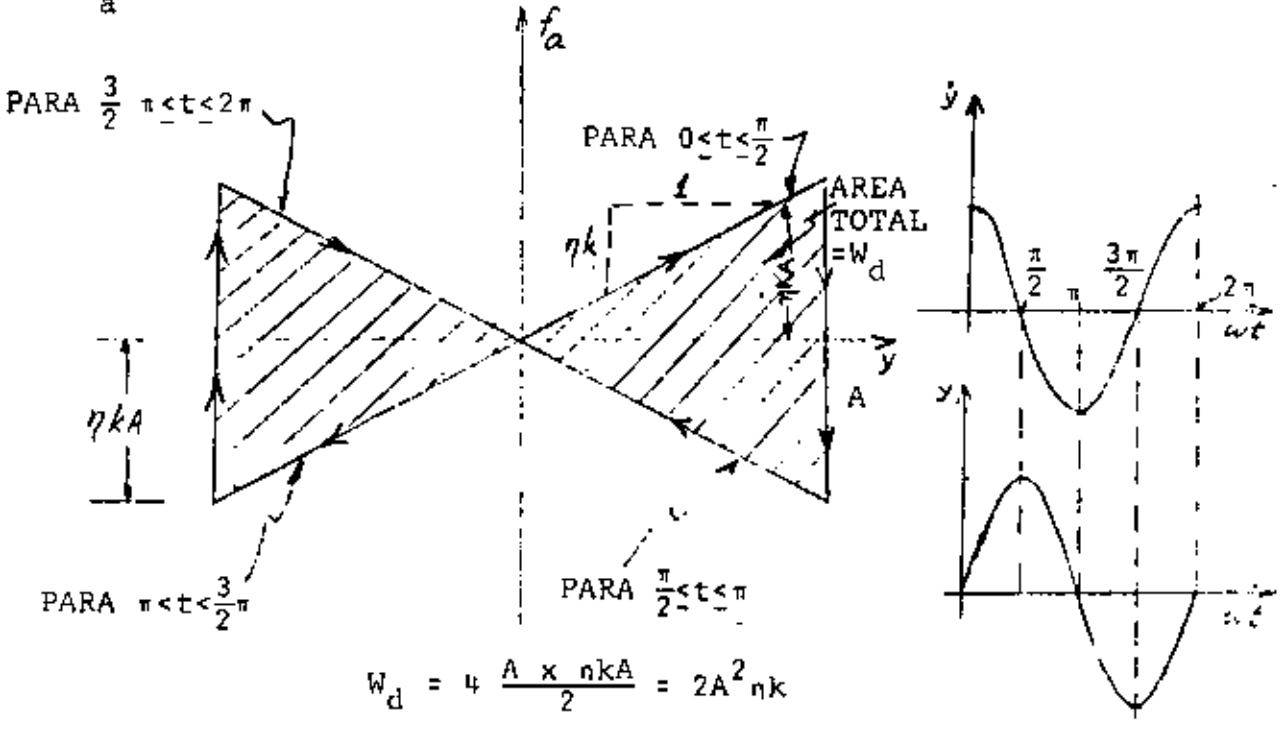

$$W_d = 4 \frac{A \times \eta kA}{2} = 2A^2 \eta k$$

SI SE CONSIDERA QUE LA ENERGIA PERDIDA POR HISTERESIS SE PUEDE REPRESENTAR MEDIANTE UN AMORTIGUADOR VISCOSO, ENTONCES, DE LA EC. (II') Y FIG 2:

$$c = \frac{2A^2 \eta k}{4\pi \frac{KA^2}{2}} = \frac{\eta}{\pi} \quad \text{o} \quad \boxed{\eta = \pi c} \qquad \text{(IV)}$$

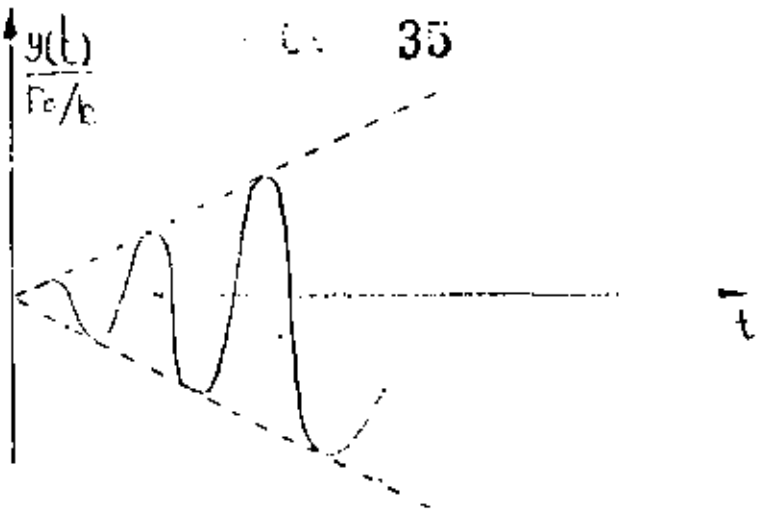

CARACTERISTICAS DINAMICAS DE LOS REGISTRADORES DE SISMOS.

SI LA ACELERACION DE LA BASE DE UN INSTRUMENTO ES ARMONICA, DADA POR LA ECUACION

$$\ddot{x}_o(t) = a \operatorname{sen}\Omega t$$

EL FACTOR DE AMPLIFICACION RESULTA SER

$$\bar{B}_d = \frac{1}{\sqrt{(1-\frac{\Omega^2}{\omega 2})^2 + (2\zeta\frac{\Omega}{\omega})^2}} \quad \frac{1}{\omega^2} = \frac{B_d}{\omega^2}$$

PUESTO QUE LA FIG I CORRESPONDE A B_d, Y EN ELLA SE OBSERVA QUE PARA $\zeta = 0.7$ SE TIENE $B_d \doteq 1$ PARA $0 \leq \Omega/\omega \leq 0.6$, SE CONCLUYE QUE EL DESPLAZAMIENTO DE LA MASA DE UN SISTEMA ES PROPORCIONAL A LA ACELERACION DE SU BASE, SI ESTE TIENE AMORTIGUAMIENTO DEL 70% Y SI LAS EXCITACIONES QUE SE TRATAN DE REGISTRAR TIENEN FRECUENCIAS INFERIORES AL 60% DE LA FRECUENCIA NATURAL DEL SISTEMA. SI ESTO SE CUMPLE, EL APARATO RESULTA SER UN ACELEROMETRO.

EN INGENIERIA SISMICA LA MAXIMA FRECUENCIA DE INTERES ES DEL ORDEN DE 10 CPS (T = 0.1 SEG), POR LO QUE LOS ACELEROMETROS TIENEN FRECUENCIA NATURAL DE 16 A 20 CPS.

POR OTRA PARTE SI LA EXCITACION DEL SUELO ES $x_o = a\,\text{sen}\Omega t$, O SEA, $\ddot{x} = -a\,\Omega^2 \text{sen}\Omega t$, ENTONCES EL FACTOR DE AMPLIFICACION RESULTA SER EL SEÑALADO EN LA ECUACION (20), ES DECIR,

$$B'_d = \frac{(\Omega/\omega)^2}{\sqrt{(1-(\Omega/\omega)^2) + (2\zeta\Omega/\omega)^2}}$$

EN LA GRAFICA CORRESPONDIENTE SE OBSERVA QUE SI $\zeta=0.5$ Y $\Omega>\omega$ EL DESPLAZAMIENTO DE LA MASA ES PROPORCIONAL AL DEL SUELO; SI ESTO SE CUMPLE, EL APARATO, CONSTITUYE UN DESPLAZOMETRO, CONOCIDO TAMBIEN COMO SISMOMETRO.

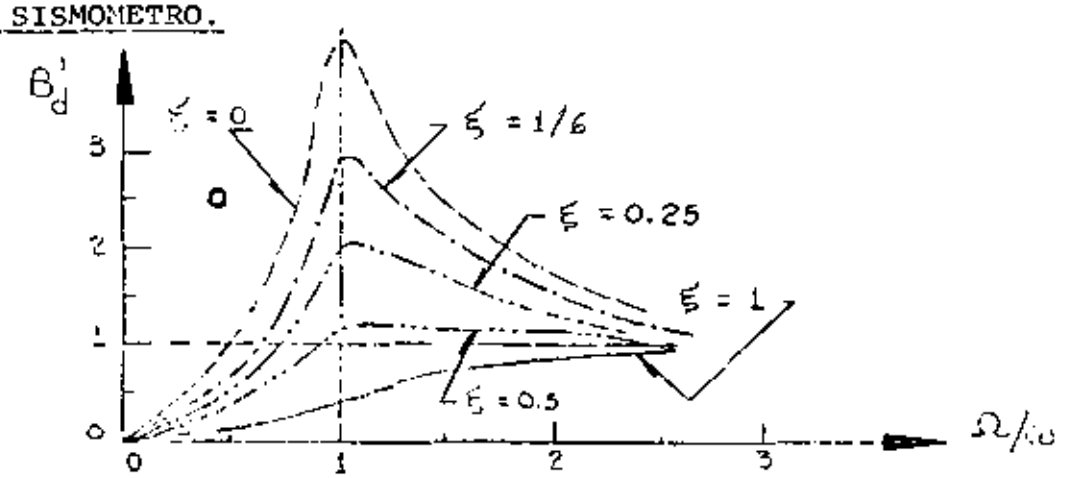

DETERMINACION EXPERIMENTAL DEL AMORTIGUAMIENTO DE UNA ESTRUCTURA MEDIANTE VIBRACIONES FORZADAS ARMONICAS

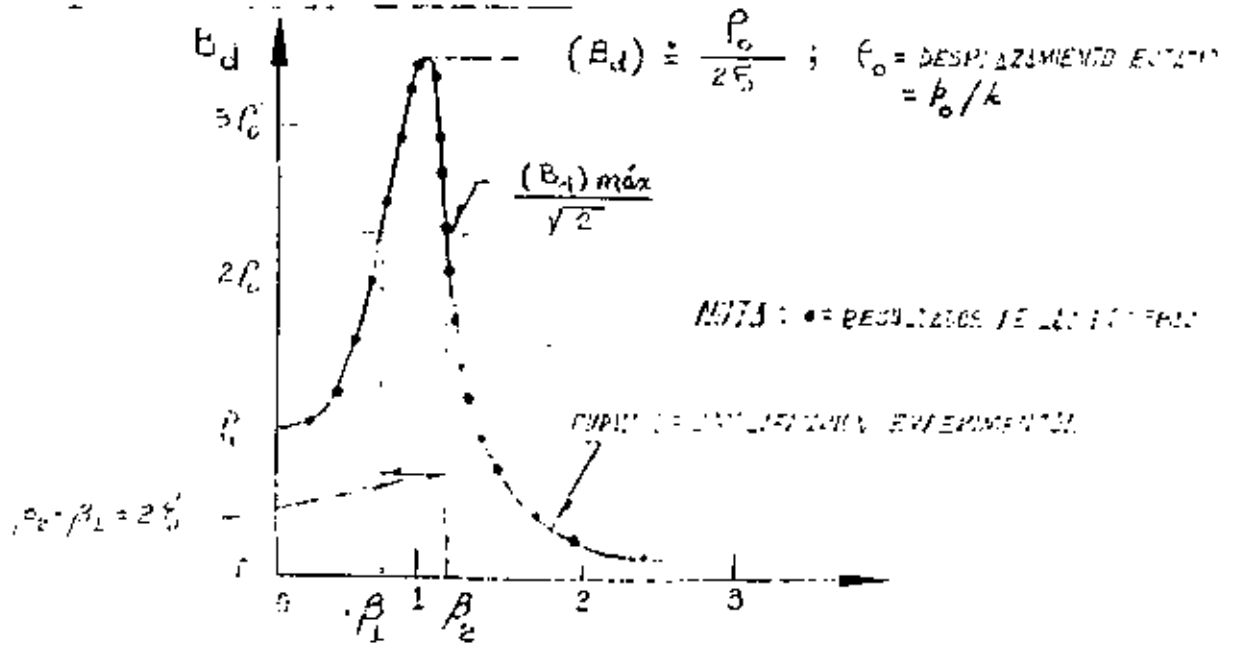

SI SE DETERMINA B_d EXPERIMENTALMENTE MEDIANTE UNA SERIE DE PRUEBAS DE VIBRACION FORZADA CON FUERZAS ARMONICAS, Y ADEMAS SE DETERMINA ρ_o, ENTONCES

$$\boxed{\zeta \doteq \frac{\rho_o}{2(B_d)_{MAX}}} \qquad (24)$$

OTRO METODO PARA DETERMINAR ζ CON BASE EN LA CURVA EXPERIMENTAL DE B_d SE CONOCE CON EL NOMBRE DE "METODO DEL ANCHO DE BANDA DE LA MITAD DE POTENCIA". ESTE SE BASA EN DETERMINAR LAS FRECUENCIAS QUE CORRESPONDEN AL VALOR rms DE LA AMPLITUD EN RESONANCIA, EL CUAL VALE $(B_d)_{MAX}/\sqrt{2}$; SEAN β_2 Y β_1 ESTAS FRECUENCIAS. DE LA ECUACION DE B_d SE OBTIENE:

$\text{rms} = \frac{A}{\sqrt{2}}$ = RAIZ CUADRADA DEL VALOR MEDIO CUADRATICO

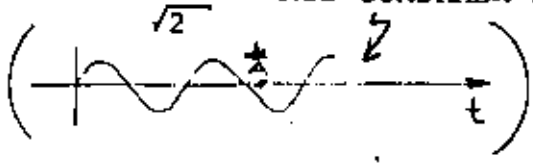

$$\frac{1}{\sqrt{2}} \frac{\rho_o}{2\zeta} = \rho_o / \sqrt{(1-\beta^2)^2 + (2\zeta\beta)^2}$$

ELEVANDO AL CUADRADO AMBOS MIEMBROS:

$$\frac{1}{8\zeta^2} = \frac{1}{(1-\beta^2)^2 + (2\zeta\beta)^2}$$

DE DONDE $\beta^2 = 1 - 2\zeta^2 \pm 2\zeta\sqrt{1+\zeta^2}$

DE AQUI, DESPRECIANDO EL TERMINO ζ^2 DEL RADICAL, SE OBTIENE

$$\beta_1^2 \doteq 1 - 2\zeta - 2\zeta^2 \quad ; \quad \beta_1 \doteq 1 - \zeta - \zeta^2$$
$$\beta_2^2 \doteq 1 + 2\zeta - 2\zeta^2 \quad ; \quad \underline{\beta_2 \doteq 1 + \zeta - \zeta^2}$$
$$\beta_2 - \beta_1 \doteq 2\zeta$$

DE DONDE $$\zeta \doteq \frac{\beta_2 - \beta_1}{2} \qquad (25)$$

EJEMPLO

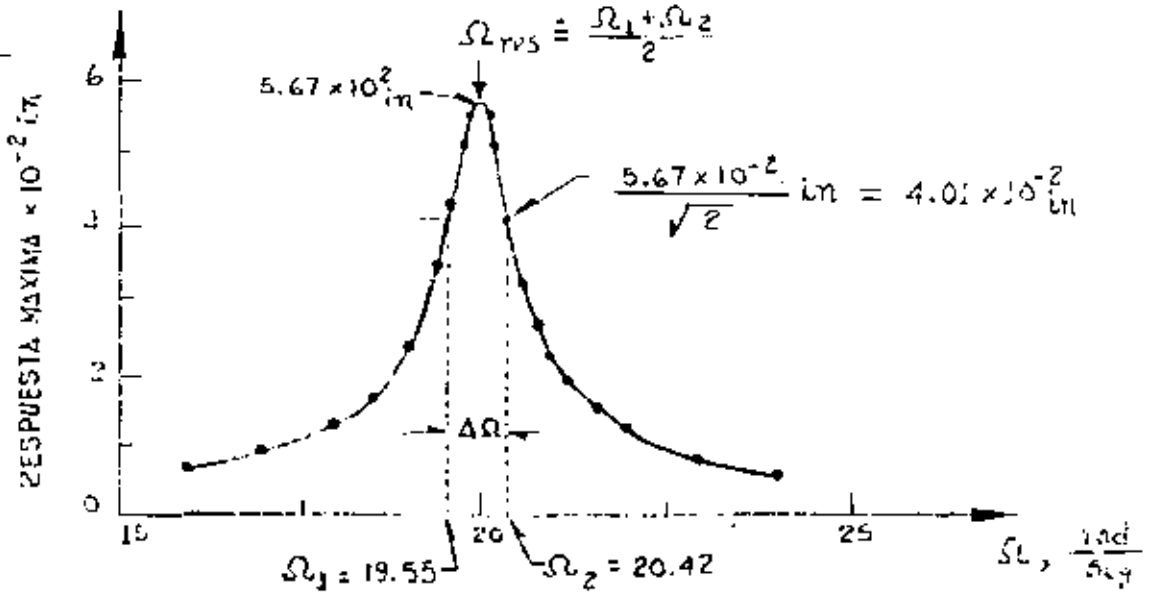

DE LA EC (25) $$A\Omega = \Omega_2 - \Omega_1 = 0.87 \ \frac{RAD}{SEG}$$

$$\zeta \doteq \frac{\beta_2 - \beta_1}{2} = \frac{\frac{\Omega_2}{\Omega_{res}} - \frac{\Omega_1}{\Omega_{res}}}{2} = \frac{\Omega_2 - \Omega_1}{\Omega_2 + \Omega_1} = \frac{0.87}{39.97} = 2.188$$

METODO NUMERICO β DE NEWMARK PARA RESOLVER EL PROBLEMA DE VIBRACIONES FORZADAS.

EL METODO QUE A CONTINUACION SE DESCRIBE ES ADAPTABLE A SISTEMAS NO LINEALES CON VARIOS GRADOS DE LIBERTAD.

PROCEDIMIENTO:

1. SEAN y_i, $\dot{y}_i$, $\ddot{y}_i$, CONOCIDOS EN EL INSTANTE t_i, Y $t_{i+1} = t_i + \Delta t$. SUPONGAMOS EL VALOR DE $\ddot{y}_{i+1}$

2. CALCULEMOS $$\dot{y}_{i+1} \doteq \dot{y}_i + (\ddot{y}_i + \ddot{y}_{i+1})\Delta t/2 \qquad (26)$$

3. CALCULEMOS $y_{i+1} \doteq y_i + \dot{y}_i \Delta t + (\frac{1}{2} - \beta)\ddot{y}_i(\Delta t)^2 + \beta \ddot{y}_{i+1}(\Delta t)$ (27)

4. CALCULEMOS UNA NUEVA APROXIMACION PARA $\ddot{y}_{i+1}$ A PARTIR DE LA ECUACION DIFERENCIAL DE EQUILIBRIO:

$$\ddot{y}_{i+1} \doteq -2\zeta\omega\dot{y}_{i+1} - \omega^2(y_{i+1} - y_{est}) - (\ddot{x}_o)_{i+1} \qquad (28)$$

DONDE $y_{est} = p(t_{i+1})/k$

5. REPITAMOS LAS ETAPAS 2 A 4 EMPEZANDO CON EL NUEVO VALOR $\ddot{y}_{i+1}$ HASTA QUE EN DOS CICLOS CONSECUTIVOS SE TENGAN VALORES DE $\ddot{y}_{i+1}$ CASI IGUALES.

SE RECOMIENDAN VALORES DE β DE 1/6 A 1/4 Y $\Delta t \doteq 0.1T$ PARA ASEGURAR CONVERGENCIA Y ESTABILIDAD.

EJEMPLO

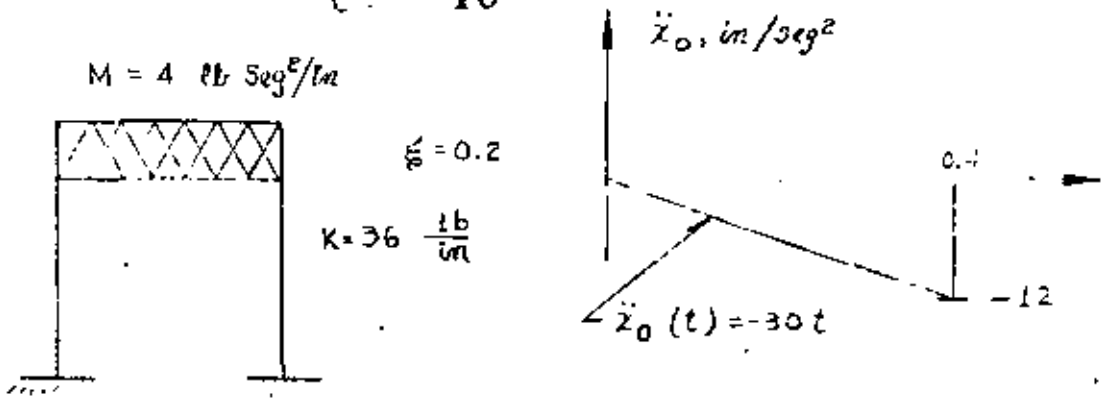

CALCULAR LA RESPUESTA DE LA ESTRUCTURA APLICANDO EL METODO β DE NEWMARK

$$\omega = \sqrt{K/M}' = \sqrt{36/4}' = 3 \frac{RAD}{SEG}$$

$$h = \zeta\omega = 0.2 \times 3 = 0.6 \quad ; \quad T = \frac{2\pi}{3} = 2.09 \text{ SEG}$$

TOMAREMOS $\beta=0.2$ Y $\Delta t = 0.2$ ($\doteq$ o.1T) SUSTITUYENDO EN LAS ECS. (26), (27) y (28):

$$\dot{y}_{i+1} \doteq y_i + 0.1 (\ddot{y}_i + \ddot{y}_{i+1})$$

$$y_{i+1} \doteq y_i + 0.2\dot{y}_i + 0.012\ddot{y}_i + 0.008\ddot{y}_{i+1}$$

$$\ddot{y}_{i+1} = -1.2\dot{y}_{i+1} - gy_{i+1} - (\ddot{x}_o)_{i+1}$$

EN t=0 SABEMOS QUE SE TIENE y=0, $\dot{y}$=0 Y $\ddot{y}$=0

EN t=0 + Δt = 0.2 SEG; SUPONGAMOS $\ddot{y}_{i+1}$ = 5.0 IN/SEG^2; $\ddot{x}_o$ =-6

$y_i = 0$

$\dot{y}_i = 0$

1ª CICLO

$$\dot{y}_{i+1} = 0 + 0.1\ (0 + 5) = 0.5 \quad ; \quad y_{i+1} = 0 + 0 + 0 + 0.008 \times 5 = 0.04$$

$$\ddot{y}_{i+1} = -1.2 \times 0.5 - 9 \times 0.04 - (-30 \times 0.2) = 5.04$$

2ª CICLO

$$\dot{y}_{i+1} = 0 + 0.1\ (0 + 5.04) = 0.504 \quad ; \quad y_{i+1} = 0 + 0 + 0 + 0.008 \times 5.04 =$$

$$= 0.04032$$

$$\ddot{y}_{i+1} = -1.2 \times 0.504 - 9 \times 0.4032 - (-6) = 5.033 \text{ IN/SEG}^2$$

ESTOS CALCULOS SE PUEDEN ORGANIZAR MEDIANTE UNA TABLA COMO LA SIGUIENTE:

t SEG	$\ddot{x}_o$ IN/SEG^2	$\ddot{y}$ ING/SEG^2	$\dot{y}$ ING/SEG	y IN
0	0	0	0	0
0.2	-6	5.0000	0.5000	0.04000
		5.040	0.5040	0.04032
		5.033	0.5033	0.04026
		5.034	0.5034	0.04027
0.4 $^-$	-12	8.0000	1.8078	0.26536
		7.442	1.7510	0.26079
		7.534	1.7602	0.26163
		7.533	1.7601	0.26162
0.4$^+$	0	-4.467	1.7601	0.26162
0.6	0	-6.000	0.7134	0.51204
		-5.464	0.7670	0.51633
		-5.550	0.7584	0.51564
		.	.	.
		.	.	.
		.	.	.

EN $t = 0.2 + \Delta t = 0.4$ SEG: $\ddot{x}_o = -30 \times 0.4 = -12$

$$\ddot{y}_i = 5.034, \quad \dot{y}_i = 0.5034, \quad y_i = 0.04027$$

SUPONIENDO $\ddot{y}_{i+1} = 8.000$ SE OBTIENE:

1er CICLO

$$\begin{cases} \dot{y}_{i+1} = 0.5034 + 0.1\ (5.034 + 8.000) = 1.8068 \\ y_{i+1} = 0.04027 + 0.2 \times 0.5034 + 0.012 \times 5.034 + 0.008 \times 8 = 0.26536 \\ \ddot{y}_{i+1} = -1.2 \times 1,8068 - 9 \times 0.26536 - (-12) = 7.442\ \text{IN/SEG}^2 \end{cases}$$

EN $t = 0.4^+$ SOLO CAMBIA $\ddot{y}$: $\ddot{y}_{0.4+} = \ddot{y}_{0.4-} + \ddot{x}_o = 7.533 - 12 = -4.467$

EN $t = 0.6$, $\ddot{y}_i = -4.467$) $\dot{y}_i = 1.7601$; $y = 0.26162$

ESPECTROS DE RESPUESTA ESTRUCTURAL

RECORDEMOS QUE LA SOLUCION DEL PROBLEMA DE VIBRACIONES FORZADAS CON EXCITACION SISMICA ES

$$Y(t) = \frac{-1}{\omega'} \int_{-\infty}^{t} \ddot{x}_o(t-\tau) e^{-\zeta\omega(t-\tau)} \operatorname{sen} \omega'(t-\tau) d\tau$$

DE LA OBSERVACION DE ESTA ECUACION SE CONCLUYE QUE EL DESPLAZAMIENTO RELATIVO, $Y(t)$, ES FUNCION DEL TIEMPO, t, EL AMORTIGUAMIENTO, ζ, Y LA FRECUENCIA CIRCULAR NATURAL, ω (O DEL PERIODO NATURAL):

$y(t) = f(t,\omega,\zeta)$

FIJEMOS UN VALOR DE ζ, POR EJEMPLO $\zeta=0$, Y LUEGO ASIGNEMOS VALORES A ω, POR EJEMPLO 0.1, 0.2. 0.3, ETC, HASTA CUBRIR UN INTERVALO DE INTERES, Y PARA CADA CASO CALCULEMOS LA FUNCION RESULTANTE DE APLICAR LA ECUACION ANTERIOR. CON ESTA OBTENEMOS

$$y_1(t) = f_1(t,\ 0.1,\ 0) = f_1(t)$$

$$y_2(t) = f_2(t,\ 0.2,\ 0) = f_2(t)$$

$$y_3(t) = f_3(t,\ 0.2,\ 0) = f_3(t)$$

SEAN $D_1 = \text{MAX}|y_1(t)| = D(\omega_1,\zeta)$

$D_2 = \text{MAX}|y_2(t)| = D(\omega_2,\zeta)$

$D_3 = \text{MAX}|y_3(t)| = D(\omega_3,\zeta)$

$\vdots$

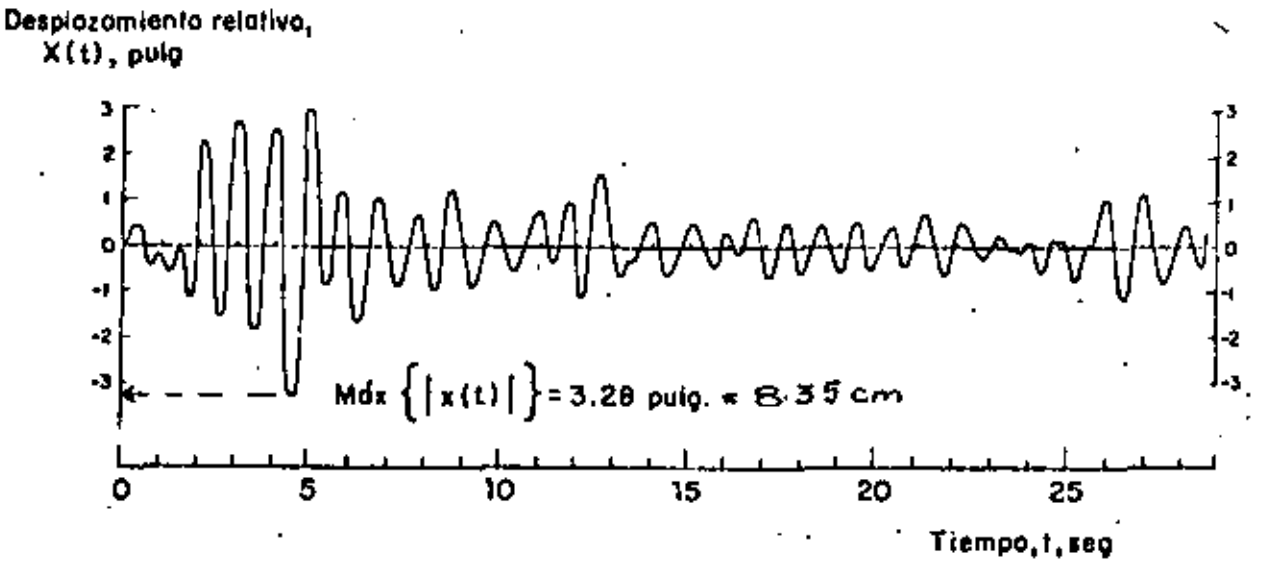

Respuesta de un sistema amortiguado simple con $T_1 = 1.0$ seg y $\zeta = 0.10$, al sismo de El Centro, Cal., 1940, componente N-S

EN TAL CASO, LA GRAFICA

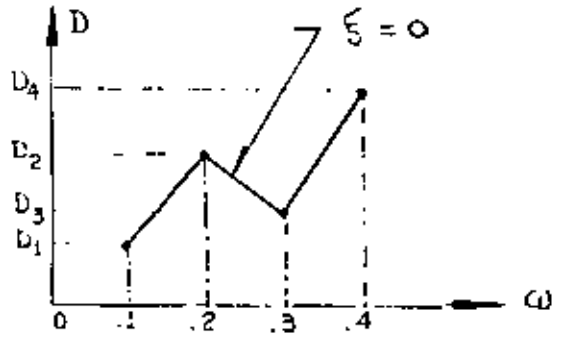

ES EL *ESPECTRO DE RESPUESTA DE DESPLAZAMIENTOS* PARA $\zeta = 0$. SI ESTE PROCESO DE REPITE FIJANDO OTROS VALORES DE ζ. POR EJEMPLO, $\zeta = 0.02$, 0.05, 0.1, 0.2, ETC, SE OBTENDRAN LOS ESPECTROS DE DESPLAZAMIENTOS CORRESPONDIENTES.

DE MANERA ANALOGA SE PUEDEN OBTENER LOS ESPECTROS PARA OTROS TIPOS DE RESPUESTA, TALES COMO *VELOCIDAD RELATIVA*, *ACELERACION ABSOLUTA*, ETC, QUE SON, RESPECTIVAMENTE

$$V = \text{MAX}\left|\dot{y}(t)\right|_{\zeta,\omega} \; ; \quad A = \text{MAX}\left|\ddot{X}(t)\right|_{\zeta,\omega} \tag{29}$$

PSEUDO - ESPECTROS

ESTADISTICAMENTE SE HA ENCONTRADO QUE

$$S_V = \omega D \doteq V \tag{30}$$

$$S_A = \omega^2 D \doteq A \doteq \omega V \tag{31}$$

A S_V Y S_A SE LES LLAMA *PSEUDOESPECTROS*.

DE LA EC. (30): $\log D = \log V - \log \omega = \log V + \log T - \log 2\pi$

DE LA EC. (31): $\log A = \log V + \log \omega = \log V - \log T + \log 2\pi$

ESTAS ECUACIONES CORRESPONDEN A LINEAS RECTAS EN PAPEL LOGARITMICO: LA PRIMERA CON PENDIENTE -1 Y LA SEGUNDA CON PENDIENTE +1, SI SE USA ω COMO VARIABLE INDEPENDIENTE; SI SE USA T, LA PRIMERA TENDRA PENDIENTE + 1, Y LA SEGUNDA, -1.

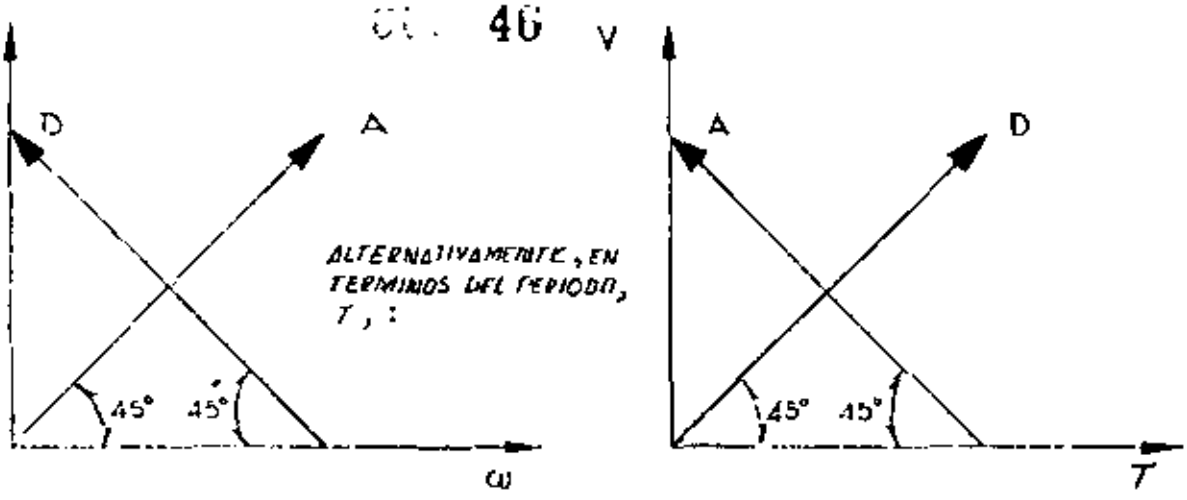

EJEMPLO

CALCULAR EL ESPECTRO CORRESPONDIENTE A LA EXCITACION (CONSIDERESE $\zeta=0$)

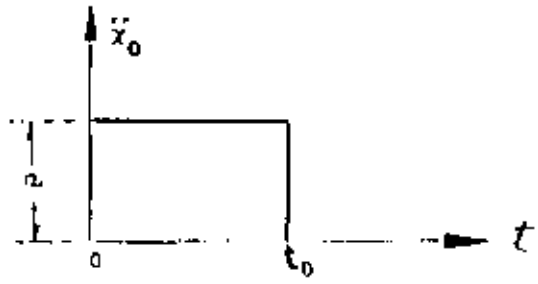

EN UN EJEMPLO ANTERIOR SE OBTUVO

$$y(t) = \frac{-a}{\omega^2}(1 - \cos\omega t), \quad \text{SI } 0 \leq t \leq t_o$$

$$D = \text{MAX}|Y(t)| = \frac{2a}{\omega^2} \quad ; \quad 0 \leq \frac{T}{2} \leq t_o, \quad (0 \leq T \leq 2t_o)$$

$$S_V = \omega D = \frac{2a}{\omega} \quad , \quad S_A = \omega V = 2a$$

Y $$D = \text{MAX}|y(t)| = \frac{2a}{\omega^2} \operatorname{sen} \frac{\omega t_o}{2} \quad , \quad \text{SI } T > 2\, t_o$$

$$S_V = \omega D = \frac{2a}{\omega} \left|\operatorname{sen} \frac{\omega t_o}{2}\right| \quad ; \quad S_A = \omega V = 2a \left|\operatorname{sen} \frac{\omega t_o}{2}\right|$$

$$\lim_{\omega \to 0} S_V = \lim_{\omega \to 0} \left\{ a t_o \, \frac{\operatorname{sen} \frac{\omega t_o}{2}}{\frac{\omega t_o}{2}} \right\} = a t_o$$

CASO PARTICULAR: SI t_o = 1 SEG y a = 100 IN/SEG^2

$$S_V = \frac{2 \times 100}{\frac{2\pi}{T}} = \frac{100}{\pi} T \, , \quad \text{SI } 0 \leq T \leq 2 \text{ SEG}$$

$$S_V = \frac{100T}{\pi}\left|\operatorname{sen}\frac{\frac{2\pi}{T}x1}{2}\right| =$$

$$= \frac{100T}{\pi}\left|\operatorname{sen}\frac{\pi}{T}\right| \text{ SI } T>2 \text{ SEG}$$

$$\lim_{T \to \infty} S_V = 100 \text{ IN/SEG}$$

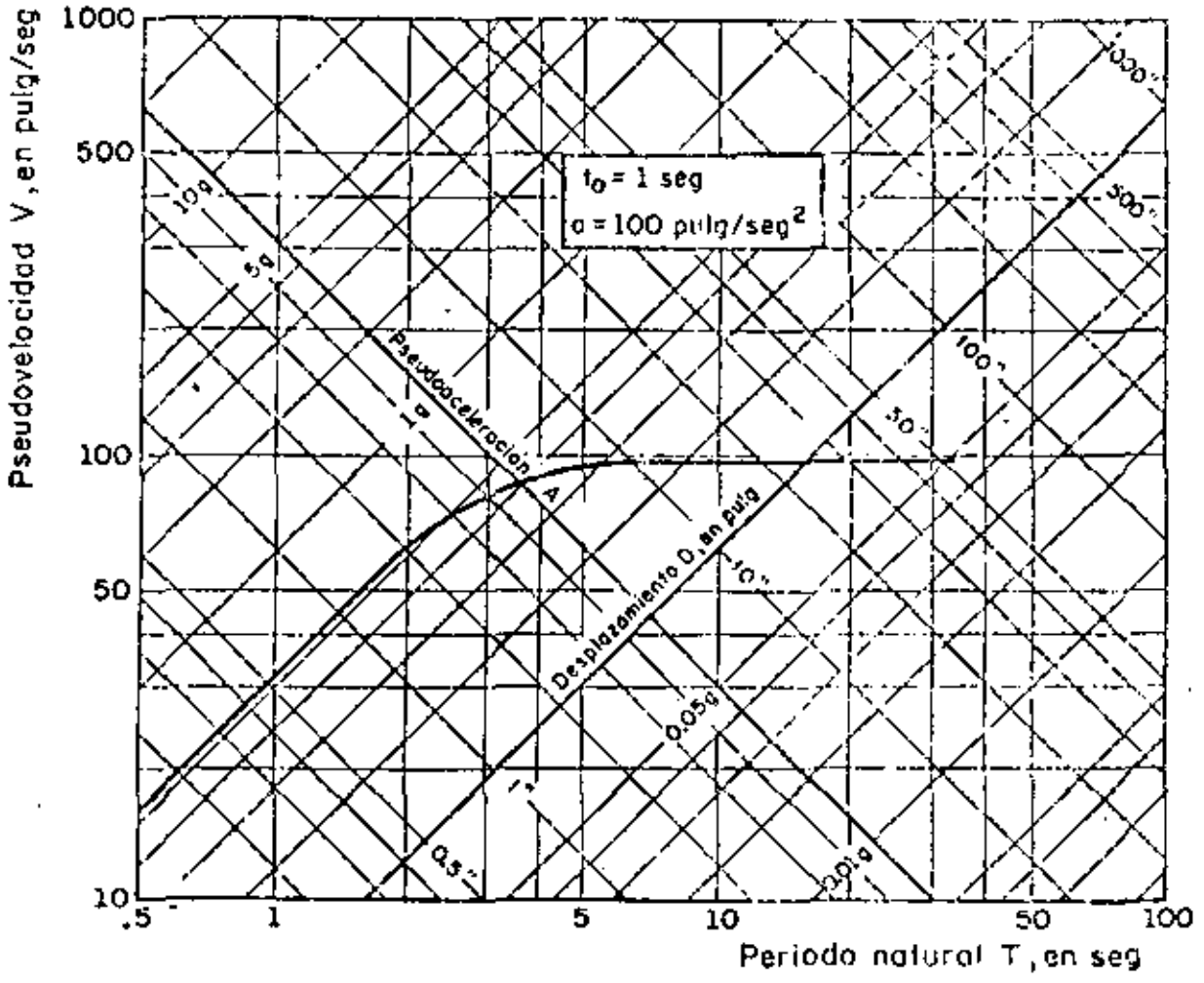

Espectro no amortiguado correspondiente a un pulso rectangular de aceleraciones. Según N. Newmark y E. Rosenblueth, ref 1

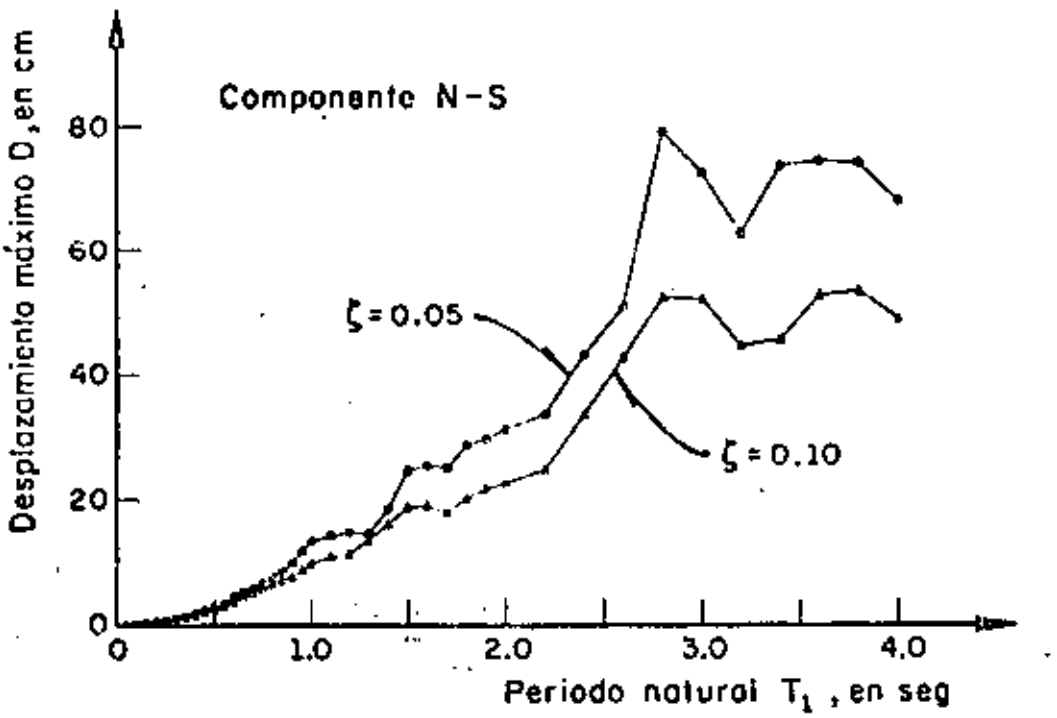

Espectro de desplazamientos. Sismo de Tokachi-Oki, Japón (1968). Según H. Tsuchida, E. Kurata y K. Sudo, ref 4

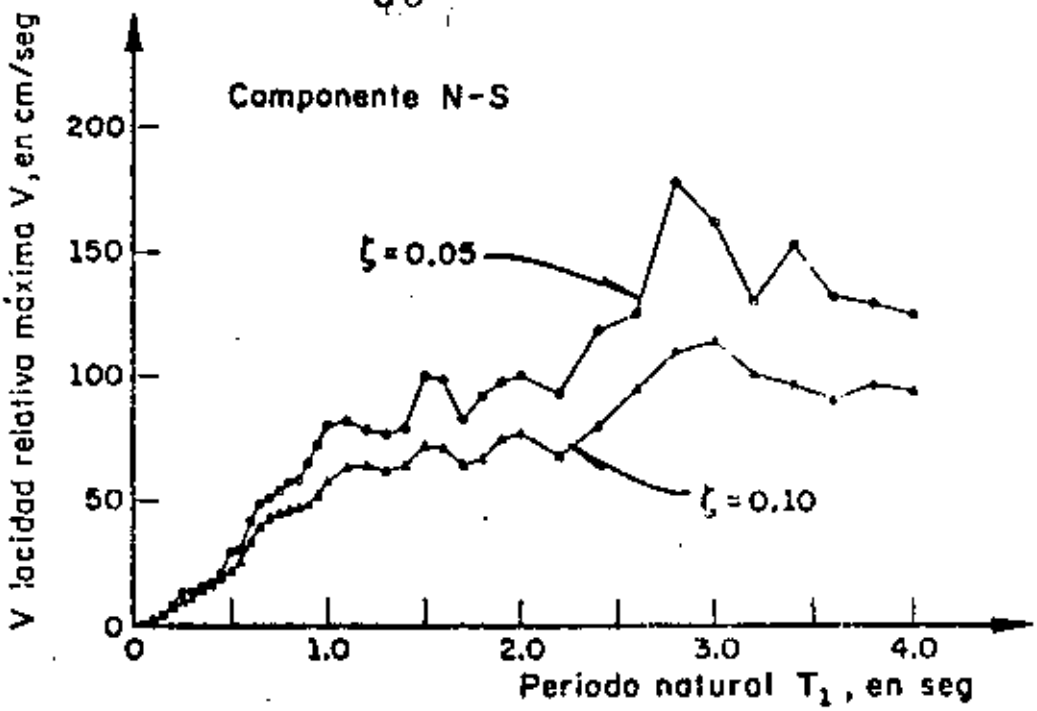

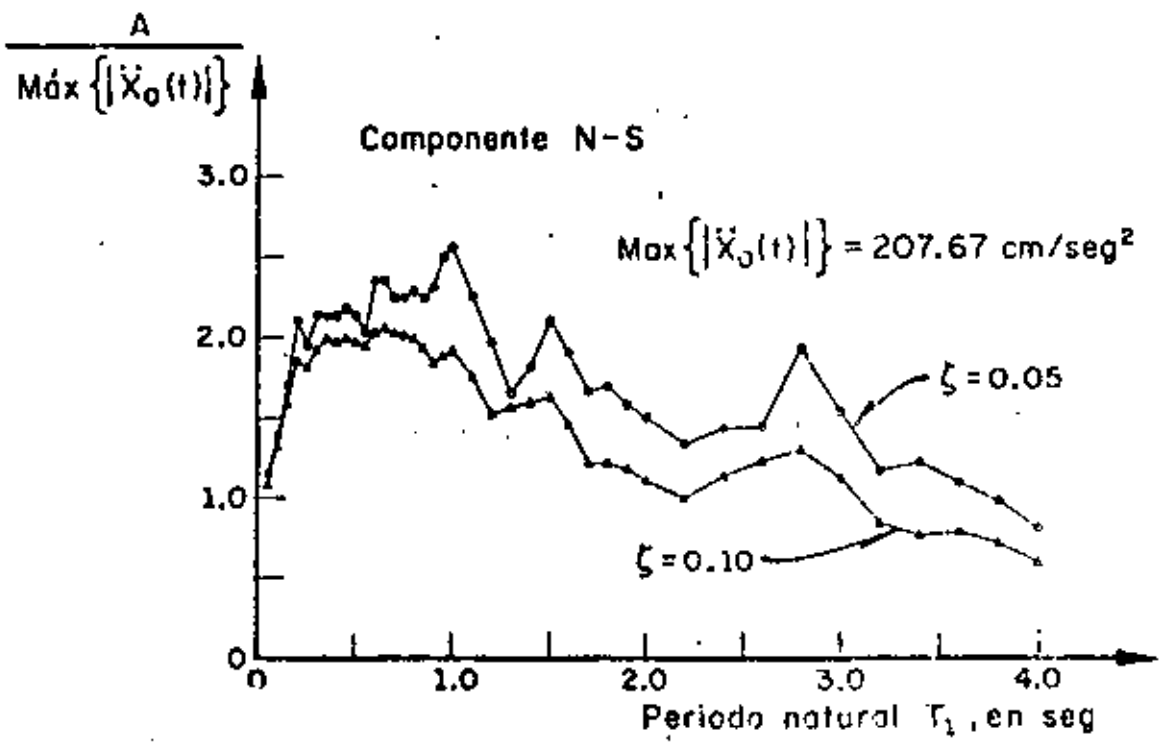

Espectros de velocidades y de aceleraciones. Sismo de Tokachi-Oki, Japón (1968). Según H. Tsuchida, E. Kurata y K. Sudo, ref 4

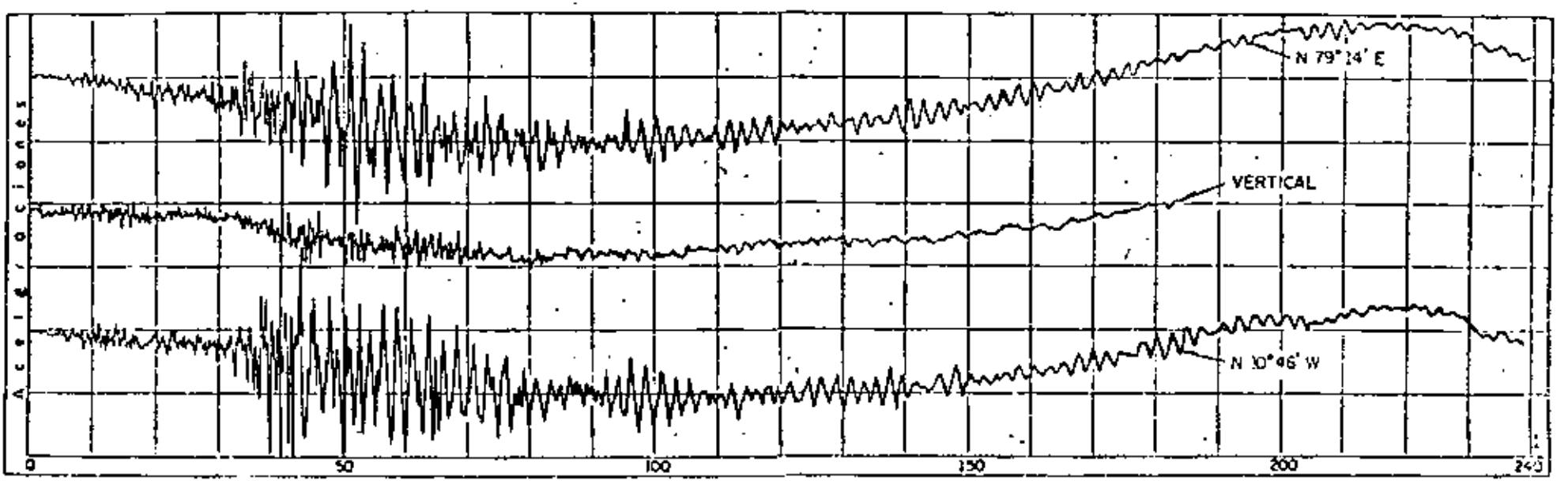

51

Acelerogramas originales del sismo registrado el 11-V-1962, en la ALAMEDA CENTRAL, Mex. D.F.

DISTRIBUCION DE FUERZAS CORTANTES DIRECTAS Y POR TORSION

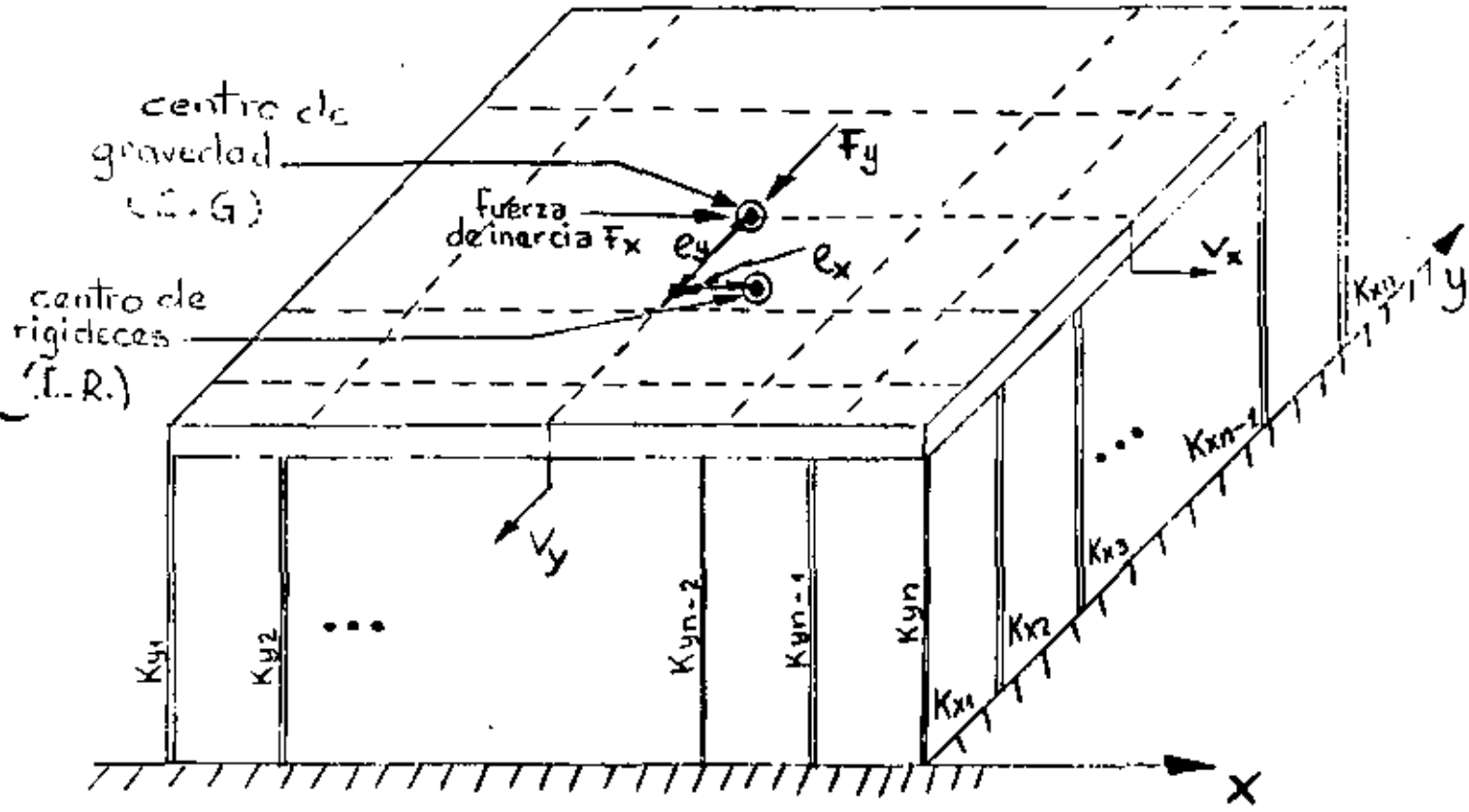

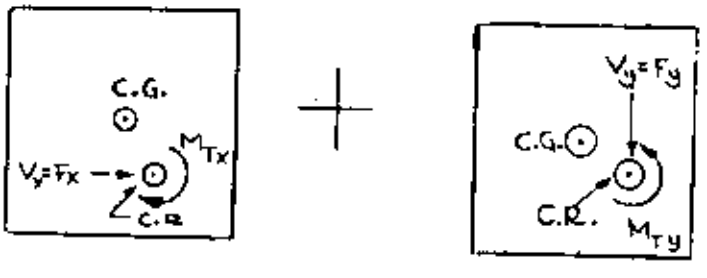

DISTRIBUCION DE LAS FUERZAS CORTANTES EN UN ENTREPISO

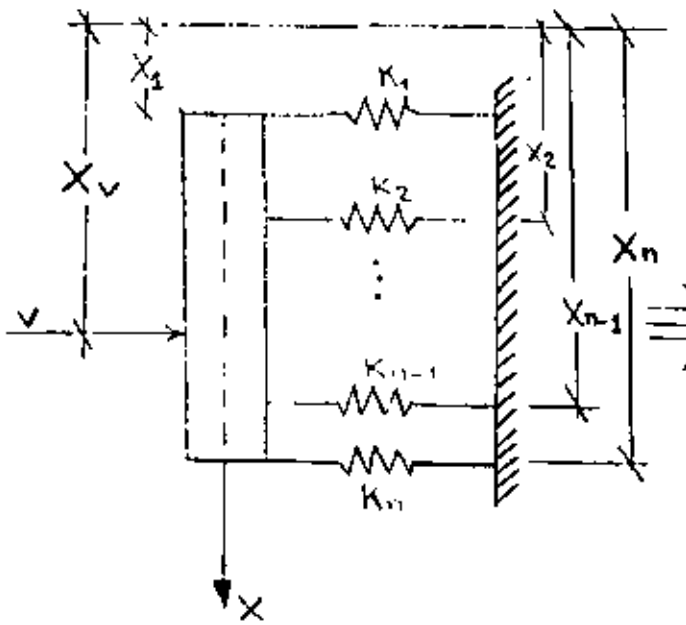

$$\Sigma F_i = K_1\delta + K_2\delta + \ldots + K_n\delta = V = K_{eq}\delta$$

$$\delta \Sigma K_i = \delta K_{eq}$$

$$K_{eq} = \sum_{i=1}^{n} K_i$$

$$\Sigma M_i = \Sigma F_i X_i = \Sigma K_i \delta X_i = \delta \Sigma K_i X_i = V X_v = K_{eq}\delta X_v$$

$$X_v = \frac{\sum_{i=1}^{n} K_i X_i}{\sum_{i=1}^{n} K_i}$$

⟸ POSICION DEL CENTRO DE RIGIDECES

54

VEAMOS COMO SE DISTRIBUYEN LAS FUERZAS CORTANTES EN LOS MARCOS

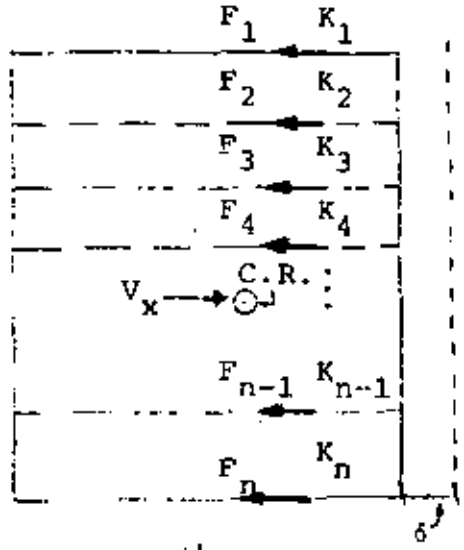

$$F_i = K_i \delta$$

$$\Sigma F_i = \Sigma K_i \delta = V_x \quad \therefore \quad \delta = \frac{V_x}{\Sigma K_i}$$

$$F_i = V_x \frac{K_i}{\sum_{i=1}^{n} K_i}$$

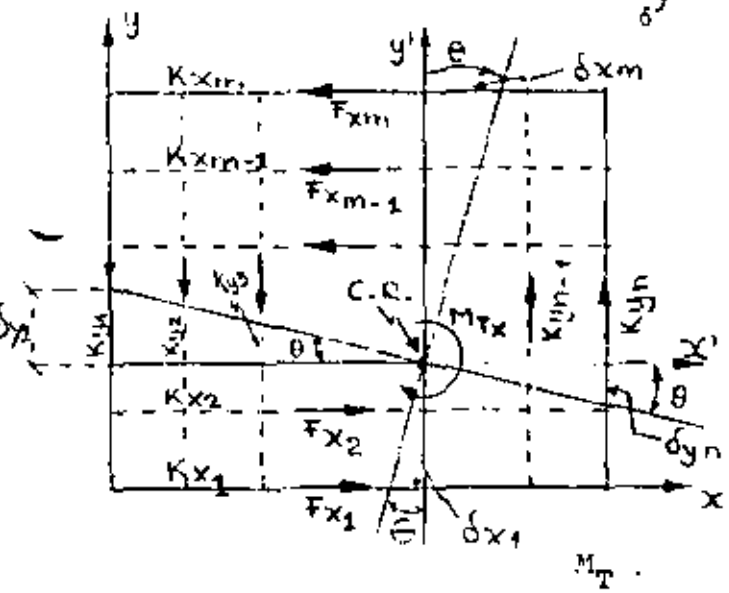

$$F_{x_i} = K_{x_i} \delta_{x_i} = K_{x_i} Y_i' \theta$$

$$F_{x_i} = K_{y_i} \delta_{y_i} = K_{y_i} X_i' \theta$$

$$\Sigma M_{C.R.} = \Sigma F_{x_i} Y_i' + \Sigma F_{y_i} X_i'$$

$$= \theta (\Sigma K_{x_i} Y_i'^2 + \Sigma K_{y_i} X_i'^2)$$

$$= M_{T_x}$$

DE DONDE $\theta = \dfrac{M_T}{\Sigma K_{x_i} Y_i'^2 + K_{y_i} X_i'^2}$

POR LO QUE

$$F_{x_i} = M_{TX} \frac{K_{x_i} Y_i'}{\Sigma K_{x_i} Y_i'^2 + K_{y_i} X_i'^2}$$

$$F_{y_i} = M_{TX} \frac{K_{y_i} X_i'}{\Sigma K_{x_i} Y_i'^2 + \Sigma K_{y_i} X_i'^2}$$

55

SISTEMAS NO LINEALES DE UN GRADO DE LIBERTAD

ECUACION DE MOVIMIENTO:

$$M\ddot{x} + Q(y,\dot{y}) = P(t) \quad ; \quad y = x - x_o = \text{DESPLAZAMIENTO RELATIVO}$$

SI $Q(y, \dot{y}) = KY + C\dot{Y}$ SE TIENE EL SISTEMA ELASTICO LINEAL

MODELOS PARTICULARES

1. RIGIDO-PLASTICO

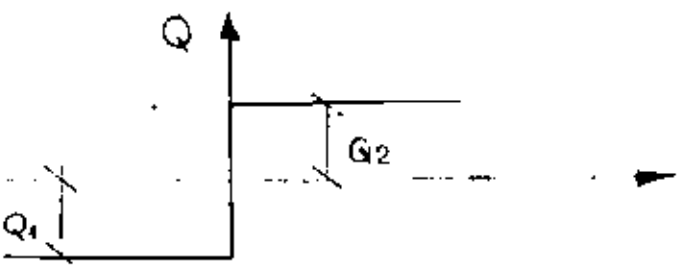

$Q = -Q_1 + C\dot{y}$, SI $\dot{y}<0$

$Q = Q_2 + C\dot{y}$, SI $\dot{y}<0$ EN DONDE C = CONSTANTE. SE HA EMPLEADO COMO MODELO EN EL ANALISIS DE TALUDES Y CORTINAS DE PRESAS DE TIERRA Y ENROCAMIENTO

2. ELASTO-PLASTICO

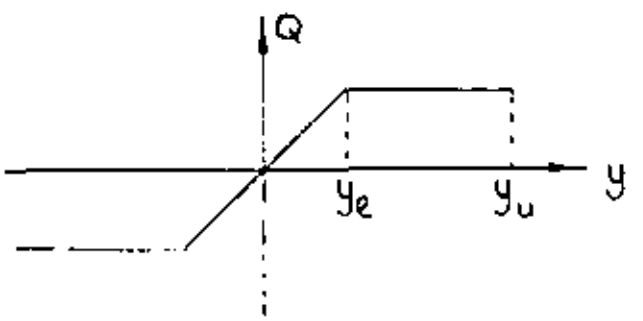

$Q = Q_1(y) + C\dot{y}$

SE EMPLEA COMO MODELO EN EL ANALISIS DE ESTRUCTURAS DUCTILES.

FACTOR DE DUCTILIDAD = $\mu = y_u/y_e$

y_u = DESPLAZAMIENTO MAXIMO QUE PUEDE SOPORTAR EL SISTEMA SIN FALLAR.

3. SISTEMA BILINEAL

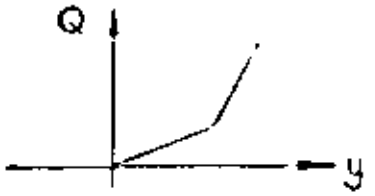

CON ENDURECIMIENTO

SE USA COMO MODELO PARA ANALISIS DE PUENTES COLGANTES

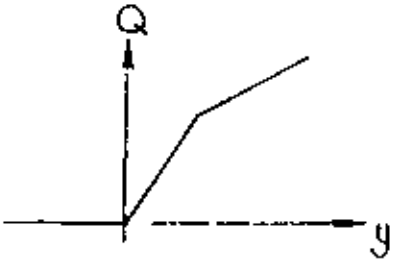

CON ABLANDAMIENTO

SE USA COMO MODELO DE SISTEMAS QUE SE DEGRADAN POR AGRIETAMIENTO (MUROS DE MAMPOSTERIA, POR EJEM)

4. TIPO MASING

(INCLUYE A LOS ANTERIORES COMO CASOS ESPECIALES)

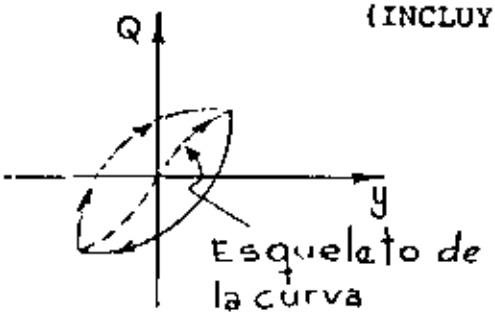

$$\frac{Q - Q_o}{2} = Q_1 \left(\frac{y - y_o}{2}\right)$$

Q_o = FUERZA EN $y = y_o$

y_o = DESPLAZAMIENTO EN EL CUAL EL PROCESO SE INVIRTIO (y CAMBIO DE SIGNO) POR ULTIMA VEZ

CASO PARTICULAR DEL ESQUELETO

$$\frac{y}{y_1} = \frac{Q}{Q_1} + \alpha \left(\frac{Q}{Q_1}\right)^r$$ (MODELO RAMBER - OSGOOD)

DONDE y_1, Q_1, α y r SON CONSTANTES POSITIVAS

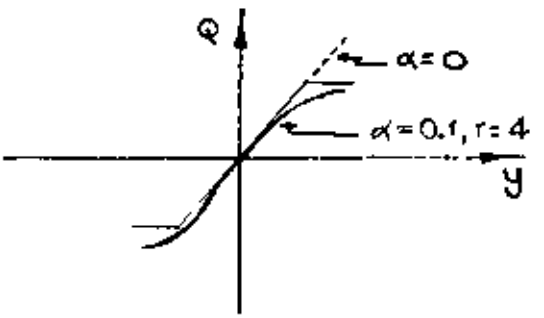

57

EJEMPLO: CASO BILINEAL

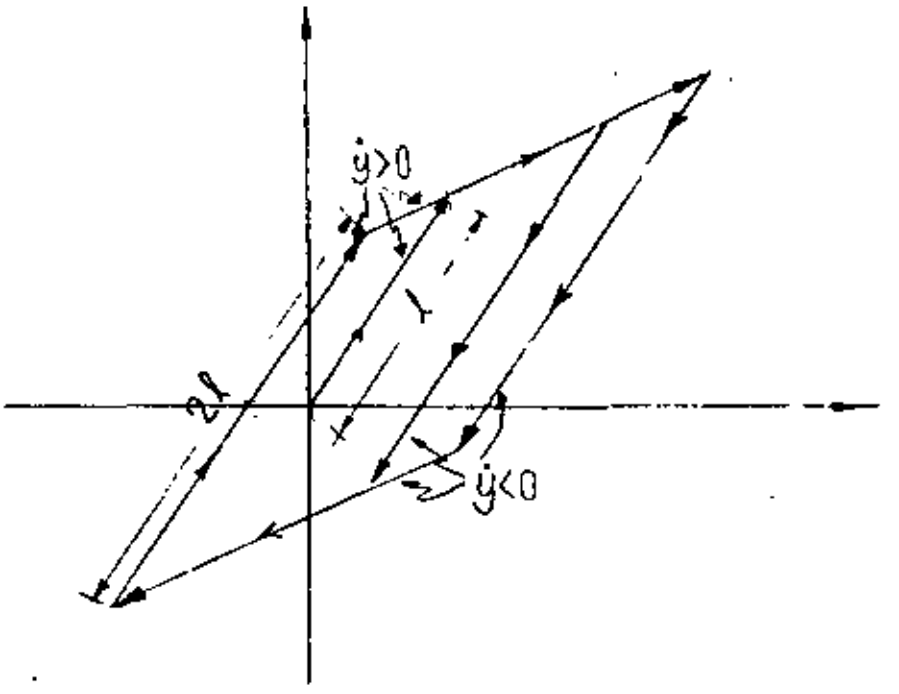

EJEMPLO CASO ELASTOPLASTICO

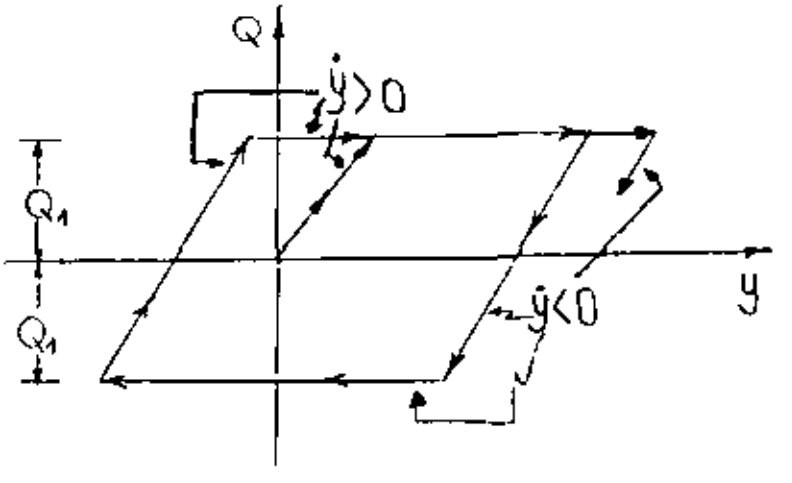

METODO β DE NEWMARK

PARA EL ANALISIS DE SISTEMAS NO LINEALES SE PUEDE USAR EL METODO β DE NEWMARK DESCRITO ANTERIORMENTE.

58

EJEMPLO

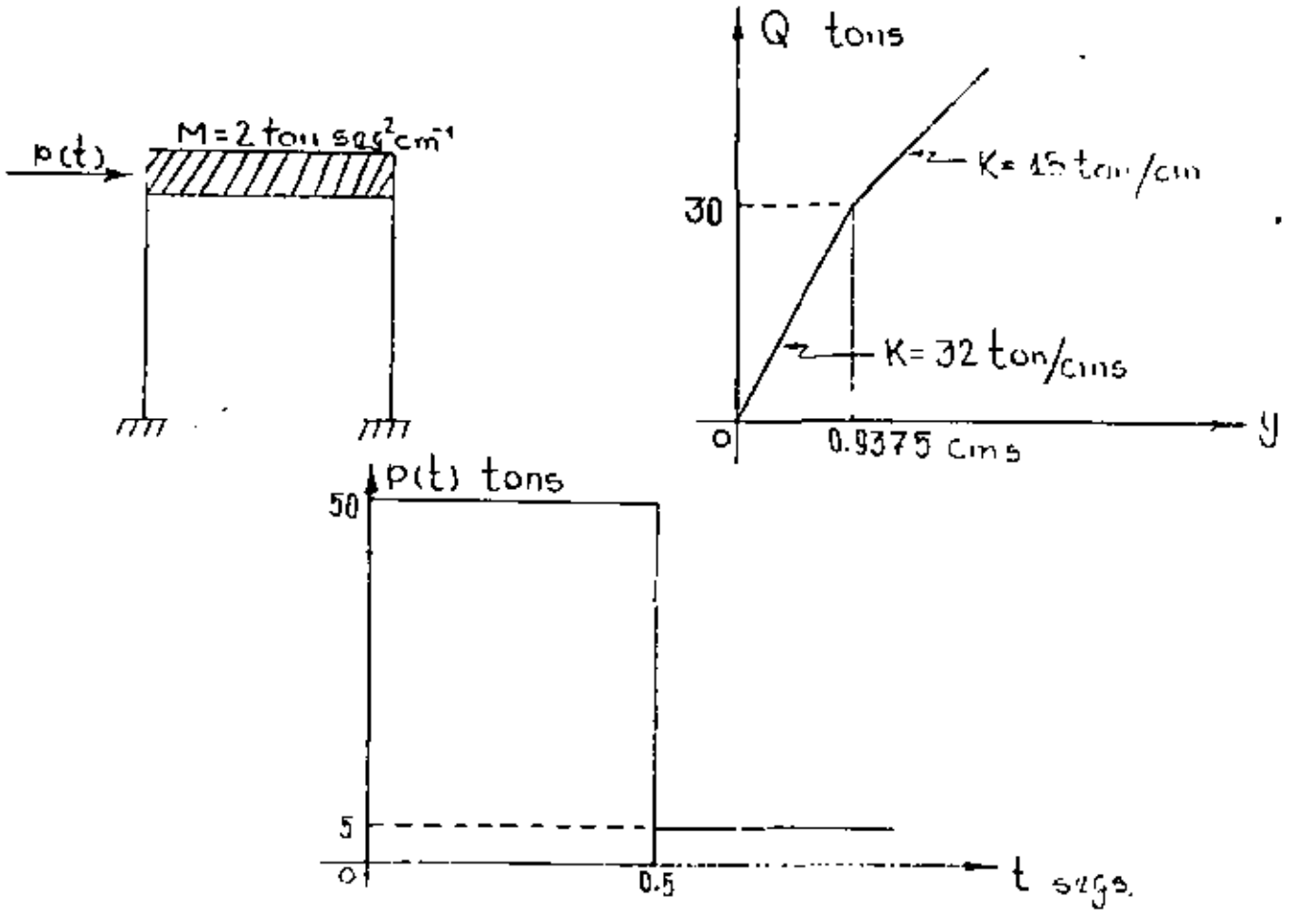

ECUACION DE EQUILIBRIO DINAMICO , $M\ddot{Y} + Q(Y) = P(t)$

$$\ddot{Y} = \frac{P(t) - Q(Y)}{M} = \frac{P(t) - Q(y)}{2} \qquad (I)$$

PARA LA APLICACION DEL METODO DE NEWMARK SE TIENEN LAS SIGUIENTES EXPRESIONES:

$$t_{i+1} = t_i + \Delta t$$

$$\dot{Y}_{i+1} = \dot{Y}_i + (\ddot{Y}_i + \ddot{Y}_{i+1})\ \Delta t/2$$

$$Y_{i+1} = Y_i + \dot{Y}_i\ \Delta t + (0.5 - \beta)\ddot{Y}_i\ (\Delta t)^2 + \beta\ \ddot{Y}_{i+1}\ (\Delta t)^2$$

CONSIDERANDO $\Delta t = 0.10$ SEG. Y $\beta = 1/6$ SE PUEDE ESCRIBIR;

$$\dot{Y}_{i+1} = \dot{Y}_i + \frac{1}{20}\,(\ddot{Y}_i + \ddot{Y}_{i+1}) \qquad \text{(II)}$$

$$Y_{i+1} = Y_i + \dot{Y}_i(0.10) + \frac{1}{600}\,(2\ddot{Y}_i + \ddot{Y}_{i+1}) \qquad \text{(III)}$$

EL PROCEDIMIENTO DE CALCULO ES COMO SIGUE:

- SE ASUME $\ddot{Y}_{i+1}$
- SE CALCULA $\dot{Y}_{i+1}$ CON LA ECUACION (II)
- SE CALCULA Y_{i+1} CON LA ECUACION (III)
- SE CALCULA UN MEJOR VALOR DE $\ddot{Y}_{i+1}$ CON LA ECUACION (I), ETC.

PARA LA FUNCION DE RESISTENCIA Q SE TIENEN LOS SIGUIENTES CASOS:

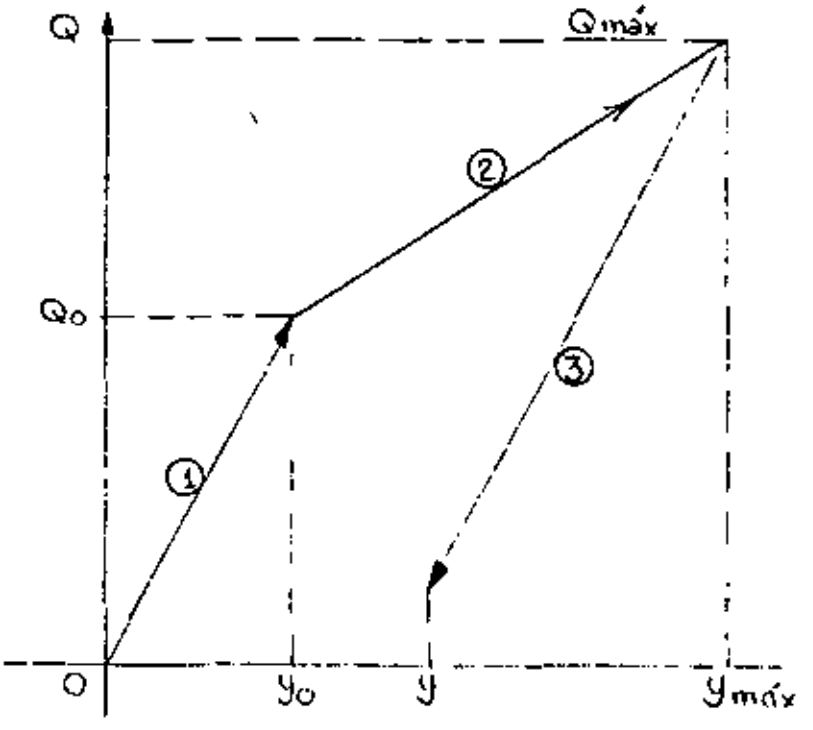

1. COMPORTAMIENTO ELASTICO , $Q = 32\ Y$ TONS
2. CAMBIO DE RIGIDEZ , $Q = 30 + 18\ (Y-Y_o)$ TON
3. DESCARGA , $Q = Q_{máx} - 32(Y_{MAX}-Y)$ TONS

ESTA ULTIMA EXPRESION MANTIENE SU VALIDEZ HASTA QUE, $(Y_{MAX}-Y) \leq 2Y_o$

60

$Y_o = 0.9375$ CMS ; $Q_o = 30.0$ TON

PARA $t = 0$, $\ddot{y} = \frac{P}{M} = \frac{50}{2} = 25$; $y = 0$; $\dot{y} = 0$

PARA $t = 0.10$, $y_i = \dot{y}_i = 0$; $\ddot{y}_i = 25$

1er. CICLO

SEA $\ddot{y}_{i+1} = 20$ COMO PRIMER TANTEO. EN TAL CASO

$$\dot{y}_{i+1} = 0 + \frac{1}{20}(0 + 25) = 2.25$$

$$y_{i+1} = 0 + 0.10 \times 0 + \frac{1}{600}(2 \times 25 + 20) = 0.1167$$

$$Q = 32 \times 0.1167 = 3.7330$$

$$\ddot{y}_{i+1} = \frac{50 - 3.733}{2} = 23.134$$

2o. CICLO

$$\dot{y}_{i+1} = 23.134/2 = 16.567$$

$$y_{i+1} = 73.134/600 = 0.1219$$

$$Q = 32 \times 0.1219 = 3.9000$$

$$\ddot{y}_{i+1} = (50 - 3.9)/2 = 23.050$$

3er. CICLO

.

.

.

4o. CICLO

$$\ddot{y}_{i+1} = 23.052$$

$$\dot{y}_{i+1} = 23.052/2 = 2.4026$$

$$y_{i+1} = 73.052/600 = 0.12175$$

$$\Omega = 32 \times 0.12175 = 3.8960$$

$$\ddot{y} = (50 - 3.8960)/2 = 23.052 \quad \ldots \text{ ETC.}$$

62

LOS CALCULOS BASICOS SE MUESTRAN EN LA TABLA SIGUIENTE:

t SEGS	p TONS	$\ddot{Y}$ CM SEG^{-2}	$\dot{Y}$ CM SEG^{-1}	Y CMS	Q TONS
0.0	50.00	25.000	0.00	0.00	0.00
0.10	50.00	20.000	2.2500	0.1167	3.7330
		23.134	2.4070	0.1219	3.9000
		23.050	2.4025	0.12175	3.3960
		23.052	2.4026	0.12175	3.8960
0.20	50.00	20.000	4.5552	0.4722	15.110
		17.445	4.4270	0.46793	14.970
		17.513	4.4310	0.46804	14.977
		17.511	4.43075	0.46204	14.977
0.30	50.00	10.000	5.8060	0.98610	30.8750
		9.560	5.7840	0.98540	30.8620
		9.569	5.7848	0.98543	30.8630
0.40	50.00	0.00	6.2630	1.5958	41.849
		4.0750	6.4670	1.6026	41.972
		4.0141	6.4640	1.6025	41.970
		4.0150	6.4640	1.60250	41.970
0.50⁻	50.00	0.00	6.6650	2.2623	53.846
		-1.9230			
		-1.9000	6.56975	2.2591	53.789
		-1.8944			
		-1.8946	6.5700	2.25912	53.789
0.50+	5.00	-24.3946	6.5700	2.25912	53.789
0.60	5.00	-30.000	3.8503	2.7848	63.251
		-29.126	3.8940	2.78626	63.278
		-29.136	3.89347	2.78624	63.277
		-29.138	3.89347	2.78624	63.277
0.70	5.00	-32.000	0.83657	3.025127	67.577
		-31.289			
		-31.320	0.87057	3.02626	67.598
		-31.299			
		-31.301	0.87147	3.02641	67.600
0.7278	5.00	-31.620	-0.00313	3.03850	67.818
		-31.409			
		-31.420	-0.000352	3.03853	67.818
		-31.4093	-0.000205	3.03853	67.818

En t=0.5 + SEG, Δy =-45/2 = -22.5 ∴ -22.5 - 1.8946 = -24.3946

CONTINUACION DEL CUADRO ANTERIOR

t	p	$\ddot{Y}$	$\dot{Y}$	Y	Q
0.80	5.0	-28.000	-2.1449	2.959611	65.293
		-30.146			
		-30.000	-2.21708	2.957874	65.237
		-30.118			
		-30.117	-2.22127	2.95777	65.234
0.90	5.0	-27.00	-5.07712	2.59025	53.473
		-24.236			
		-25.00	-4.97712	2.59358	53.580
		-24.290			
		-24.294	-4.94182	2.59476	53.617
		-24.308	-4.94242	2.59474	53.617
1.00	5.0	-14.00	-6.85782	1.99614	34.461
		-14.7305			
		-14.7200	-6.89382	1.99494	34.423
		-14.7120	-6.89342	1.99495	34.423

EN ESTOS CALCULOS SE INTRODUJO $t = 0.50^-$ Y 0.50^+ PORQUE PARA ESTE INSTANTE SE PRODUCE UN CAMBIO BRUSCO EN LA CARGA P(t) DE 50.00 TONS A 5.00 TONS, CON LO CUAL SE PRODUCE UN CAMBIO BRUSCO EN LA ACELERACION DEL SISTEMA $\ddot{Y}$. EN ESTE INSTANTE NO SE PRODUCEN CAMBIOS EN $\dot{Y}$ Y Y. EL TIEMPO t = 0.7273 SEG. SE INTRODUJO POR LA NECESIDAD DE CALCULAR LOS VALORES DE $\dot{Y}$ Y DE Q, PUES A PARTIR DE DICHO INSTANTE SE INICIA LA DESCARGA DEL SISTEMA. ESTA CONDICION SE ENCONTRO SOBRE LA BASE DE APROXIMAR $\dot{Y}$ A CERO, OBTENIENDOSE $Y_{MAX=3.03853}$ CMS y Q_{MAX} = 67.818 TON.

EN EL CUADRO SIGUIENTE SE PRESENTA UN RESUMEN DE LOS RESULTADOS.

64

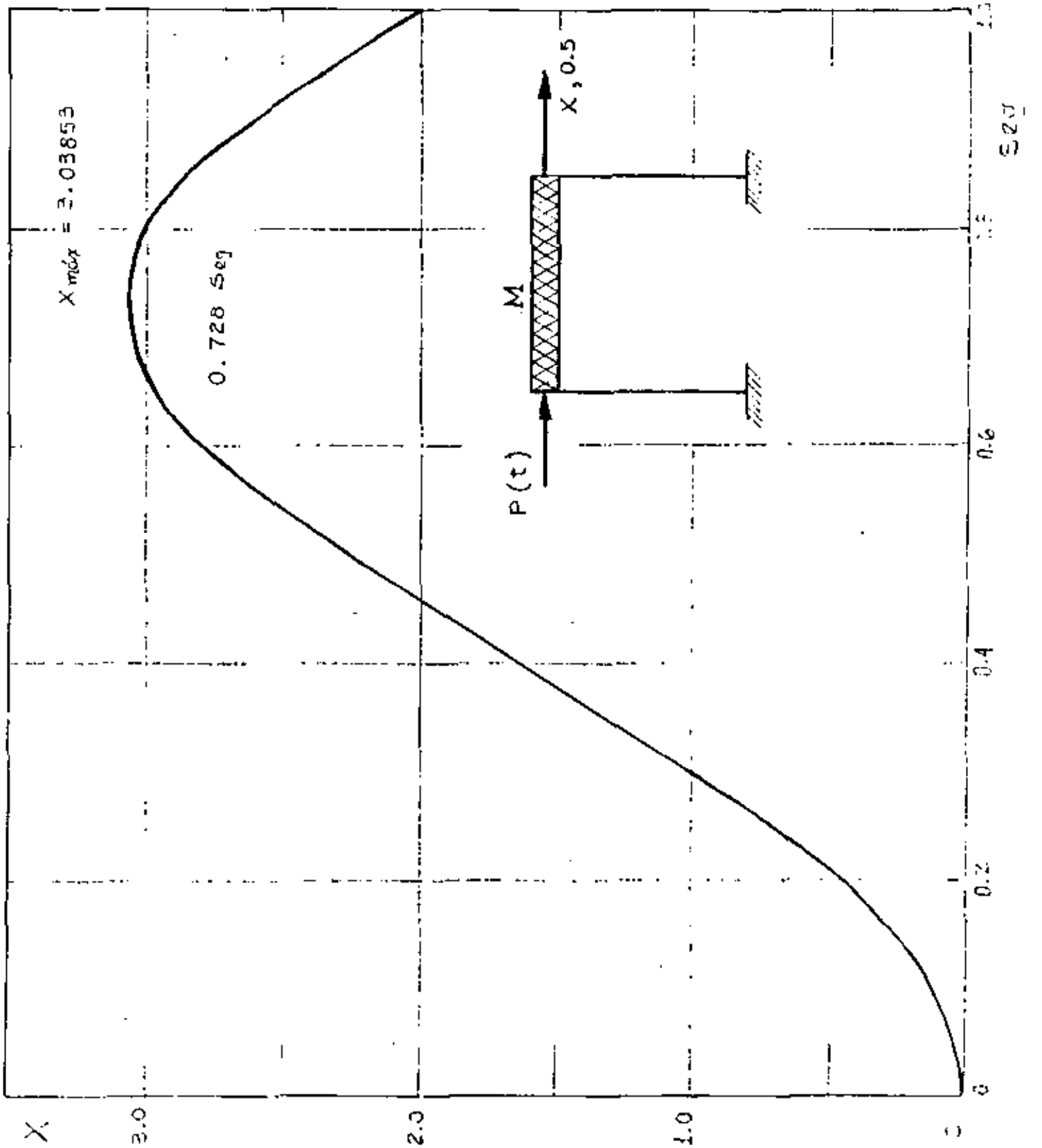

t Seg.	$\ddot{Y}$ (supuesta) Cm Seg^{-2}	P Ton	Y Cm.	Q Ton	$\ddot{Y}$ (calculado) Cm Seg^{-2}	$\dot{Y}$ Cm Seg^{-1}	N O T A S
0.0	- -	50.00	0.00	0.00	25.00	0.00	
0.10	23.0520	50.00	0.12175	3.896	23.0520	2.40260	
0.20	17.5110	50.00	0.46804	14.977	17.5110	4.43075	
0.30	9.5690	50.00	0.98543	30.863	9.5690	5.78480	— CAMBIO DE RIGIDEZ
0.40	4.0150	50.00	1.60250	41.970	4.0150	6.4640	
0.50⁻	-1.8946	50.00	2.25912	53.789	-1.8946	6.5700	
0.50+	- -	5.00	2.25912	53.789	-24.3945	6.5700	— CAMBIO DE CARGA
0.60	-29.1380	5.00	2.78624	63.277	-29.1380	3.89347	
0.70	-31.3010	5.00	3.02641	67.600	-31.3010	0.87147	
0.7278	-31.4093	5.00	3.03853	67.818	-31.4093	-0.000205	— Qmáx, Ymáx.
0.800	-30.1170	5.00	2.95777	65.234	-30.1170	-2.22127	
0.90	-24.3080	5.00	2.59474	53.617	-24.3080	-4.94242	
1.00	-14.7120	5.00	1.99495	34.423	-14.7120	-6.89342	

RESPUESTA MAXIMA

$Y_{máx} = 3.03853$ cms

$Q_{máx} = 67.818$ tons

66

CRITERIOS PARA TRAZAR ESPECTROS DE DISEÑO ELASTOPLASTICOS A PARTIR DEL ELASTICO

1. CRITERIO DE IGUAL DESPLAZAMIENTO MAXIMO DEL SISTEMA ELASTICO Y EL ELASTOPLASTICO DE IGUAL PERIODO:

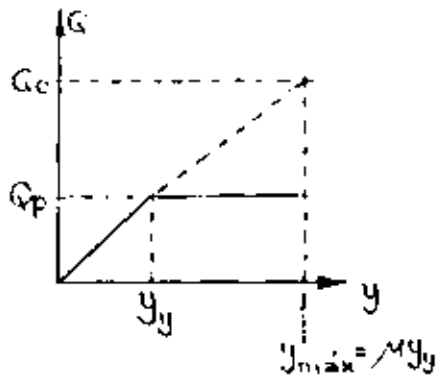

$$Q_p = Ky_y = \frac{Ky_{MAX}}{\mu} = \frac{Q_e}{\mu}$$

$$y_{MAX} = D_e = \mu y_y = \mu D_p$$

$$D_p = \frac{De}{\mu}$$

2. CRITERIO DE IGUAL ENERGIA ABSORVIDA POR LA ESTRUCTURA:

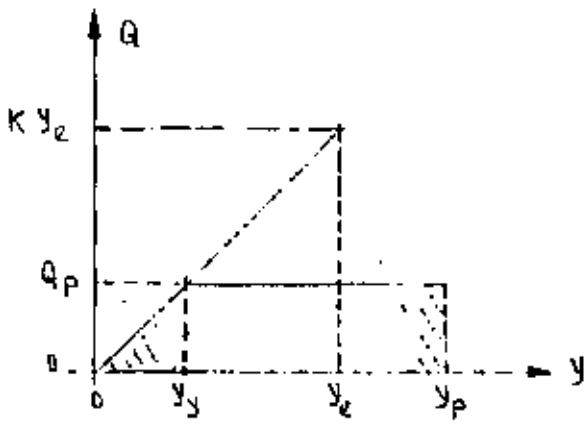

$$\frac{Ky_e y_e}{2} = \frac{Ky_y y_y}{2} + Ky_y(y_p - y_y)$$

$$\frac{1}{2} y_e^2 = \frac{1}{2} y_y^2 + y_y y_p - y_y^2 = y_y y_p - \frac{y_y^2}{2}$$

$$\frac{1}{2} \left(\frac{y_e}{y_y}\right)^2 = \frac{y_p}{y_y} - \frac{1}{2} = \mu - \frac{1}{2}$$

$$\frac{y_e}{y_y} = \sqrt{2\mu - 1}$$

$$y_y = \frac{y_e}{\sqrt{2\mu - 1}}$$

$$y_{y\_MAX} = D_p = \frac{y_e]_{MAX}}{\sqrt{2\mu - 1}} = \frac{D_e}{\sqrt{2 - 1}}$$

POR LO TANTO

$$D_p = D_e/\sqrt{2\mu - 1} \qquad Y \qquad Q_p = Q_e/\sqrt{2\mu - 1}$$

AMORTIGUAMIENTO HISTERETICO

SI SE CUENTA CON EQUIPO PARA MEDIR EL ANGULO DE FASE ENTRE LA FUERZA DE EXCITACION Y EL DESPLAZAMIENTO RESULTANTE, SE PUEDE EVALUAR EXPERIMENTALMENTE EL AMORTIGUAMIENTO DEL SISTEMA CON UNA SOLA PRUEBA DE VIBRACION ARMONICA EN RESONANCIA. ESTA SE LOGRA CUANDO SE AJUSTA LA FRECUENCIA DEL EXCITADOR DE TAL MANERA QUE EL ANGULO DE FASE SEA 90°, YA QUE:

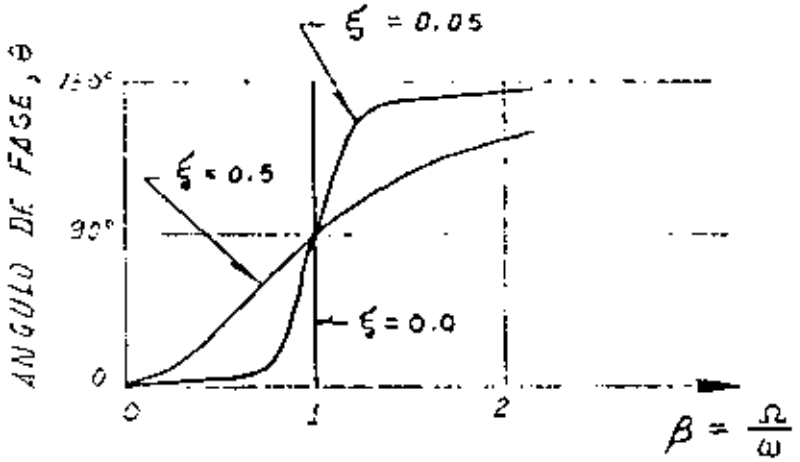

EN ESTAS CONDICIONES LA FUERZA DE EXCITACION QUEDA EN FASE CON LA VELOCIDAD DE LA MASA YA QUE

$$y = A \operatorname{sen}(\omega t - \theta) = -A \cos\omega t, \quad \text{SI } \theta = 90°$$

Y $\quad \dot{y} = A\omega \operatorname{sen}\omega t \quad ; \quad \ddot{y} = A\omega^2 \cos\omega t$

Y DE LA ECUACION DIFERENCIAL DE EQUILIBRIO:

$$MA\omega^2 \cos\omega t + CA\omega \operatorname{sen}\omega t + K(-A\cos\omega t) = p_o \operatorname{sen}\omega t$$

SE VE QUE SE DEBE CUMPLIR QUE:

$$CA\omega = p_o \quad , \text{ DE DONDE } \boxed{C = \frac{p_o}{A\omega}} \qquad (I)$$

DE LAS ECUACIONES ANTERIORES SE DEDUCE QUE:

$$y^2 = A^2 \cos^2\omega^2 \; ; \quad \frac{y^2}{A^2} = \cos^2\omega t$$

Y

$$p^2 = p_o^2 \operatorname{sen}^2\omega t \; ; \quad \frac{p^2}{p_o^2} = \operatorname{sen}^2\omega t$$

SUMANDO:

$$\frac{y^2}{A^2} + \frac{p^2}{p_o^2} = \operatorname{sen}^2\omega t + \cos^2\omega t$$

QUE ES LA ECUACION DE UNA ELIPSE CON LOS EJES COORDENADOS y Y p, ASI (fig 1):

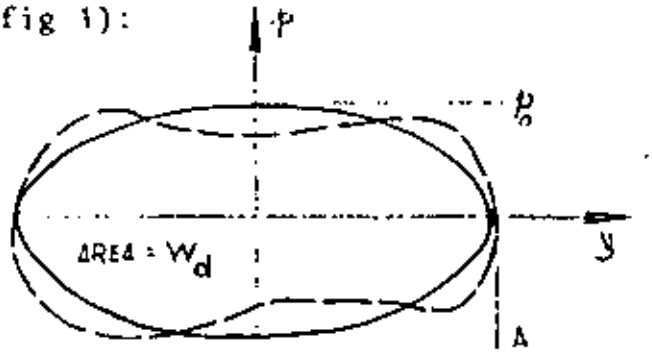

FIG 1

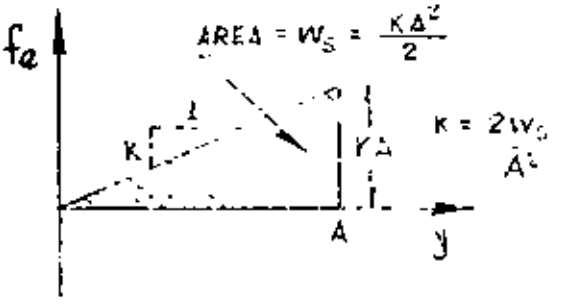

FIG 2

SI EL AMORTIGUAMIENTO NO ES EXACTAMENTE VISCOSO, LA GRAFICA QUE SE OBTENDRIA DE p CONTRA y NO SERIA EXACTAMENTE ELIPTICA; SINO ALGO COMO LA LINEA PUNTEADA AHI MOSTRADA. EN ESTE CASO SE PUEDE UTILIZAR UN AMORTIGUAMIENTO *VISCOSO EQUIVALENTE*, DE TAL MANERA QUE EL AREA W_d, DE ESTA CURVA SEA IGUAL A LA DE LA ELIPSE EQUIVALENTE, $W_{eq}=\pi A p_o$, ES DECIR

$$W_d = \pi A p_o \text{ , DE DONDE } p_o = \frac{W_d}{\pi A}$$

POR LO QUE, DE LA EC. (I)

$$\boxed{C_{eq} = \frac{W_d}{\pi \omega A^2}} \qquad \text{(II)}$$

ADEMAS, $C_{cr} = 2\sqrt{KM} = 2K/\omega$; DE FIG. 2 : $C_{cr} = 2(\frac{2W_S}{A^2})/\omega$, DE DONDE

$$\zeta_{eq} = \frac{C_{eq}}{C_{cr}}$$

$$\boxed{\zeta_{eq} = W_d/(4\pi W_S)} \qquad \text{(II')}$$

METODO β DE NEWMARK

SISTEMAS ELASTICOS LINEALES DE VARIOS GRADOS DE LIBERTAD

PARA CALCULAR LA RESPUESTA DE UN SISTEMA DE N GRADOS DE LIBERTAD Y COMPORTAMIENTO ELASTICO LINEAL SE EMPLEAN LAS MISMAS ECUACIONES QUE PARA UN SISTEMA DE UN GRADO DE LIBERTAD.

$$\dot{x}_j(t_{i+1}) = \dot{x}_j(t_i) + [\ddot{x}_j(t_i) + \ddot{x}_j(t_{i+1})]\,\frac{\Delta t}{2}$$

$$x_j(t_{i+1}) = x_j(t_i) + \dot{x}_j(t_i)\Delta t + [(1/2-\beta)\ddot{x}_j(t_i) + \beta\ddot{x}_j(t_{i+1})](\Delta t)^2$$

EN DONDE $j = 1,2,\ldots,N$.

EN ESTE CASO SE RECOMIENDA TAMBIEN UN VALOR DE β COMPRENDIDO ENTRE 1/4 Y 1/6, Y QUE $\Delta t \leq 0.1\ T_N$, EN DONDE T_N ES EL PERIODO NATURAL DE VIBRACION MAS PEQUEÑO.

EJEMPLO

SEA UN SISTEMA DE DOS GRADOS DE LIBERTAD CON AMORTIGUAMIENTO NULO, CUYAS MATRICES DE MASAS Y RIGIDECES SON:

$$\underline{K} = \begin{bmatrix} 10 & 1 \\ 1 & 5 \end{bmatrix} \quad , \qquad \underline{M} = \begin{bmatrix} 2 & 0 \\ 0 & 1 \end{bmatrix}$$

USANDO EL METODO β DE NEWMARK CON $\Delta t = 0.2$ seg Y $\beta = 1/6$ CALCULE LA RESPUESTA DINAMICA ANTE UNA EXCITACION DADA POR LOS DESPLAZAMIENTOS DEL SUELO:

$x_o = 1.2\ t$ SI $0 \leq t \leq 2$ seg (x_o EN CENTIMETROS)

$x_o = 4.8 - 1.2\ t$ SI $2 \leq t \leq 4$ seg

$x_o = 0$ SI $t < 0$ o $t > 4$ seg

PUESTO QUE ESTA EXCITACION IMPLICA QUE $\ddot{x}_o(t) = 0$ PARA TODO t, SE TIENE QUE LA ECUACION MATRICIAL DE EQUILIBRIO RESULTA SER

$$\underline{M\ddot{Y}} + \underline{KY} = \underline{M\ddot{Y}} + \underline{Q} = \underline{0}$$

POR LO QUE

$$m_1 \ddot{y}_1 + Q_1 = 0 \rightarrow \ddot{y}_1 = Q_1/m_1$$

$$m_2 \ddot{y}_2 + Q_2 = 0 \rightarrow \ddot{y}_2 = Q_2/m_2$$

EN DONDE $y_1 = x_1 - x_o$ Y $y_2 = x_2 - x_o$.

CON $\Delta t = 0.2$ seg Y $\beta = 1/6$, LAS ECUACIONES DEL METODO β DE NEWMARK QUEDAN EN LA FORMA

$$\dot{x}_j(t_{i+1}) = \dot{x}_j(t_i) + 0.1[\ddot{x}_j(t_i) + \ddot{x}_j(t_{i+1})]$$

$$x_j(t_{i+1}) = x_j(t_i) + 0.1\ \dot{x}_j(t_i) + 0.04[\ddot{x}_j(t_i)/3 + \ddot{x}_j(t_{i+1})/6]$$

EN $t = 0$, $y_i = x_i = 0$, $\dot{y}_i = \dot{x}_i = 0$, $\ddot{y}_i = \ddot{x}_i = 0$.

EN $t = 0.2$, $x_o = 1.2 \times 0.2 = 0.24$ cm; SUPONGAMOS $\ddot{x}_1 = \ddot{y}_1 = 1.35$ Y $\ddot{x}_2 = \ddot{y}_2 = 1.50$ cm/seg:

PRIMER CICLO

PARA LA MASA 1: $\dot{x}_1 = 0 + 0.1\ (0 + 1.35) = 0.135$ cm/seg

$x_1 = 0 + 0 + 0.04(0 + 1.35/6) = 0.009$ cm

$y_1 = 0.009 - 0.24 = -0.231$ cm

PARA LA MASA 2: $\dot{x}_2 = 0 + 0.1(0 + 1.50) = 0.15$

$x_2 = 0 + 0 + 0.04(0 + 1.50/6) = 0.01$

$y_2 = 0.01 - 0.24 = -0.23$ cm

$$Q = \begin{bmatrix} Q_1 \\ Q_2 \end{bmatrix} = \begin{bmatrix} 10 & 1 \\ 1 & 5 \end{bmatrix} \begin{bmatrix} -0.231 \\ -0.230 \end{bmatrix} = \begin{bmatrix} -2.540 \\ -1.381 \end{bmatrix}$$

POR LO QUE $\ddot{y}_1 = \ddot{x}_1 = 2.54/2 = 1.27 \neq 1.35$

$\ddot{y}_2 = \ddot{x}_2 = 1.381/1 = 1.381 \neq 1.50$

SEGUNDO CICLO

$\dot{x}_1 = 0.1 \times 1.27 = 0.127$

$x_1 = 0.04 \times 1.27/6 = 0.0085$

$y_1 = 0.0085 - 0.24 = -0.2315$

$\dot{x}_2 = 0.1 \times 1.381 = 0.138$

$x_2 = 0.04 \times 1.381/6 = 0.0092$

$y_2 = 0.0092 - 0.24 = -0.2308$

$$Q = \begin{bmatrix} 10 & 1 \\ 1 & 5 \end{bmatrix} \begin{bmatrix} -0.2315 \\ -0.2308 \end{bmatrix} = \begin{bmatrix} -2.546 \\ -1.386 \end{bmatrix}$$

DE DONDE $\ddot{x}_1 = \ddot{y}_1 = 2.546/2 = 1.273 \doteq 1.27$

$\ddot{x}_2 = \ddot{y}_2 = 1.386/1 = 1.386 \doteq 1.381$

EN $t = 0.2 + 0.2 = 0.4$ seg SE TIENEN $x_o = 1.2 \times 0.4 = 0.48$,

$x_1(t_i) = 0.0085$; $x_2(t_i) = 0.0092$

$\dot{x}_1(t_i) = 0.127$; $\dot{x}_2(t_i) = 0.138$

$\ddot{x}_1(t_i) = 1.273$; $\ddot{x}_2(t_i) = 1.386$

PRIMER CICLO

SUPONIENDO $\ddot{x}_1(t_{i+1}) = 2.3$ Y $\ddot{x}_2(t_{i+1}) = 2.1$ SE OBTIENEN:

$\dot{x}_1 = 0.127 + 0.1(1.273 + 2.3) = 0.484$

$x_1 = 0.0085 + 0.2 \times 0.127 + 0.04(1.273/3 + 2.3/6) = 0.0662$

$y_1 = 0.0662 - 0.48 = -0.4138$

$\dot{x}_2 = 0.138 + 0.1(1.386 + 2.1) = 0.486$

$x_2 = 0.0092 + 0.2 \times 0.138 + 0.04(1.386/3 + 2.1/6) = 0.0693$

$y_2 = 0.0693 - 0.48 = -0.4107$

$$Q = \begin{bmatrix} 10 & 1 \\ 1 & 5 \end{bmatrix} \begin{bmatrix} -0.4138 \\ -.4107 \end{bmatrix} = \begin{bmatrix} -4.548 \\ -2.468 \end{bmatrix}$$

DE DONDE $\ddot{x}_1 = \ddot{y}_1 = 4.548/2 = 2.274 \neq 2.3$

$\ddot{x}_2 = \ddot{y}_2 = 2.468 \neq 2.1$

ETCETERA. LOS RESULTADOS DEL PROBLEMA SE PRESENTAN EN LA TABLA 1.

Tomado del libro de N. Newmark y E.Rosenblueth D.

TABLA 2.1. *Ejemplo 2.7*

t seg	Q_1 ton	$\ddot{x}$ cm/seg²	$\dot{x}$ cm/seg	x_1 cm	$x_1 - x_2$ cm	Q_2 ton	$\ddot{x}$ cm/seg²	$\dot{x}$ cm/seg	x_2 cm	$x_2 - x_3$ cm	x_3 cm
0	0	0	0	0	0	0	0	0	0	0	0
0.2	2.540	1.350	0.135	0.0090	-0.2310	1.580	1.500	0.150	0.0100	-0.2300	0.24
0.2	2.546	1.270	0.127	0.0085	-0.2315	1.586	1.580	0.158	0.0092	-0.2308	0.24
0.2	2.546	1.273	0.127	0.0085	-0.2315	1.586	1.586	0.158	0.0092	-0.2308	0.24
0.4	4.548	+2.300	0.484	+0.0662	-0.4138	2.468	2.100	0.486	+0.0695	-0.4107	0.48
0.4	4.548	2.274	0.481	0.0660	-0.4140	2.455	2.468	0.523	0.0718	-0.4082	0.48
0.4	4.548	2.274	0.481	0.0660	-0.4140	2.455	2.455	0.522	0.0717	-0.4083	0.48
0.4	4.548	2.274	0.481	0.0660	-0.4140	2.455	2.455	0.522	0.0717	-0.4083	0.48
0.6	5.585	2.700	0.978	0.2105	-0.3095	2.960	3.200	1.088	0.2301	-0.4899	0.72
0.6	5.581	2.793	0.987	0.2141	+0.5089	2.967	2.960	1.064	0.2285	-0.4915	0.72
0.6	5.580	2.790	0.987	0.2141	+0.5089	2.966	2.967	1.065	0.2296	-0.4914	0.72
0.6	5.580	2.790	0.987	0.2141	-0.5089	2.966	2.966	1.065	0.2296	-0.4914	0.72
0.8	5.409	2.900	1.556	0.4630	-0.4950	2.790	2.980	1.660	0.5010	-0.4590	0.96
0.8	5.423	2.704	1.536	0.4637	+0.4963	2.798	2.790	1.641	0.4937	+0.4607	0.96
0.8	5.422	2.711	1.537	0.4638	+0.4962	2.797	2.798	1.642	0.4938	+0.4602	0.96
0.8	5.422	2.711	1.537	0.4638	-0.4962	2.797	2.797	1.642	0.4998	-0.4602	0.96
1.0	4.104	2.150	2.023	0.8216	+0.3784	1.977	2.200	2.142	0.8802	-0.3198	1.20
1.0	4.111	2.052	2.013	0.8210	+0.3790	1.985	1.977	2.120	0.8787	+0.3213	1.20
1.0	4.111	2.055	2.014	0.8210	+0.3790	1.985	1.985	2.121	0.8787	+0.3213	1.20
1.0	4.111	2.055	2.014	0.8210	-0.3790	1.985	1.985	2.121	0.8787	+0.3213	1.20
1.2	1.931	0.950	2.315	1.2575	-0.1825	0.712	0.700	2.390	1.3341	-0.1059	1.44
1.2	1.930	0.965	2.316	1.2576	-0.1824	0.712	0.712	2.391	1.3341	-0.1059	1.44
1.2	1.930	0.965	2.316	1.2576	+0.1824	0.712	0.712	2.391	1.3341	-0.1059	1.44
1.4	- 0.653	-0.320	2.381	1.7316	0.0516	-0.735	-0.800	2.382	1.8165	0.1365	1.68
1.4	- 0.652	-0.326	2.380	1.7315	0.0515	+0.735	-0.735	2.388	1.8169	0.1369	1.68
1.4	+ 0.652	+0.326	2.380	1.7315	0.0515	- 0.735	-0.735	2.388	1.8169	0.1369	1.68
1.6	- 3.085	-1.500	2.197	2.1932	0.2732	- 2.026	+2.100	2.104	2.2707	0.3507	1.92
1.6	- 3.040	-1.541	2.193	2.1929	0.2729	- 2.029	+2.026	2.114	2.2712	0.3512	1.92
1.6	- 3.080	-1.540	2.193	2.1929	0.2729	- 2.029	-2.029	2.114	2.2712	0.3512	1.92
1.8	- 4.830	+2.500	1.789	2.5943	0.4343	- 2.869	-2.900	1.618	2.6471	0.4871	2.16
1.8	+ 4.836	-2.415	1.797	2.5949	0.4349	+ 2.871	+2.869	1.621	2.6473	0.4873	2.16
1.8	- 4.836	-2.418	1.797	2.5949	0.4349	+ 2.871	+2.871	1.621	2.6473	0.4873	2.16
2.0	- 5.547	- 2.900	1.275	2.9034	0.5034	- 3.069	+ 3.000	1.033	2.9132	0.5132	2.40
2.0	- 5.549	- 2.773	1.278	2.9036	0.5036	- 3.068	- 3.069	1.027	2.9127	0.5127	2.40
2.0	- 5.549	+2.774	1.278	2.9036	0.5036	3.068	- 3.068	1.027	2.9127	0.5127	2.40

TABLA 2.1. *Ejemplo 2.7 (Cont.)*

t seg	Q_j ton	$\ddot{x}$ cm/seg²	$\dot{x}$ cm/seg	x_j cm	$x_j - x_p$ cm	Q_p ton	$\ddot{x}$ cm/seg²	$\dot{x}$ cm/seg	x_j cm	$x_j - x_p$ cm	x_p cm
2.2	-10.156	-5.200	0.481	3.0075	0.9275	-5.332	-5.460	0.174	3.0408	0.8808	2.16
2.2	-10.165	-5.078	0.495	3.0083	0.9283	-5.337	-5.332	0.187	3.0417	0.8817	2.16
2.2	-10.165	-5.083	0.493	3.0083	0.9283	-5.337	-5.337	0.186	3.0417	0.8817	2.16
2.4	-12.578	-6.900	-0.709	3.0731	1.1531	-6.386	-6.200	-0.968	2.9665	1.0465	1.92
2.4	-12.617	-6.269	-0.644	3.0772	1.1572	-6.583	-6.386	-0.987	2.9652	1.0452	1.92
2.4	-12.615	-6.309	-0.646	3.0770	1.1570	-6.583	-6.383	-0.986	2.9652	1.0452	1.92
2.4	-12.615	-6.308	-0.646	3.0770	1.1570	-6.383	-6.383	-0.986	2.9652	1.0452	1.92
2.6	-12.388	-6.200	-1.897	2.8725	1.1425	-5.958	-6.000	-2.224	2.6429	0.9629	1.68
2.6	-12.368	-6.154	-1.896	2.8725	1.1425	-5.959	-5.958	-2.220	2.6432	0.9632	1.68
2.6	-12.388	-6.194	-1.896	2.8725	1.1425	-5.959	-5.959	-2.220	2.6432	0.9632	1.68
2.8	- 9.573	-4.300	-2.945	2.5390	0.8990	-4.155	- 4.100	-3.206	+2.0925	0.6525	1.44
2.8	- 9.540	-4.787	-2.994	2.5388	0.8988	-4.120	- 4.155	-3.242	2.0921	0.6521	1.44
2.8	- 9.541	-4.770	-2.997	2.5389	0.8989	-4.120	- 4.150	-3.241	2.0921	0.6521	1.44
2.8	- 9.541	-4.770	-2.992	2.5389	0.8989	-4.150	- 4.150	-3.241	2.0921	0.6521	1.44
3.0	- 4.667	-2.500	-3.719	1.6502	0.4502	-1.376	- 1.400	-5.766	1.2853	0.1853	1.20
3.0	- 4.656	-2.343	-3.703	1.6513	0.4513	-1.378	- 1.376	-5.764	1.2854	0.1854	1.20
3.0	- 4.656	-2.345	-3.704	1.6513	0.4513	-1.378	- 1.378	-5.764	1.2854	0.1854	1.20
3.2	1.590	0.800	-3.859	0.8845	-0.0755	1.748	1.700	-3.732	0.6755	-0.3245	0.96
3.2	1.106	0.545	-3.884	0.8828	-0.0772	1.748	1.748	-3.727	0.6759	-0.3241	0.96
3.2	1.105	0.553	-3.883	0.8829	-0.0771	1.748	1.748	-3.727	0.6759	-0.3241	0.96
3.2	1.105	0.553	-3.883	0.8829	-0.0771	1.748	1.748	-3.727	0.6759	-0.3241	0.96
3.4	6.608	3.600	-3.468	0.1357	-0.5843	4.506	4.700	-3.082	-0.0649	-0.7849	0.72
3.4	6.629	3.304	-3.428	0.1357	-0.5843	4.515	4.506	-3.101	-0.0652	-0.7852	0.72
3.4	6.628	3.314	-3.429	0.1358	-0.5842	4.515	4.515	-3.100	-0.0661	-0.7861	0.72
3.4	6.628	3.314	-3.429	0.1358	-0.5842	4.515	4.515	-3.100	+0.0661	-0.7861	0.72
3.6	10.575	5.400	-2.568	-0.4718	-0.9518	6.251	6.900	-1.528	-0.5759	-1.0559	0.48
3.6	10.589	5.269	-2.579	-0.4725	-0.9525	6.277	6.251	-2.023	-0.5842	-1.0642	0.48
3.6	10.589	5.299	-2.577	-0.4725	-0.9525	6.277	6.277	-2.020	-0.5841	-1.0641	0.48
3.6	10.525	5.299	-2.577	-0.4725	-0.9525	6.277	6.277	-2.020	-0.5841	-1.0641	0.48
3.8	12.759	6.700	-1.427	-0.0760	-1.1160	6.612	6.800	-0.732	-0.0591	-1.0591	0.24
3.8	12.264	6.130	-1.434	-0.0764	-1.1164	6.618	6.612	-0.731	-0.0603	-1.1003	0.24
3.8	12.264	6.132	-1.434	-0.0764	-1.1164	6.618	6.618	-0.730	-0.0603	-1.1003	0.24
4.0	11.323	5.600	-0.260	+1.0441	+1.0441	5.454	5.400	0.472	-0.8824	-0.8824	0
4.0	11.319	5.661	-0.255	+1.0437	+1.0437	5.453	5.454	0.477	0.8817	-0.8817	0
4.0	11.319	5.660	-0.255	+1.0437	+1.0437	5.453	5.453	0.477	-0.8817	-0.8817	0
4.2	10.705	5.350	0.846	+0.9831	0.9831	5.330	5.330	1.565	-0.8191	-0.8191	0
4.2	10.705	5.352	0.846	+0.9834	0.9834	5.329	5.330	1.562	-0.8189	-0.8189	0

SISTEMA DE VARIOS GRADOS DE LIBERTAD Y COMPORTAMIENTO INELASTICO

Ejemplo de aplicación de Newmark

Calcular mediante el método de Newmark los desplazamientos máximos absolutos del 1º y 2º nivel de la estructura mostrada cuando es excitada por un desplazamiento súbito de 2 cm en su base.

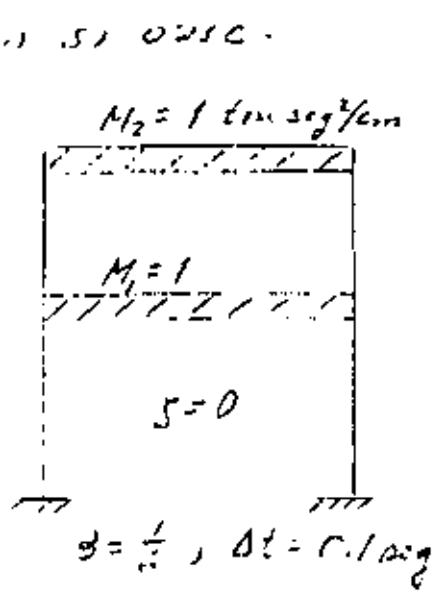

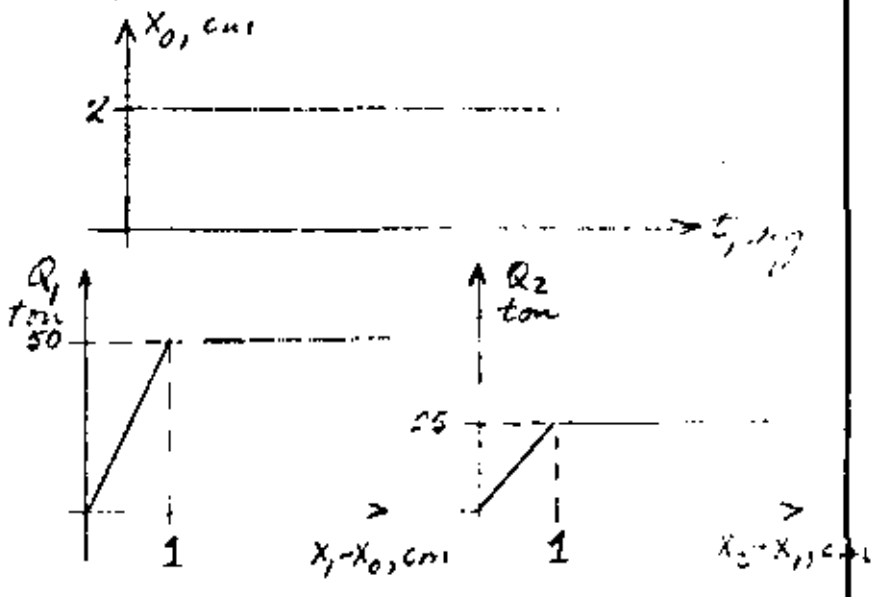

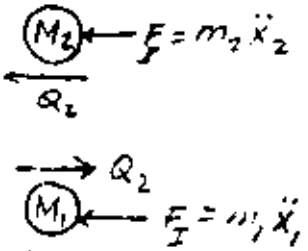

$$M \ddot{X} + Q = 0$$

$$M_1 \ddot{X}_1 + Q_1 - Q_2 = 0$$

$$M_2 \ddot{X}_2 + Q_2 = 0$$

$$\Downarrow$$

$$\left.\begin{aligned} \ddot{X}_1 &= \frac{Q_2 - Q_1}{M_1} \\ \ddot{X}_2 &= -\frac{Q_2}{M_2} \end{aligned}\right\} \quad (1)$$

En vez de suponer $\ddot{x}_1$ y $\ddot{x}_2$ al inicio de cada ciclo, suponemos Q_1 y Q_2 y calculamos ambas aceleraciones con base en ellas mediante la ec. (1). Las ecuaciones para la velocidad y el desplazamiento son:

$$\left.\begin{aligned} \dot{x}_{i+1} &= \dot{x}_i + 0.05(\ddot{x}_i + \ddot{x}_{i+1}) \\ x_i &= x_i + 0.1\dot{x}_i + \frac{1}{600}(2\ddot{x}_i + \ddot{x}_{i+1}) \end{aligned}\right\} \quad (2)$$

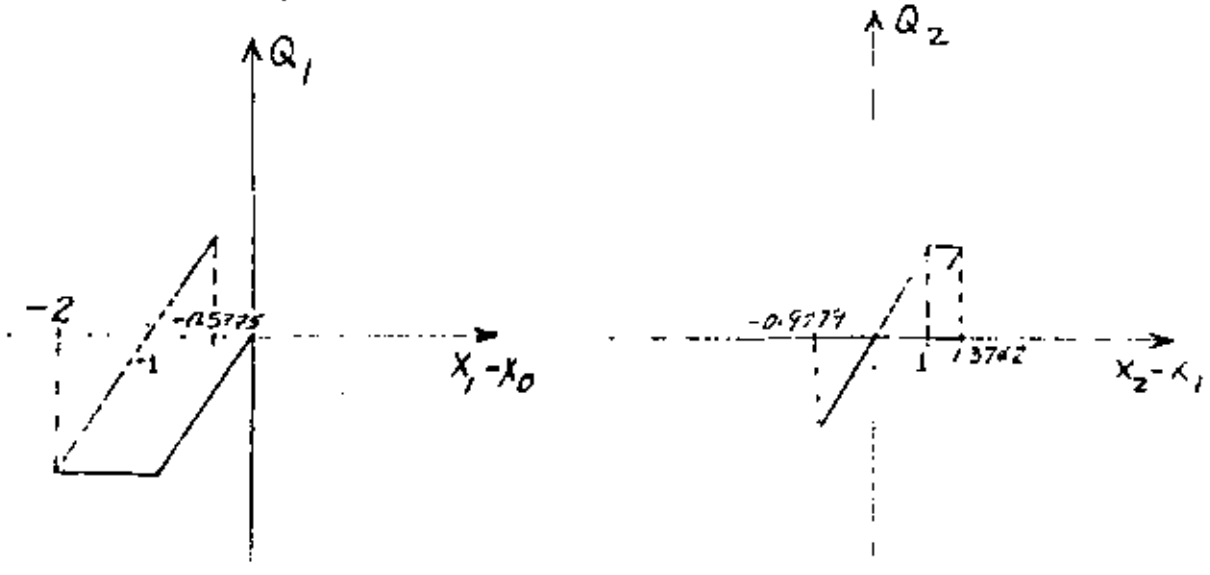

t seg	x_o cm	Q_i ton	Q_2 ton	$\ddot{x}_1$ cm/seg^2	$\ddot{x}_2$ cm/seg^2	$\dot{x}_1$ cm/seg	x_1 cm	$\dot{x}_2$ cm/seg	x_2 cm	x_1-x_0 cm	x_2-x_1 cm	$\dot{x}_1-x_0$ cm/seg	$\dot{x}_2-x_1$ cm/seg	OBSERVACIONES
0.0	2.0	-50.00	0.00	50.00	0.00	0.00	0.00	0.00	0.00	-2.00	0.00	0.00	0.00	
0.1	2.0	-37.500	-6.25	37.5	6.250	4.375	0.229	0.3125	0.0104	-1.771	-0.2185	4.375	-4.063	
		-38.550	-5.463	32.3·	5.463	4.115	0.2205	0.2731	0.0091	-1.7795	-0.2113	4.115	-3.842	
		-38.975	-5.283	33.5125	5.283	4.1756	0.2225	0.2641	0.0088	-1.7774	-0.2136	4.1756	-3.9114	
		-38.875	-5.34	33.593	5.340	4.1796	0.2226	0.2670	0.0089	-1.7773	-0.2137	4.1796	-3.9126	
		-38.870	-5.343	33.530	5.3425	4.1765	0.2225	0.2671	0.0089	-1.7774	-0.2135	4.1765	-3.9093	
0.2	0.2	-20.00	-10.00	10.00	10.00	6.353	0.7685	1.0342	0.070	-1.2314	-0.6984	6.353	-5.3188	
		-11.575	-17.46	1.575	17.46	5.9317	0.7545	1.4072	0.083	-1.2455	-0.6919	5.9317	-4.5244	
		-12.275	-16.7975	-5.185	16.7975	5.5937	0.7432	1.3741	0.0814		-0.6617			
		-12.84	-16.5446	-3.9575	16.5446	5.6551	0.7453	1.3614	0.0809		-0.6643			
		-12.735	-16.6076	-3.8096	16.6076	5.6625	0.7455	1.3646	0.0810		-0.6644			
		-12.7216	-16.6100	-3.886	16.6100	5.6587	0.7454	1.3647	0.0811	-1.2546	-0.6642	5.6587	-4.294	
0.3	2.0	10.000	-25.00	-35.00	25.00	3.7144	1.2399	3.4452	0.3146		-0.9252			
		11.995	-23.1324	-36.995	23.132	3.6146	1.2366	3.3518	0.3114		-0.9251			
		11.83	-23.1277	-34.963	23.127	3.7162	1.2400	3.3510	0.3114		-0.9285			
		12.00	-23.2129	-35.13	23.213	3.7080	1.2397	3.3558	0.3116		-0.9280			
		11.9885	-23.2018	-35.202	23.202	3.7043	1.2396	3.3552	0.3116	-0.7604	-0.9279	3.7043	-0.3491	
0.4	2.0	25.000	-15.00	-40.000	15.000	-0.1193	1.4219	5.3067	0.7520		-0.6698			
		21.095	-16.745	-36.095	16.7457	0.0563	1.4272	5.3853	0.7544		-0.6727			
		21.360	-16.8193	-38.1057	16.8193	-0.0341	1.4245	5.3886	0.7545		-0.6699			
		21.225	-16.7493	-38.0443	16.7493	-0.0313	1.4245	5.3854	0.7544	-0.5755	-0.6700	-0.0313	5.4067	*
0.5	2.0	15.00												
		12.64	-10.00	-25.0	10.00	-3.1835	1.2528	6.7228	1.3654		0.1126			
		12.87	2.8159	-22.64	-2.8159	-3.0655	1.2568	6.0818	1.3440		0.0872			
		13.89	2.1819	-10.024	-2.1819	-2.4347	1.2778	6.1137	1.3451		0.0673			
		13.75	1.6833	-11.7081	-1.683	-2.5189	1.2750	6.1387	1.3459		0.0709			
		13.72	1.7853	-11.9459	-1.7853	-2.5308	1.2746	6.1336	1.3457	-0.7254	0.0741	-2.5308	8.6644	
0.6	2.0	0.000	15.000	15.000	-15.000	-1.6915	1.0524	5.2943	1.8745		0.8221			
		2.62	20.550	12.38	-20.55	-2.5090	1.0023	5.0168	1.9188		0.9165			
		0.115	22.9139	20.435	-22.9189	-2.1063	1.0157	4.8986	1.9149		0.8992			
		0.785	22.4804	22.1289	-22.4804	-1.9866	1.0185	4.9203	1.9156		0.8971			
		0.925	22.4285	21.5554	-22.4285	-2.050	1.0176	4.9229	1.9157		0.8987			
		0.88	22.4532	21.5485	-22.4532	-2.050	1.0176	4.9216	1.9156	-0.9824	0.8990	-2.050	6.9716	
0.615	2.00	-3.00	25.000	28.000	-25.000	-1.6905	0.9894	4.5657	1.9867		0.9973			
		-0.53	24.9334	25.51	-24.9334	-1.6967	0.9894	4.5659	1.9867	-1.0106	0.9973	-1.6967	6.2626	**

* $x_1-x_0=x_1$ SE HACE CASI CERO, CAMBIO DE POSITIVO A NEGATIVO. $|x_1|$máx = 1.4245 cm

** CAMBIO DE RIGIDEZ EN EL 2o. PISO x_2-x_1 = 1.00, Q_2 = 25

t seg	x_o cm	Q_1 ton	Q_2 ton	$\ddot{x}_1$ cm/seg^2	$\ddot{x}_2$ cm/seg^2	$\dot{x}_1$ cm/seg	x_1 cm	$\dot{x}_2$ cm/seg	x_2 cm	x_1-x_0 cm	x_2-x_1 cm	$\dot{x}_1-\dot{x}_0$ cm/seg	$\dot{x}_2-\dot{x}_1$ cm/seg	OBSERVACIONES
0.70	2.00	-10.000	25.000	35.000	-25.000	0.8696	0.9484	2.441	2.285		1.3366			
		-2.580	25.000	27.580	-25.000	0.5728	0.9405	2.441	2.285		1.3445			•
		-2.975	25.000	27.975	-25.000	0.5886	0.9409	2.441	2.285		1.3441			
		-2.955	25.000	27.955	-25.000	0.5878	0.9409	2.441	2.285	-1.0591	1.3441	0.5878	1.8532	
0.735	2.00	-1.000	25.000	26.000	-25.000	1.5368	0.98065	1.565	2.3549					
		-0.9675	25.000	25.9675	-25.000	1.5367	0.98065	1.566	2.3549					
		-0.9671	25.000	25.9671	-25.000	1.5367	0.98065	1.566	2.3549	-1.1093	1.3742	1.5367	0.0293	
0.80	2.00	5.000	20.000	15.000	-20.000	2.8823	1.1282	0.09128	2.4068		1.2756			
		6.365	22.575	16.245	-22.595	2.9196	1.0449	0.01343	2.4053		1.3604			
		6.570	22.4619	18.085	-22.469	2.9748	1.1300	0.0173	2.4053		1.2753			
		6.435	22.5613	16.0948	-22.5613	2.9151	1.1288	0.0144	2.4053	-0.8712	1.2765	2.9151	-2.9007	**

** x_2 SE HACE CASI CERO

$|x_2|$máx = 2.4053 cm

PROBLEMA DE VIBRACIONES DE TORSION ACOPLADA CON TRASLACION

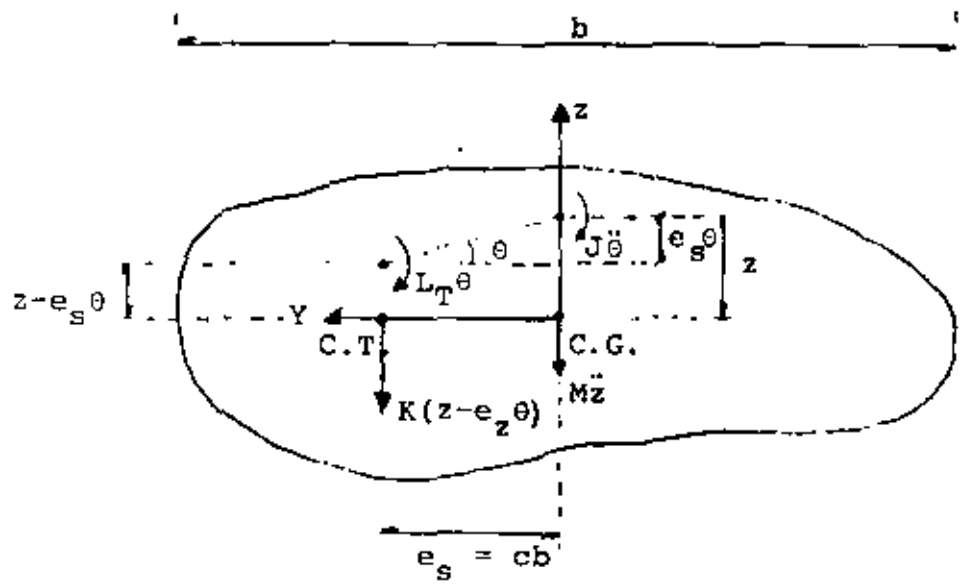

$$\Sigma F_z = M\ddot{z} + K(z-e_s\theta) = 0 \qquad (1)$$

$$\Sigma M_{C.G.} = J\ddot{\theta} + L_t\theta - K(z-e_s\theta)\ e_s = 0$$

$$J\ddot{\theta} + L\theta - Ke_s z = 0 \qquad (2)$$

EN DONDE $L = L_t + Ke_s^2$

PUESTO QUE LAS VIBRACIONES SON ARMONICAS:

$\ddot{\theta} = -\omega^2\theta$ y $\ddot{z} = -\omega^2 z$

$-\omega^2 Mz + Kz - Ke_s\theta = 0$

$(K - \omega^2 M)z - Ke_s\theta = 0 \qquad (1')$

$$- J\omega^2\theta + L_T\theta - Ke_s z = 0$$

$$(L_T - J\omega^2)_0 - Ke_s z = 0 \qquad (2')$$

$$\text{Det} \begin{bmatrix} K - \omega^2 M & - Ke_s \\ - Ke_s & L_T - J\omega^2 \end{bmatrix} = 0$$

$$(K - \omega^2 M)\ (L_T - J\omega^2) - K^2 e_s^2 = 0$$

$$KL_T - KJ\omega^2 - \omega^2 ML_T + MJ\omega^4 - K^2 e_s^2 = 0$$

$$\omega^4 - \frac{KJ + ML_T}{MJ}\,\omega^2 + \frac{KL_T}{MJ} - \frac{K^2 e_s^2}{MJ} = 0$$

DIVIENDO POR $(K/M)^2$:

$$\frac{\omega^4}{(K/M)^2} - \frac{\omega^2}{K/M}\,\frac{KJ + ML_T}{(MJ)(K/M)} + \frac{KL_T}{MJ(K/M)^2} - \frac{K^2 e_s^2}{MJ(K/M)^2} = 0$$

SI $\lambda^2 = \omega^2/(K/M)$ Y CONSIDERANDO $e_s = cb$:

$$\lambda^4 - \lambda^2\left(1 + \frac{L_T/J}{K/M}\right) + \frac{L_T/J}{K/M} - \frac{c^2}{J/(Mb^2)} = 0$$

SI $(L_T/J)/(K/M) = \eta$ y $j^2 = J/(Mb^2)$

$$\lambda^4 - \lambda^2(1 + \eta) + \eta - c^2/j^2 = 0$$

$$\therefore \lambda_{1,2} = \frac{\eta + 1}{2} \pm \sqrt{\frac{(\eta + 1)^2}{4} + \frac{c^2}{j^2}}$$

$$\Rightarrow \omega_1^2 = \lambda_1\,(K/M) \text{ y } \omega_2^2 = \lambda_2\,(K/M)$$

SUSTITUYENDO A ω^2, EN (1') O EN (2'):

$$\underline{z}_1 = \begin{bmatrix} z_1 \\ \theta_1 \end{bmatrix} = \begin{bmatrix} 1 \\ \dfrac{1 - \lambda_1^2}{cb} \end{bmatrix} ;$$

SUSTITUYENDO A ω_2^2:

$$\underline{z}_2 = \begin{bmatrix} z_2 \\ \theta_2 \end{bmatrix} = \begin{bmatrix} 1 \\ \dfrac{1 - \lambda_2^2}{cb} \end{bmatrix} \quad o: \quad \underline{z}_n = \begin{bmatrix} 1 \\ \dfrac{1 - \lambda_n^2}{cb} \end{bmatrix}$$

SOLUCION GENERAL PARA EL CASO $\xi = 0$

$$y(t) = C_1 \operatorname{sen} \omega t + C_2 \cos \omega t + \frac{P_o}{M} \frac{\operatorname{sen} \Omega t}{\omega^2 - \Omega^2}$$

SI EL SISTEMA PARTE DEL REPOSO, LAS CONDICIONES INICIALES SON $y(0) = 0$ Y $\dot{y}(0) = 0$. EN ESTE CASO:

$$y(0) = 0 = C_1 \operatorname{sen}(\omega 0) + C_2 \cos(\omega 0) + \frac{P_o}{M} \frac{\operatorname{sen}(\Omega 0)}{\omega^2 - \Omega^2} = 0$$

$$= 0 + C_2 + 0 = C_2 = 0$$

$$\dot{y}(0) = C_1 \omega \cos(\omega 0) - C_2 \omega \operatorname{sen}(\omega 0) + \frac{P_o \Omega}{M} \frac{\cos(\Omega 0)}{\omega^2 - \Omega^2} = 0$$

$$= C_1 \omega + \frac{P_o \Omega}{M} \cdot \frac{1}{\omega^2 - \Omega^2} = 0$$

$$\therefore \quad C_1 = \frac{-P_o}{M} \frac{(\Omega/\omega)}{\omega^2 - \Omega^2}$$

$$y(t) = \frac{P_o}{M} \left(\frac{\operatorname{sen} \Omega t}{\omega^2 - \Omega^2} - \frac{\Omega}{\omega} \frac{\operatorname{sen} \omega t}{\omega^2 - \Omega^2} \right)$$

$$y(t) = \frac{(P_o/M)}{(1 - \omega^2/\Omega^2)} \left[\operatorname{sen} \omega t - \frac{\Omega}{\omega} \operatorname{sen} \omega t \right] \qquad (20')$$

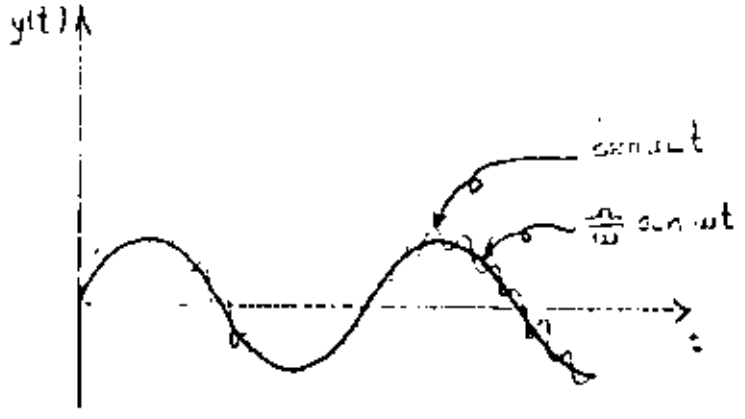

INSTITUTO DE INGENIERIA

ESTUDIO ESTADISTICO DE LOS CRITERIOS PARA ESTIMAR LA RESPUESTA SISMICA DE SISTEMAS LINEALES CON DOS GRADOS DE LIBERTAD

OCTAVIO A RASCON
AUGUSTO G VILLARREAL

OCTUBRE 1973 323

UNIVERSIDAD NACIONAL AUTONOMA DE MEXICO

Estudio estadístico de los criterios para estimar la respuesta sísmica de sistemas lineales con dos grados de libertad

Octavio A. Rascón
Augusto G. Villarreal*

RESUMEN

El objeto de este trabajo es verificar el grado de aproximación de dos métodos que con frecuencia se utilizan para estimar la respuesta sísmica máxima de sistemas lineales con varios grados de libertad. Para ello se aplica el método de Monte Carlo en el estudio de tres tipos de estructuras con dos grados de libertad: torsión y traslación, cabeceo y traslación, y traslación en dos pisos. Como excitaciones se utilizan sismos simulados y reales; se comparan las respuestas estimadas con las exactas, se hacen recomendaciones acerca del empleo de dichos métodos, y se obtienen las distribuciones de probabilidades de los cocientes de las respuestas exactas entre las estimadas.

ABSTRACT

The purpose of this work is to verify the degree of approximation of two methods used frequently for estimating the maximum seismic response of linear systems with various degrees of freedom. To do this, the Monte Carlo method is used in the study of three types of structures with two degrees of freedom: torsion and translation, rocking and translation, and translation in a two story building. Simulated and real earthquakes are used as ground excitations; estimated responses are compared with the exact ones, recommendations for the use of such methods are given, and the probability distributions of the ratios of exact to estimated responses are obtained.

1. INTRODUCCION

En este trabajo se analiza el comportamiento dinámico de algunos tipos de estructuras de comportamiento lineal de dos grados de libertad cuando se les sujeta a solicitaciones sísmicas. El objeto es verificar el grado de aproximación de dos métodos propuestos por Rosenblueth (refs 1 y 2) para estimar la respuesta máxima total, mediante su comparación con las respuestas máximas exactas obtenidas con el método de análisis modal, al superponer en el tiempo los efectos del sismo en los dos modos naturales de vibración de la estructura.

El método 1 consiste en estimar la respuesta máxima total, Q, extrayendo la raíz cuadrada de la suma de los cuadrados de la respuesta en cada modo natural de vibración, Q_i, es decir

$$Q = \sqrt{\sum_{i=1}^{n} Q_i^2} \qquad (1.1)$$

* Profesores investigadores, Instituto de Ingeniería, UNAM

donde n es el total de grados de libertad del sistema.

El método 2 consiste en aplicar la fórmula

$$Q = \sqrt{\sum_{i=1}^{n} Q_i^2 + \sum_{i \neq j} \sum \frac{Q_i\, Q_j}{1 + \epsilon^2_{ij}}} \qquad (1.2)$$

siendo

$$\epsilon_{ij} = \frac{\omega_i' - \omega_j'}{\xi_i' \omega_i + \xi_j' \omega_j} \qquad (1.3)$$

donde

Q_i	respuesta máxima en el i-ésimo modo de vibración, tomada con el mismo signo que el de la correspondiente función de transferencia cuando esta alcanza su valor máximo absoluto
ω_i	i-ésima frecuencia circular natural de vibracion del sistema sin amortiguamiento
$\omega_i' = \omega_i \sqrt{1 - \xi_i^2}$	i-ésima frecuencia circular natural de vibración del sistema amortiguado
ξ_i	fracción del amortiguamiento crítico en el i-ésimo modo natural
$\xi_i' = \xi_i + 2/(\omega_i S)$	fracción del amortiguamiento crítico equivalente
S	duración del sismo con el que se excita al sistema

El interés primordial al realizar esta verificación radica en que el método 1, actualmente en uso en varios reglamentos de construcción (refs 3 y 4), podría llegar a sustituirse por el método 2.

Se han propuesto otros procedimientos para estimar Q (ref 5) que son función no lineal de los resultados del método 1; sin embargo, no se discuten en este trabajo porque han sido estudiados con base en estructuras sin amortiguamiento, las cuales, como se verá, conducen a conclusiones diferentes de las que corresponden a estructuras amortiguadas.

Para realizar estadísticamente este estudio, se emplearon técnicas de reducción de variancia del método de Monte Carlo.

En cuanto al análisis, este se limita a tres casos, los cuales se detallan en el Apéndice:

1. Torsión en estructuras de un piso, considerando que las respuestas dinámicas son la fuerza cortante y el momento torsionante.

2. Cabeceo en estructuras de un piso, considerando como respuestas la fuerza cortante y el momento de cabeceo.

3. Traslación en estructuras de dos pisos, tomando en cuenta las fuerzas cortantes en los entrepisos uno y dos.

2. CALCULO DE LAS RESPUESTAS MAXIMAS

Las respuestas elásticas máximas de los diversos tipos de estructuras se calcularon utilizando:

a) Método 1 (ec 1.1, criterio del Reglamento de Construcciones del Departamento del Distrito Federal, ref 3)

b) Método 2 (ec 1.2 y nuevo criterio de Rosenblueth, ref 2)

c) Análisis modal (respuesta exacta).

Los resultados del análisis modal sirvieron como base de comparación del grado de aproximación de las estimaciones logradas con los otros dos criterios.

Como excitaciones sísmicas se emplearon cuatro sismos simulados de acuerdo con el método indicado en la ref 6 (figs 1 a 4), y uno real (fig 5), registrado en la zona blanda de la ciudad de México (ref 7).

El análisis de los tres casos se realizó empleando el método de Monte Carlo, que consiste en estudiar el comportamiento de un modelo matemático determinado, mediante la simulación de los datos de entrada (generalmente en computadora digital) y del estudio estadístico de los resultados. Cada vez que se introduce un conjunto de datos y se obtiene la respuesta del modelo, se dice que se efectúa un *experimento conceptual* del problema; la colección de resultados constituye la *muestra* que sirve de base para inferir cuál es el grado de aproximación con que dicho modelo matemático representa el fenómeno para el cual se formuló.

Conforme aumenta el número de parámetros que intervienen en el modelo matemático, se incrementa la cantidad de experimentos necesaria para dilucidar cuáles influyen en el problema, es decir, para verificar si en los resultados que se obtienen al variar los valores de los parámetros existen diferencias estadísticas significativas; sin embargo, eso representa un costo de computación que en ocasiones hace prohibitivo tal tipo de estudios, a menos que se emplee alguna técnica de *reducción de variancia* (refs 11 y 12), lo que permite un ahorro considerable en el número de experimentos necesario para obtener conclusiones adecuadas.

La técnica de reducción de variancia que se emplea en este trabajo es muy común y consiste en:

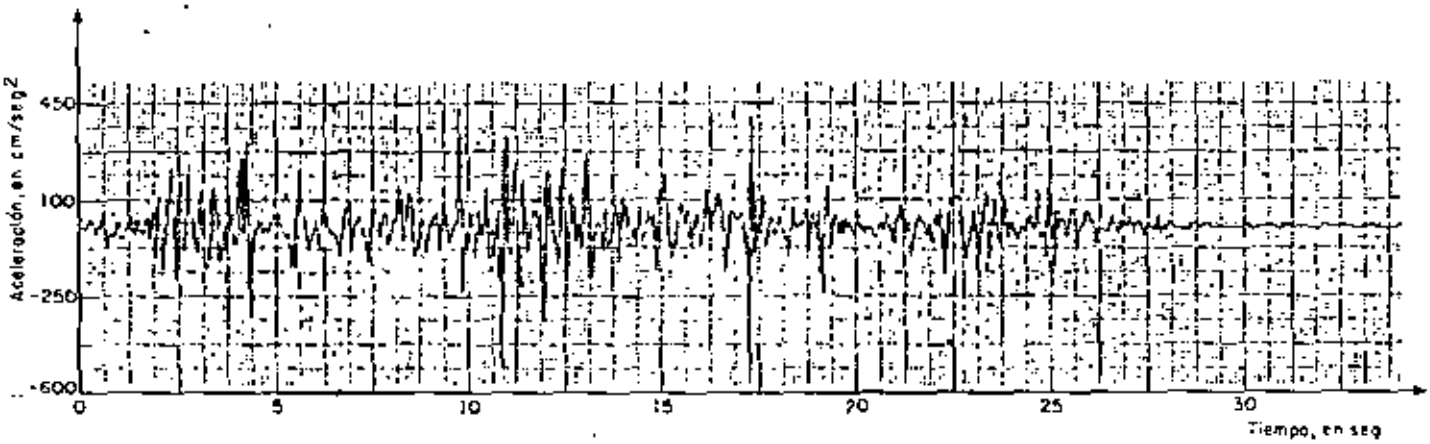

Fig 1. Sismo simulado No 1

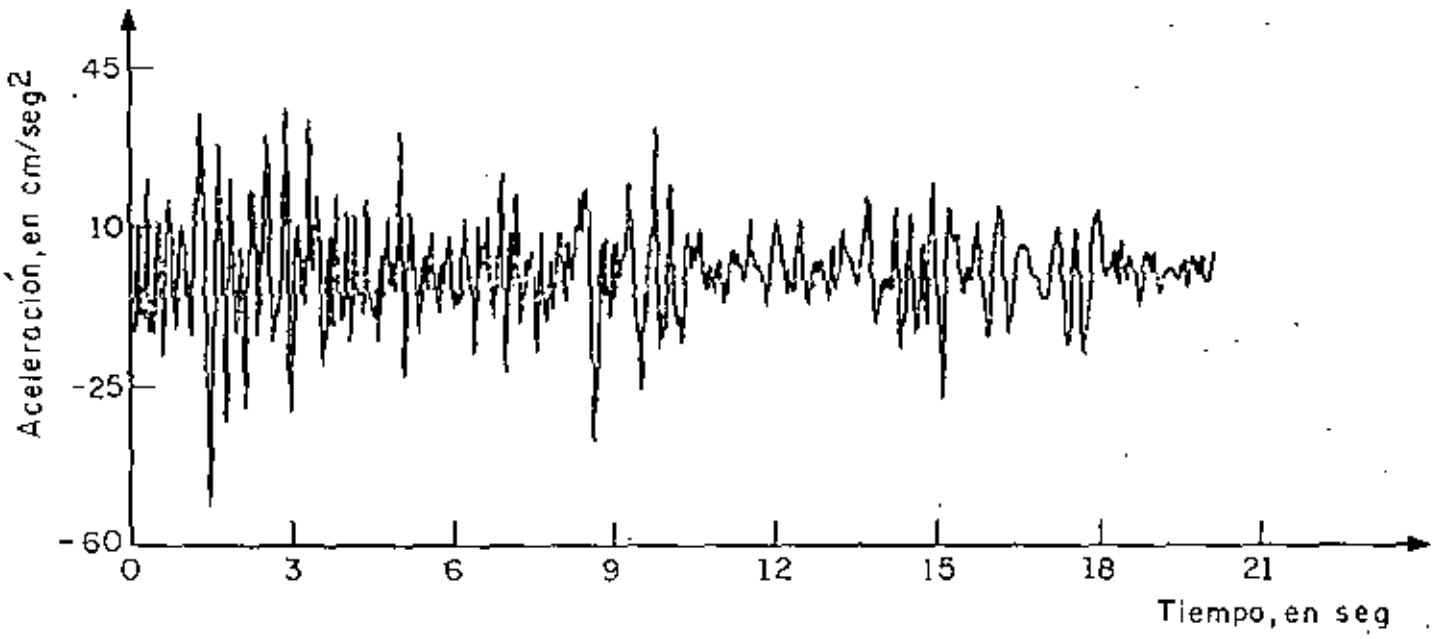

Fig 2. Sismo simulado No 2

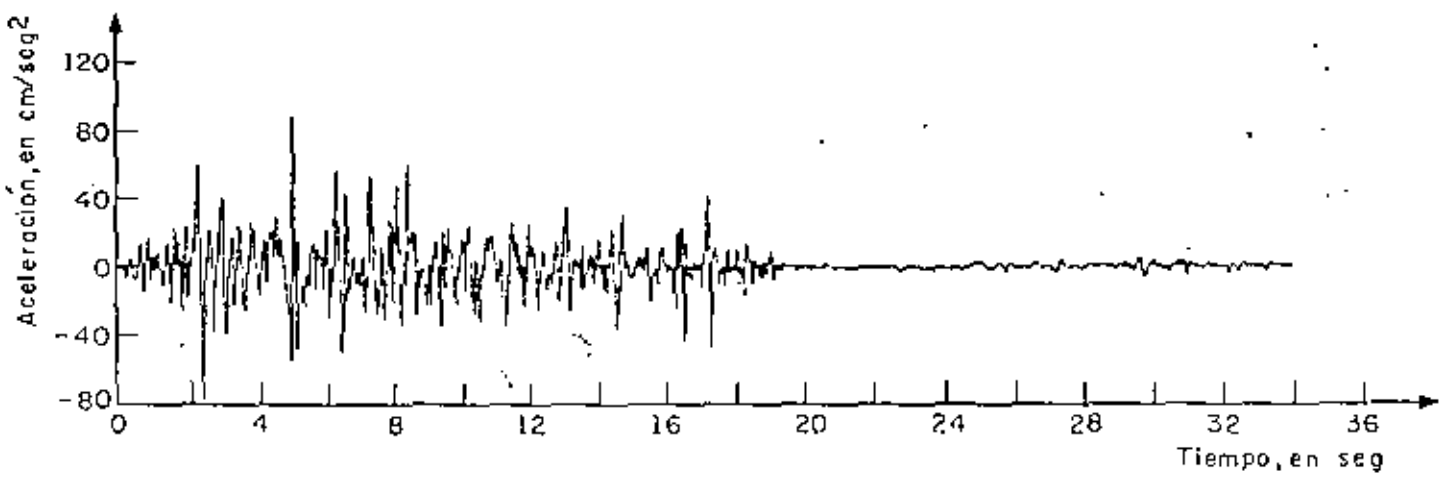

Fig 3. Sismo simulado No 3

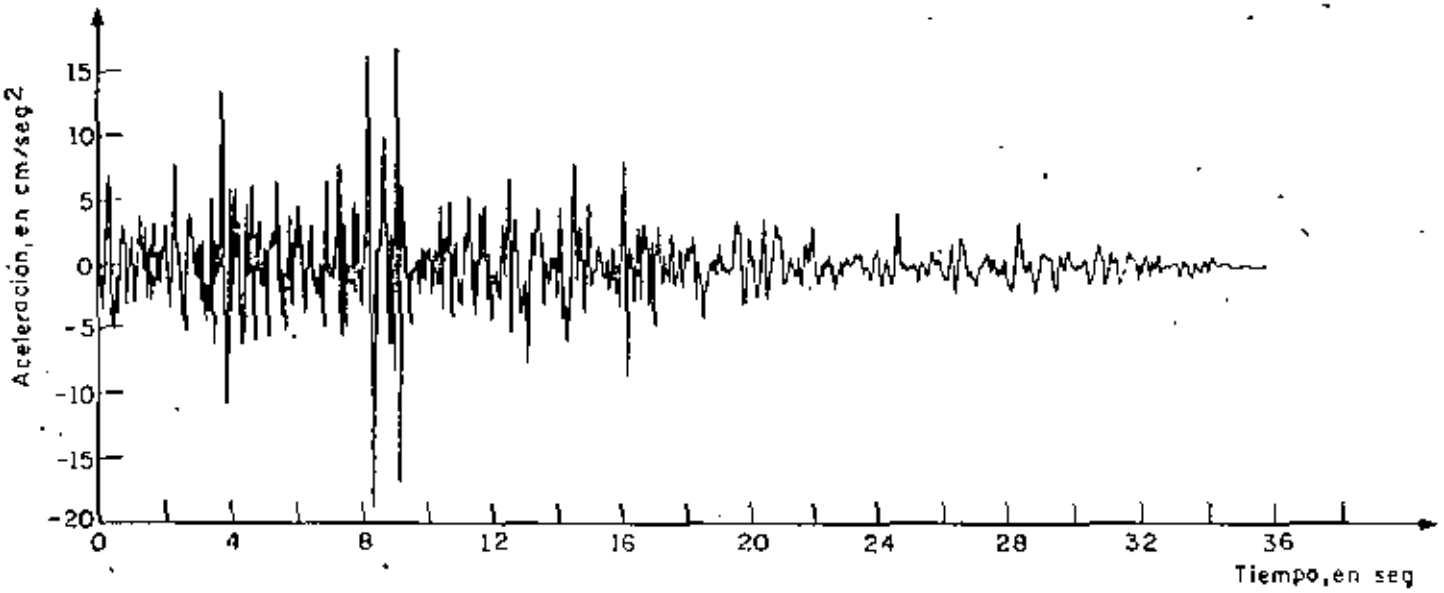

Fig 4. Sismo simulado No. 4

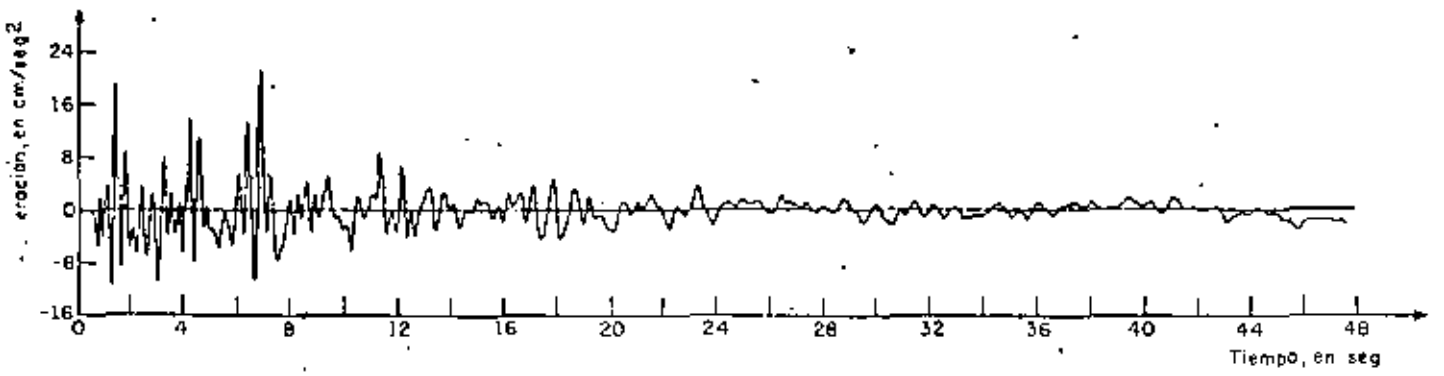

Fig 5. Sismo real registrado en la Alameda Central, México, D. F., el 10 de diciembre de 1961

a) Asignar diversos valores a cada parámetro que interviene en el problema, de manera que se cubran los intervalos de interés de cada uno.

b) Calcular la respuesta máxima exacta y las estimadas con los métodos 1 y 2 para cada combinación de valores de los diferentes parámetros.

c) Obtener las respuestas normalizadas dividiendo los valores exactos entre los estimados; esto se hace para cada combinación de valores de los parámetros, con lo cual se elimina la dispersión en los resultados ocasionada por la magnitud y variación con el tiempo de los datos de entrada (se reduce la variancia).

d) Estudiar si existen diferencias estadísticas significativas entre los resultados obtenidos al variar los valores asignados a uno de los parámetros. Si las hay, se infiere que los resultados logrados con cada valor de dicho parámetro corresponden a poblaciones estadísticas diferentes; en caso contrario, la población estadística es la misma y, por consiguiente, las muestras respectivas pueden agruparse en una sola de mayor tamaño, a partir de la cual es factible obtener conclusiones más generales y confiables acerca del modelo en estudio, ya que la variancia del promedio de la estimación se reduce en proporción a 1/n (ref 11). Esta etapa se repite sucesivamente para cada uno de los parámetros restantes, con lo que se realiza, de hecho, un análisis de variancia.

2.1 Resultados del problema de torsión (caso 1)

Para diseño sísmico de edificios, los elementos mecánicos que usualmente interesa conocer son las fuerzas y momentos que obran sobre cada elemento estructural. Para simplificar, con objeto de aislar los efectos de la fuerza cortante y del momento torsionante, en este problema de torsión se considerará una estructura (fig 6) con masa uniformemente distribuida, con un solo muro en dirección Z que resista la fuerza cortante directa, y dos idénticos en dirección Y (per-

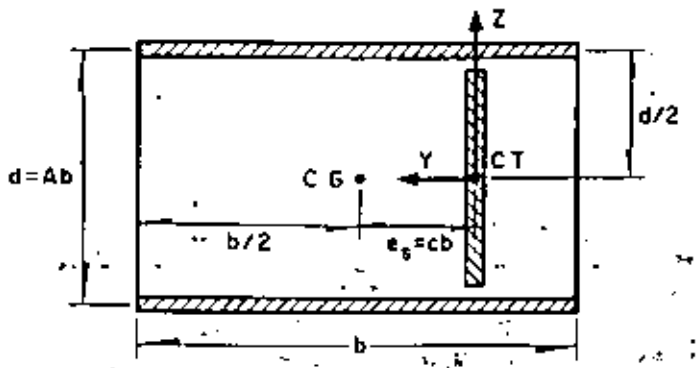

Fig 6. Estructura tipo considerada en el problema de torsión

pendicular al movimiento), de manera que cada uno de estos últimos resista una fuerza cortante igual a M/d, donde M es el momento torsionante dinámico y d es la separación de los dos muros. En este caso, la estructura presenta excentricidad solo en dirección perpendicular a la de excitación, Z.

Los parámetros que se escogieron para estudiar el problema de torsión fueron (fig 6):

$A = b/d$

b dimensión en la dirección Y

$c = e_s/b$

T_1 periodo fundamental de vibración $= \omega_1/2\pi = \lambda_1/(2\pi K/m)$

ζ fracción de amortiguamiento respecto al crítico en ambos modos de vibración

η cociente de la frecuencia angular entre la lineal $= (L/J)/(K/m)$

Los valores que se asignaron a A, b y c son los consignados en la tabla 1; los de ζ son 0, 0.05 y 0.10; los de η, 0.5, 0.9, 1.0, 1.1, 1.5, 2.0, 2.5, 3 y 4, y los de T_1, 0.1, 0.3, 0.5, 0.7, 1.0, 1.5, 2, 3 y 4 seg. Los casos de $\eta = 1$, 0.9 y 1.1 se estudiaron con especial cuidado debido a que para valores de $\eta = 1$ y cercanos, sucede que las dos frecuencias naturales de vibración resultan más próximas entre sí (ec A.3) y, en consecuencia, el término ϵ_{12}^2 de las ecs A.8 y A.9 del Apéndice puede asumir valores pequeños (ec 1.3), en cuyo caso se pueden presentar diferencias considerables entre los resultados de ambos métodos, puesto que el término de la doble suma de la ec 1.2 asume valores tanto mayores cuanto menores son los de ϵ_{12}^2.

Para cada uno de los casos de la tabla 1 se obtuvieron las fuerzas cortantes y los momentos torsionantes máximos correspondientes a todas las combinaciones de ζ, T_1 y η.

En las figuras que aparecen más adelante no se hace distinción de los resultados obtenidos con cada sismo ni con cada combinación de A, b y c, ya que las muestras respectivas se mezclaron al no haberse encontrado diferencias estadísticas significativas con un 95 por ciento de nivel de confianza en los mismos, a pesar de la marcada diferencia entre los valores de dichos parámetros y de las características de los sismos, tales como duración y frecuencia dominante.

2.1.1 Momento torsionante

En las figs 7 a 9 se presentan los resultados correspondientes a los casos en los que $T_1 = 2.0$ seg y $\zeta = 0$, 0.05 y 0.10, respectivamente. En el eje de las abscisas se localizan los valores de η, y en el de las ordenadas los cocientes de los momentos torsionantes exactos, M, entre los estimados, $\hat{M}$ y $\tilde{M}$, con los métodos 1 y 2, respectivamente (Apéndice).

En la fig 7, en la que el amortiguamiento es nulo, se aprecia mayor dispersión en los resultados de ambos métodos que corresponden a $\eta = 0.9$, 1.0 y 1.1 que para los demás valores de η. En cambio, en las figs 8 y 9, que corresponden a $\zeta = 0.05$ y $\zeta = 0.10$, respectivamente, se observa que la dispersión de los resultados del método 2 es prácticamente la misma para todos los valores de η (el coeficiente de variación es cercano a 0.2), cosa que no sucede con los resultados del método 1; para los cuales se tiene mayor dispersión cuando $\eta = 0.9$, 1.0 y 1.1. Estas observaciones llevan a la conclusión de que para el método 1 no se pueden mezclar las muestras correspondientes a todos los valores de η, ya que los resultados dependen de este parámetro; mientras que para el método 2 podrían mezclarse las que no se refieren a amortiguamiento nulo si se verificara que los valores medios correspondientes a cada η son estadísticamente iguales.

Para lograr dicha verificación, se investigó primero si los resultados del método 2 son independientes del periodo fundamental, T_1. Con este fin se trazó un juego de figuras del mismo tipo que las figs 10 a 12, que corresponden a $\eta = 1.0$ con $\zeta = 0$, 0.05 y 0.10, respectivamente. En la fig 10, que corresponde a $\zeta = 0$, se observa que los resultados sí dependen de T_1, ya que los valores medios son sensiblemente más grandes para periodos mayores de 1.0 seg que para los menores. Por lo contrario, en las figs 11 y 12 se nota que los valores medios son prácticamente independientes de T_1 en el intervalo de periodos estudiado, por lo que las muestras de cada periodo pueden agruparse en una sola (esta conclusión también es válida para los resultados del método 1).

Para verificar estadísticamente la conclusión anterior, se realizó una prueba de hipótesis acerca de si la pendiente de la recta que se ajusta a los datos puede considerarse nula, habiéndose aceptado con 95 por ciento de nivel de confianza.

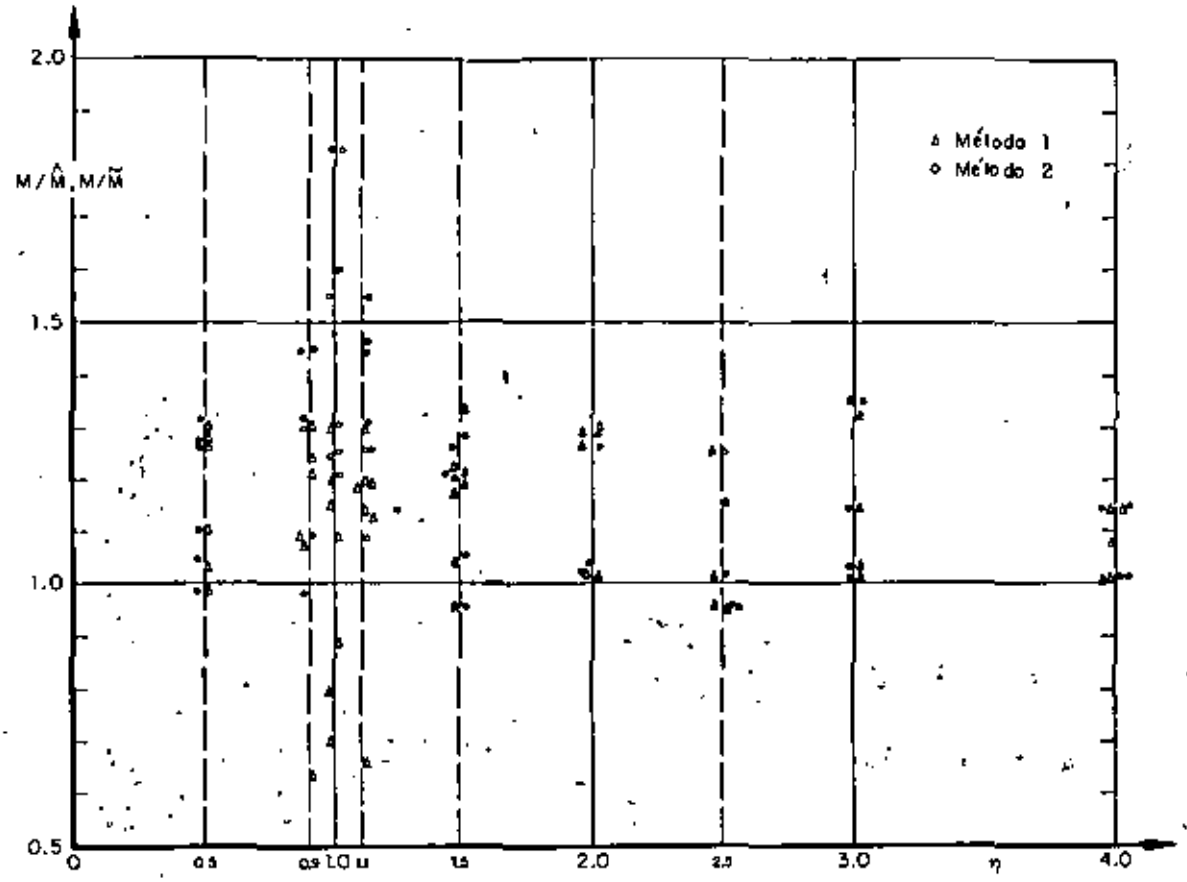

Fig 7. Resultados de los momentos torsionantes para $T_1 = 2.0$ seg. y $\xi = 0$

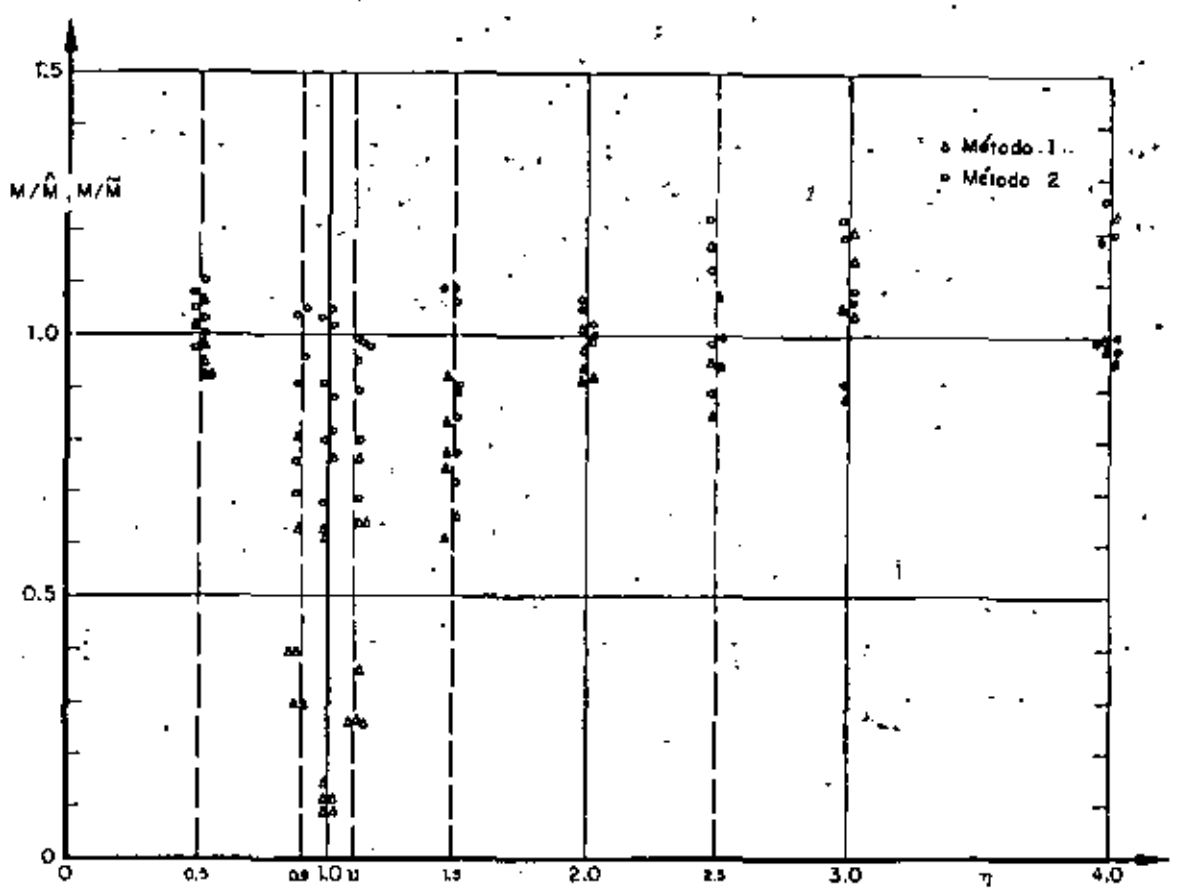

Fig 8. Resultados de los momentos torsionantes para $T_1 = 2.0$ seg. y $\xi = 0.05$

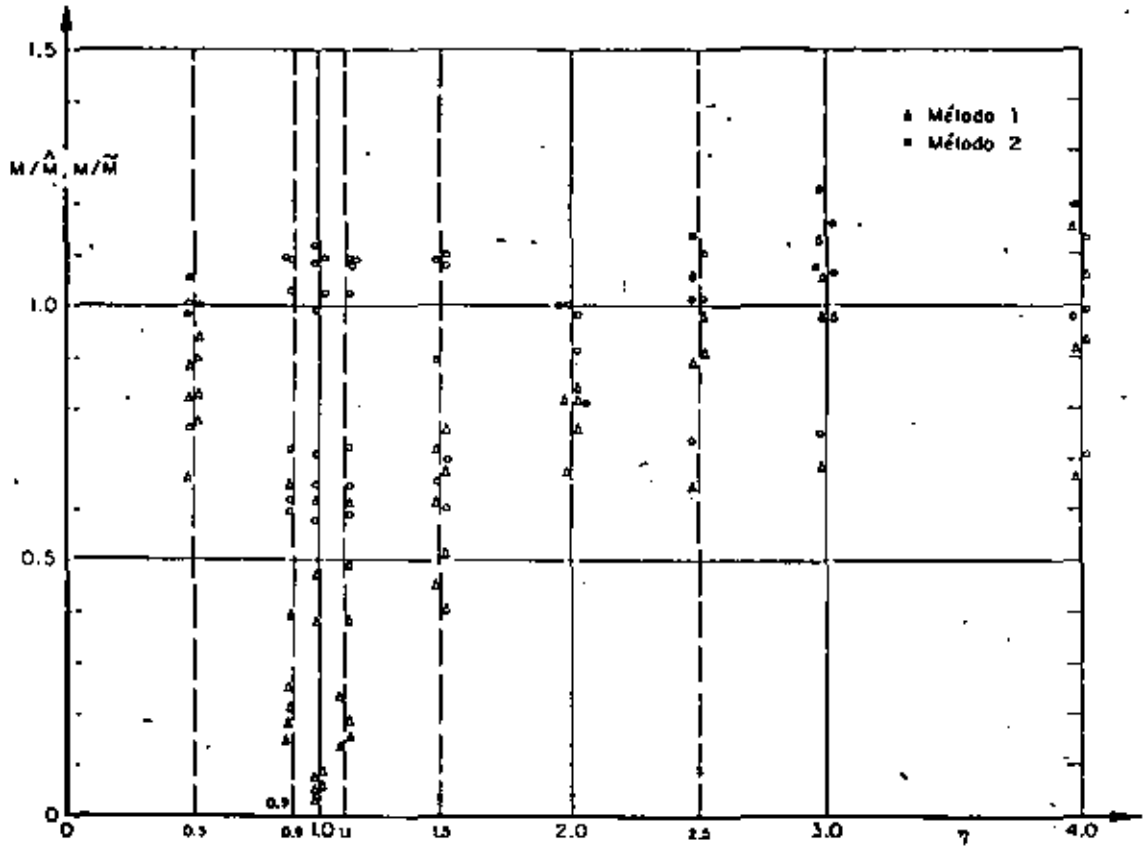

Fig 9. Resultados de los momentos torsionantes para $T_j = 2.0$ seg, y $\xi = 0.10$

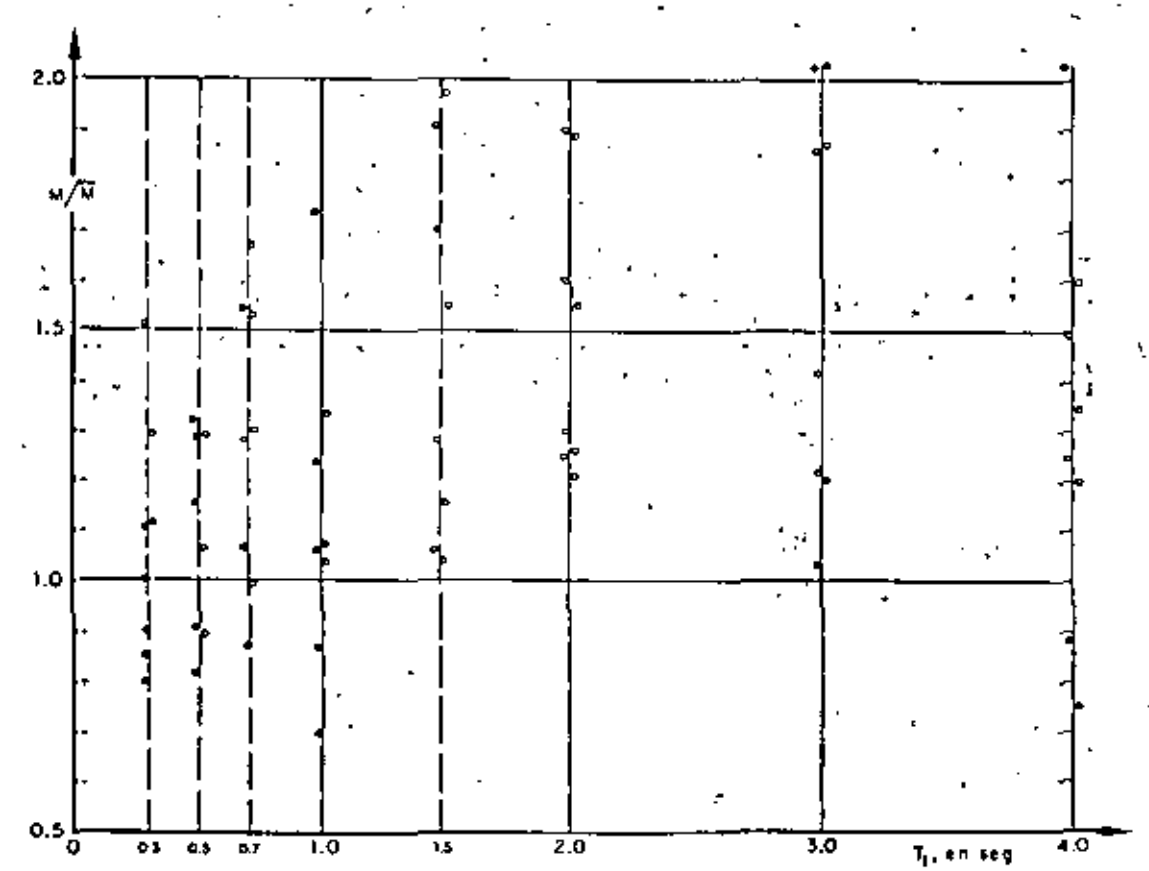

Fig 10. Resultados de los momentos torsionantes para $\eta = 1.0$, y $\xi = 0$, Método 2

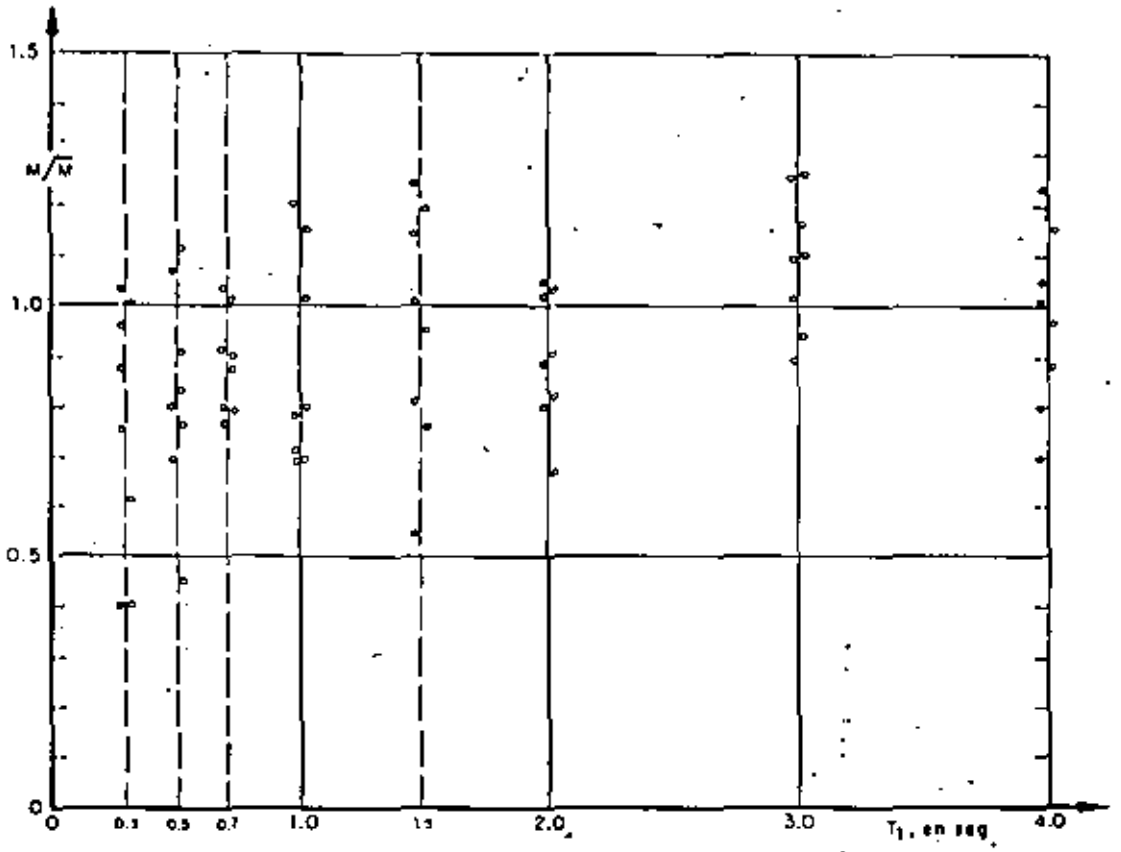

Fig 11. Resultados de los momentos torsionantes para $\eta = 1.0$, y $\zeta = 0.05$, Método 2

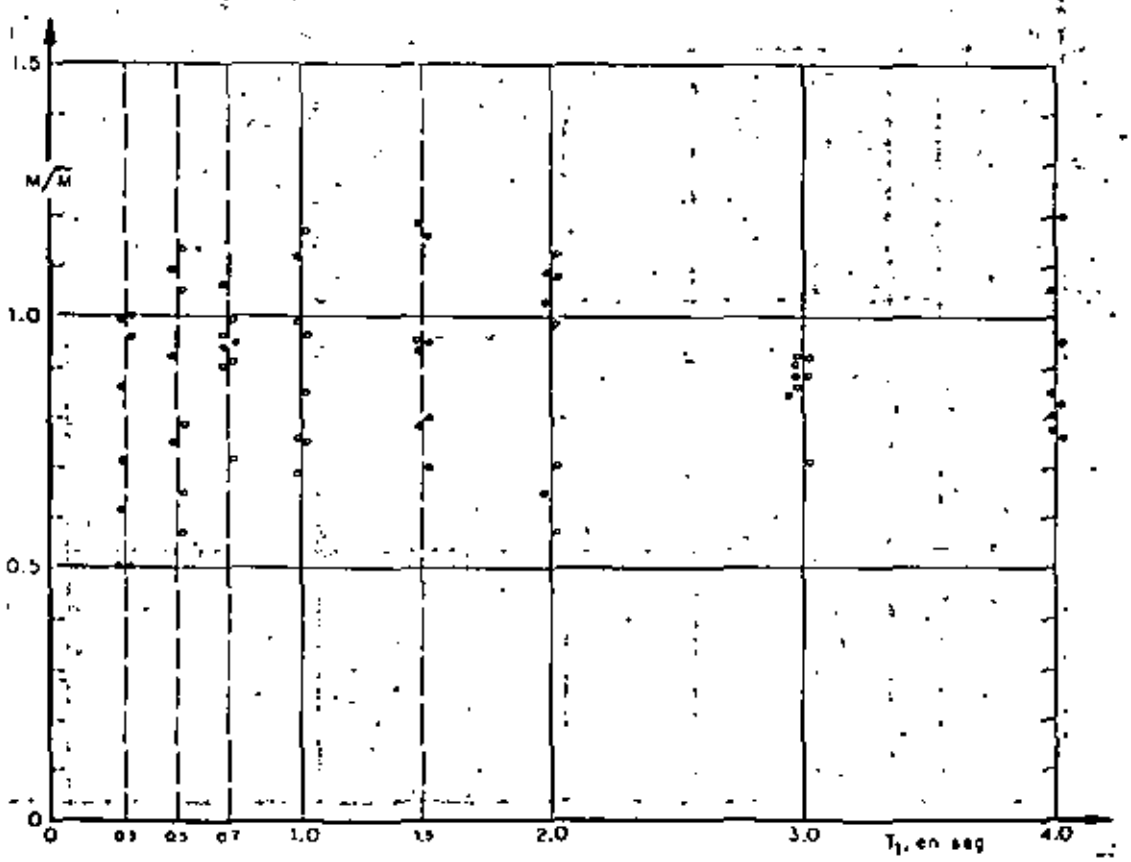

Fig 12. Resultados de los momentos torsionantes para $\eta = 1.0$, y $\zeta = 0.10$. Método 2

En la fig 13 se presentan en el eje de las ordenadas los promedios, $(M/\hat{M})$ y $(M/\tilde{M})$, de los resultados obtenidos respectivamente con los métodos 1 y 2, considerando que estos son independientes de T_1; en el eje de las abscisas se localizan los valores de η. Se observa que, para $\eta = 0.9$, 1.0 y 1.1, el método 2 sobrestima ligeramente la respuesta media (en 10 por ciento), tendiendo a subestimarla en 5 por ciento conforme los valores de η se alejan de 1.0, cuando $\zeta = 0.05$ y 0.10

Con objeto de verificar si con el método 2 los resultados son independientes de η, se realizaron pruebas de hipótesis de igualdad de medias, siendo aceptables con 95 por ciento de nivel de confianza. Por lo contrario, los resultados del método 1 no fueron independientes de η, lo cual es obvio, puesto que con $\zeta = 0.10$ se tiene que el promedio de $M/\hat{M}$ es 0.31 para $\eta = 1$ (el mínimo valor fue 0.04 y el máximo 0.68), y 0.99 para $\eta = 4$ (el mínimo fue 0.66 y el máximo 1.28).

En la fig 13 se observa también que los promedios obtenidos con el método 1 se acercan a los exactos conforme η aumenta, presentándose mayores errores para valores de η muy cercanos a 1.0, para el cual las frecuencias naturales de la estructura resultan más próximas entre sí (ec A.3), lo que trae como consecuencia que en muchas ocasiones las respuestas máximas en ambos modos de vibración ocurran simultáneamente y con signo contrario, por lo que la respuesta combinada máxima es la suma algebraica de ambas respuestas, que da resultados menores que los de la ec A.11.

Otra conclusión inmediata que se obtiene de la fig 13 es que los resultados del método 2 son prácticamente independientes de ζ cuando $\zeta \geq 0.05$ y que el método 1 pierde aproximación conforme aumenta ζ, y η se aproxima a 1

De lo anterior se concluye también que en estructuras amortiguadas, que son las de interés práctico, el método 2 proporciona, en promedio, mejores resultados que el método 1, aunque el 2 subestime más y con mayor frecuencia la respuesta máxima. En estructuras no amortiguadas, que únicamente son de interés académico, el método 1 proporciona mejores resultados.

Otro punto importante de discusión es el del cociente de la excentricidad dinámica exacta, e_d, entre la estática, e_s. En las figs 14 a 16 se tiene η en el eje de las abscisas, y e_d/e_s en el eje de las ordenadas.

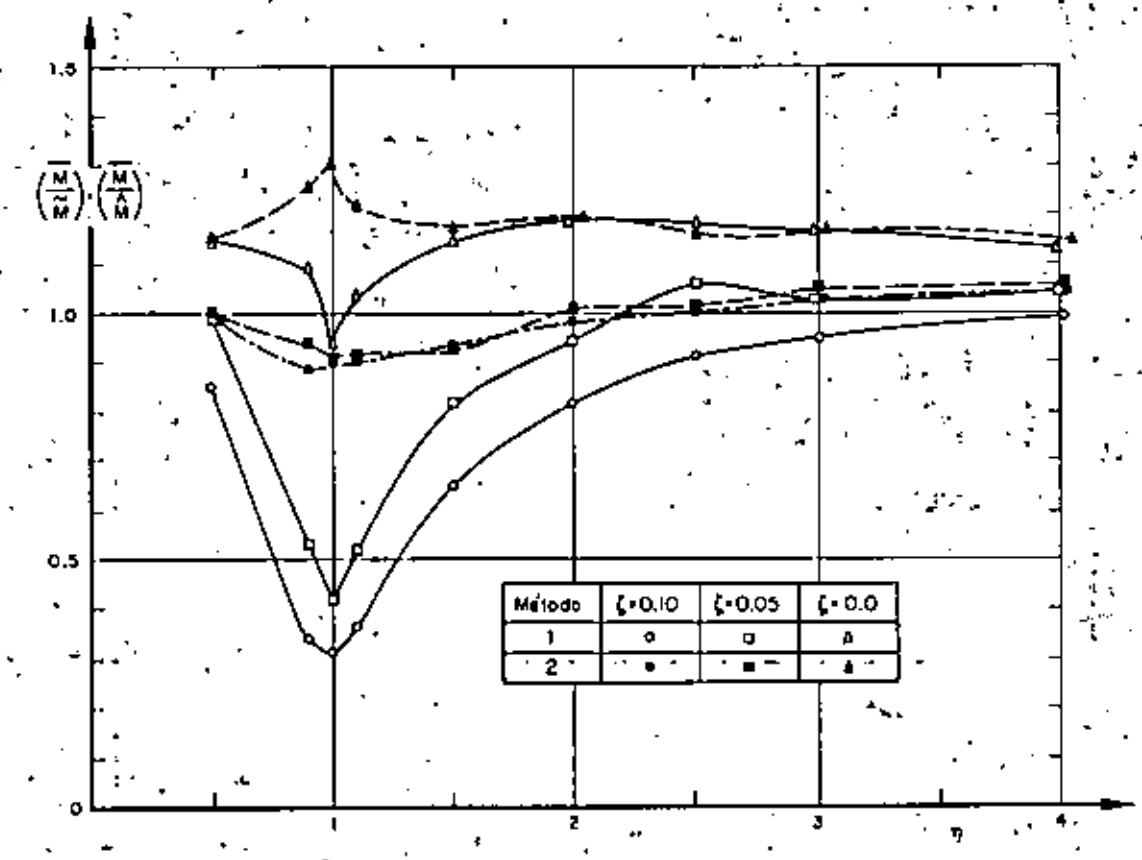

Fig 13. Variación con η de los promedios de los momentos torsionantes estimados

Se observa en la fig 14, que corresponde a amortiguamiento nulo, que para $\eta = 0.9$, 1.0 y 1.1 hay una marcada diferencia entre los resultados obtenidos con el caso I con los casos II y III (la de estos últimos entre sí no es tan importante). Así, cuando $\eta = 1.0$, en el caso I el promedio de e_d/e_s fue 38.5 y la desviación estándar 16.6; en el caso II estos parámetros estadísticos valieron 5.4 y 0.6, respectivamente. Para valores de η separados de 1.0 en 0.5 unidades o más hay diferencias menos apreciables entre los resultados de los tres casos. Además, e_d/e_s disminuye rápidamente conforme η se aleja de 1.0.

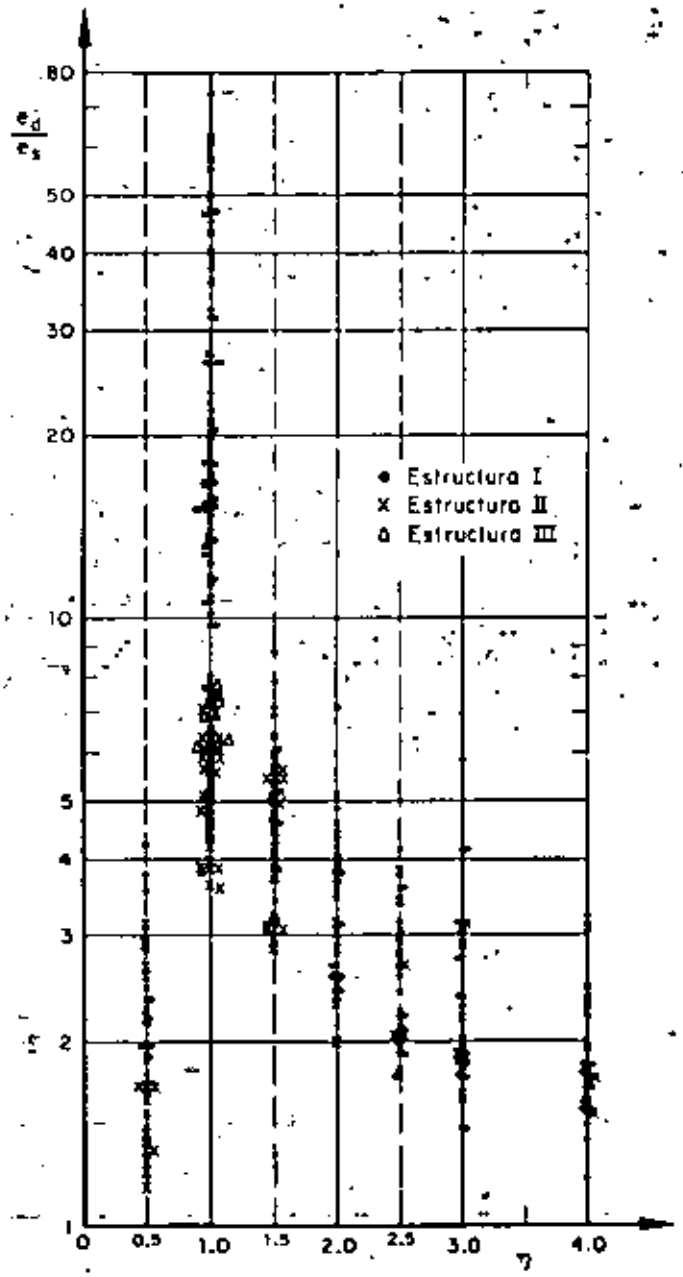

Fig 14. Cocientes de la excentricidad dinámica exacta entre la estática, para $\zeta = 0$

En las figs 15 y 16, para $\zeta = 0.05$ y 0.10, respectivamente, casi no hay diferencias entre los resultados de los dos casos, aunque persiste la dependencia respecto a η. Comparando estas tres últimas figuras se nota también que e_d/e_s disminuye conforme el amortiguamiento aumenta. Así, para $\zeta = 0.05$ el promedio fue 4.6 y la desviación estándar 1.3, mientras que para $\zeta = 0.10$, los valores correspondientes fueron 2.7 y 0.7.

De las figs 15 y 16 se concluye que la disposición del Reglamento de Construcciones del Departamento del Distrito Federal de que se tome $e_d/e_s = 1.5$ subestima el valor promedio para todos los valores de η mayores de 0.5 y menores de 4.0 (aquí se omitió el término $\pm 0.05b$ que se agrega a 1.5 en la disposición del Reglamento, porque dicho término tiene como finalidad prevenir excentricidades accidentales ocasionadas por variaciones imprevisibles de masas y rigideces y posibles excitaciones torsionales).

Con objeto de estimar probabilidades de eventos relacionados con los momentos torsionantes, se trazaron en papel de probabilidades los datos de frecuencias acumuladas correspondientes a diferentes casos. Las distribuciones de probabilidades empleadas fueron la logarítmico normal, la extrema tipo II y la normal, de las cuales, por apreciación visual, se consideró que esta última daba en general mejores resultados (figs 17 a 19).

Para verificar que las poblaciones bajo estudio tienen distribuciones normales, se realizaron pruebas de hipótesis estadísticas con un 95 por ciento de nivel de confianza.

Los resultados fueron:

Método 1

(Con resultados de $\eta = 1.5$, 2.0, 2.5, 3.0 y 4.0 mezclados; fig 17)

$\zeta = 0$: se rechaza la hipótesis nula de que la distribución es normal con media 1.16 y desviación estándar 0.12 (esta hipótesis se rechaza también con un 99 por ciento de nivel de confianza)

$\zeta = 0.05$ y $\zeta = 0.10$: se aceptan las hipótesis nulas de que las distribuciones son normales con medias 0.96 y 0.85, y desviaciones estándar 0.15 y 0.17, respectivamente.

Método 2

(Con resultados de $\eta = 1.5$, 2.0, 2.5, 3.0 y 4.0 mezclados; fig 18)

$\zeta = 0$, 0.05 y 0.10: se aceptan las hipótesis de que las distribuciones son normales con medias 1.15, 1.06 y 1.00, y desviaciones estándar 0.15, 0.15 y 0.15, respectivamente. Para $\zeta = 0.05$, la hipótesis se acepta con 99 por ciento de nivel de confianza; las otras con 95 por ciento.

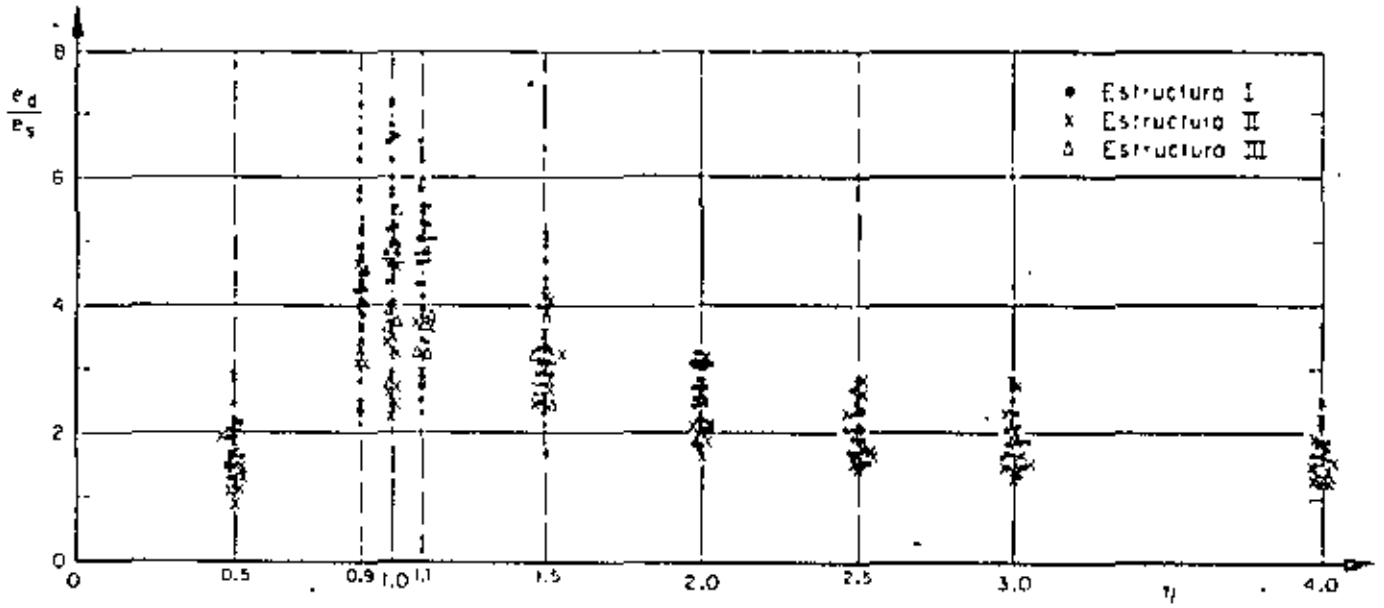

Fig 15. Cocientes de la excentricidad dinámica exacta entre la estática, para $\zeta = 0.05$

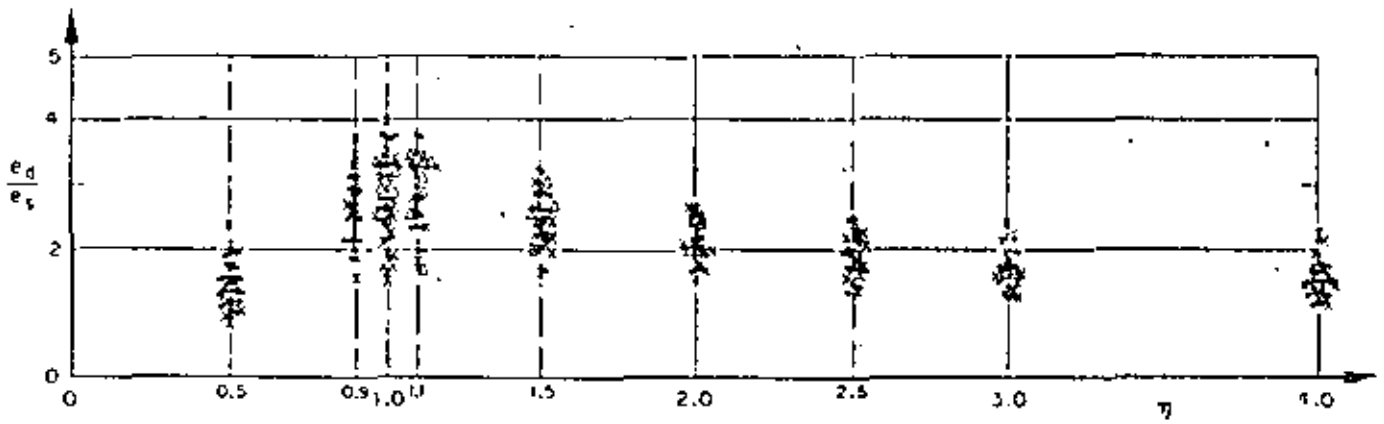

Fig 16. Cocientes de la excentricidad dinámica exacta entre la estática, para $\zeta = 0.10$

Además, para $\zeta = 0.10$ se estudió el caso en que se mezclaron los resultados de $\eta = 1$ y $\eta = 1.1$ (fig 19), obteniéndose una distribución normal con media 0.88 y desviación estándar 0.17. También se mezclaron los resultados de los valores de η de 1 a 4, para los cuales se obtuvo una distribución de igual tipo con media 0.95 y desviación estándar 0.16. Ambas hipótesis fueron aceptables, pero con 97.5 por ciento de nivel de confianza.

En todos los casos descritos en que se acepta la hipótesis nula, se observa que la desviación estándar es muy semejante, ya que varía de 0.15 a 0.17, mientras que la media va de 0.86 a 1.15.

2.1.2 Fuerza cortante

Los resultados obtenidos con los métodos 1 y 2, correspondientes a $\eta = 1.0$ y $\zeta = 0$, se muestran en la fig 20. En el eje de las abscisas se tienen los periodos fundamentales, T_1, y en el de las ordenadas las fuerzas cortantes normalizadas, $V/\hat{V}$ y $V/\tilde{V}$, obtenidas al dividir las fuerzas cortantes, V, calculadas mediante análisis modal entre las estimadas con los métodos 1 y 2, $\hat{V}$ y $\tilde{V}$, respectivamente.

De la fig 20 y otras similares se concluyó que las fuerzas cortantes normalizadas obtenidas con ambos métodos son independientes del periodo fundamental, T_1, con 95 por ciento de nivel de confianza. Además, para valores de η menores de 0.9 y mayores de 1.1, los resultados fueron independientes de los parámetros A, b y c, con errores de ± 5 por ciento. Esta independencia también se obtuvo para el método 2, inclusive cuando $\eta = 0.9$, 1.0 y 1.1, con errores máximos de 40 por ciento en defecto y 20 por ciento en exceso para $\zeta = 0$, tendiendo a reducirse conforme aumenta el amortiguamiento; así, para $\zeta = 0.05$, se obtuvieron errores máximos de ± 20 por ciento, y para $\zeta = 0.10$ de ± 10 por ciento.

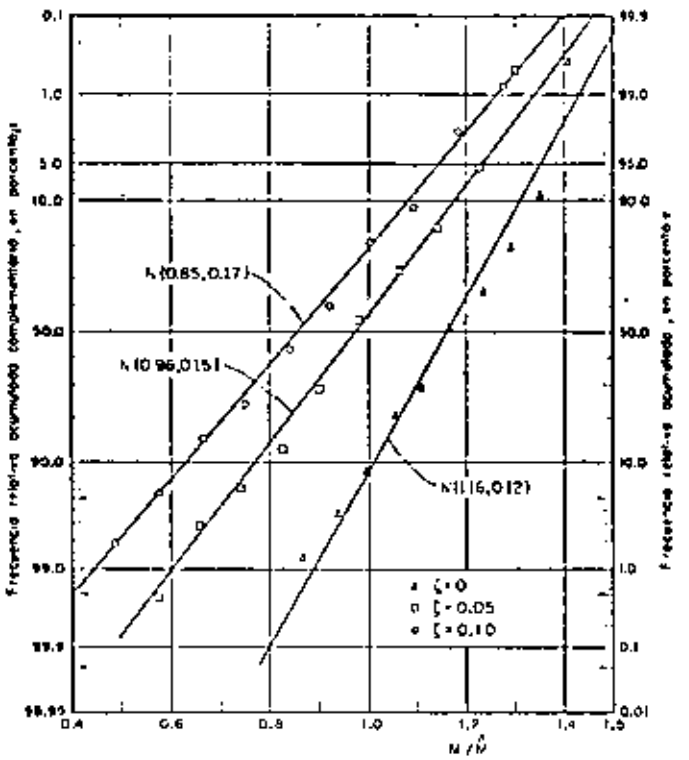

Fig 17. Resultados de los momentos torsionantes para $\eta = 1.5, 2.0, 2.5, 3.0$ y 4.0 mezclados. Papel de probabilidades normal, método 1

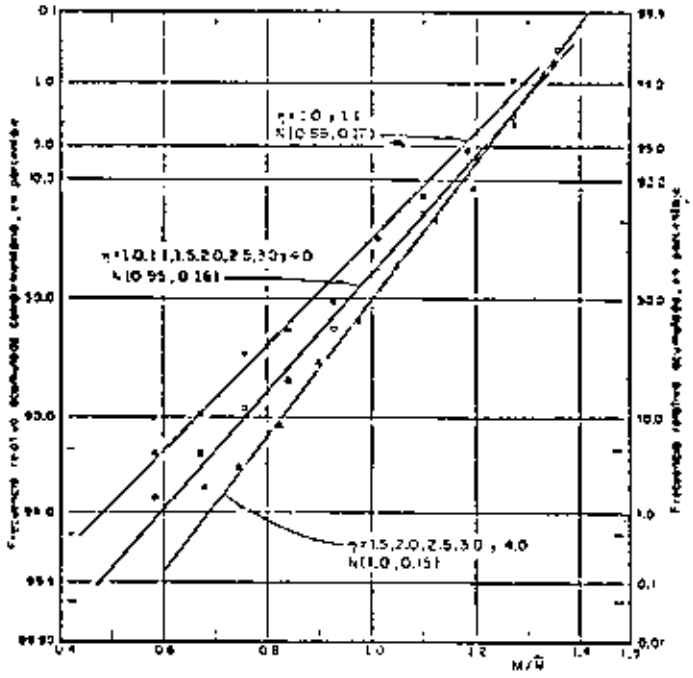

Fig 19. Resultados del método 2 para $\zeta = 0.10$

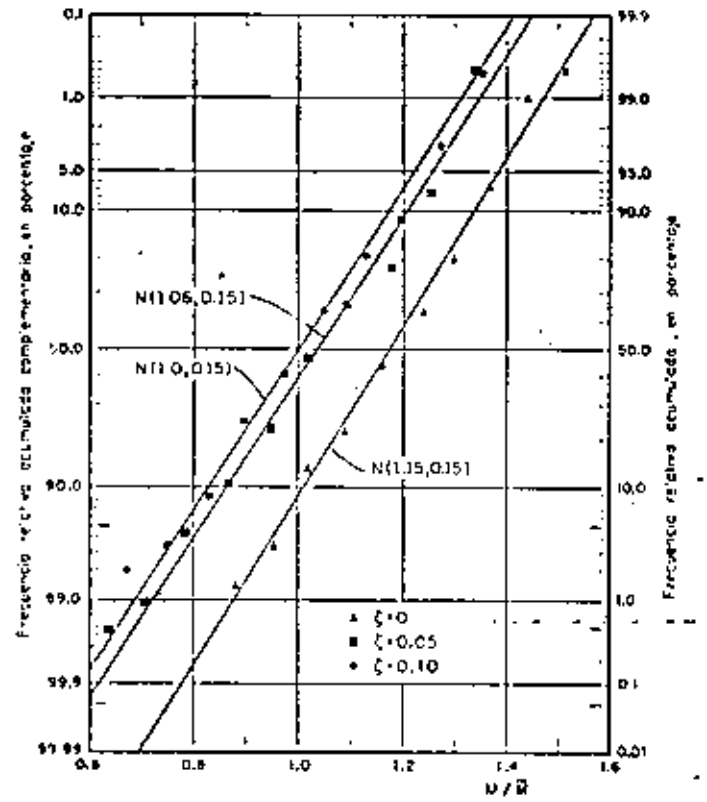

Fig 18. Resultados de los momentos torsionantes para $\eta = 1.5, 2.0, 2.5, 3.0$ y 4.0 mezclados. Papel de probabilidades normal, método 2

Para el método 1, con $\eta = 1.0$, los errores máximos fueron: 41 por ciento en defecto para la estructuración del caso I y 32 por ciento en defecto en los casos II y III. Los errores medios respectivos fueron 36 y 15 por ciento, ambos en defecto. Para $\eta = 1.1$, la estructuración del caso I tuvo errores máximos de ± 5 por ciento, y las tipo II y III, 38 por ciento en defecto y 11 por ciento en exceso.

Respecto al amortiguamiento, se concluyó que las fuerzas cortantes normalizadas son prácticamente independientes de este; así, para $\eta = 1$, los promedios globales de los métodos 1 y 2 fueron 1.23 y 1.11, respectivamente, para $\zeta = 0$; para $\zeta = 0.05$ de 1.30 y 1.02, y para $\zeta = 0.10$ de 1.30 y 1.0.

Como puede apreciarse mediante los promedios citados en el párrafo anterior, los resultados que se obtienen con el método 2 son mejores que los del 1 cuando $\eta = 1.0$. Una conclusión semejante se obtuvo cuando $\eta = 0.9$ y 1.1, aunque las diferencias se redujeron en un 10 por ciento. Para valores de η fuera del intervalo $0.9 \leqslant \eta \leqslant 1.1$, los resultados de ambos métodos fueron prácticamente iguales.

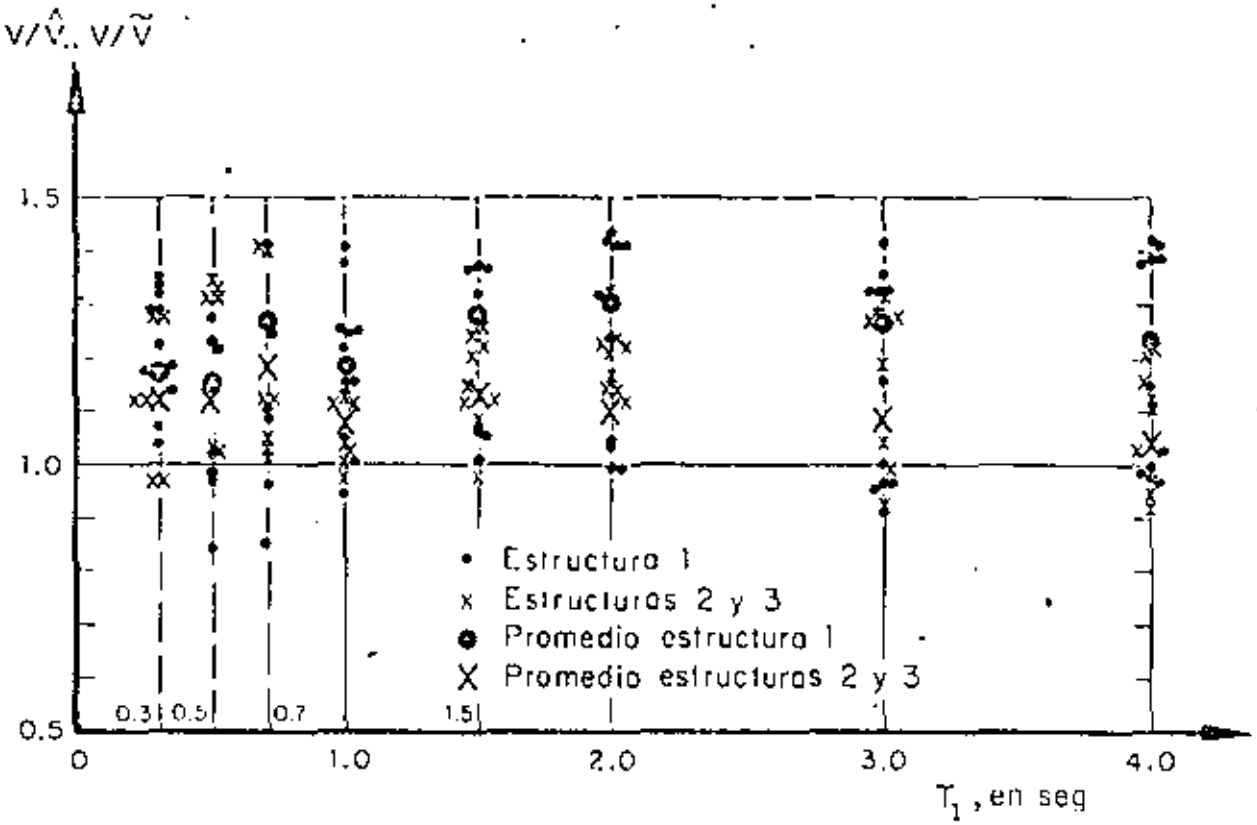

Fig 20. Fuerzas cortantes normalizadas estimadas con los métodos 1 y 2, para $\eta = 1.0$ y $\zeta = 0$

3.2 Resultados del problema de cabeceo (caso 2)

Los parámetros que se escogieron para estudiar el problema de cabeceo fueron:

m masa total

L distancia del suelo al centro de gravedad } periodo

T_1 periodo fundamental

ζ fracción de amortiguamiento respecto al crítico en ambos modos de vibración

η_c cociente de la frecuencia angular entre la lineal

Los valores que se asignaron a T_1 fueron 0.3, 0.7, 1.0, 1.5, 2.0, 3.0 y 4.0 seg; a ζ, 0, 0.05 y 0.10, y a η_c, 0.2, 0.5, 1.0, 1.5, 2.0, 2.5, 3.0 y 4.0. En cuanto a m y L, únicamente se usaron 2.0 ton seg^2/m y 4 m, respectivamente, ya que por los resultados (fuerzas y momentos normalizados) que se obtuvieron con estas combinaciones se juzgó innecesario el uso de otros valores; por la misma razón se emplearon únicamente tres de los sismos del problema de torsión.

En este problema, igual que en el de torsión, no hubo diferencias apreciables entre los resultados obtenidos con los tres sismos que se emplearon como excitación, por lo cual se agruparon los resultados en una sola muestra. Además, tanto las fuerzas cortantes como los momentos de cabeceo máximos normalizados fueron estadísticamente independientes del periodo fundamental, T_1, con nivel de confianza de 95 por ciento.

Otra conclusión interesante es que los resultados obtenidos con los métodos 1 y 2 (Apéndice) son prácticamente iguales, con diferencias máximas entre ellos de 5 por ciento. Esto se debe a que los valores de ϵ_{12}^2 (ec 1.3) son grandes porque las frecuencias de vibración no resultan con valores muy cercanos entre sí, aun cuando se usaron η_c muy pequeñas, de manera que el radical de la ec A.17 fuera también pequeño y, por tanto, que las diferencias entre las dos frecuencias fundamentales fueran mínimas. Esto hace que los términos que contienen a ϵ_{12}^2 en las ecs A.24 y A.25 resulten muy pequeños y que estas ecuaciones sean casi iguales a las ecs A.22 y A.23, respectivamente.

Aprovechando las conclusiones anteriores, se acumularon las muestras correspondientes a todos los periodos fundamentales, y para cada amortiguamiento se elaboraron dos gráficas: una de fuerzas cortantes y otra de momentos de cabeceo normalizados, empleando únicamente los resultados del método 2. En ellas, el eje de las abscisas representó a η_c, y el de las ordenadas a los cocientes $V/\tilde{V}$ o $M/\tilde{M}$, donde V y M denotan la fuerza cortante y el momento de cabeceo exactos, y $\tilde{V}$ y $\tilde{M}$ los mismos elementos mecánicos estimados con el método 2.

Debido a que las conclusiones obtenidas de esas gráficas son prácticamente las mismas, en este trabajo solo se reproduce la correspondiente a las fuerzas cortantes con $\zeta = 0.10$ (fig 21). Dichas conclusiones fueron, además de las mencionadas, las siguientes:

— Los resultados son estadísticamente independientes de η con 95 por ciento de nivel de confianza, cuando $\zeta \geq 0.05$

— La respuesta normalizada se subestima con mayor frecuencia que lo que se sobrestima, en proporción de 2 a 1

— El error máximo en defecto fue 29 por ciento, y en exceso, 22 por ciento

— El promedio global de los resultados con $\zeta \geq .05$ es 1.05, y el coeficiente de variación, 10 por ciento

— Los resultados varían ligeramente al introducir amortiguamiento a la estructura; se hace notar que para $\zeta = 0$, la respuesta normalizada promedio se subestima aproximadamente en 10 por ciento más que con $\zeta = 0.05$ y 0.10 (fig 22). En estos dos últimos casos no se aprecia diferencia significativa en los promedios de las respuestas ni en las dispersiones. Así, los errores máximos que se tuvieron para $\zeta = 0.05$ alcanzaron 31 por ciento en defecto y 19 por ciento en exceso; en cuanto a $\zeta = 0.10$ fueron, respectivamente, 27 y 21 por ciento

— Dado que existe gran incertidumbre en otros factores del diseño sísmico, tales como magnitud del sismo de diseño (o en las amplitudes del espectro de diseño), contenido de frecuencias, duración y variación temporal del mismo, se puede concluir que las estimaciones obtenidas con los dos métodos son, en promedio, satisfactorias en este tipo de estructuras.

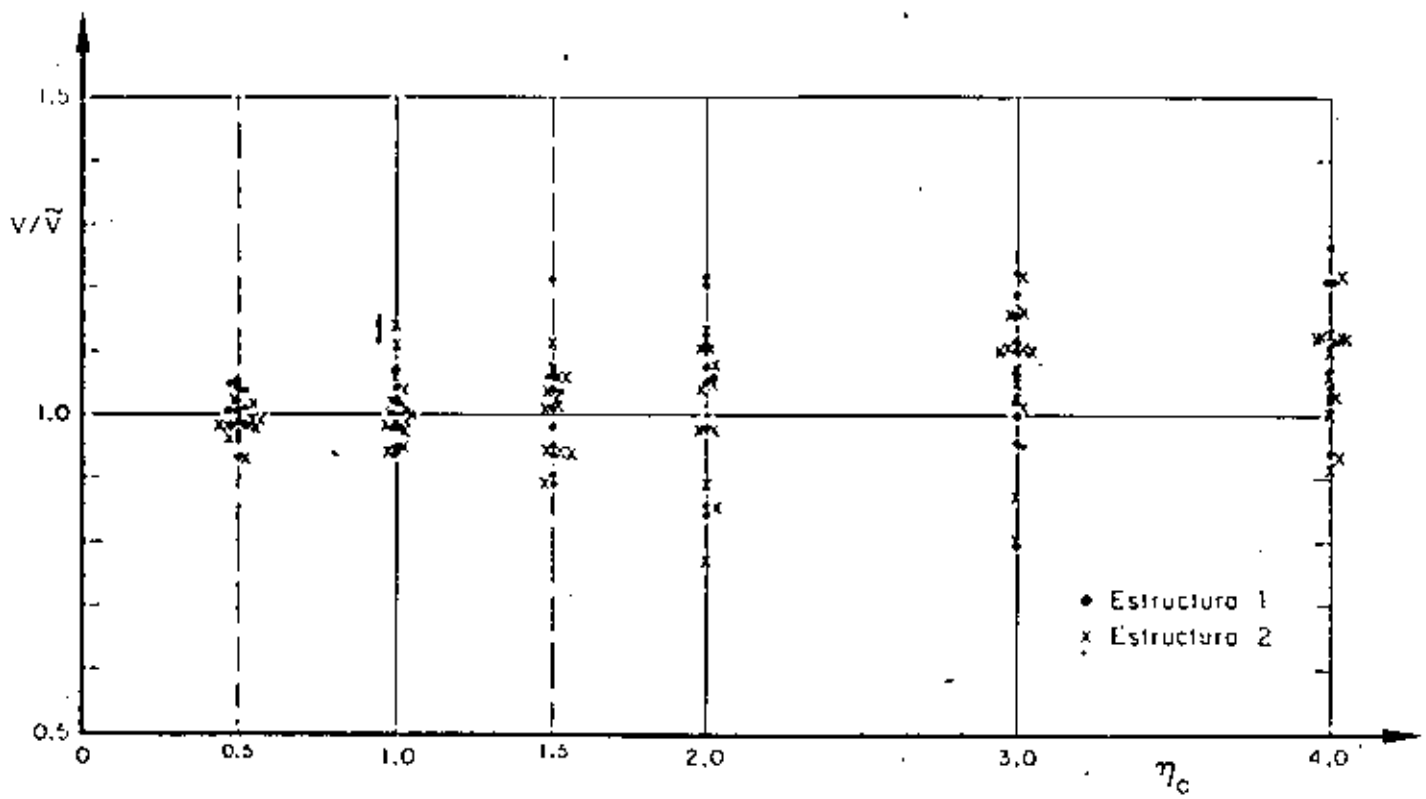

Fig 21. Fuerzas cortantes normalizadas estimadas con el método 2, para $\zeta = 0.10$. Problema de cabecco

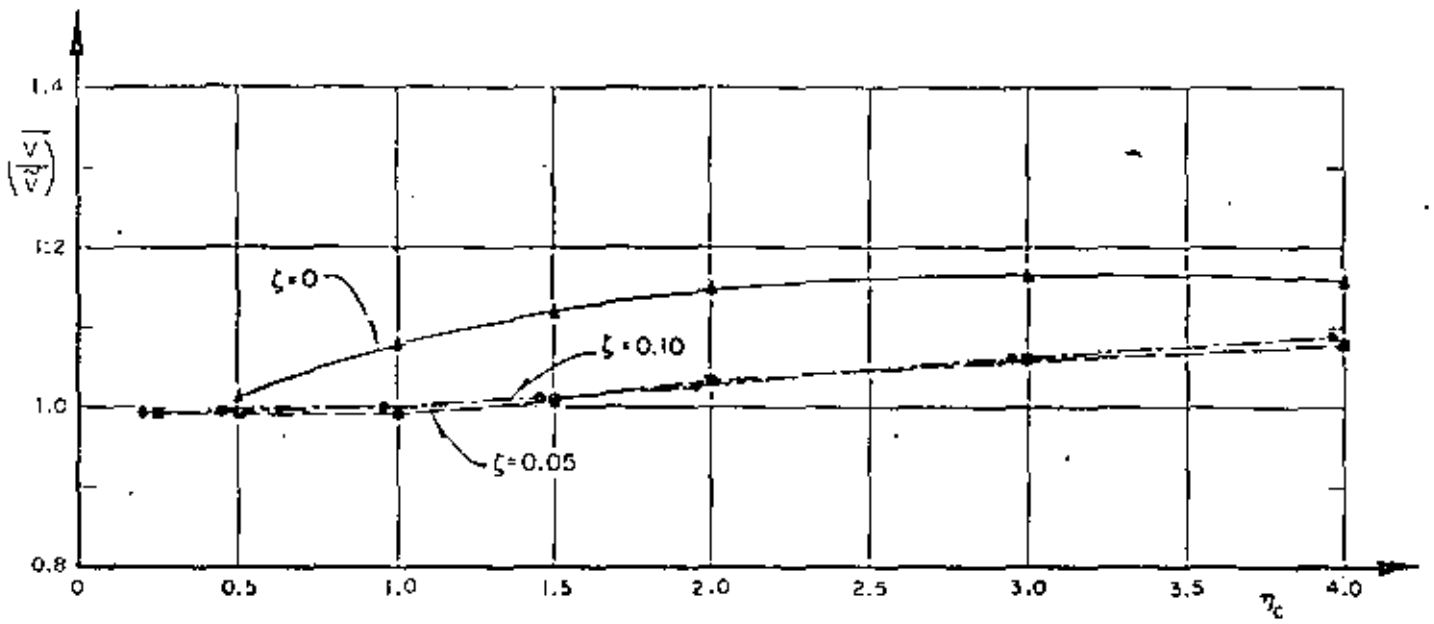

Fig 22. Variación con η_c de los promedios de las fuerzas cortantes estimadas con el método 2. Problema de cabeceo

2.3 Resultados del problema de traslación (caso 3)

Para estudiar este problema se escogieron como parámetros:

=	$(k_2/m_2)/(k_1/m_1)$
T_1	periodo fundamental
ζ	fracción de amortiguamiento respecto al crítico en ambos modos de vibración
m_2/m_1	relación de masas

Los valores que se asignaron a η_t fueron 0.1, 0.2, 0.5, 1.0, 1.5 y 3; a T_1, 0.3, 1.0 y 4.0 seg; a ζ, 0, 0.05 y 0.10; y a m_2/m_1, 0.5 1.0 y 2.0

Los resultados se analizaron mediante gráficas con η_1 o T_1 en el eje de las abscisas, y cocientes de las fuerzas cortantes exactas entre las estimadas en el eje de las ordenadas (fuerzas cortantes normalizadas). Debido a que los resultados no difirieron mucho de los de cabeceo, se empleó únicamente un sismo como excitación. Las conclusiones a que se llegó son:

— Las estimaciones que se obtienen con los métodos 1 y 2 son prácticamente iguales, debido a que los valores de las frecuencias de vibración no resultan muy cercanas entre sí en cada caso, lo cual hace que las $c_{1,2}^2$ (ec 1.3) resulten grandes y, por tanto, que el término de las ecs A.36 y A.37 que las incluye sea muy pequeño, en cuyo caso las ecs A.34 y A.35 son casi iguales a las ecs A.36 y A.37, respectivamente.

Lo se observó aun cuando se estudiaron casos adicionales de m_2/m_1 y η_t, para los cuales el radical de la ec A.29 fue mínimo, con lo cual hubo las diferencias mínimas posibles entre las dos frecuencias fundamentales y, por tanto, los valores más pequeños de $c_{1,2}^2$. Esto ocurre cuando

$$\eta_t = \frac{1 - m_2/m_1}{(1 + m_2/m_1)^2}, \text{ si } m_2/m_1 < 1$$

Dichos casos adicionales fueron: $m_2/m_1 = 0.2$ con $\eta_t = 0.555$; $m_2/m_1 = 0.5$ con $\eta_t = 0.222$, y $m_2/m_1 = 0.8$ con $\eta_t = 0.062$. En estos, la diferencia máxima que se obtuvo entre los resultados de los dos métodos fue de 13 por ciento, siendo mejores los del método 2

— Las estimaciones normalizadas son estadísticamente independientes del periodo fundamental, T_1, con nivel de confianza de 95 por ciento

— En la fig 23 se observa que las estimaciones de V_1 y V_2 tienen, en promedio, errores muy parecidos, por lo que en las conclusiones no es necesario hacer distinciones entre ellas

— La respuesta se sobrestima solamente en 30 por ciento de los casos. El error máximo en exceso que se observó fue 46 por ciento, y en defecto 41 por ciento. El coeficiente de variación para $\zeta = 0.10$ alcanzó 12 por ciento

— En la fig 24 se observa que los promedios de las estimaciones con $\zeta = 0.05$ y 0.10 son mejores que las que corresponden a $\zeta = 0$, lo cual hace pensar que las conclusiones obtenidas en la ref 5 respecto a $\zeta = 0$ no pueden generalizarse para $\zeta > 0$

— Los promedios globales de las fuerzas cortantes normalizadas fueron, para $\zeta = 0$, 1.15; para $\zeta = 0.05$, 1.04, y en cuanto a $\zeta = 0.10$, 1.04. Además, se observó que respecto a $\zeta = 0.05$ y 0.10, los resultados son muy similares, es decir, son independientes de ζ si $\zeta \geq 0.05$

— Las medias de los resultados normalizadas son estadísticamente independientes de la relación de masas, m_2/m_1, con un nivel de confianza de 95 por ciento, pero los casos especiales de m_2/m_1 y η_t indicados anteriormente tuvieron mayor dispersión

— Para $\zeta = 0.05$ y 0.10, las estimaciones normalizadas son estadísticamente independientes de η_t, con un nivel de confianza de 95 por ciento, como puede apreciarse en la fig 24 en la que aparecen únicamente los resultados del método 2. Para $\zeta = 0$ esta hipótesis no se aceptó

— Por la misma razón indicada en el último párrafo de conclusiones del problema de cabeceo, las estimaciones obtenidas con ambos métodos son en promedio satisfactorias en este tipo de estructuras

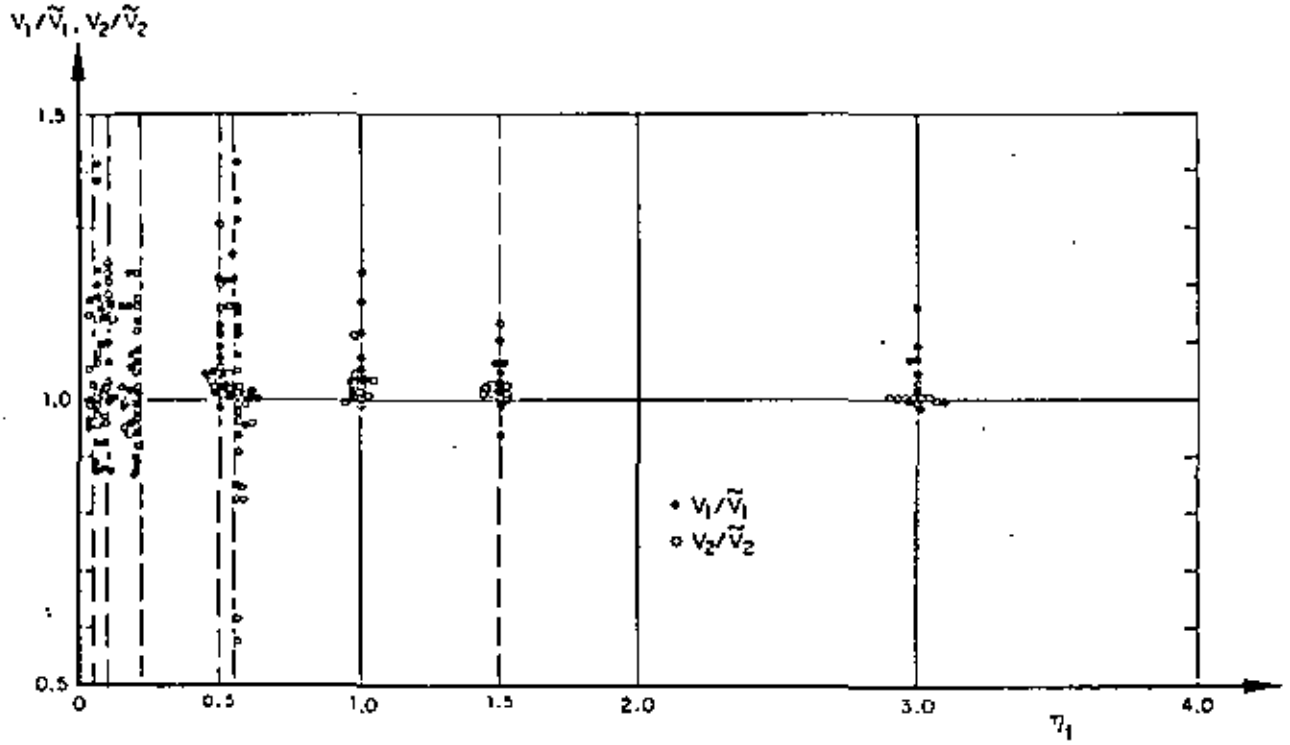

Fig 23. Fuerzas cortantes estimadas con el método 2, para $\zeta = 0.10$. Problema de traslación

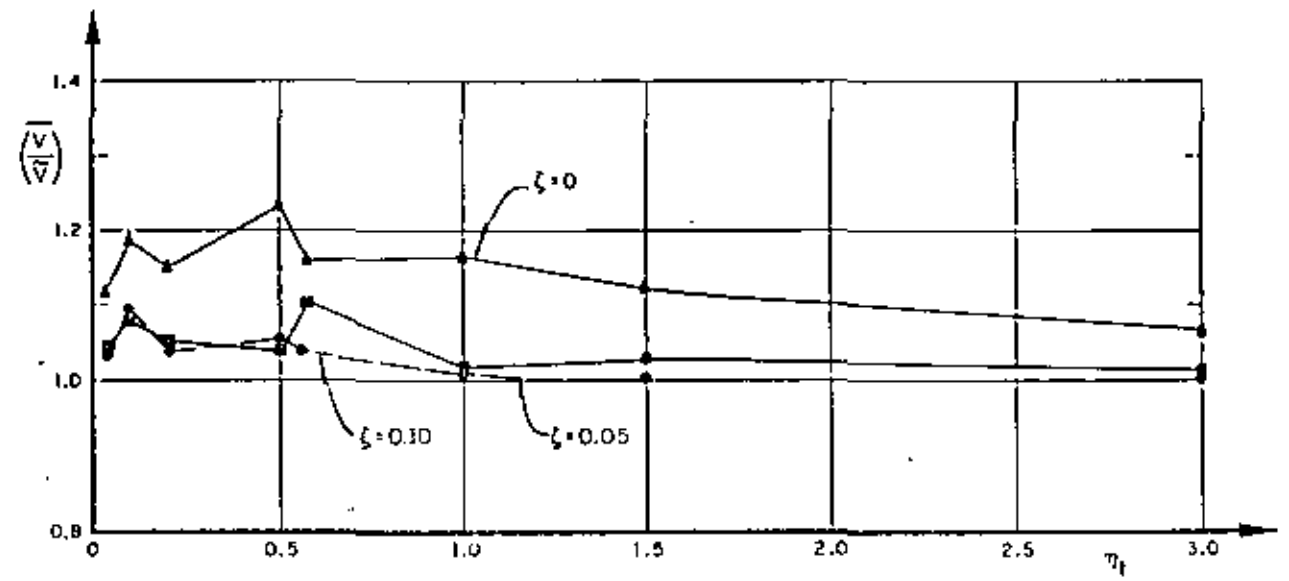

Fig 24. Variación con η_t de los promedios de las fuerzas cortantes estimadas con el método 2. Problema de traslación

3. CONCLUSIONES

El resumen de las conclusiones obtenidas de los tres problemas estudiados es:

En cabeceo y traslación:

— En promedio las estimaciones normalizadas de las respuestas máximas logradas con los métodos 1 y 2 son satisfactorias y prácticamente iguales; esto último debido a que $c^2_{12} >> 0$

— La respuesta se subestimó con mayor frecuencia que lo que se sobrestimó, reduciéndose el error al considerar amortiguamiento en la estructura. Además, los valores exactos divididos entre los estimados fueron estadísticamente independientes de T_1 y η_c o η_1, así como del tipo de respuesta que se trate (momento de cabeceo o fuerza cortante)

En torsión:

— Las conclusiones sí difieren al tomar en cuenta el momento torsionante o la fuerza cortante. Además, debido a que en algunos casos c^2_{12} es pequeña, los dos métodos dan resultados diferentes

— Las estimaciones del momento torsionante al considerar amortiguamiento estructural nulo dependen en gran medida de la relación de frecuencias, η. Además, estos difieren al usar el método 1 o el 2, siendo más aproximados los del 1 para valores de η comprendidos en el intervalo o $0.5 \leqslant \eta \leqslant 1.5$ o muy parecidos fuera de él

— Para los tres amortiguamientos estudiados, los resultados del método 2 son estadísticamente independientes de η, no así los del 1; son mejores los del método 2 cuando $\zeta = 0.05$ y 0.10

— Cuando se tenga $0.5 \leqslant \eta \leqslant 2$, se recomienda usar el método 2; en los demás casos es indistinto el empleo de cualquiera de los dos métodos

— La relación de excentricidad dinámica a excentricidad estática se subestima en las disposiciones del Reglamento de Construcciones del Distrito Federal, siendo esto más cuando el valor de η queda comprendido entre 0.8 y 2. En particular, para $0.9 \leqslant \eta \leqslant 1.1$ esta relación vale, en promedio, 4.6 para $\zeta = 0.05$ y 2.7 para $\zeta = 0.10$. De lo anterior se concluye que es necesario realizar estudios exhaustivos sobre este aspecto, considerando vibración torsional en estructuras de varios pisos y con comportamiento inelástico

— Las distribuciones de probabilidades del cociente del valor exacto sobre el estimado son normales con desviación estándar cercana a 0.16 y media comprendida en el intervalo 1 ± 0.12 (fig 19)

APENDICE

A.1 ANALISIS DINAMICO DE UNA ESTRUCTURA SUJETA A TORSION

La fig A.1 representa un edificio de un piso, de forma arbitraria, con la línea del centro de torsión (CT) al centro de gravedad (CG) perpendicular a la dirección del sismo considerado.

En dicha figura se tiene que

m masa total del sistema

J momento polar de masa respecto al centro de gravedad

L_t rigidez torsional respecto al centro de torsión

K rigidez lineal en la dirección del movimiento

e_s excentricidad estática

b dimensión de la estructura en dirección Y

$c = e_s/b$

Considerando que la rigidez torsional respecto al centro de gravedad es

$$L = L_t + K e_s^2$$

y aplicando el principio de D'Alambert para obtener las ecuaciones de equilibrio del sistema en vibraciones libres, se llega al siguiente sistema de ecuaciones diferenciales lineales de segundo orden (ref 8)

$$\begin{aligned} m\ddot{z} + K(z - e_s \Phi) &= 0 \\ J\ddot{\Phi} + L\Phi - K e_s z &= 0 \end{aligned} \qquad (A.1)$$

Sustituyendo en la ec A.1 a $\ddot{z} = -\omega^2 z$ y $\ddot{\Phi} = -\omega^2 \Phi$ (por ser vibraciones libres), donde ω es la frecuencia circular natural del sistema, y resolviendo el sistema de ecuaciones algebraicas resultante, se obtiene la ecuación característica:

$$\lambda^4 - \lambda^2(1 + \eta) + \eta - c^2/j^2 = \qquad (A.2)$$

donde $\lambda^2 = \omega^2/(k/m)$, $j^2 = J/(mb^2)$ y $\eta = (L/J)/(K/m)$. Las raíces de la ec A.2 son

$$\lambda^2_{1,2} = \frac{\eta + 1}{2} \pm \sqrt{\frac{(\eta - 1)^2}{4} + \frac{c^2}{j^2}} \qquad (A.3)$$

mientras que los vectores de las configuraciones modales son

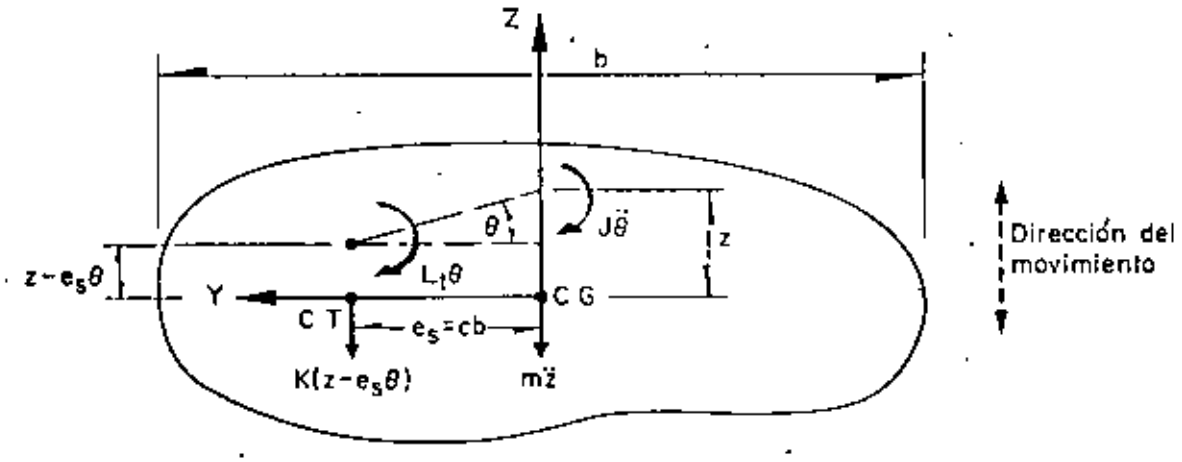

Fig A.1. Diagrama de cuerpo libre de una estructura sujeta a torsión y traslación (vista superior)

$$\begin{bmatrix} z_n \\ \\ \Phi_n \end{bmatrix} = \begin{bmatrix} 1 \\ \\ 1-\lambda_n^2 \\ cb \end{bmatrix} ; n = 1, 2 \qquad (A.4)$$

En términos de las raíces $\lambda_{1,2}^2$ de la ec A.3, se puede demostrar (ref 8) que los coeficientes de participación de los modos 1 y 2 (las proporciones en que contribuyen los modos a la respuesta total del sistema) se encuentran dados por

$$C_n = \frac{c^2}{c^2 + (1-\lambda_n^2)^2 j^2} ; n = 1, 2 \qquad (A.5)$$

Ahora, si se suponen conocidas las aceleraciones espectrales de cada modo, a_n, la fuerza cortante máxima vale

$$V_n = m\, a_n\, C_n ; n = 1, 2 \qquad (A.6)$$

y el momento torsionante máximo respecto al centro de torsión es

$$M_n \frac{(1-\lambda_n^2)\, J\, V_n}{cbm} ; n = 1, 2 \qquad (A.7)$$

Una vez conocidos los valores de V_1, V_2, M_1 y M_2, la aplicación de la ec 1.2 conduce a la estimación de la fuerza cortante y del momento torsionante máximos mediante el método 2; ellos son, respectivamente

$$\bar{V} = \sqrt{V_1^2 + V_2^2 + 2\frac{V_1\, V_2}{1+\epsilon_{12}^2}} \qquad (A.8)$$

$$\bar{M} = \sqrt{M_1^2 + M_1^2 - 2\frac{M_1\, M_2}{1+\epsilon_{12}^2}} \qquad (A.9)$$

donde ϵ_{ij}^2 se obtiene aplicando la ec 1.3. El signo negativo asociado al doble producto que aparece en la ec A.9 se debe a que las funciones de transferencia de los momentos en el primero y segundo modos tienen signo contrario, ya que el factor $(1 - \lambda_n^2)$ que aparece en la ec A.7 es positivo para el primer modo (n = 1) y negativo para el segundo (n = 2), lo cual se demuestra como sigue:

De la ec A.3

$$\lambda_1^2 = \frac{\eta+1}{2} - \sqrt{\frac{(\eta-1)^2}{4} + \frac{c^2}{j^2}}$$

por lo que

$$\lambda_1^2 < \frac{\eta+1}{2} - \frac{\eta-1}{2} = 1$$

Análogamente

$$\lambda_2^2 = \frac{\eta+1}{2} + \sqrt{\frac{(\eta-1)^2}{4} + \frac{c^2}{j^2}}$$

de ahí que, si $\eta \geq 1$

$$\lambda_2^2 \geq \frac{\eta + 1}{2} + \frac{\eta - 1}{2} = \eta$$

o, si $\eta \leq 1$

$$\lambda_2^2 \geq \frac{\eta + 1}{2} + \frac{1 - \eta}{2} = 1$$

En consecuencia, $(1 - \lambda_1^2) \geq 0$ y $(1 - \lambda_2^2) \leq 0$

Además, según el Reglamento del Distrito Federal (método 1) las respuestas dinámicas máximas del mismo sistema estarían dadas por (ec 1.1)

$$\tilde{V} = \sqrt{V_1^2 + V_2^2} \qquad \text{(A.10)}$$

$$\tilde{M} = \sqrt{M_1^2 + M_2^2} \qquad \text{(A.11)}$$

Finalmente, por el método exacto, las resouestas máximas totales, V y M, se obtienen localizando los máximos en el tiempo, t, de las sumas de las respuestas (cortante o momento, según sea el caso) en los modos 1 y 2, es decir,

$$V = \text{Máx} \left| \left\{ m C_1 a_1 (t) + m C_2 a_2 (t) \right\} \right| =$$

$$= \text{Máx} \left| \left\{ V_1 (t) + V_2 (t) \right\} \right| \qquad \text{(A.12)}$$

$$M = \text{Máx} \left| \left\{ \Gamma_1 V_1 (t) + \Gamma_2 V_2 (t) \right\} \right| \qquad \text{(A.13)}$$

donde

$$\Gamma_n = \frac{(1 - \lambda_n^2) J}{cbm} \; ; \; n = 1, 2 \qquad \text{(A.14)}$$

A.2 ANALISIS DINAMICO DE UNA ESTRUCTURA SUJETA A CABECEO

Es frecuente que en la práctica se presenten estructuras constituidas por una hilera de columnas o una sola columna que sostiene una losa o un cascarón (péndulos invertidos), tal como la que aparece en la fig A.2. La respuesta dinámica de una estructura de este tipo se debe obtener (ref 9) considerando el efecto que la inercia rotacional de la cubierta induce en el movimiento total del sistema.

En la fig A.2 se empleó la notación:

- W peso de la cubierta más la parte tributaria de la columna
- m W/g
- g aceleración de la gravedad
- J_c momento de inercia de la masa de la cubierta respecto al eje Z
- E módulo de elasticidad del material de la columna
- I_c momento de inercia de la sección transversal de la columna respecto al eje Z
- CG centro de gravedad de la cubierta
- L distancia del suelo al centro de gravedad

El diagrama de cuerpo libre de la estructura anterior aparece en la fig A.3, en la cual se tiene que (ref 9)

- K rigidez por traslación $= 3EI_c/L^3$
- K_r rigidez por rotación $= EI_c/L$
- x desplazamiento del centro de gravedad de la cubierta
- Φ rotación del centro de gravedad de la cubierta

$\alpha = (x - k_r \gamma \phi)/k$

$\beta = (\phi - k \gamma x)/k$

$\gamma = L^3/2 EI_c$

$k = 1 - K L^3/4EI_c = 0.25$

Las ecuaciones diferenciales de movimiento correspondientes al diagrama de cuerpo libre de la estructura son

$$\begin{aligned} m \ddot{x} + (Kx - K K_r \gamma \Phi)/k &= 0 \\ J_c \ddot{\Phi} + (K_r \Phi - K K_r \gamma x)/k &= 0 \end{aligned} \qquad \text{(A.15)}$$

Considerando que se satisfacen las relaciones $\ddot{x} = -\omega^2 x$ y $\ddot{\delta} = -\omega^2 \theta$, donde ω es la frecuencia circular natural de vibración de la estructura, y resolviendo el sistema de ecuaciones A.15, se obtiene la ecuación característica

$$\omega^4 - \frac{K J_c + m K_r}{m J_c k} \omega^2 + \frac{K K_r}{4 m J_c k^2} = 0 \qquad \text{(A.16)}$$

que es una ecuación de segundo grado en ω^2. Si se efectúan algunas transformaciones algebraicas y se considera que

- $K/m = p^2$ cuadrado de la frecuencia circular natural por traslación

$K_t/J_c = \Omega^2$ cuadrado de la frecuencia circular natural por rotación

$\lambda = \omega^2/p^2$

$\lambda_c = \Omega^2/p^2$

se llega a

$$\gamma_{1,2} = 2\,(1 + \eta_c \pm \sqrt{(1+\eta_c)^2 - \eta_c}) \qquad \text{(A.17)}$$

Por otra parte, los vectores de las configuraciones modales son

$$\begin{bmatrix} x_n \\ \\ \Phi_n \end{bmatrix} = \begin{bmatrix} 1 \\ \\ \dfrac{4-\lambda_n}{2L} \end{bmatrix} \quad ; n = 1, 2 \qquad \text{(A.18)}$$

Se puede demostrar (ref 9) que los coeficientes de participación correspondientes a los modos 1 y 2 se encuentran dados por la expresión

$$C_n = \frac{x_n\, m}{x_n^2\, m + \Phi_n^2\, J_c}; \; n = 1, 2 \qquad \text{(A.19)}$$

Partiendo del hecho de que se conocen las aceleraciones espectrales de cada modo, a_n, la fuerza cortante máxima y el momento máximo de cabeceo correspondientes valen

$$V_n = m\, a_n\, C_n\, x_n = m\, a_n\, C_n ; n = 1, 2 \qquad \text{(A.20)}$$

$$M_n = J\, a_n\, C_n\, \Phi_n = J\, a_n\, C_n \frac{4-\lambda_n}{2L} =$$

$$= \frac{(4-\lambda_n)\, J_c}{2\, Lm}\, V_n \qquad \text{(A.21)}$$

Las respuestas dinámicas de la estructura de acuerdo con los criterios del Reglamento de Construcciones del D. F. (método 1) y de Rosenblueth (método 2), se obtienen haciendo uso de las ecuaciones

$$\tilde{V} = \sqrt{V_1^2 + V_2^2} \qquad \text{(A.22)}$$

$$\tilde{M} = \sqrt{M_1^2 + M_2^2} \qquad \text{(A.23)}$$

$$\tilde{V} = \sqrt{V_1^2 + V_2^2 + 2\,\frac{V_1\, V_2}{1+\epsilon_{12}^2}} \qquad \text{(A.24)}$$

$$\tilde{M} = \sqrt{M_1^2 + M_2^2 - 2\,\frac{M_1\, M_2}{1+\epsilon_{12}^2}} \qquad \text{(A.25)}$$

donde ϵ_{12}^2 se calcula mediante la ec 1.3. El signo menos aparece en la ec A.25 debido a que la función de transferencia del segundo modo es de signo opuesto a la del primero, ya que se puede demostrar, a partir de la ec A.17, que $\lambda_1 \leq 4$ y $\lambda_2 \geq 4$, por lo que el factor $4 - \lambda_n$ que aparece en la ec A.21 tiene signo positivo en el modo 1, y negativo en el 2.

La respuesta dinámica exacta se obtiene utilizando las expresiones

$$V = \text{Máx} \left| \left\{ C_1\, m\, x_1\, a_1(t) + C_2\, m\, x_2\, a_2(t) \right\} \right| \qquad \text{(A.26)}$$

$$M = \text{Máx} \left| \left\{ C_1\, J_c\, \Phi_1\, a_1(t) + C_2\, J_c\, \Phi_2\, a_2(t) \right\} \right| \qquad \text{(A.27)}$$

A.3 ANALISIS DINAMICO DE UNA ESTRUCTURA SUJETA A TRASLACION

Consideremos ahora el caso de una estructura de cortante de dos pisos, en la cual no existe rotación en los planos horizontales en los niveles de los pisos (fig A.4).

La ecuación matricial de equilibrio de este sistema es (ref 10)

$$\begin{bmatrix} m_1\,\omega^2 - K_1 - K_2 & K_2 \\ \\ K_2 & m_2\,\omega^2 - K_2 \end{bmatrix} \begin{bmatrix} z_1 \\ \\ z_2 \end{bmatrix} = |0| \qquad \text{(A.28)}$$

donde m_1 y m_2 son las masas concentradas en los niveles 1 y 2, y K_1 y K_2 son las rigideces de los entrepisos 1 y 2, respectivamente.

Partiendo de este sistema de ecuaciones y haciendo $\eta_1 = (K_2/m_2)/(K_1/m_1)$ y $\lambda = \omega^2/(K_1/m_1)$, se obtienen las raíces

$$\lambda_{1,2}^2 = \frac{1}{2}\left[\eta_1 + (m_2/m_1)\,\eta_1 + 1\right] \pm$$

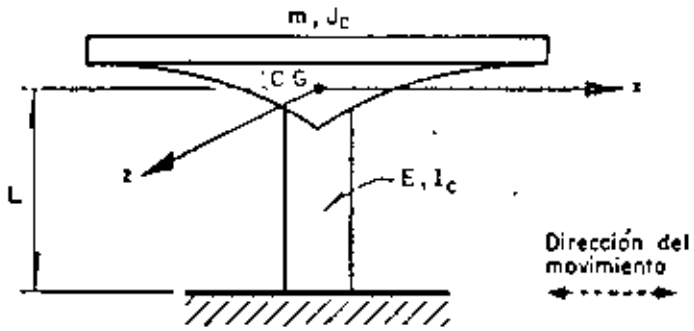

Fig A.2. Estructura en forma de péndulo invertido (vista lateral)

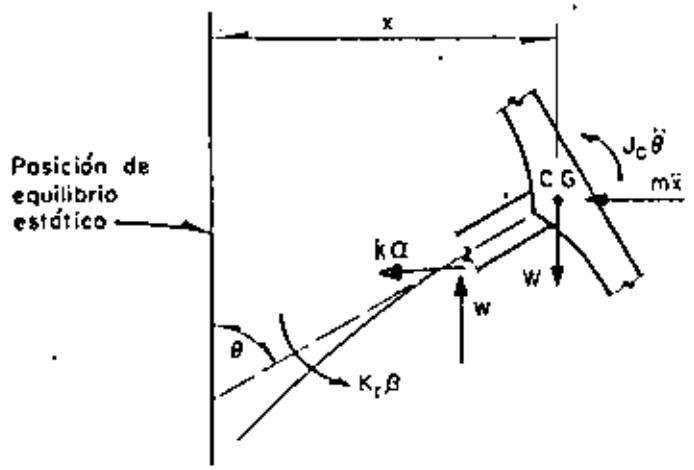

Fig A.3. Diagrama de cuerpo libre de la estructura de la fig A.2

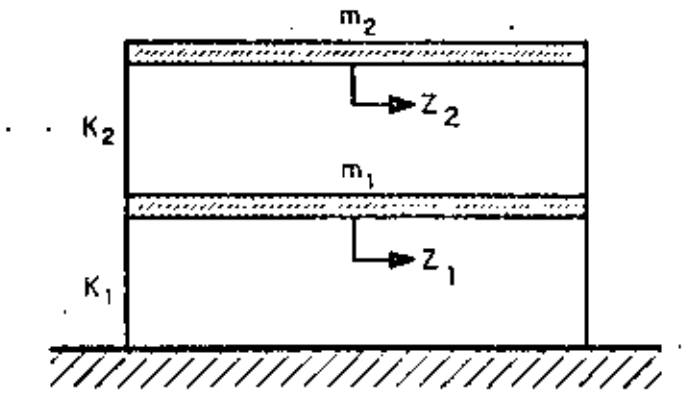

Fig A.4. Estructura de dos pisos sujeta a traslación (vista lateral)

$$\pm\frac{1}{2}\sqrt{\left[\eta_1+(m_2/m_1)\,\eta_1+1\right]^2-4\,\eta_1} \qquad \text{(A.29)}$$

Además, los vectores de configuraciones modales resultan ser

$$\begin{bmatrix} z_{1,n} \\ z_{2,n} \end{bmatrix} = \begin{bmatrix} 1 \\ 1+\dfrac{(K_1/m_1)-\omega_n^2}{\eta_1\,(K_1/m_1)(m_2/m_1)} \end{bmatrix}; \; n=1,2 \qquad \text{(A.30)}$$

Además, se puede demostrar (ref 10) que los coeficientes de participación de los modos 1 y 2 se encuentran dados por

$$C_n=\frac{z_{1,n}+(m_2/m_1)\,z_{2,n}}{z_{1,n}^2+(m_2/m_1)\,z_{2,n}^2};\; n=1,2 \qquad \text{(A.31)}$$

Si se conocen las aceleraciones espectrales de cada modo, a_n, la fuerza cortante máxima correspondiente al entrepiso 1 en cada modo vale

$$V_{1,n}=C_n\,a_n\,(m_1\,z_{1,n}+m_2\,z_{2,n})\;;\; n=1,2 \qquad \text{(A.32)}$$

en tanto que la fuerza cortante máxima correspondiente al entrepiso 2 es

$$V_{2,n}=C_n\,a_n\,m_2\,z_{2,n}\;;\; n=1,2 \qquad \text{(A.33)}$$

Ya conocidos los valores de $V_{1,n}$ y $V_{2,n}$, las respuestas máximas dinámicas totales de la estructura estimadas con los métodos 1 y 2 se calculan haciendo uso de las fórmulas

$$\hat{V}_1=\sqrt{V_{1,1}^2+V_{1,2}^2} \qquad \text{(A.34)}$$

$$\hat{V}_2=\sqrt{V_{2,1}^2+V_{2,2}^2} \qquad \text{(A.35)}$$

$$\tilde{V}_1=\sqrt{V_{1,1}^2+V_{1,2}^2+2\,\frac{V_{1,1}\,V_{1,2}}{1+\epsilon_{12}^2}} \qquad \text{(A.36)}$$

$$\tilde{V}_2=\sqrt{V_{2,1}^2+V_{2,2}^2-2\,\frac{V_{2,1}\,V_{2,2}}{1+\epsilon_{12}^2}} \qquad \text{(A.37)}$$

donde ϵ_{12}^2 se calcula mediante la ec 1.3

Finalmente, las respuestas máximas dinámicas de la estructura en cuestión se pueden obtener mediante el método exacto haciendo uso de las ecuaciones

$$V_1 = \text{Máx} \left| \left\{ \sum_{n=1}^{2} C_n \, a_n(t) \left[m_1 \, z_{1,n} + m_2 \, z_{2,n} \right] \right\} \right| \qquad \text{(A.38)}$$

$$V_2 = \text{Máx} \left| \sum_{n=1}^{2} C_n \, a_n(t) \, m_2 \, z_{2,n} \right| \qquad \text{(A.39)}$$

REFERENCIAS

1. E. Rosenblueth, "A Basis for Aseismic Design", Tesis doctoral, *Universidad de Illinois*, Urbana (1951)

2. E. Rosenblueth, "Sobre la respuesta sísmica de estructuras de comportamiento lineal", *Segundo Congreso Nacional de Ingeniería Sísmica*, Veracruz (1968)

3. "Reglamento de Construcciones para el Distrito Federal", *Diario Oficial*, México, D. F. (feb 1966)

4. "Los Angeles City Building Code", Los Angeles, Cal. (1966)

5. R. Husid, "Estimación de la respuesta máxima de tranques de tierra sometidos a la acción de terremotos", *Tercer Congreso Nacional de Ingeniería Sísmica*, Acapulco (1971)

6. O. A. Rascón, "Modelo estocástico para simular registros de temblores en terreno duro", Tesis doctoral, *Facultad de Ingeniería, UNAM*, México, D. F. (1968)

7. M. Chávez, O. A. Rascón y L. Alonso, "Un nuevo método para corrección de la línea base de registros de temblores", *Tercer Congreso Nacional de Ingeniería Sísmica*, Acapulco (1971)

8. J. Elorduy, y E. Rosenblueth, "Torsiones sísmicas en edificios de un piso", Informe 164. *Instituto de Ingeniería, UNAM*, México, D. F. (1968)

9. O. A. Rascón, "Efectos sísmicos en estructuras en forma de péndulo invertido", *Revista de la Sociedad Mexicana de Ingeniería Sísmica*, Vol 3, No 1, México, D. F. (1965), pp 8-16

10. E. Rosenblueth, y L. Esteva, "Folleto complementario: diseño sísmico de edificios, proyecto de Reglamento de Construcciones en el Distrito Federal", *Ediciones Ingeniería*, México, D. F. (1962)

11. T. Naylor et al, "Técnicas de simulación en computadoras", *Limusa-Wiley*, México, D. F. (1971)

12. J. Hammersley y D. Handscomb, "Monte-Carlo Methods", *Methuen*, Londres (1964)

DIVISION DE EDUCACION CONTINUA
FACULTAD DE INGENIERIA U.N.A.M.

CURSOS DE INGENIERIA CIVIL EN EL PROYECTO DE PLANTAS HIDROELECTRICAS.

INGENIERIA SISMICA

PROF. DR. OCTAVIO A. RASCON CHAVEZ.

AGOSTO, 1981.

5. EJEMPLOS DE ANALISIS SISMICO DE ACUERDO CON EL REGLAMENTO DE CONSTRUCCIONES PARA EL DISTRITO FEDERAL - 1977

Por Dr. Octavio A. Rascón Ch.

5.1 EJEMPLO DEL METODO SIMPLIFICADO

La figura siguiente muestra esquemáticamente las plantas, alturas y pesos de una estructura. Se verificará que se satisface las condiciones que se exigen en el artículo 238 y se efectuará el análisis mediante el método simplificado.

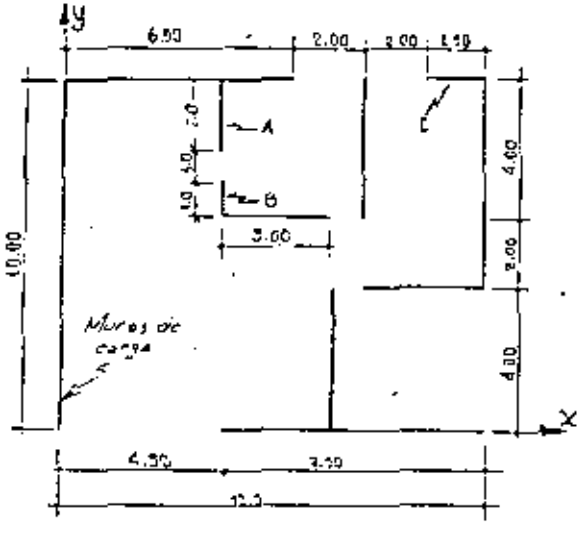

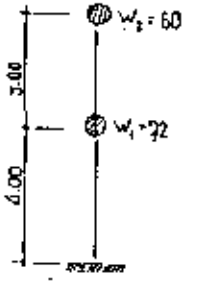

Nota: las distancias están en metros y los pesos en toneladas.

Los muros son de tabique recocido, de 14 cm de espesor, cuya resistencia al esfuerzo cortante es 1.5 kg/cm²

PLANTA DE DOS PISOS

Observando la planta se puede afirmar que más del 75% de las cargas verticales están soportadas por los muros. Se aprecia también que existen en cada dirección dos muros perimetrales paralelos; las longitudes en que estos muros están ligados a las losas son, en la dirección X: 7.50 m y 6.50 m, mayores que 0.5 x 12 = 6.00 m, y en la dirección Y, 10.00 m y 6.00 m, mayores que 0.5 x 10 = 5.00 m. La relación entre la longitud y anchura de la planta es 12/10 = 1.2, menor que 2.0; la relación entre la altura y la dimensión mínima en planta es 7/10 = 0.7, menor que 1.5 y la altura del edificio es menor que 13 m. En conclusión se puede aplicar el método simplificado en ambas direcciones.

Paso 1. Se determina el coeficiente sísmico de acuerdo con la tabla del artículo 239. Suponiendo que la estructura se edificará en la zona I y teniendo en cuenta que la altura es 7 m, encontramos que el coeficiente sísmico es 0.08

Paso 2. Se calculan las fuerzas y cortantes sísmicas, de la manera especificado en el artículo 240, es decir, como se indica en la tabla siguiente:

Nivel o entrepiso i	W_i ton	h_i m	$W_i h_i$ ton-m	P_i ton	V_i ton
2	60	7	420	6.30	6.32
1	72	4	288	4.32	10.62
Sumas	132		708	10.62	

donde: h_i es la altura del nivel i respecto a la base,

$$P_i = \frac{W_i h_i}{\Sigma W_i h_i}(0.08\Sigma W_i) + \frac{W_i h_i}{708}(.08 \times 132) = 0.015\, W_i h_i$$

Las fuerzas P_i actúan en las direcciones X y Y

Paso 3. Se calculan las fuerzas resistentes en las direcciones X, Y. Los muros cuya relación $\frac{h}{L}$ sea menor que 1.33 tendrán una capacidad de 1.5 kg/cm² (sin ninguna reducción), en la planta baja esto ocurre para muros con una longitud mayor que 4.0/1.33 = 3 m.

En la dirección X hay (6.5+3.0+3.5+7.5) = 20.5 m que cumplen tal condición, y (10.0+4.0+4.0+6.0) = 24 m, en la dirección Y.

Los muros A, B y C tienen L < 3.0 m y sus esfuerzos resistentes se reducen a

$$\sigma_A = 1.5\ (1.33 \times \frac{2.0}{4.0})^2 = 0.66\ kg/cm^2$$

$$\sigma_B = 1.5\ (1.33 \times \frac{1.0}{4.0})^2 = 0.17\ kg/cm^2$$

$$\sigma_C = 1.5\ (1.33 \times \frac{1.5}{4.0})^2 = 0.37\ kg/cm^2$$

La resistencia total en la dirección x es:

$$\frac{2050 \times 14 \times 1.5 + 150 \times 14 \times .37}{1000} = 43.83\ ton$$

y en la dirección Y:

$$\frac{2400 \times 14 \times 1.5 + 200 \times 14 \times 0.66 + 100 \times 14 \times .17}{1000} =$$

52.49 ton

ambas mayores que la fuerza cortante actuante 10.62 ton.

5.2 EJEMPLO DE ANALISIS ESTATICO

En las figuras siguientes se muestran la elevación y las plantas esquemáticas de un hospital de tres niveles que se construirá en la zona de terreno firme del Distrito Federal.

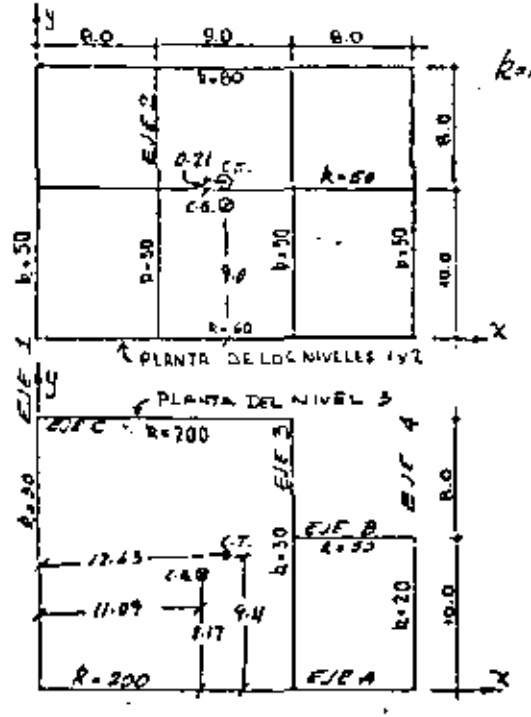

Rigidez de entrepiso

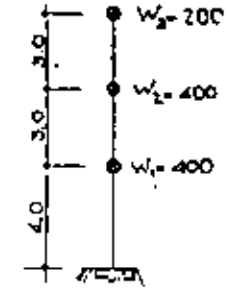

Nota: las distancias están en metros, los pesos en toneladas y las rigideces de entrepiso en toneladas sobre centímetro.

Los detalles constructivos y los materiales que se usarán permiten utilizar Q=4. Se dan los valores de las rigideces de entrepiso de los marcos, los pesos concentrados en los niveles y las dimensiones. Se determinarán las fuerzas cortantes que correspondan a cada marco utilizando el método estático propuesto en el artículo 240 del Reglamento.

Paso 1. Determinación del coeficiente sísmico: el artículo 240 especifica que la relación entre la fuerza cortante en la base V y el peso total W igual a $\frac{c}{Q}$ o a_o, el que sea mayor. El valor de C se obtiene de la tabla del artículo 234 y el de a_o, de la tabla del artículo 236, y son parte de la definición del espectro de diseño sísmico.

Enseguida se indican los valores correspondientes a la zona de terreno firme (zona I) y a un edificio que se va a usar como hospital (construcción del grupo A, según el artículo 232):

$a_o = 0.03$, $c = 0.16$; $C=0.16 \times 1.3=0.208$

Usar $\frac{C}{Q} = \frac{0.208}{4} = 0.052 > a_o$

Paso 2. Cálculo de fuerzas sísmicas en los niveles: según el artículo 240 la fuerza sísmica P_i en el nivel i es igual a $C_i W_i$, donde W_i es el peso de tal nivel y C_i es una constante proporcional a h_i, que es la correspondiente altura con respecto a la base. Digamos:

$$P_i = C_i W_i = a\, h_i W_i$$

Para determinar a se toma en cuenta que

$$\frac{V}{W} = \frac{\Sigma P_i}{\Sigma W_i} = \text{coeficiente sísmico} = S_a$$

$$\therefore S_a = \frac{a \Sigma h_i W_i}{\Sigma W_i} \quad \text{de donde:} \quad a = \frac{S_a \Sigma W_i}{\Sigma h_i W_i}$$

$$\boxed{P_i = \frac{W_i h_i}{\Sigma W_i h_i} S_a \Sigma W_i}$$

El cálculo de las P_i para este ejemplo se presenta en la siguiente tabla

Nivel o entrepiso i	W_i (ton)	h_i (m)	$W_i h_i$	P_i (ton)	V_i (ton)
3	200	10	2000	16.25	16.25
2	400	7	2800	22.75	39.00
1	400	4	1600	13.00	52.00
Sumas	1000		6400	52.00	

$S_a = 0.052$

$P_i = \frac{0.052 \times 1000}{6400} W_i h_i$

$P_i = 0.008125\, W_i h_i$

Paso 3. Determinación de la posición de las fuerzas cortantes, los centros de rigidez de cada piso, y los momentos torsionantes:

Las fuerzas en los niveles P_j están ubicadas en los centros de gravedad de las cargas W_j. Como las fuerzas cortantes son resultado de las fuerzas P_j, su ubicación estará dada por:

$$X_V = \frac{\Sigma P_j X_j}{V} \quad ; \quad Y_V = \frac{\Sigma P_j Y_j}{V}$$

donde $V = \Sigma P_j$ y las sumas son sólo hasta el nivel en que está aplicada la fuerza cortante V. Supondremos en este ejemplo que los centros de gravedad de las cargas coinciden con el centro de gravedad de las áreas de las plantas, es decir que, con referencia a los ejes indicados en las figuras donde se presentan las plantas, las cordenadas de los puntos de aplicación de las fuerzas sísmicas en los niveles son

Nivel j	X_j (m)	Y_j (m)
3	11.09	8.17
1,2	12.50	9.00

En la siguiente tabla se muestran los cálculos para determinar la posición de las fuerzas cortantes.

Nivel o entrepiso	FUERZAS EN DIRECCION X						FUERZAS EN DIRECCION Y					
	P_j	Y_j	$P_j Y_j$	$\Sigma P_j Y_j$	V	Y_V	P_j	X_j	$P_j X_j$	$\Sigma P_j X_j$	V	X_V
3	16.25	8.17	132.76	132.76	16.25	8.17	16.25	11.09	180.21	180.21	16.25	11.09
2	22.75	9.00	204.75	337.51	39.00	8.65	22.75	12.50	284.38	464.59	39.00	11.91
1	13.00	9.00	117.00	454.51	52.00	8.74	13.00	12.50	162.50	627.09	52.00	12.06

El centro de torsión es el punto por el que debe pasar la línea de acción de la fuerza cortante sísmica para que el movimiento relativo de los niveles que limitan el entrepiso sea exclusivamente de traslación. Si esto no ocurre existe torsión o rotación relativa entre tales niveles. Las expresiones para calcular el centro de torsión será, en cada entrepiso:

$$X_T = \frac{\Sigma K_y X}{\Sigma K_y} \quad ; \quad Y_T = \frac{\Sigma K_x Y}{\Sigma K_x}$$

donde K_y son las rigideces de entrepiso de los marcos orientados en la dirección Y, cuya posición está dada por X. K_x son las rigideces de entrepiso de los marcos orientados en la dirección x, cuya posición está dada por Y. Las sumas se refieren a todos los marcos que hay en el entrepiso en la correspondiente dirección

En la siguiente tabla se muestran los cálculos para el ejemplo que estamos tratando.

MARCOS EN LA DIRECCION Y											
ENTRE PISO	EJE 1		EJE 2		EJE 3		EJE 4		ΣK_y	$\Sigma K_y X$	X_T
	K_y	X	K_y	X	K_y	X	X_y	X			
3	30	0	—	—	30	17	20	25	80	1010	12.63
2	50	0	50	8	50	17	50	25	200	2500	12.50
1	50	0	50	8	50	17	50	25	200	2500	12.50

MARCOS EN LA DIRECCION X								
ENTRE-PISO	EJE A		EJE B		EJE C		ΣK_x	$\Sigma K_x Y$	Y_T
	K_x	Y	K_x	Y	K_x	Y			
3	200	0	50	10	200	18	450	4100	9.11
2	60	0	50	10	80	18	190	1940	10.21
1	60	0	50	10	80	18	190	1940	10.21

Para determinar los momentos torsionantes es necesario conocer las excentricidades calculadas de las fuerzas cortantes y añadir las amplificaciones prescritas en el punto VII del art 240. Esto se hace en las siguientes tablas, donde también se calculan los momentos torsionantes.

$e_1 = 1.5\, e_s + 0.1b$

$e_2 = e_s - 0.1b$

SISMO EN DIRECCION X

ENTRE-PISO	Y_v (m)	Y_T (m)	$e_s = Y_v - Y_T$ (m)	b (m)	e_1 (m)	e_2 (m)	V_x (m)	M_{1x} (ton-m)	M_{2x} (ton-m)
3	8.17	9.11	-0.94	18.0	-3.21	0.86	16.25	-52.16	13.98
2	8.65	10.21	-1.56	18.0	-4.14	0.24	39.00	-161.46	9.36
1	8.74	10.21	-1.47	18.0	-4.01	0.33	52.00	-208.52	17.16

SISMO EN DIRECCION Y

ENTRE PISO	X_v (m)	X_T (m)	$e_s = X_v - X_T$ (m)	b (m)	e_1	e_2	V_y	M_{1y}	M_{2y}
3	11.09	12.63	-1.54	25.0	-4.81	0.96	16.25	-78.16	15.6
2	11.91	12.50	-0.59	25.0	-3.39	1.91	39.00	-132.21	74.49
1	12.06	12.50	-0.44	25.0	-3.16	2.06	52.00	-164.32	107.12

PASO 4 .Distribución de las fuerzas cortantes sísmicas en los marcos. La fuerza cortante que debe resistir un marco cualquiera debe ser la suma de dos efectos: el debido a la fuerza cortante del piso actuando en el centro de rigideces y el debido al momento torsionante del piso. Cuando todos los marcos son paralelos a uno de los ejes X o Y, son válidas las siguientes expresiones:

DISTRIBUCION DE FUERZAS CORTANTES DIRECTAS Y POR TORSION

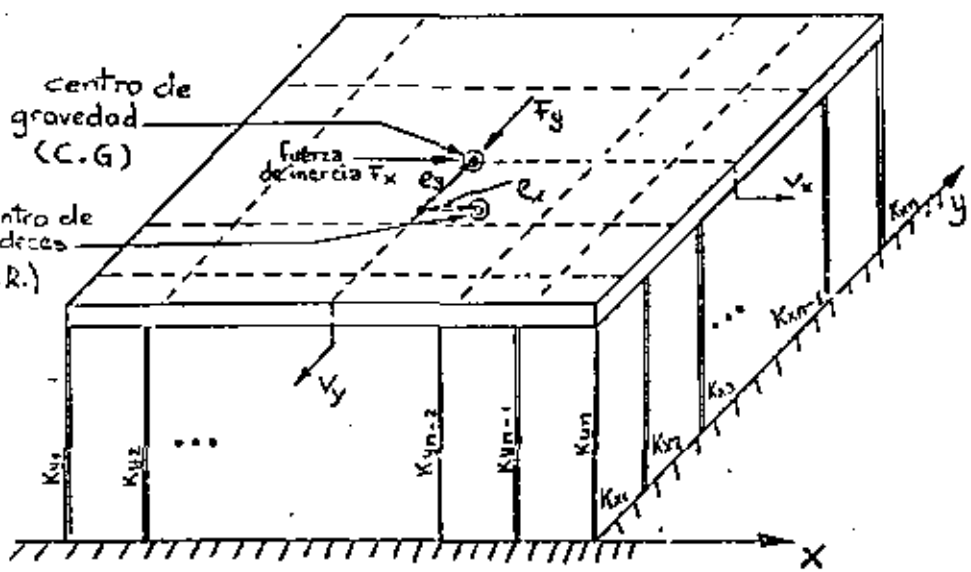

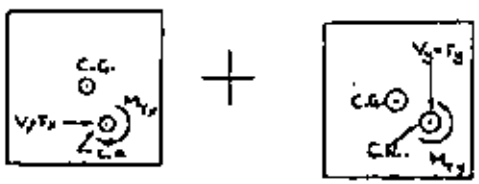

DISTRIBUCION DE LAS FUERZAS CORTANTES EN UN ENTREPISO

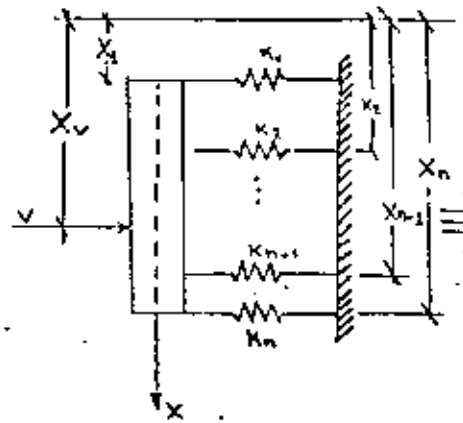

$$\Sigma F_i = K_1\delta + K_2\delta + \ldots + K_n\delta = V = K_{eq}\delta$$

$$\delta\Sigma K_i = \delta K_{eq}$$

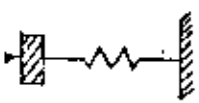

$$K_{eq} = \sum_{i=1}^{n} K_i$$

$$\Sigma M_i = \Sigma F_i X_i = \Sigma K_i \delta X_i = \delta \Sigma K_i X_i = V X_v = K_{eq}\delta X_v$$

$$X_v = \frac{\sum_{i=1}^{n} K_i X_i}{\sum_{i=1}^{n} K_i}$$

← POSICION DEL CENTRO DE RIGIDECES

VEAMOS COMO SE DISTRIBUYEN LAS FUERZAS CORTANTES EN LOS MARCOS

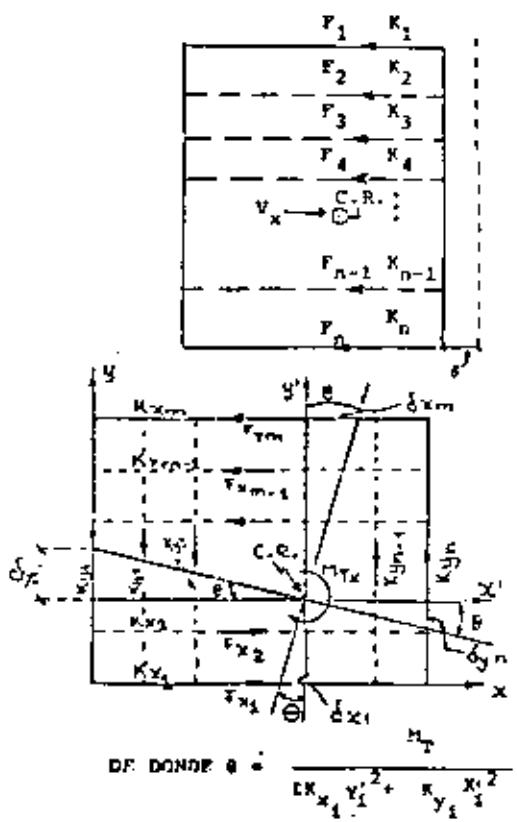

$$F_i = K_i \delta$$

$$\Sigma F_i = \Sigma K_i \delta = V_x \quad \therefore \quad \delta = \frac{V_x}{\Sigma K_i}$$

$$F_i = V_x \frac{K_i}{\sum_{i=1}^{n} K_i}$$

$$F_{x_i} = K_{x_i} \delta_{x_i} = K_{x_i} Y_i' \theta$$

$$F_{x_i} = K_{y_i} \delta_{y_i} = K_{y_i} X_i' \theta$$

$$M_{C.R.} = \Sigma F_{x_i} Y_i' + \Sigma F_{y_i} X_i'$$

$$= \theta(\Sigma K_{x_i} Y_i'^2 + \Sigma K_{y_i} X_i'^2)$$

$$= M_{Tx}$$

DE DONDE $\theta = \dfrac{M_T}{\Sigma K_{x_i} Y_i'^2 + K_{y_i} X_i'^2}$

POR LO QUE

$$F_{x_i} = M_{TX} \frac{K_{x_i} Y_i'}{\Sigma K_{x_i} Y_i'^2 + K_{y_i} X_i'^2}$$

y

$$F_{y_i} = M_{TX} \frac{K_{y_i} X_i'}{\Sigma K_{x_i} Y_i'^2 + \Sigma K_{y_i} X_i'^2}$$

PARA LOS MARCOS PARALELOS A X

1. $V_X \dfrac{K_x}{\Sigma K_x}$ (Sismo en X) Directo

2. $\dfrac{M_y K_x \bar{Y}}{R_o}$ (Sismo en X) torsión

3. $\dfrac{|M_y K_x \bar{Y}|}{R_o}$ (Sismo en Y) torsión

PARA MARCOS PARALELOS A Y

1. $V_Y \dfrac{K_Y}{\Sigma K_Y}$ (Sismo en Y) Directo

2. $\dfrac{M_y K_y \bar{X}}{R_o}$ (Sismo en Y) torsión

3. $\dfrac{|M_x K_y \bar{X}|}{R_o}$ (Sismo en X) torsión

donde $R_o = \Sigma K_x \bar{Y}^2 + \Sigma K_y \bar{X}^2$

$\bar{X}$, $\bar{Y}$ son las coordenadas de los marcos con respecto al centro de torsión: $\bar{X} = X - X_T$

$\bar{Y} = Y - Y_T$

Nótese que las contribuciones directas (1) y las de torsión que se producen en los marcos perpendiculares a la dirección del sismo (3) son siempre positivas. La contribución (2) puede ser positiva o negativa. Los valores de M_x y M_y se escogerán, para cada marco, de forma que produzcan la máxima contribución.

El art 237 del Reglamento exige que las estructuras se analicen bajo la acción de dos componentes otorgonales del movimiento del terreno y que en cada sección crítica se sumarán vectorialmente los efectos gravitacionales con los de un componente del movimiento del terreno y, cuando sea significativo, 0.3 de los efectos del otro. En rigor tal combinación debe hacerse a nivel de desplazamiento y de elementos mecánicos, pero es razonable efectuarla a nivel de

fuerzas cortantes, que es como se hace en las siguientes tablas.

ENTRE PISO 3 V_x = 16.25 ton X_T = 12.63 m

V_y = 16.25 ton Y_T = 9.11 m

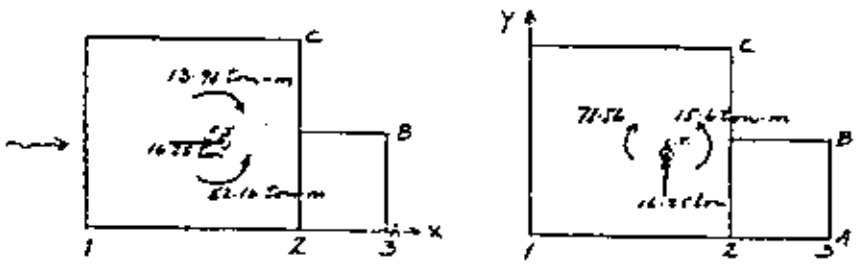

MARCO	K_x	Y	$\bar{Y}$= Y-Y_T	$K_x \bar{Y}$	$K_x \bar{Y}^2$	Sismo en X Dir.	Sismo en X Tors	en Y Tors	1(X) + .3(Y)	.3(X) + 1(Y)	V Diseño
A	200	0.	-9.11	-1822.	16 598.42	7.22	2.33	3.48	10.59	6.35	10.59
B	50	10.	0.89	44.5	39.61	1.81	0.02	0.09	1.86	0.64	1.86
C	200	18.	8.89	1778	15 806.42	7.22	0.61	3.40	8.85	5.75	8.85
Σ	450			Σ 0	32 444.45	16.25					21.30

MARCO	K_y	X	$\bar{X}$= X-X_T	$K_y \bar{X}$	$K_y \bar{X}^2$	Sismo en Y Dir.	Sismo en Y Tors	en X Tors	1(X) + .3(Y)	.3(X) + 1(Y)	V Diseño
1	30	0	-12.63	-378.9	4785.51	6.09	0.72	0.48	2.52	6.95	6.95
2	30	17.	4.37	131.1	572.91	6.09	0.05	0.17	2.01	6.19	6.19
3	20	25.	12.37	247.4	3060.38	4.07	0.09	0.35	1.60	4.26	4.26
Σ	80			Σ 0	8418.76	16.25					17.39

Σ = 40,863.21

Como comprobación la suma de $K_x \bar{Y}$ y $K_y \bar{X}$ debe ser cero, la suma de los cortantes directos debe ser igual a los respectivos actuantes y la de los de diseño debe ser mayor que tal valor.

ENTREPISO 2

V_x = 39.0 ton V_y = 39.0 ton

X_T = 12.50 m Y_T = 10.21 m

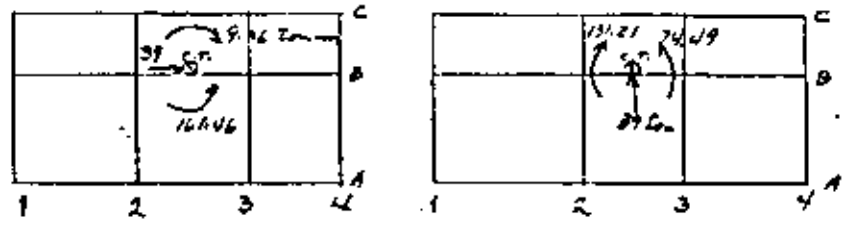

MARCO	K_x	Y	$\bar{Y}$= Y-Y_T	$K_x \bar{Y}$	$K_x \bar{Y}^2$	Sismo en X Dir	Sismo en X Tors	en Y Tors	1(X) + .3(Y)	.3(X) + 1(Y)	V diseño
A	60	0	-10.21	-612.6	6254.7	12.32	3.44	2.82	16.61	7.55	16.61
B	50	10	-0.21	-10.5	2.2	10.26	0.06	0.05	10.34	3.15	10.34
C	80	18	7.79	623.2	4854.7	16.42	0.20	2.86	17.48	7.85	17.48
Σ	190			Σ 0	11111.6	39.0					44.43

MARCO	K_y	X	$\bar{X}$= X-X_T	$K_y \bar{X}$	$K_y \bar{X}^2$	Sismo en Y Dir	Sismo en Y Tors	en X Tors	1(X) + .3(Y)	.3(X) + 1(Y)	V diseño
1	50	0	-12.5	-625	7812.5	9.75	2.87	3.51	7.30	13.67	13.67
2	50	8	- 4.5	-225	1012.5	9.75	1.03	1.26	4.49	11.16	11.16
3	50	17	4.5	225	1012.5	9.75	0.58	1.26	4.49	11.16	11.16
4	50	25	12.5	625	7812.5	9.75	1.62	3.56	7.30	13.67	13.67
	200			= 0	17650.0	39.0					49.66

Σ = 28,761.6

De manera similar resulta para el primer entrepiso:

Marco	A	B	C	1	2	3	4
V diseño	21.91	16.78	21.33	17.93	14.78	14.78	17.93

Al lado se muestran las fuerzas que servirán para analizar los marcos 1 y A

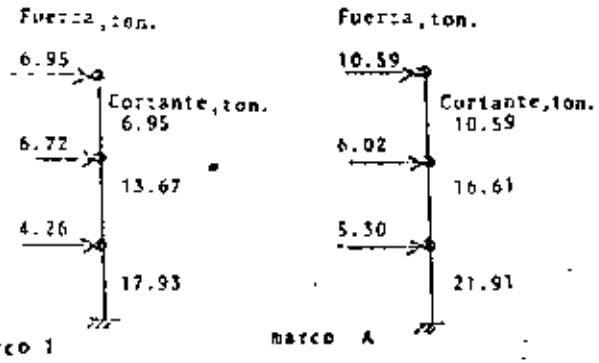

Dividiendo las fuerzas cortantes entre las rigideces de entrepiso se pueden calcular los desplazamientos de entrepiso, para revisar si son o no aceptables; es importante tener presente que deben multiplicarse por Q, puesto que la reducción por ductilidad se aplica sólo a las fuerzas y no a los desplazamientos. Para los marcos 1 y A tenemos:

	Marco 1			Marco A			
Entrepiso	V (ton)	K (ton/cm)	$\delta = Q\frac{V}{K}$ (cm)	V (ton)	K (ton/cm)	$\delta = Q\frac{V}{K}$ (cm)	$\delta_{máx}$ (cm)
1	17.93	50	1.43	21.91	60	1.46	3.20
2	13.67	50	1.09	16.61	60	1.11	2.40
3	6.95	30	0.93	10.59	200	0.21	2.40

$\delta_{máx} = 0.008\ h$ (art 242) Todas las deformaciones son aceptables

5.2 EJEMPLO DE REDUCCION DE LAS FUERZAS CORTANTES EN ANALISIS ESTATICO, TOMANDO EN CUENTA EL VALOR DEL PERIODO FUNDAMENTAL.

En la tabla siguiente se muestran los valores de los pesos, rigideces de entrepiso, fuerzas cortantes obtenidas en el ejemplo 5.2.

Para calcular el periodo fundamental, el inciso II del artículo 240 da la expresión:

$$T = 6.3 \left(\frac{\sum W_i X_i^2}{g \sum P_i X_i}\right)^{1/2}$$

donde g es la aceleración de la gravedad.

Los cálculos se presentan en la siguiente tabla:

Entrepiso o nivel	W_i (ton)	P_i (ton)	K_i (ton/cm)	V_i (ton)	δ_i (cm)	X_i (cm)	X_i^2	$W_i X_i^2$ (ton-cm^2)	$P_i X_i$ (ton-cm)
3	200	16.25	80	16.25	0.2031	0.6581	.43310	86.620	10.694
2	400	22.75	200	39.00	0.1950	0.4550	.20703	82.810	10.351
1	400	13.00	200	52.00	0.2600	0.2600	.06760	27.040	3.380
Σ								196.67	24.425

$$T = 6.3 \left(\frac{1}{981} \times \frac{196.67}{24.425}\right)^{1/2} = 0.571 \text{ seg}$$

Para la zona 1, $T_1 = 0.3$ y $T_2 = 0.8$ seg

Entonces:

$$0.3 < 0.571 < 0.8 \quad , \quad T_1 < T < T_2$$

por lo que no se permite reducción en este caso.

EJEMPLO DE ANALISIS DINAMICO

Calcular las fuerzas cortantes de diseño sísmico según el Regla[illegible] del DDF, de una estructura de dos grados de libertad, con $m_1 = 4$ y $m_2 = 2$ ton seg^2/cm, y $k_1 = 60$ y $k_2 = 40$ ton/cm.

La estructura será tipo B y se construirá en la zona II.

Utilizar el método de análisis dinámico.

Solución

Las frecuencias se obtienen resolviendo el determinante:

$$|[K] - \omega^2[M]| = 0 = (100 - 4\omega^2)(40 - 2\omega^2) - 40^2 = 0$$

donde $[K] = \begin{bmatrix} k_1+k_2 & -k_2 \\ -k_2 & k_2 \end{bmatrix} = \begin{bmatrix} 100 & -40 \\ -40 & 40 \end{bmatrix}$, y $[M] = \begin{bmatrix} 4 & 0 \\ 0 & 2 \end{bmatrix}$

$\omega_1^2 = 9.139$, $\omega_1 = 2.853$; $T_1 = 2.203$ seg

$\omega_2^2 = 36.861$, $\omega_2 = 6.071$; $T_2 = 1.035$ seg

Los vectores modales se obtuvieron resolviendo los sistemas de ecuaciones

$$\begin{bmatrix} 100 - 4(\omega_i^2) & -40 \\ -40 & 40 - 2(\omega_i^2) \end{bmatrix} \begin{Bmatrix} x_1 \\ x_2 \end{Bmatrix} = \begin{Bmatrix} 0 \\ 0 \end{Bmatrix}$$

$z_1^T = [0.5931, 1]$; $z_2^T = [-0.8431, 1]$

Consideremos que se trata de una estructura tipo B que se construirá en la zona II.

En tal caso: $C = 0.20$, $a_o = 0.045$, $T_1 = 0.5$, $T_2 = 2.0$ y $r = 2/3$

Considérese $Q = 2$. El espectro sísmico será entonces:

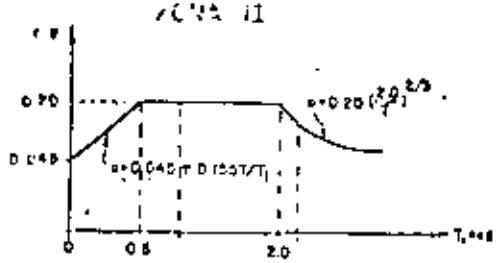

Para $T = 2.20$ seg, $a = 0.2\left(\frac{2.0}{2.2}\right)^{2/3} = 0.188g$

Para $T = 1.03$ seg, $a = 0.20g$

Las ordenadas espectrales reducidas serán:

$A_1 = 0.188g/2 = 0.094g$; $A_2 = 0.20g/2 = 0.10g$

Coeficientes de participación:

$$a_1 = \frac{z_1^T M i}{z_1^T M z_1} = \frac{\sum m_i z_{i1}}{\sum m_i z_{i1}^2} = \frac{4.37}{3.41} = 1.28$$

$$M i = \begin{bmatrix} m_1 & 0 \\ 0 & m_2 \end{bmatrix} \begin{bmatrix} 1 \\ 1 \end{bmatrix} = \begin{bmatrix} m_1 \\ m_2 \end{bmatrix} ; \quad z_1^T M i = \begin{bmatrix} z_{11} & z_{21} \end{bmatrix} \begin{bmatrix} m_1 \\ m_2 \end{bmatrix} = z_{11} m_1 + z_{21} m_2$$

$$= 0.5931 \times 4 + 1 \times 2 = 4.37$$

$$M z_1 = \begin{bmatrix} m_1 & 0 \\ 0 & m_1 \end{bmatrix} \begin{bmatrix} z_{11} \\ z_{21} \end{bmatrix} = \begin{bmatrix} m_1 z_{11} \\ m_2 z_{21} \end{bmatrix} ; \quad z_1^T M z_1 = \begin{bmatrix} z_{11} & z_{21} \end{bmatrix} \begin{bmatrix} m_1 z_{11} \\ m_2 z_{21} \end{bmatrix} = m_1 z_{11}^2 + m_2 z_{21}^2$$

$$= (0.5931)^2 \times 4 + 1^2 \times 2 = 3.41$$

Análogamente

$$a_2 = \frac{z_{12} m_1 + z_{22} m_2}{z_{12}^2 m_1 + z_{22}^2 m_2} = \frac{-0.8431 \times 4 + 1 \times 2}{(-0.8431)^2 \times 4 + 1^2 \times 2} = \frac{-1.37}{4.84} = -0.28$$

$$Y_1 = \frac{a_1}{\omega_1^2} A_1 \Sigma_1 = \frac{0.094 \times 981 \times 1.28}{8.139} \begin{bmatrix} 0.5931 \\ 1 \end{bmatrix} = \begin{bmatrix} 8.60 \\ 14.50 \end{bmatrix} \text{ cm}$$

$$Y_2 = \frac{a_2}{\omega_2^2} A_2 \Sigma_2 = \frac{-0.28 \times 0.1 \times 981}{36.761} \begin{bmatrix} -0.5441 \\ 1 \end{bmatrix} = \begin{bmatrix} 0.63 \\ -0.75 \end{bmatrix} \text{ cm}$$

Desplazamientos Relativos:

$$\Delta y_1 = \begin{bmatrix} 8.60 \\ 5.90 \end{bmatrix} \text{ cm} \; ; \qquad \Delta y_2 = \begin{bmatrix} 0.63 \\ -1.38 \end{bmatrix} \text{ cm}$$

Fuerzas Cortantes

MODO	ENTREPISO	Δy	K	CORTANTE
1	1	8.60	60	516 ton.
	2	5.90	40	236 ton.
2	1	0.63	60	37.8 ton.
	2	−1.38	40	−55.2 ton.

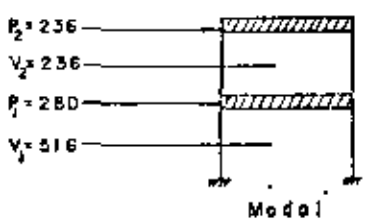

Modo 1

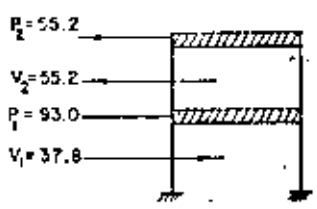

Modo 2

Fuerzas Totales

$V_1 = 516 + 37.8 = 553.8$ ton. ; $V_2 = 236 + 55.2 = 291.2$ ton.

...ón ... ...:

$V_1 = \sqrt{516^2 + 37.8^2} = \sqrt{267684} = 517.38$ ton

$V_2 = \sqrt{236^2 + 55.2^2} = \sqrt{58743} = 242.37$ ton

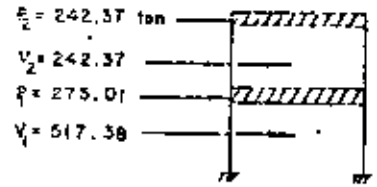

5.3 EJEMPLO DE ANALISIS DINAMICO

for O.A. RASCON CH.

El art 241 del Reglamento acepta que el análisis dinámico puede hacerse por el método denominado modal (en realidad debe llamarse modal espectral), y se aplicará este método al edificio del ejemplo 5.2, cuando el sismo actúa en la dirección Y.

PASO 1. Determinación de modos y frecuencias de vibrar.

El Reglamento exige que se consideren todos los modos con período mayor o igual que 0.4 seg, y nunca menos de 3 modos. Cuando se tienen definidas las rigideces de entrepiso y las masas, el edificio se puede idealizar como se ilustra enseguida:

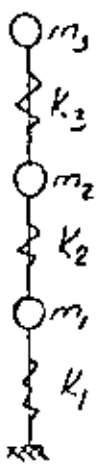

M_i = masa del nivel i

K_i = rigidez del entrepiso i = Σ rigideces de entrepiso de los marcos en esa dirección

En el ejemplo:

$$m_1 = m_2 = \frac{400}{981} = 0.407750 \frac{T\text{-seg}^2}{cm}$$

$$m_3 = \frac{200}{981} = 0.203875 \frac{T\text{-seg}^2}{cm}$$

$K_1 = 50 \times 4 = 200$ T/cm $= K_2$

$K_3 = 30 + 30 + 20 = 80$ T/cm

Con estos valores se pueden determinar los períodos y modos de vibrar por varios procedimientos de los que ilustraremos dos:

I. *Método matricial*

Las matrices de masas y de rigideces del sistema son:

$$\underline{M} = \begin{vmatrix} m_1 & 0 & 0 \\ 0 & m_2 & 0 \\ 0 & 0 & m_3 \end{vmatrix} \quad ; \quad \underline{K} = \begin{vmatrix} K_1+K_2 & -K_2 & \\ -K_2 & +K_2+K_3 & -K_3 \\ & -K_3 & K_3 \end{vmatrix}$$

$$M = \begin{vmatrix} 0.40775 & 0 & \\ 0 & 0.40775 & 0 \\ 0 & 0 & 0.203875 \end{vmatrix} \quad ; \quad \underline{K} = 80 \begin{vmatrix} 5 & -2.5 & 0 \\ -2.5 & 3.5 & -1 \\ 0 & -1 & 1 \end{vmatrix}$$

Necesitamos los valoes de ω^2 que cumplen:

$$(\underline{K} - \omega^2 \underline{M})\ \underline{X} = 0 \qquad (a)$$

es decir $|\underline{K} - \omega^2 \underline{M}| = 0$, o sea:

$$80 \begin{vmatrix} .5 - 0.40775 \frac{\omega^2}{80} & -2.5 & 0 \\ -2.5 & 3.5 - 0.40775 \frac{\omega^2}{80} & -1 \\ 0 & -1 & 1 - 0.203875 \frac{\omega^2}{80} \end{vmatrix} = 0$$

haciendo $\frac{\omega^2}{80} = y$ y desarrollando el determinante se llega a:

$$y^3 - 25.7539\, y^2 + 157.91\, y - 184.42 = 0 \qquad (b)$$

cuyas soluciones son:

$y_1 = 1.525$

$y_2 = 7.030$

$y_3 = 17.190$

que, teniendo en cuenta que $T = 2\pi/\omega$, conducen a:

$\omega_1^2 = 122.0$, $\omega_1 = 11.05\ seg^{-1}$; $T_1 = 0.5686$ seg

$\omega_2^2 = 562.4$, $\omega_2 = 23.71\ seg^{-1}$; $T_2 = 0.2650$ seg

$\omega_3^2 = 1536.2$, $\omega_3 = 37.08\ seg^{-1}$; $T_3 = 0.1694$ seg

Los modos se calculan a partir de la expresión (a), reemplazando los valores correspondientes de ω^2. Para $\omega_1^2 = 122$, tenemos:

$$\begin{bmatrix} (400 - 122\times .40775) & -200 & 0 \\ -200 & (280 - 122\times .40775) & -80 \\ 0 & -80 & (80 - 122\times .203875) \end{bmatrix} \begin{bmatrix} x_1 \\ x_2 \\ x_3 \end{bmatrix} = \begin{bmatrix} 0 \\ 0 \\ 0 \end{bmatrix}$$

$$350.2545\, x_1 - 200\, x_2 = 0 \quad \therefore x_2 = 1.751\, x_1$$

$$-200\, x_1 + 230.2545\, x_2 - 80\, x_3 = 0$$

$$-80.\, x_2 + 55.1275\, x_3 = 0 \quad \therefore x_3 = 1.45117\, x_2$$

Si tomamos $x_1 = 1$, entonces: $x_2 = 1.751$

$x_3 = 2.541$

y el vector que corresponde al primer modo es:

$$\underline{\phi}_1 = \begin{bmatrix} 1.000 \\ 1.751 \\ 2.541 \end{bmatrix}$$

Análogamente se obtienen los vectores correspondientes a los modos segundo y tercero:

$$\underline{\phi}_2 = \begin{bmatrix} 1.000 \\ 0.853 \\ -1.969 \end{bmatrix} \quad ; \quad \underline{\phi}_3 = \begin{bmatrix} 1.000 \\ -0.803 \\ 0.321 \end{bmatrix}$$

que dibujados aparecen como:

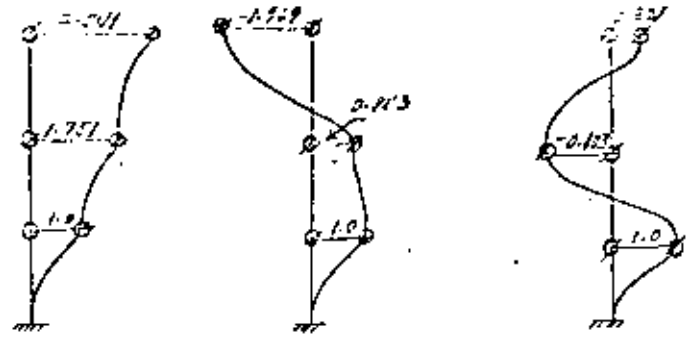

$T_1 = 0.5686$ seg $T_2 = 0.2650$ seg $T_3 = 0.1694$ seg

La matriz modal $\underline{R}$ es:

$$\underline{R} = [\underline{\phi}_1 \ \ \underline{\phi}_2 \ \ \underline{\phi}_3]$$

$$R = \left[\begin{array}{c|c|c} 1.0 & 1.0 & 1.0 \\ 1.751 & 0.853 & -0.803 \\ 2.541 & -1.969 & 0.321 \end{array}\right]$$

E. Métodos de Stodolla-Newmark y Holzer

Estos métodos son apropiados para usarse con calculadoras de escritorio. El Método de Stodolla-Newmark se presta a mucha precisión, y sirve para el 1er modo:

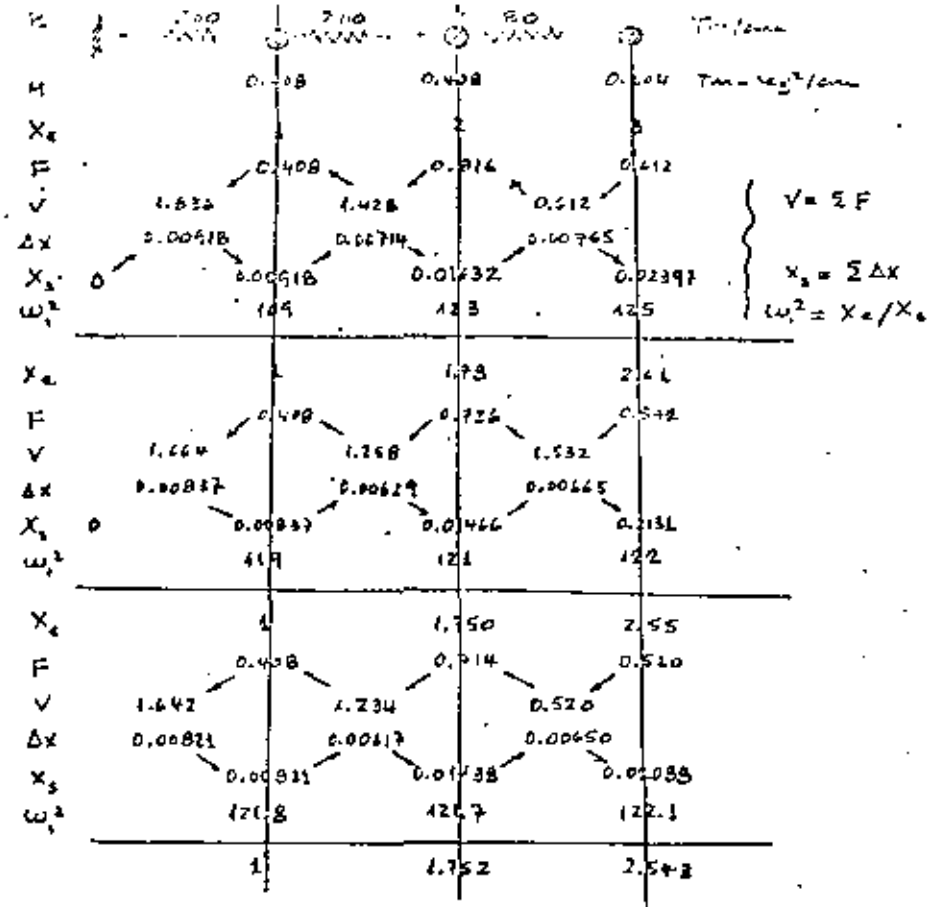

Para ω_1^2 podemos tomar el promedio del último ciclo:

$$\omega_1^2 = 121.9\ seg^{-2} \quad ; \quad \Phi_1 = \begin{Bmatrix} 1.00 \\ 1.752 \\ 2.543 \end{Bmatrix}$$

$$T_1 = 0.5686\ seg$$

El método de Holzer sirve para los modos superiores y para este ejemplo se aplica como sigue:

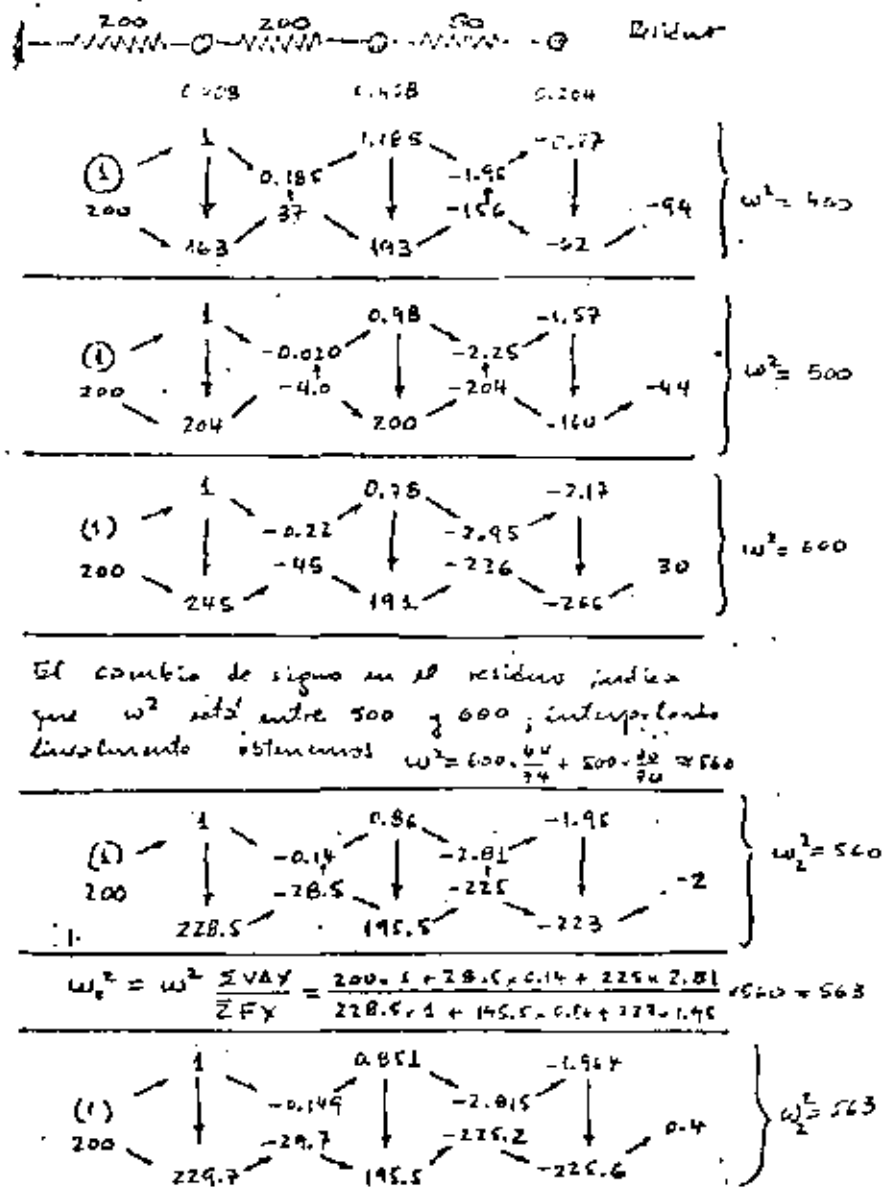

La fréquence du second mode est donc :

$$\omega_2^2 = \frac{200\cdot 1 + 29.7 \cdot (-.149) + 225.7 \cdot 7.815}{29.7 + 199.5 \cdot (-.851) + 225.6 \cdot 1.964} \times 568 = 5062.5$$

$$T_2 = 0.2660 \text{ s} \qquad \underline{\Phi}_2 = \begin{Bmatrix} 1.00 \\ 0.851 \\ -1.964 \end{Bmatrix}$$

K

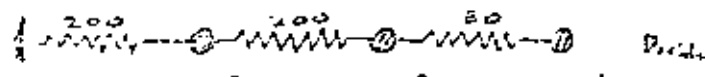

MA						
X		1	-0.04	-2.44		$\omega^2 = 1000$
ΔX	(1)		-1.04	-2.40		
V	200	-208		-192	306	
F		408	-16	-448		
X		1	-1.06	4.90		$\omega^2 = 1500$
ΔX	(1)		-2.06	2.96		
V	200	-412		237	-344	
F		612	-649	581		
X		1	-0.52	-1.06		$1000 + \frac{344}{450}$
ΔX	(1)		-1.52	-0.53		$+1500 \times \frac{306}{450}$
V	200	-304		-42	223	$= 1235$
F		504	-262	-265		
X		1	-0.74	-.01		$1235 + \frac{344}{547}$
ΔX	(1)		-1.74	0.73		$+1500 \times \frac{223}{547}$
V	200	-347		58	61	$= 1340$
F		547	-405	-3		
X		1	-0.79	0.25		$1340 + \frac{344}{405}$
ΔX	(1)		-1.79	1.04		$+1500 \times \frac{61}{405}$
V	200	-357		83	13	$= 1365$
F		557	-440	70		

$$\omega_3^2 = \frac{200\cdot 1 + 357 \cdot (-1.79) + 83 \cdot 1.04}{557 \cdot 1 + 440 \cdot (-.79) + 70 \cdot 0.25} \times 1365 = 1390$$

X		1	-0.80	0.30		$\omega^2 = 1390$
ΔX	(1)		-1.80	1.10		
V	200	-359		88	4	
F		559	-447	84		

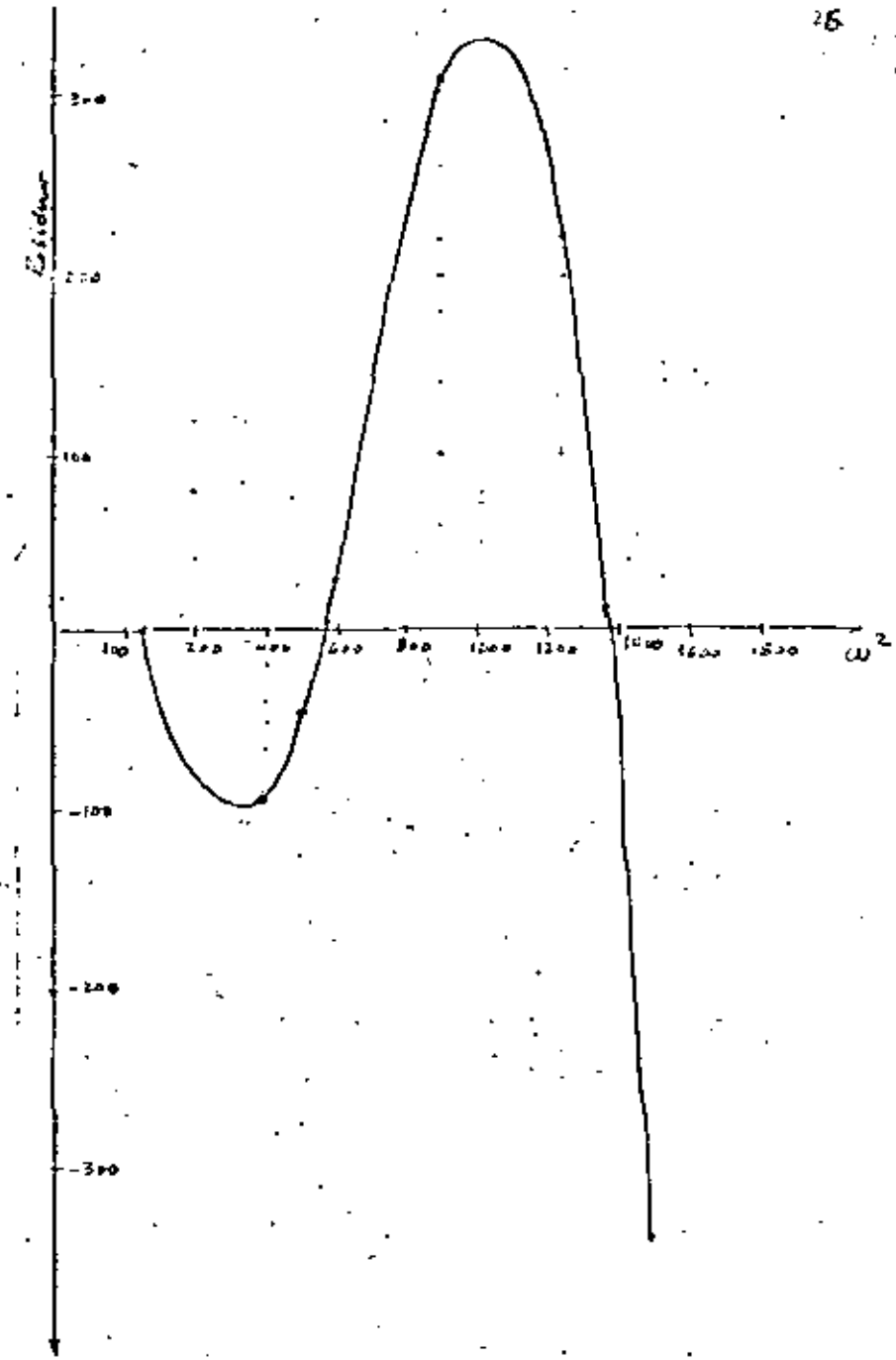

$$\omega_3^2 = \frac{200 \times 1 + 359 \times 1.8 - 88 \times 1.1}{559 \times 1 + 447 \times 0.8 + 84 \times 0.5} \times 1370 = 1372$$

podemos tomar entonces:

$$\omega_3^2 = 1372 \qquad \underline{\beta}_3 = \begin{Bmatrix} 1.00 \\ -0.80 \\ 0.30 \end{Bmatrix}$$

$$T_3 = 0.1696$$

Estos resultados prácticamente coinciden con los del método matricial.

PASO II Obtención de las ordenadas espectrales de diseño.

El espectro para diseño sísmico está definido en el art 236 (acápite II) La estructura que estamos tratando se encuentra en la zona I, y le corresponden, siendo la estructura del grupo A:

$a_o = 0.05$, $T_1 = 0.3$, $T_2 = 0.8$, $r = 1/2$ } de la tabla del art 236

$c = 0.16 \times 1.3 = 0.208$ } de la tabla del art 234.

y el espectro queda como la siguiente figura:

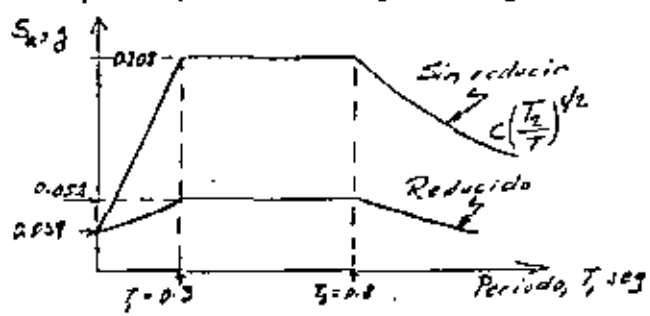

Tiene que aplicarse luego la reducción por ductilidad que consiste en dividir entre el factor Q'

$$Q' = \begin{cases} Q & \text{si } T > T_1 \\ 1 + (Q-1)\frac{T}{T_1} & \text{si } T \leq T_1 \end{cases}$$

Para el primer modo $T = 0.5686 > 0.30 = T_1$ entonces $Q' = 4$ y la ordenada espectral y la aceleración correspondientes valen:

$$S_{a1} = \frac{0.208}{4} = 0.052 \quad , \quad a_1 = 0.052g = 51 \text{ cm/seg}^2$$

Para el segundo modo, $T = 0.2650 < 0.30$, por tanto:

$$Q' = 1 + (4-1)\frac{0.2650}{0.3} = 3.650$$

$$S_{a2} = \frac{0.039 + (0.208 - 0.039) \times 0.2650/0.3}{3.65} = 0.05158$$

$$a_2 = 0.05158g = 50.6 \text{ cm/seg}^2$$

y, para el tercer modo, $T = 0.1694 < 0.30$, entonces:

$$Q' = 1 + (4-1)\frac{0.1694}{0.3} = 2.694$$

$$S_{a3} = \frac{0.039 + (0.208 - 0.039) \times 0.1694/0.3}{2.694} = 0.049899$$

$$a_3 = 0.049899\,g = 48.95 \text{ cm/seg}^2$$

PASO III Cálculo de las fuerzas cortantes máximas para cada modo de vibración.

La siguiente expresión sirve para calcular los desplazamientos de entrepiso:

$$\underline{U}_{j\max} = \frac{a_j}{\omega_j^2} \; C_j \; \underline{\phi}_j$$

donde ω_j es la frecuencia del modo j; $\underline{\phi}_j$ el correspondiente vector [illegible], a_j, la ordenada espectral respectiva y C_j, que se denomina coeficiente de participación del j-ésimo modo, está dado por:

$$C_j = \frac{\sum_i m_i \phi_{ji}}{\sum_i m_i \phi_{ji}^2}$$

en esta expresión m_i es la masa del nivel i, y ϕ_{ji} es la componente i del vector modal j.

Los valores de C_j para los modos 1, 2, 3 son:

$$C_1 = \frac{0.40775 \times 1 + 0.40775 \times 1.751 + 0.203875 \times 2.541}{0.40775 \times 1^2 + 0.40775 \times (1.751)^2 + 0.203875 \times (2.541)^2} = 0.5510$$

$$C_2 = \frac{0.40775 \times 1 + 0.40775 \times 1.751 + 0.203876 \times (-1.969)}{0.40775 \times 1^2 + 0.40775 \times 1.751^2 + 0.203875 \times (-1.969)^2} = 0.2369$$

$$C_3 = \frac{0.40775 \times 1 + 0.40775 \times (-0.803) + 0.203875 \times 0.321}{0.40775 \times 1^2 + 0.40775 \times (-0.803)^2 + 0.203875 \times 0.321^2} = 0.2107$$

y los desplazamientos máximos son:

$$U_1 = \frac{51.0}{122} \times 0.5510 \begin{Bmatrix} 1.000 \\ 1.751 \\ 2.541 \end{Bmatrix} = \begin{Bmatrix} 0.2304 \\ 0.4035 \\ 0.5855 \end{Bmatrix} \; ; \; \Delta\underline{u}_1 = \begin{Bmatrix} 0.2304 \\ 0.1731 \\ 0.1820 \end{Bmatrix}$$

$$\underline{U}_2 = \frac{50.6}{562.4} \times 0.2369 \begin{Bmatrix} 1.000 \\ 0.683 \\ -1.969 \end{Bmatrix} = \begin{Bmatrix} 0.0223 \\ 0.0182 \\ -.0420 \end{Bmatrix} \; ; \; \Delta\underline{u}_2 = \begin{Bmatrix} 0.0213 \\ -.0031 \\ -.0602 \end{Bmatrix}$$

$$\underline{U}_3 = \frac{48.95}{1375.2} \times 0.2107 \begin{Bmatrix} 1.000 \\ -0.803 \\ 0.321 \end{Bmatrix} = \begin{Bmatrix} 0.0075 \\ -.0060? \\ 0.0024 \end{Bmatrix} \; ; \; \Delta\underline{u}_3 = \begin{Bmatrix} 0.0075 \\ -.0135 \\ 0.0084 \end{Bmatrix}$$

Los vectores $\Delta\underline{u}$ son los desplazamientos de entrepiso.

Las fuerzas cortantes se obtienen multiplicando los desplazamientos de entrepiso por la respectiva rigidez, como se hace en la siguiente tabla:

MODO	ENTREPISO	Δ	K	CORTANTE
1	1	0.2304	200	46.08
	2	0.1731	200	34.62
	3	0.1820	80	14.56
2	1	0.0213	200	4.26
	2	-.0031	200	-0.62
	3	-.0602	80	-4.82
3	1	0.0075	200	1.50
	2	-.0135	200	-2.70
	3	0.0084	80	0.67

PASO IV Superposición de los efectos de los modos considerados.

El artículo 241 autoriza, cuando no hay apéndices o no consideran los grados de libertad correspondientes a torsión, que se puede estimar cualquier respuesta de interés R en la expresión

$R = \sqrt{R_i^2}$ DONDE R_i ES LA RESPUESTA QUE SE OBTIENE EN EL MODO i.

LAS FUERZAS CORTANTES SERIAN ASI:

ENTREPISO	CORTANTE
1	$\sqrt{46.06^2 + 4.26^2 + 1.50^2}$ = 46.30 ton
2	$\sqrt{34.62^2 + 0.62^2 + 2.70^2}$ = 34.73 ton
3	$\sqrt{14.56^2 + 4.82^2 + 0.67^2}$ = 15.35 ton

5.4 EJEMPLO DE CALCULO DEL MOMENTO DE VOLTEO

Se calculará el momento de volteo para el edificio del ejemplo 5.3.

De acuerdo con el inciso VI del art 240 del Reglamento, el momento de volteo que se puede obtener integrando el diagrama de cortantes, puede reducirse "tomándolo igual al calculado multiplicado por 0.8 + 0.2z (siendo z la relación entre la altura a la que se calcula el factor reductivo por momento de volteo y la altura de la construcción), pero no menor que el producto de la fuerza cortante en el nivel en cuestión multiplicada por el conteo de gravedad de la parte de la estructura que se encuentra por encima de dicho nivel".

Esta última distancia se puede calcular sabiendo que:

$$h_{Gj} = \frac{\sum_i W_i h_i}{\sum_i W_i}$$ donde W_i y h_i son el peso y la altura del nivel i, y la suma se hace para todos los niveles que están encima

$d_j = h_{Gj} - h_j$ de aquel en el cual se calcula el momento de volteo (nivel j)

Las fuerzas cortantes obtenidas en el ejemplo 3, así como las fuerzas correspondientes en los niveles se muestran a continuación:

Diagrama de cortantes

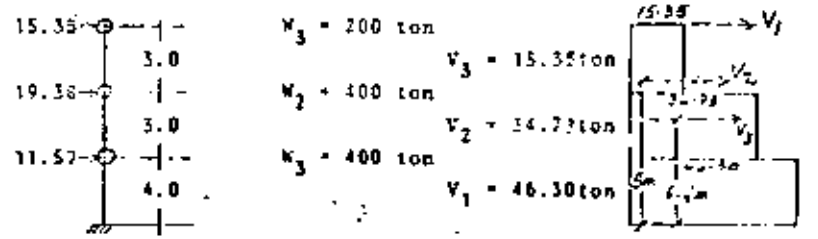

En las siguientes tablas se muestran los cálculos necesarios para determinar los momentos de volteo reducidos en los tres niveles

NIVEL	W_i (Ton)	ΣW_i (ton)	h_j (m)	$W_i h_i$ (ton-m)	$\Sigma W_i h_i$ (ton-m)	h_{Gj} (m)
3	200	200	10	2000	2000	10.0
2	400	600	7	2800	4800	8.0
1	400	1000	4	1600	6400	6.4

NIVEL j	h_{Gj} (m)	h_j (m)	h_{pj} (m)	V_j (ton)	$h_{pj}V_j$ (ton-m)	Mcal (ton-m)	d_j (ton-m)	M_1 (ton-m)
2	10	7	3	15.35	46.05	46.05	3.0	46.05
1	8.0	4	3	34.71	104.19	150.24	4.0	138.92
0	6.4	0	4	46.30	185.20	335.44	6.4	296.32

$M_{cal} = \Sigma h_{pj} V_j$; $M_1 = V_j d_j$; $M_2 = M_{cal} \times F$

NIVEL	z	Factor reductivo F	M_2 (ton-m)	USAR
2	7/10 = 0.7	0.8+0.14=0.94	43.29	46.05
1	4/10 = 0.4	0.8+0.08=0.88	132.21	138.92
0	0/10 = 0.	0.8+0 =0.80	268.35	296.32

USAR el mayor entre M_1 y M_2

5.5. *EJEMPLO DE UN EDIFICIO CON APENDICES*

Supóngase que el edificio que se presentó en el ejemplo 5.1 tiene sobre el tercer nivel un tanque de almacenamiento que pesa 10 toneladas y que está soportado por dos marcos que tienen 3 metros de altura sobre el tercer nivel como se indica en la figura. En este ejemplo se calcula la distribución de fuerzas sísmicas que corresponden a este caso, con el método estático del Reglamento.

Esquemáticamente el edificio queda como se muestra en la figura siguiente:

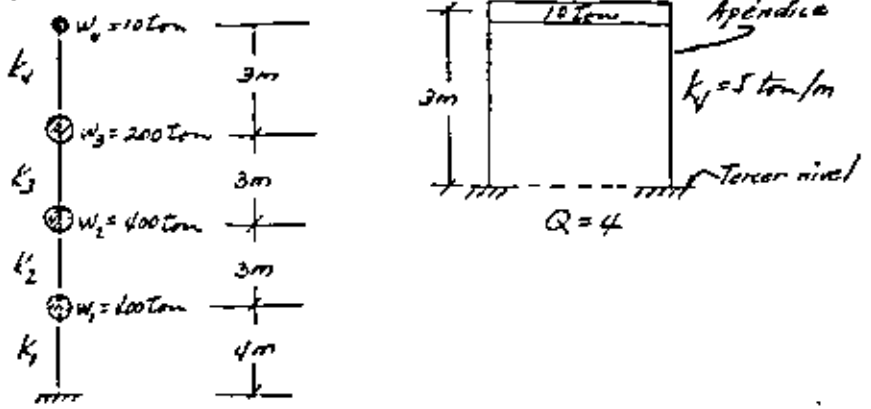

En el inciso V del art 240 del Reglamento se establece que debe suponerse que sobre los apéndices actúa la misma distribución de aceleraciones que le correspondería como si estuviese apoyado directamente sobre el terreno, multiplicada por $\frac{C' + a_o}{a_o}$ donde c' es el mismo factor por el que se multiplican los pesos a la altura de desplante del apéndice cuando se valúan las fuerzas laterales sobre la construcción.

Recordemos que según el método estático la fuerza sísmica es proporcional a $W_i\ h_i$, según se muestra en la figura.

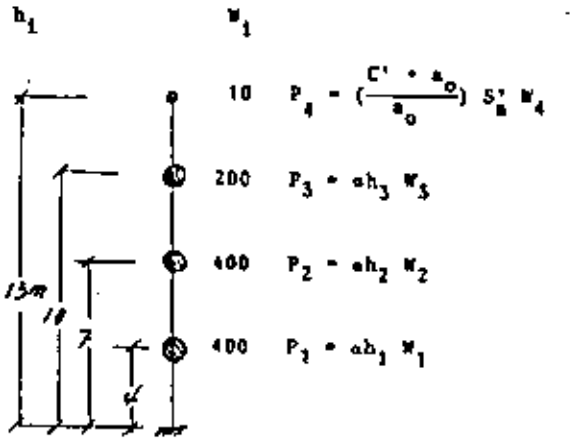

El factor por el que se multiplica el peso en el nivel de desplante del apéndice es αh_3, y teniendo presente que para la zona I se tiene $a_o = 0.03$, se llega a que:

$$\frac{C' + a_o}{a_o} = \frac{\alpha h_3 + 0.03}{0.03}$$

Si el apéndice estuviese apoyado directamente en el suelo, la ordenada espectral que le correspondería sería el mayor entre $\frac{C}{Q}$ y a_o, que según se vió en el ejemplo 5.4 valen:

$\frac{C}{Q} = \frac{0.208}{4} = 0.052$

$a_0 = 0.03$

} Entonces para el apéndice se toma $S_a' = 0.052$

Para el edificio completo se tiene, también como se vió en el ejemplo 5.1, que

$$S_a = 0.052$$

y para conocer a debemos tomar en cuenta que:

$$\frac{\Sigma P_i}{\Sigma W_i} = S_a$$

Es decir:

$$a(h_1 W_1 + h_2 W_2 + h_3 W_3) + \left(\frac{ah_3 + 0.03}{0.03}\right) S_a' W_4 = S_a(W_1 + W_2 + W_3 + W_4)$$

$$a(4\times400 + 7\times400 + 10\times200) + \frac{a_x 10\, S_a'\, x 10}{0.03} = S_a(400+400+200+10) - S_a'\, x 10$$

reemplazando los valores de S_a' y S_a y despejando:

$$a = 0.007911$$

y la distribución de fuerzas es:

		cortante
$P_4 = \frac{0.00791 \times 10 + 0.03}{0.03} \times 0.052 \times 10$	= 1.89	1.89
$P_3 = 0.007911 \times 10 \times 200$	= 15.82	17.71
$P_2 = 0.00791 \times 7 \times 400$	= 22.15	39.86
$P_1 = 0.00791 \times 4 \times 400$	= 12.66	52.52

Comprobación: $\frac{52.52}{1010} = 0.052 = S_a$

centro de educación continua
división de estudios de posgrado
facultad de ingeniería unam

CURSOS DE INGENIERIA CIVIL EN EL PROYECTO DE PLANTAS HIDROELECTRICAS.
C.F.E.

INGENIERIA SISMICA.

DR. OCTAVIO RASCON CHAVEZ.

JUNIO, 1981.

Efectos sísmicos en estructuras en forma de péndulo invertido

Octavio RASCON CH. *

INTRODUCCION

En la práctica se presentan estructuras constituidas por una sola columna la cual sostiene una cubierta que puede ser una losa o un cascarón. Su comportamiento dinámico debe estudiarse considerando el efecto que la inercia rotacional de la cubierta induce en el movimiento total de la estructura.

A principios de este año se presentó en California, EUA, un trabajo[1] en el cual se trató este problema desde un punto de vista energético. Se calculó sólo el periodo fundamental y con base en él, la respuesta de la estructura a un determinado temblor. Los periodos calculados para cuatro estructuras de este tipo ya construidas fueron menores que los medidos *in situ*. La discrepancia fue atribuida a efectos de rotación y traslación de la base.

El objeto de este trabajo es introducir un análisis modal, el cual nos proporcionará los efectos del acoplamiento que existe entre los modos de vibración. También se tomarán en cuenta en forma aproximada los efectos de rotación y traslación de la base.

CALCULO DE FRECUENCIAS Y CONFIGURACIONES MODALES DE VIBRACION

1. *Suelo rígido*

Para el caso en que el centro de gravedad de la cubierta se encuentra localizado en la prolongación del eje de la columna, el movimiento de la estructura podrá estudiarse en dos direcciones perpendiculares entre sí. En tal caso el problema podrá discretizarse como de dos modos de vibración acoplados en cada dirección.

Para el cálculo de las frecuencias de vibración se idealizará la estructura como de comportamiento lineal, constituida por una cubierta infinitamente rígida de masa simétricamente distribuida y soportada por una sola columna. Como primer caso se considerará al suelo infinitamente rígido (fig. 1).

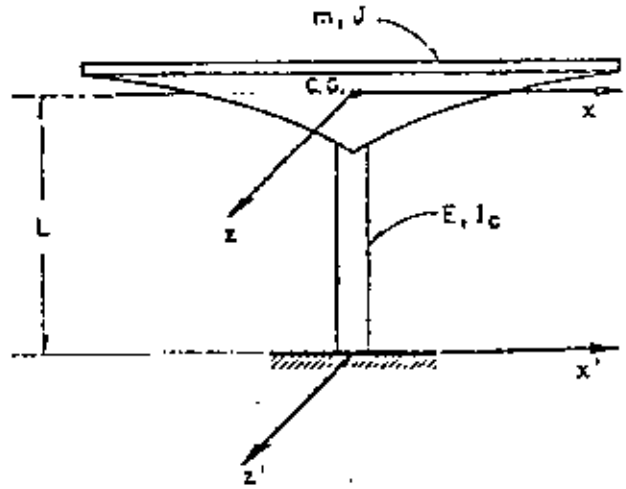

FIG. 1. *Péndulo invertido*

En fig 1

W = peso de la cubierta más la parte tributaria de la columna

J = momento de inercia de la masa de la cubierta respecto al eje z

E = módulo de elasticidad del material de la columna

I_c = momento de inercia de la sección transversal de la columna con respecto al eje z

$C.G.$ = centro de gravedad de la cubierta

L = distancia de C.G. al suelo.

Para la columna mostrada en las figs. 2*a* y 2*b*.

k = rigidez por traslación (fuerza horizontal aplicada en C.G. necesaria para que este se desplace la unidad)

k_r = rigidez por rotación (par aplicado en C.G. necesario para producir un giro unitario a la altura de C.G.

θ = rotación en C.G. debida a la fuerza k

δ = desplazamiento lateral de C.G. debido al momento k_r.

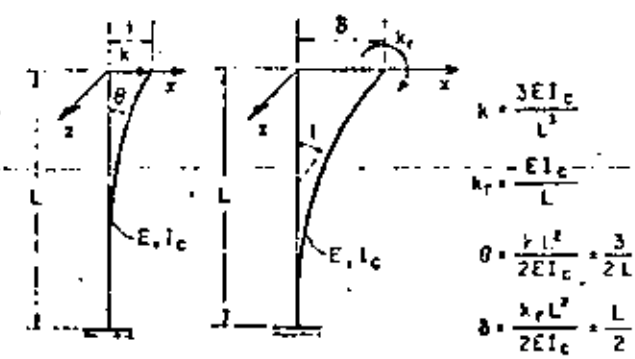

FIG. 2. *Rigideces*

* Asistente de Investigador, Instituto de Ingeniería, UNAM.

Despreciando las deformaciones por cortante, las expresiones para k, k_r, Θ y δ pueden encontrarse por estática y valen

$$k = 3EI_c/L^3; \qquad (1a)$$

$$k_r = EI_c/L; \qquad (2a)$$

$$\Theta = 1.5/L \qquad (1b)$$

$$\delta = L/2 \qquad (2b)$$

Para una fuerza de magnitud αk, el desplazamiento será α y el giro $\alpha\Theta$. Para un par de magnitud βk, el giro será β y el desplazamiento $\beta\delta$. Al aplicarse ambos simultáneamente, el desplazamiento total de C.G. será x_1 y el giro ϵ_1 (fig. 3).

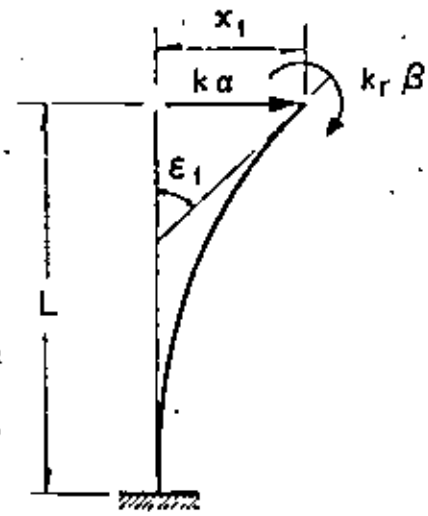

$$x_1 = \alpha + \beta\,\delta$$

$$\epsilon_1 = \alpha\,\theta + \beta$$

FIG. 3. *Desplazamientos y giros totales*

Por tanto los valores de x_1 y ϵ_1 quedan dados por

$$x_1 = \alpha + \beta\delta \qquad (3)$$

$$\epsilon_1 = \alpha\Theta + \beta \qquad (4)$$

Resolviendo el sistema de ecuaciones 3 y 4 para α y β, y utilizando las ecs 1*b* y 2*b* se obtiene

$$\alpha = (x_1 - k_r\gamma\epsilon_1)/\kappa; \qquad (5a)$$

$$\beta = (\epsilon_1 - k\gamma x_1)/\kappa \qquad (5b)$$

en las cuales

$$\gamma = L^2/2EI_c; \qquad (6a)$$

$$\kappa = 1 - kL^3/4EI_c = 0.25 \qquad (6b)$$

Para las oscilaciones del péndulo mostrado en la fig 1, el diagrama de cuerpo libre de la cubierta está indicado en la fig 4. Las ecuaciones de movimiento, despreciando efectos gravitacionales, serán

$$m\ddot{x}_1 + k\alpha = 0 \qquad (7)$$

$$J\ddot{\epsilon}_1 + k_r\beta = 0 \qquad (8)$$

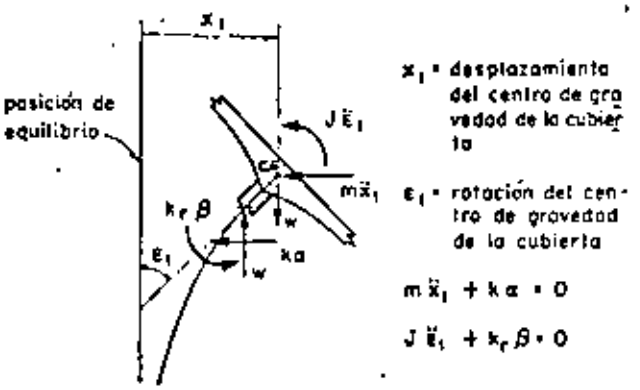

FIG. 4. *Diagrama de cuerpo libre*

Sustituyendo a (5a) y (5b) en (7) y (8) se obtiene

$$m\ddot{x}_1 + (kx_1 - kk_r\gamma\epsilon_1)/\kappa = 0 \qquad (9)$$

$$J\ddot{\epsilon}_1 + (k_r\epsilon_1 - kk_r\gamma x_1)/\kappa = 0 \qquad (10)$$

Las ecs. 9 y 10 se pueden expresar matricialmente en la forma

$$\begin{bmatrix} m & 0 \\ 0 & J \end{bmatrix}\begin{bmatrix} \ddot{x}_1 \\ \ddot{\epsilon}_1 \end{bmatrix} + \frac{1}{\kappa}\begin{bmatrix} k & -\gamma kk_r \\ -\gamma kk_r & k_r \end{bmatrix}\begin{bmatrix} x_1 \\ \epsilon_1 \end{bmatrix} = 0 \qquad (11)$$

Utilizando las ecs 1a, 2a y 6a se encuentra que

$$\gamma kk_r = Lk/2 \qquad (12)$$

Puesto que el movimiento es armónico se tiene que

$$\ddot{x}_1 = -\omega^2 x_1 \quad \text{y} \quad \ddot{\epsilon}_1 = -\omega^2\epsilon_1 \qquad (13)$$

en donde ω es la frecuencia circular natural de vibración.

Sustituyendo las ecs. 12 y 13 en (11) se obtiene

$$-\begin{bmatrix} m & 0 \\ 0 & J \end{bmatrix}\omega^2\begin{bmatrix} x_1 \\ \epsilon_1 \end{bmatrix} + \frac{1}{\kappa}\begin{bmatrix} k & -\frac{Lk}{2} \\ -\frac{Lk}{2} & k_r \end{bmatrix}\begin{bmatrix} x_1 \\ \epsilon_1 \end{bmatrix} = 0 \qquad (14)$$

Factorizando en la ec. 14

$$\left\{\frac{1}{\kappa}\begin{bmatrix} k & -\frac{Lk}{2} \\ -\frac{Lk}{2} & k_r \end{bmatrix} - \omega^2\begin{bmatrix} m & 0 \\ 0 & J \end{bmatrix}\right\}\begin{bmatrix} x_1 \\ \epsilon_1 \end{bmatrix} = 0 \qquad (15)$$

La ec 15 representa un sistema de ecuaciones homogéneas, el cual, para tener solución diferente de la trivial, necesita que su determinante sea nulo. Por tanto

$$\begin{vmatrix} \frac{k}{\kappa} - m\omega^2 & -\frac{Lk}{2\kappa} \\ -\frac{Lk}{2\kappa} & \frac{k_r}{\kappa} - J\omega^2 \end{vmatrix} = 0 \qquad (16)$$

Desarrollando el determinante se llega a

$$mI\omega^4 - \frac{1}{\kappa}(kI + mk_r)\omega^2 + \frac{1}{4\kappa^2}(4kk_r - L^2k^2) = 0 \qquad (17)$$

Dividiendo ambos miembros entre mI y considerando que $L^2k^2 = 3kk_r$ se obtiene

$$\omega^4 - \frac{kI + mk_r}{mI\kappa}\omega^2 + \frac{kk_r}{4mI\kappa^2} = 0 \qquad (18)$$

que es una ecuación de segundo grado en ω^2, cuyas soluciones son

$$\omega^2_{1,2} = \frac{kI + mk_r}{2mI\kappa} \pm \sqrt{\frac{(kI + mk_r)^2}{4m^2I^2\kappa^2} - \frac{kk_r}{4mI\kappa^2}} \qquad (19)$$

Dividiendo numerador y denominador de (19) entre mI

$$\omega^2_{1,2} = \frac{k/m + k_r/I}{2\kappa} \pm \frac{1}{2\kappa}\sqrt{(k/m + k_r/I)^2 - (k/m)(k_r/I)} \qquad (20)$$

Llamando a

$k/m = p^2$ = cuadrado de la frecuencia circular natural por traslación

$k_r/I = \Omega^2$ = cuadrado de la frecuencia circular natural por rotación

se obtiene

$$\omega^2_{1,2} = 2\left(p^2 + \Omega^2 \pm \sqrt{(p^2 + \Omega^2)^2 - p^2\Omega^2}\right) \qquad (21)$$

Dividiendo ambos miembros de (21) entre p^2 y haciendo $\omega^2/p^2 = \lambda$ y $\Omega^2/p^2 = \mu$ se llega a

$$\lambda_{1,2} = 2\left(1 + \mu \pm \sqrt{(1 + \mu)^2 - \mu}\right) \qquad (22)$$

Es interesante notar que si $I = 0$ (masa concentrada) de la ec 17 se obtiene $\omega^2 = k/m = p^2$.

Las configuraciones modales pueden obtenerse de cualquiera de las dos ecuaciones algebraicas contenidas en la ecuación matricial dada en ec 15. La primera de ellas es

$$\left(\frac{k}{\kappa} - m\omega_n^2\right)x_{1,n} - \frac{Lk}{2\kappa}\epsilon_{1,n} = 0 \qquad (23)$$

donde el índice n indica el número del modo y de la cual se obtiene

$$x_{1,n}/\epsilon_{1,n} = \frac{Lk}{2\kappa}\Big/\left(\frac{k}{\kappa} - m\omega_n^2\right) \qquad (24)$$

dividiendo numerador y denominador de (24) entre m y considerando que $\kappa = 0.25$, $k/m = p^2$ y que $\lambda_n = \omega_n^2/p^2$ se llega a

$$x_{1,n}/\epsilon_{1,n} = 2L/(4 - \lambda_n) \qquad (25)$$

Si se desean tomar en cuenta las deformaciones por cortante basta con modificar las rigideces mediante un análisis de estática y partir de nuevo de la ec 17 sin considerar que $L^2k^2 = 3kk_r$. Si existe excentricidad en alguna dirección su efecto podrá tomarse en cuenta introduciendo un grado de libertad adicional.

En las figs 5 y 6 se encuentran representados los resultados de las ecs 22 y 25.

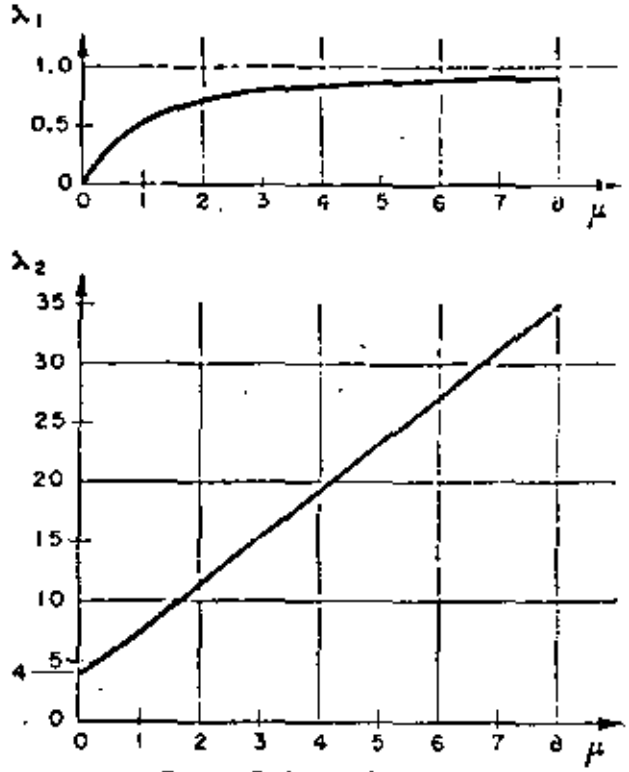

FIG. 5. *Gráfica de frecuencias*

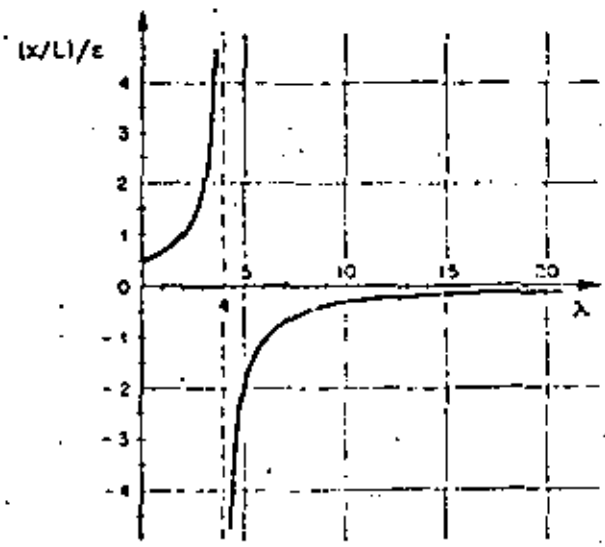

FIG. 6. *Gráfica* $(x/L)/\epsilon$ *vs* λ

2. *Suelo flexible*

Al oscilar una estructura cimentada en suelo blando, existe interacción dinámica suelo-estructura que en la mayoría de los casos no debe despreciarse al calcular las frecuencias y los modos de vibración. En lo que sigue se propone la adaptación de un método numérico para tomar en cuenta dicho efecto.

Las restricciones del suelo serán idealizadas mediante resortes de comportamiento lineal; uno para desplazamientos lineales horizontales y otro para deformaciones angulares de cabeceo de la cimentación [2,3].

En la fig. 7 se hace referencia a los parámetros que a continuación se mencionan

K = rigidez del resorte correspondiente a la traslación de la base $= C_r A$

C_r = coeficiente de cortante elástico uniforme del suelo.

A = área de contacto de la cimentación.

R = rigidez del resorte correspondiente a rotación de la base $= C_\varphi I_b - W'\bar{y}$

C_φ = coeficiente de compresión elástica no uniforme del suelo.

I_b = momento de inercia de área de la base de la cimentación con respecto al eje z'

W' = peso de la estructura

$\bar{y}$ = altura del centro de gravedad de la estructura sobre el nivel de desplante

$F = m\omega_n^2 x$

x = desplazamiento total en C.G.

$M = J\omega_n^2 \varepsilon$

ε = desplazamiento angular total en C.G.

L' = altura de C.G. sobre el nivel de desplante

x_0 = traslación de la base

ε_0 = rotación de la base

$x_1 = \alpha + \beta\delta$

$\varepsilon_1 = \beta + \alpha\Theta$

$x_2 = L'\varepsilon_0$

$\alpha = F/k$

$\beta = M/k_r$

J, L, δ, Θ, k, k_r, x_1, ε_1 y W ya definidos anteriormente.

El problema será resuelto utilizando un procedimiento iterativo y la tabulación propuesta por N. M. Newmark[4]: se despreciarán la variación de la rigidez de la columna debida a la fuerza normal W y los momentos en la misma, causados por la excentricidad del peso debida a deformaciones de la columna.

Sean

F_s = fuerza horizontal en la base de la cimentación $= F$

M_s = momento flexionante en la base de la cimentación $= M + FL'$

$x_0 = F_s/K$

$\varepsilon_0 = M_s/R$

A continuación se describe el procedimiento a seguir:

1. Suponer valores para x y ε
2. Calcular F y M usando las expresiones $F = m\omega_n^2 x$ y $\varepsilon = J\omega_n^2 \varepsilon$. En esta etapa el valor de ω_n aún no se conoce; por tanto se llevará como factor común en el resto del cálculo

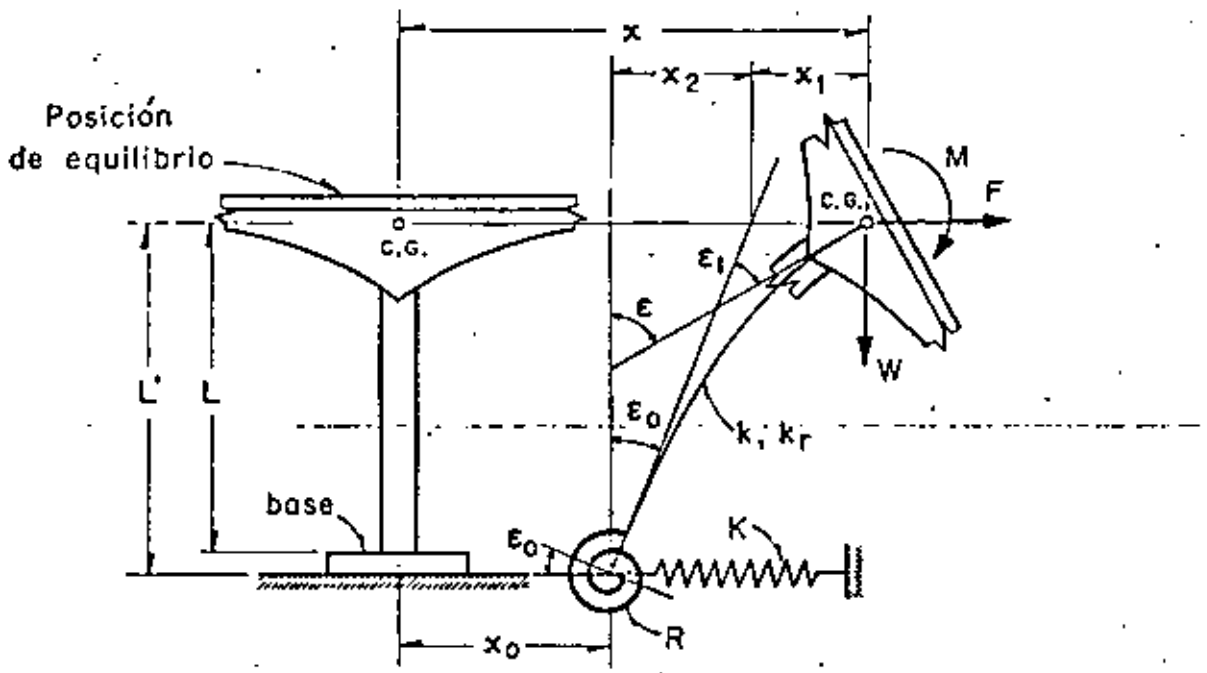

Fig. 7. *Modelo de interacción dinámica suelo-estructura*.

3. Calcular la fuerza y el momento en la base mediante las fórmulas

$$F_0 = F \quad \text{y} \quad M_0 = M + FL'$$

4. Encontrar los valores de los desplazamientos $x_0 = F_0/K$ y $\epsilon_0 = M_0/R$
5. Calcular los valores de los parámetros $\alpha = F/k$ y $\beta = M/k_r$
6. Efectuar los productos $\beta\delta$ y $\alpha\theta$
7. Calcular $x_1 = \alpha + \beta\delta$ y $\epsilon_1 = \beta + \alpha\theta$
8. Efectuar el producto $x_2 = L'\epsilon_0$
9. Calcular los desplazamientos lineales y angulares totales de C.G. mediante las expresiones

$$x' = x_0 + x_1 + x_2 \quad \text{y} \quad \epsilon' = \epsilon_0 + \epsilon_1$$

10. Encontrar el valor de ω_n^2 mediante los cocientes x/x' y ϵ/ϵ'
11. Si los valores de ω_n^2 calculados en el paso anterior son aproximadamente iguales, el proceso habrá concluido. En caso contrario repítase la secuela utilizando como valores de partida para x y ϵ los encontrados en etapa 9 o valores cuyo cociente sea igual al de x' entre ϵ'. El proceso deberá continuarse hasta lograr la aproximación deseada.

EJEMPLO DE APLICACION

Con motivo de ilustrar los conceptos enunciados anteriormente se calcularán las frecuencias y modos de vibración de un cascarón ya construido en California, EUA (fig 8). Los datos necesarios han sido extraídos de la ref 1. Se computarán también las respuestas sísmicas suponiendo que esa estructura fuera a construirse en la zona blanda de la ciudad de México. Se utilizarán por tanto los parámetros elásticos de las arcillas del Valle de México y los espectros de diseño propuestos en el reglamento de construcción para el Distrito Federal [5].

Los datos necesarios de la estructura son

$L = 419$ cm
$L' = 480$ cm
$\bar{y} = 249$ cm
$W = 20,450$ kg ($m = 20.81$ kg seg^2/cm)
$W' = 43,600$ kg
$I_0 = 1.775 \times 10^{10}$ cm^4
$I_r = 1.065 \times 10^{10}$ cm^4
$k = 1.266 \times 10^4$ kg/cm
$k_r = 7.41 \times 10^8$ kg cm/rad
$J = 1.386 \times 10^8$ kg seg^2 cm
$\theta = 0.00358$ rad/cm
$\delta = 208$ cm/rad

Las expresiones para C_r y C_ϕ son las siguientes [5]:

$$C_r = F_1 \frac{E'}{1-\nu^2} \frac{1}{\sqrt{A}}; \quad C_\phi = F_2 \frac{E'}{1-\nu^2} \frac{1}{\sqrt{A}} \quad (26)$$

En ecs 26

E' = módulo de elasticidad del suelo
ν = relación de Poisson del suelo
A = área de contacto de la cimentación
F_1, F_2 = factores de forma de la cimentación

Para el caso de la zona blanda del Valle de México un valor representativo de E' es 50 kg/cm^2 y $\nu = 0.5$ [4]. Para una cimentación cuadrada los valores de F_1 y F_2 son 0.704 y 2.11 respectivamente.

Sustituyendo valores en ecs 26 se obtiene

$$C_r = 0.123 \text{ kg/cm}^3$$
$$C_\phi = 0.369 \text{ kg/cm}^3$$

Caso 1. Suelo rígido

a) *Cálculo de frecuencias y modos de vibración*

Para el cálculo de las frecuencias de vibración usaremos la fórmula dada en ec 22. Los valores de los parámetros a sustituir son

$$p^2 = k/m = 608 \text{ (rad/seg)}^2$$
$$\Omega^2 = k_r/J = 535 \text{ (rad/seg)}^2$$
$$\mu = \Omega^2/p^2 = 0.882$$

con los cuales

$$\lambda_{1,2} = 2(1.882 \pm \sqrt{3.55 - 0.882}) = 0.494; 7.034$$

Por tanto

$$\omega_1 = \sqrt{0.494 \times 608} = \sqrt{300} = 17.32 \text{ rad/seg}$$

$$\omega_2 = \sqrt{7.034 \times 608} = \sqrt{4260} = 65.30 \text{ rad/seg}$$

Los periodos naturales son

$T_1 = 2\pi/\omega_1 = 0.362$ seg (T_1 obtenido de un registro de vibraciones libres de la estructura y reportado en ref 1 = 0.483 seg)

$T_2 = 2\pi/\omega_2 = 0.096$ seg

Comparando los valores calculado y medido de T_1 se puede ver la importancia de la interacción dinámica suelo-estructura.

Las relaciones modales se obtienen de las ecs. 25 y sus valores son

$$x_1/\epsilon_1 = \frac{2 \times 419}{1 - 0.494} = 238 \text{ cm/rad}$$

$$x_2/\epsilon_2 = \frac{2 \times 419}{1 - 7.034} = 275 \text{ cm/rad}$$

b) *Respuesta sísmica*

Para el cálculo de la respuesta sísmica de sistemas de varios grados de libertad es necesario calcular los coeficientes de participación de cada modo de vibración. Se puede demostrar [3] que para este caso es aplicable la siguiente ecuación

$$C_n = \frac{X_n^T M \bar{1}}{X_n^T M X_n} \quad (27)$$

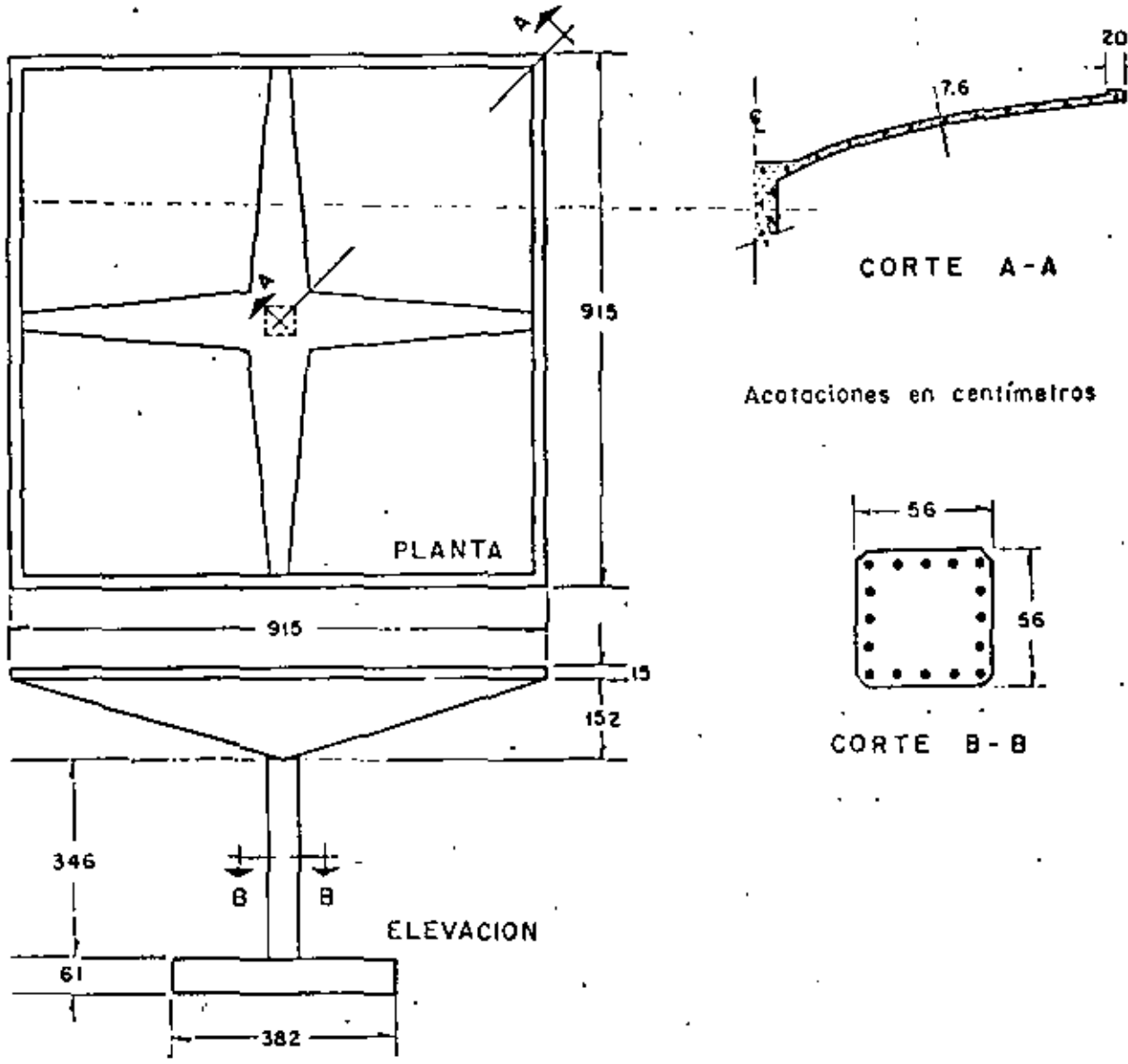

FIG. 8. *Cascarón utilizado para ejemplo.* (Después de R. McLean)

en la cual

$\bar{I}$ es un vector que representa los desplazamientos estáticos de cada grado de libertad de la estructura inducidos por un desplazamiento estático unitario de la base.

$\bar{X}_n$ es el vector modal para el enésimo modo (n)

$\bar{M}$ es la matriz de inercia y

$\bar{X}_n^T$ es el vector traspuesto de $\bar{X}_n$.

Para nuestro caso se tendrá

$$\bar{I} = \begin{bmatrix} X_{rot} \\ t_{rot} \end{bmatrix} = \begin{bmatrix} 1 \\ 0 \end{bmatrix}$$

$$\bar{X}_1 = \begin{bmatrix} 238 \\ 1 \end{bmatrix}, \qquad \bar{X}_2 = \begin{bmatrix} -275 \\ 1 \end{bmatrix}$$

$$\bar{X}_1^T = \begin{bmatrix} 238 & 1 \end{bmatrix}, \qquad \bar{X}_2^T = \begin{bmatrix} -275 & 1 \end{bmatrix}$$

$$\bar{M} = \begin{bmatrix} m & 0 \\ 0 & J \end{bmatrix} = \begin{bmatrix} 20.81 & 0 \\ 0 & 1.386 \times 10^6 \end{bmatrix}$$

Sustituyendo valores en ec 27 y efectuando los productos matriciales en ella indicados se obtiene

$$C_1 = \frac{4.960}{2.566 \times 10^6} = 0.00193$$

$$C_2 = \frac{-5.720}{2.959 \times 10^6} = -0.00193$$

El valor absoluto de la respuesta máxima en cada uno de los modos será [7].

$$\begin{bmatrix} V_n = \text{fuerza cortante} \\ M_n = \text{momento flexionante} \end{bmatrix} = |C_n| \begin{bmatrix} m & 0 \\ 0 & I \end{bmatrix} \times$$

$$\times \begin{bmatrix} x_n \\ \epsilon_n \end{bmatrix} S_{an} \qquad (28)$$

donde

S_{an} = ordenada del espectro de aceleraciones afectada por el coeficiente sísmico $C = 0.15$.

El espectro que será utilizado es el propuesto en el reglamento de construcciones del Distrito Federal [8] (fig. 9). Los valores de las ordenadas espectrales correspondientes a T_1 y T_2 son 100 cm/seg² y 80.6 cm/seg² respectivamente.

Sustituyendo valores en ec 28 se llega a

$$\begin{bmatrix} V_1 \\ M_1 \end{bmatrix} = \begin{bmatrix} 957 \text{ kg} \\ 268{,}000 \text{ kg cm} \end{bmatrix} \qquad (29)$$

$$\begin{bmatrix} V_2 \\ M_2 \end{bmatrix} = \begin{bmatrix} 893 \text{ kg} \\ 216{,}000 \text{ kg cm} \end{bmatrix} \qquad (30)$$

El criterio propuesto en ref. 8 será utilizado para el cálculo de la respuesta total (considerando los efectos combinados de los dos modos). Por lo anterior la respuesta total de la estructura valdrá

$$V = \sqrt{V_1^2 + V_2^2} \quad ; \quad M = \sqrt{M_1^2 + M_2^2} \qquad (31a, 31b)$$

En ecs 31a y 31b

V = fuerza cortante total en la columna

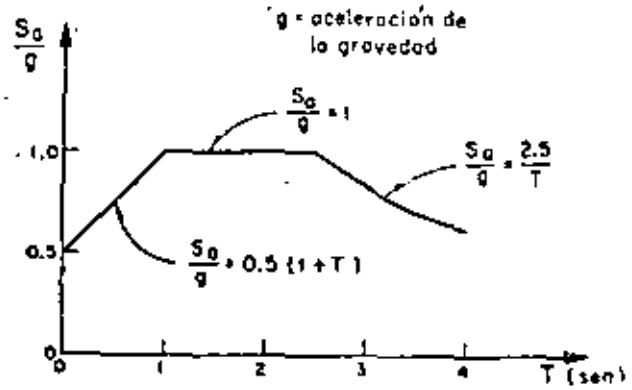

FIG. 9. *Espectro de aceleraciones* (Después de E. Rosenblueth y L. Esteva)

M = momento flexionante total en C. G.

Sustituyendo los valores dados en ecs 29 y 30 en (31) se obtiene

$$V = 1{,}310 \text{ kg} \quad ; \quad M = 344{,}000 \text{ kg cm}$$

El momento en la base de la columna valdrá

$$M_b = 344{,}000 + 1{,}310 \times 419 = 893{,}000 \text{ kg cm}$$

Los resultados de este caso se resumen en la fig. 10a.

CASO 2. SUELO FLEXIBLE

a) Cálculo de frecuencias y modos de vibración.

Para considerar las restricciones del suelo emplearemos el método propuesto anteriormente procediendo en forma tabular. Sustituyendo valores en ecuaciones para K y R se obtienen 1.88×10^5 kg/cm y 6.35×10^8 kg cm/rad respectivamente.

PRIMER MODO

Parámetros	*Valores (1er. ciclo)*		*Factor común*
x, ϵ (supuestos)	$x = 400$ cm	$\epsilon = 1$ rad	
$F = m\omega_1^2 x$, $M = I\omega_1^2 \epsilon$	$F = 8320$	$M = 1{,}386{,}000$	ω_1^2
$F_0 = F$, $M_0 = M + FL'$	$F_0 = 8320$	$M_0 = 5{,}376{,}000$	ω_1^2
$x_0 = F_0/K$, $\epsilon_0 = M_0/R$	$x_0 = 0.4420$	$\epsilon_0 = 0.00847$	ω_1^2
$\alpha = F/k$, $\beta = M/k_\epsilon$	$\alpha = 0.6570$	$\beta = 0.00187$	ω_1^2
$\beta\delta$, $\alpha\theta$	$\beta\delta = 0.3892$	$\alpha\theta = 0.00235$	ω_1^2
$x_1 = \alpha + \beta\delta$, $\epsilon_1 = \beta + \alpha\theta$	$x_1 = 1.0462$	$\epsilon_1 = 0.00422$	ω_1^2
$x_2 = \epsilon_0 L'$	$x_2 = 4.0650$	———	ω_1^2
$x' = x_0 + x_1 + x_2$, $\epsilon' = \epsilon_0 + \epsilon_1$	$x' = 5.5532$	$\epsilon' = 0.01269$	ω_1^2
$\omega_1^2 = x/x'$, $\omega_1^2 = \epsilon/\epsilon'$	72.0	78.7	

$$x'/\epsilon' = 438, \quad \bar{X}_1^t = [438\ 1]$$

PRIMER MODO

Parámetros	*Valores (2º ciclo)*		*Factor común*
x, e	438	1	
F, M	9130	1,386.000	ω_1^2
F_o, M_o	9130	5,766.000	ω_1^2
x_o, e_o	0.4860	0.00910	ω_1^2
α, β	0.7210	0.00187	ω_1^2
$\beta\delta, \alpha\theta$	0.3892	0.002585	ω_1^2
x_1, e_1	1.1102	0.004455	ω_1^2
x_2, e_2	4.365	———	ω_1^2
x', e'	5.961	0.013565	ω_1^2
ω_1^2	73.5	75.8	—

Suponiendo que la aproximación es suficiente resulta

$$x'/e' = 440, \quad \bar{X}_1^T = [440, 1], \quad \omega_1^2 \doteq 74 \text{ (rad/seg)}^2$$

$$T_1 = 0.731 \text{ seg.}$$

El procedimiento para el cómputo de los parámetros del segundo modo es el mismo, sólo que la configuración supuesta deberá "limpiarse", antes de proseguir el cálculo, de las componentes del primer modo que pudiera contener. Se demuestra[1] que si $\bar{X}_2'$ es el vector de la configuración supuesta, el vector libre de componentes del primer modo queda dado por

$$\bar{X}_2 = \bar{X}_2' - \frac{\bar{X}_2'^T \bar{M} \bar{X}_1}{\bar{X}_1^T M X_1} X_1 \qquad (32)$$

Suponiendo para el primer ciclo

$$\bar{X}_2' = \begin{bmatrix} -150 \\ 1 \end{bmatrix}$$

y sustituyendo valores en la ecuación matricial 32 se obtiene

$$\bar{X}_2 = \begin{bmatrix} -151 \\ 1 \end{bmatrix}$$

que nos da los valores de partida para el primer ciclo de cálculo.

SEGUNDO MODO

Parámetros	*Valores (1er. ciclo)*		*Factor común*
x, e	—151	1	
F, M	—3143	1.386.000	ω_2^2
F_o, M_o	—3143	—123,000	ω_2^2
x_o, e_o	—0.1672	—0.0001940	ω_2^2
α, β	—0.2481	0.0018700	ω_2^2
$\beta\delta, \alpha\theta$	0.3892	—0.0008890	ω_2^2
x_1, e_1	0.1411	0.0009810	ω_2^2
x_2, e_2	—0.0930	———	ω_2^2
x', e'	—0.1191	0.0007870	ω_2^2
ω_2^2	1267	1270	—

$x'/e' = -151, \ \bar{X}_2^T = [-151\ 1], \ T_2 = 0.176$ seg.

En este caso se supuso un valor cercano al real y por tanto sólo se necesitó un ciclo para que se obtuviera la aproximación deseada. Si el valor supuesto no hubiese sido ese sino otro cualquiera seguramente no hubiera sido suficiente un ciclo de cálculo. En los ciclos subsiguientes se procedería en igual forma que antes: suponer inicialmente la configuración obtenida en el ciclo anterior; limpiarla de las componentes del primer modo; etc.

b) Respuesta sísmica

Los valores de los coeficientes de participación y de las ordenadas espectrales para este caso son:

$$C_1 = 0.001689, \qquad C_2 = -0.001689$$

$$S_{a1} = 127.4 \text{ cm/seg}^2, \qquad S_{a2} = 86.6 \text{ cm/seg}^2$$

Las respuestas máximas para cada modo valen

$$\begin{bmatrix} V_1 \\ M_1 \end{bmatrix} = \begin{bmatrix} 1.970 \text{ kg} \\ 298.200 \text{ kg cm} \end{bmatrix}$$

$$\begin{bmatrix} V_2 \\ M_2 \end{bmatrix} = \begin{bmatrix} 461 \text{ kg} \\ 203.000 \text{ kg cm} \end{bmatrix}$$

Las respuestas máximas totales serán (fig 10b)

$$V = 2,030 \text{ kg}$$

$$M = 361,000 \text{ kg cm}$$

$$M_b = 1,209.000 \text{ kg cm}$$

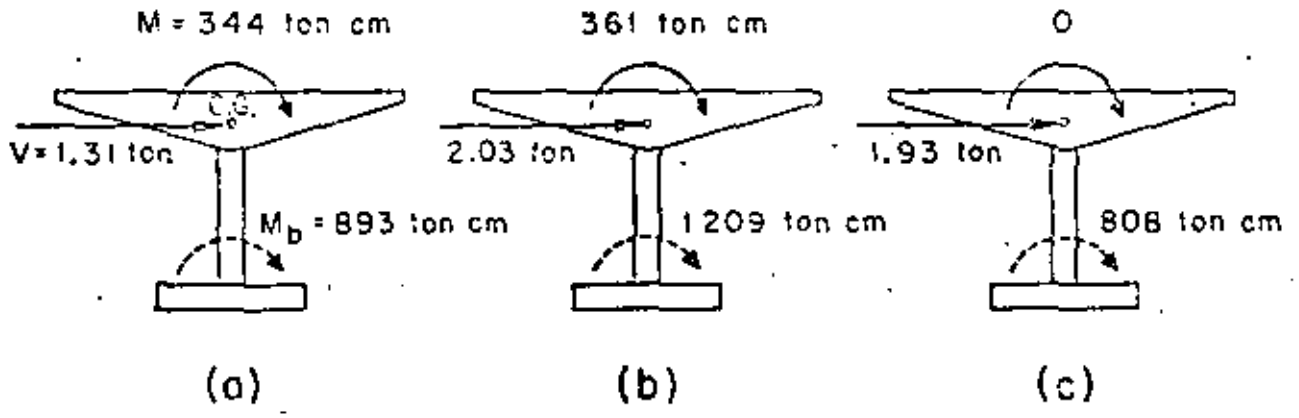

FIG. 10. *Respuestas sísmicas*

CASO 3. BASE RÍGIDA Y MASA CONCENTRADA

Para comparación de resultados se verá cuál es el valor de la respuesta máxima en el caso de despreciar la inercia rotacional y la interacción suelo-estructura.

Para este caso $p^2 = 608$ (rad/seg)^2, $T = 0.325$ seg, $0.15S_a = 92.6$ cm/seg^2, $V = mS_a = 1.930$ kg y $M_b = 808.000$ kg cm (fig 10c).

CONCLUSIONES

En la siguiente tabla se resumen los resultados de los tres casos, indicados como porcentajes del segundo caso.

Concepto	*Caso 1*	Caso 2	Caso 3
V	64.4%	100%	95.0%
M	95.2%	100%	0 %
M_b	73.8%	100%	66.7%

Los resultados de la tabla anterior dan una idea clara de la importancia que tiene el considerar la inercia rotacional de la cubierta y la interacción suelo-estructura. La importancia del primer concepto aumentará conforme mayor sea el momento de inercia de masa de la cubierta con respecto al eje z. El último concepto es tanto más importante cuanto más blando sea el suelo de cimentación. En particular puede observarse que en el tipo de solución 3 no se obtiene momento flexionante a la altura de C.G. Esto puede traer consigo serios errores en la cuantía del acero de refuerzo necesario en la unión columna-cubierta que es donde más ductilidad necesita desarrollarse.

AGRADECIMIENTO

El autor manifiesta su agradecimiento a los doctores E. Rosenblueth y J. A. Nieto, así como al Ing. E. del Valle por sus valiosos comentarios y sugerencias.

REFERENCIAS

1. McLean, R. S., "Inverted pendulum structures", technical report of *Consulting Civil and Structural Engineers*, Fullerton, Cal. (ene. 1965).
2. Barkan, D. D., "Dynamics of bases and foundations", McGraw Hill Book Co. Inc. (1962).
3. Jacobsen, L. S., y Ayre, R. S., "Engineering vibrations", McGraw Hill Book Co. Inc. (1958).
4. Newmark, N. M., "Numerical procedure for computing deflections, moments and buckling loads", *Transactions ASCE*, Vol. 108 (1943), pp. 1161-1234.
5. Rosenblueth, E. y Esteva, L., *"Proyecto de reglamento de las construcciones en el Distrito Federal. "Folleto complementario. Diseño sísmico de edificios"*, Ediciones Ingeniería, México (1962).
6. Marsal, R., y Mazari, M., *"El subsuelo de la Ciudad de México"*, Publicación del Instituto de Ingeniería UNAM (1962).
7. Newmark, N. M., y Rosenblueth, E., *"Earthquake Engineering"*, será publicado por Prentice-Hall, Inc.
8. Rosenblueth, E., "Some applications of probability theory in aseismic design", *Proceedings, 1st World Conference on Earthquake Engineering*, Berkeley, Cal. (1956), paper 8.

DIVISION DE EDUCACION CONTINUA
FACULTAD DE INGENIERIA U.N.A.M.

C U R S O :

" I N G E N I E R I A S I S M I C A "

VIBRACION DE VIGAS DE CORTANTE Y FLEXION

DR. OCTAVIO A. RASCON CHAVEZ

JUNIO, 1981.

VIGAS DE CORTANTE NO AMORTIGUADAS

SON SISTEMAS CONTINUOS CUYOS CAMBIOS DE PENDIENTE SON PROPORCIONALES AL CORTANTE QUE ACTUA EN LA SECCION.

SEAN m y p LA MASA Y FUERZA EXTERNA DISTRIBUIDAS POR UNIDAD DE LONGITUD, Y SEA k LA RIGIDEZ POR CORTANTE:

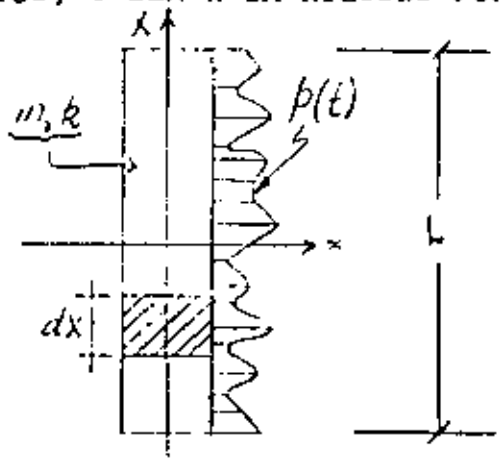

$k = FAG$

F = FACTOR DE FORMA

A = AREA SECCION TRANSVERSAL

G = MODULO DE ELASTICIDAD DINAMICO AL CORTANTE

$$F_I = mdX \frac{\partial^2 x}{\partial t^2}$$

POR EQUILIBRIO:

$$\frac{\partial S}{\partial x} dx + pdx - m \frac{\partial^2 x}{\partial t^2} dx = 0$$

$$m \frac{\partial^2 x}{\partial t^2} - k \frac{\partial^2 x}{\partial x^2} = p(t) \qquad (1)$$

LA EC HOMOGENEA QUEDA (CON p=0)

$$(2)\quad \frac{\partial^2 x}{\partial t^2} - v^2 \frac{\partial^2 x}{\partial X^2} = 0 \; ; \quad v^2 = \frac{k}{m}$$

ESCRIBIENDO $x(t) = Z_n(X)\theta_n(t)$, LA EC (2) QUEDA

$$Z_n \ddot{\theta}_n - v^2 Z_n'' \theta_n = 0$$

$$\frac{\ddot{\theta}_n(t)}{\theta_n(t)} - v^2 \frac{Z_n''}{Z_n} = 0 \Rightarrow \frac{\ddot{\theta}_n(t)}{\theta_n(t)} = v^2 \frac{Z_n''}{Z_n} = \omega_n^2 = \text{CONSTANTE}$$

$$\Rightarrow \ddot{\theta}_n + \omega_n^2 \theta_n = 0 \; ; \quad Z_n'' + \frac{\omega_n^2}{v^2} Z_n = 0$$

$$\theta_n = \operatorname{sen}\omega_n(t-t_n), \quad Z_n = A_n \operatorname{sen}\frac{\omega_n}{v}(X-a_n)$$

$$\therefore x_n = A_n \operatorname{sen}\left[\frac{\omega_n}{v}(X-a_n)\right]\operatorname{sen}\left[\omega_n(t-t_n)\right], \quad n=1,2\ldots$$

LAS CONSTANTES a_n Y ω_n SE DETERMINAN EN CADA PROBLEMA EN FUNCION DE LAS CONDICIONES DE FRONTERA

CONDICION DE ORTOGONALIDAD

$$\int_0^L x_n(X)x_j(X) = 0, \text{ SI } n \neq j$$

EJEMPLO 1: CUERDA VIBRANTE DE LONGITUD L Y EXTREMOS FIJOS:

EN EL EXTREMO X=0 SE TENDRA

$$(3)\quad x(0,t) = 0 \Rightarrow \frac{\omega_n a_n}{v} = j\pi \; ; \quad j = 0,1,2,\ldots$$

EN EL EXTREMO X = L SE TENDRA

$$(4)\quad x(L,t) = 0 \quad \Rightarrow \quad \frac{\omega_n L}{v} = n\pi \quad ; \quad n = 1,2,\ldots$$

PUESTO QUE EN LA EC (3) SE TOMA j=0, YA QUE j=1,2,... DAN LA MISMA SOLUCION, LO CUAL CONDUCE A $a_n = 0$

DE LA EC (4): $\omega_n = \frac{n\pi v}{L}$; $n = 1,2,\ldots$

FRECUENCIA FUNDAMENTAL

SI $n=1$, $\omega_1 = \frac{\pi v}{L}$ $\therefore$ $\omega_n = n\,\omega_1$

Y $T_1 = \frac{2L}{v}$ $T_n = \frac{T_1}{n}$

LAS CONFIGURACIONES MODALES QUEDAN:

$$Z_n = A_n \operatorname{sen}\frac{n\pi X}{L} \quad ; \quad x(t,X) = A_n \operatorname{sen}\frac{n\pi X}{L} \operatorname{sen}\frac{n\pi v}{L}(t-tn)$$

CONDICION DE ORTOGONALIDAD:

$$\int_0^L A_i \operatorname{sen}\frac{i\pi X}{L}\, A_j \operatorname{sen}\frac{j\pi X}{L} dx = 0, \quad \text{SI} \quad i \neq j$$

EJEMPLO 2: VIGA DE CORTANTE APOYADA EN X = 0 Y LIBRE EN X = L

DE $x(0,t) = 0 \Rightarrow a_n = 0$

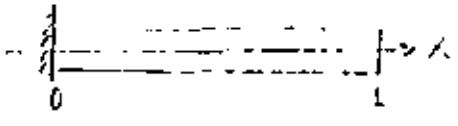

DE $x'(L,t) = 0$ (PUESTO QUE EN X = L SE DEBE CUMPLIR QUE LA FUERZA CORTANTE, S, SEA NULA),

$$x'(X,t) = A_n \frac{\omega_n}{v} \cos\frac{\omega_n X}{v} \operatorname{sen}\omega_n(t-t_n)$$

$$\therefore \quad x'(L,t) = 0 = \cos \frac{\omega_n L}{v} \Rightarrow \frac{\omega_n L}{v} = \frac{\pi}{2}(2n-1)$$

$$O \quad \omega_n = \frac{v}{L} \frac{\pi}{2} (2n-1) \qquad n = 1,2,\ldots$$

$$SI \quad n=1, \ \omega_1 = \frac{\pi v}{L.2} \Rightarrow T_1 = \frac{4L}{v}$$

$$\therefore \quad \omega_n = \omega_1(2n-1) \ ; \quad T_n = \frac{T_1}{2n-1}$$

$$ASI: \ T_2 = \frac{T_1}{3} \ , \ T_3 = \frac{T_1}{5} \ , \ ETC.$$

DISTRIBUCION DE CORTANTES:

$$S_n = k \frac{\partial x}{\partial X} = A_n \ k \ \frac{\omega_n}{v} \cos \frac{\omega_n X}{v} \ \text{sen}\omega_n(t-t_n)$$

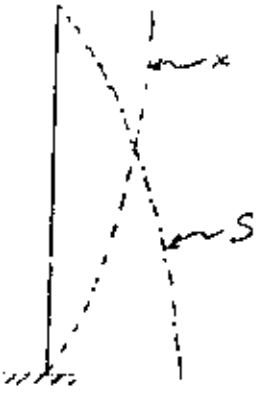

1er. MODO (FUNDAMENTAL)

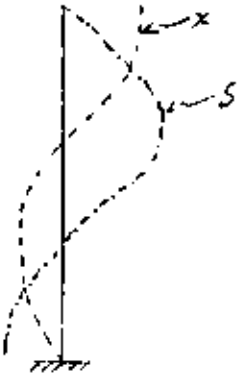

2o. MODO

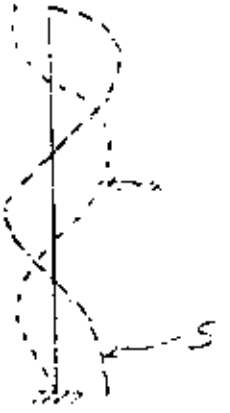

3er. MODO

SEA $\ddot{x}_o(t)$ LA EXCITACION DEL TERRENO. LA RESPUESTA, $x(t)$, DEL SISTEMA ES

$$(3)\quad x(t) = -\sum_{n=1}^{\infty} \frac{a_n}{\omega_n} \operatorname{sen} \frac{\omega_n}{v} X \int_o^t \ddot{x}_o(\tau) \operatorname{sen}\omega_n(t-\tau)\,d\tau$$

DONDE

$$(4)\quad a_n = \frac{\int_o^L n \operatorname{sen} \frac{\omega_n v}{X}\,dx}{\int_o^L n \operatorname{sen}^2 \frac{\omega_n v}{X}\,dx} = \frac{4}{(2n-1)\pi}$$

TAREA: DEMOSTRAR ECS (3) Y (4) Y ESTUDIAR SECCION 3.15.

EJEMPLO: CALCULAR EL LIMITE SUPERIOR DEL CORTANTE EN UNA VIGA DE CORTANTE A CUYA BASE SE LE SOMETE A UNA ACELERACION CONSTANTE, a.

EL ESPECTRO DE ESTA EXCITACION ES $V = a/\omega$

POR LO TANTO, $S \leq k \left| \frac{\partial}{\partial X} \left(\sum_{n=1}^{\infty} \frac{a_n}{\omega_n} \operatorname{sen} \frac{\omega_n}{v} X \right) \right| V$

$$S \leq \left| \sum_{n=1}^{\infty} \frac{k a_n V}{\omega_n} \frac{\omega_n}{v} \cos \frac{\omega_n}{v} X \right| = \frac{4k}{\pi} \frac{a}{\frac{k}{m}} \left| \sum_{n=1}^{\infty} \frac{\operatorname{sen} \frac{\pi}{2L}(2n-1)X}{(2n-1)\frac{v}{L}\frac{\pi}{2}(2n-1)} \right|$$

$$S \leq \frac{8aLm}{\pi^2} \sum_{n=1}^{\infty} \frac{1}{(2n-1)^2} \left| \cos \frac{(2n-1)\pi X}{2L} \right| \quad ; \text{ EN } X=0$$

$$S \leq (8aLm)/\pi^2 \underbrace{\sum_{n=1}^{\infty} \frac{1}{(2n-1)^2}}_{\pi^2/8} = aLm$$

VIBRACION DE VIGAS EN FLEXION

a. AMORTIGUAMIENTO NULO

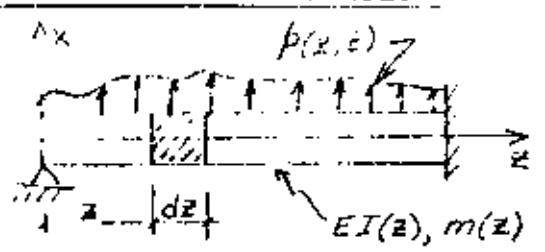

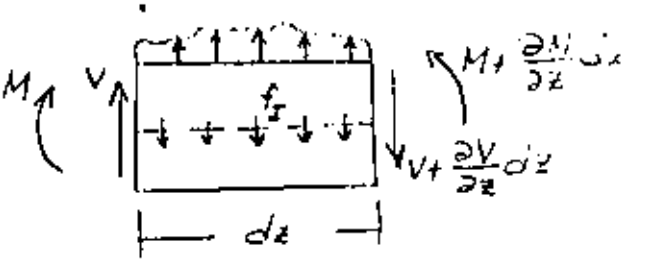

$$V + pdz - (V + \frac{\partial V}{\partial z}\, dz) - f_I dz = 0 \qquad (1)$$

EN DONDE $f_I dz = mdx \ \frac{\partial^2 x}{\partial t^2}$ (2)

SUSTITUYENDO (2) EN (1) Y SIMPLIFICANDO:

$$\frac{\partial V}{\partial z} = p - m \frac{\partial^2 x}{\partial t^2} \qquad (3)$$

$$M + Vdz - (M + \frac{\partial M}{\partial z}\, dz) = 0 \qquad \frac{\partial M}{\partial z} = V \qquad (4)$$

(DESPRECIANDO LOS TERMINOS DE SEGUNDO ORDEN DE LOS MOMENTOS DE p Y f_I)

SUSTITUYENDO (4) EN (3) SE OBTIENE

$$\frac{\partial^2 M}{\partial z^2} + m\frac{\partial^2 x}{\partial t^2} = p \qquad (4')$$

TOMANDO EN CUENTA QUE $\frac{M}{EI} = \frac{\partial^2 x}{\partial z^2}$ SE OBTIENE FINALMENTE

$$\frac{\partial^2}{\partial z^2}(EI \frac{\partial^2 x}{\partial z^2}) + m\frac{\partial^2 x}{\partial t^2} = p \qquad (5)$$

8

b. AMORTIGUAMIENTO VISCOSO

- FUERZA DE AMORTIGUAMIENTO POR VELOCIDAD TRANSVERSAL $= c(z)\frac{\partial x}{\partial t}$

$$\frac{\partial V}{\partial z} = p - m\frac{\partial^2 x}{\partial t^2} - c\frac{\partial x}{\partial t} \qquad (6)$$

- FUERZA DE AMORTIGUAMIENTO POR DEFORMACION DE LA VIGA. ACEPTANDO LA HIPOTESIS DE NAVIER DE DEFORMACION PLANA

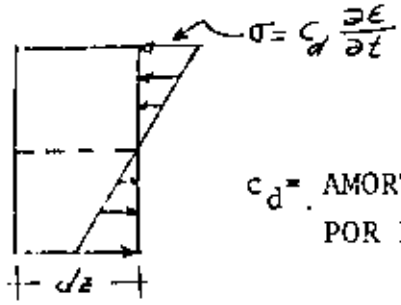

$$M_{amort} = \int \sigma y da = c_d I(z)\frac{\partial^3 x}{\partial z^2 \partial t}$$

c_d = AMORTIGUAMIENTO POR DEFORMACION

INCORPORANDO EL MOMENTO DEBIDO AL AMORTIGUAMIENTO EN LA EC. (5)

$$\frac{\partial^2}{\partial z^2}\left(EI\frac{\partial^2 x}{\partial z^2} + C_d I\frac{\partial^3 x}{\partial z^2 \partial t}\right) + m\frac{\partial^2 x}{\partial t^2} + c\frac{\partial x}{\partial t} = p \qquad (6)$$

SI LA EXCITACION ES POR MOVIMIENTO DE LOS APOYOS, SE PUEDE DEMOSTRAR (CLOUGH Y PENZIEN, PAG 303) QUE:

$$\frac{\partial^2}{\partial z^2}\left(EI\frac{\partial^2 x}{\partial z^2} + C_d I\frac{\partial^3 x}{\partial z^2 \partial t}\right) + m\frac{\partial^2 x}{\partial t^2} + c\frac{\partial x}{\partial t} = p_{efect.}$$

EN DONDE

$$p_{efect} = \frac{-\partial^2}{\partial z^2}\left(EI\frac{\partial^2 x_s}{\partial z^2} + C_d I\frac{\partial^3 x_s}{\partial z^2 \partial t}\right) - m\frac{\partial^2 x_s}{\partial t^2} - c\frac{\partial x_s}{\partial t} \qquad (7)$$

$$x(z,t) = x_{est}(z,t) + x(z,t)$$
$$t0t$$

x_s = DESPLAZAMIENTO PSEUDOESTATICO OCASIONADO POR EL MOV. DE LOS APOYOS DE MANERA ESTATICA

x = DESPLAZAMIENTO DINAMICO

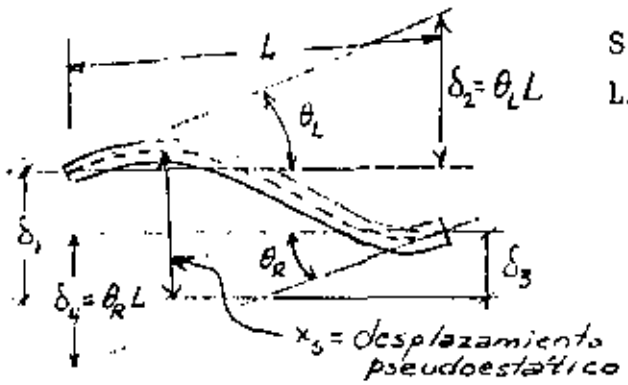

SI SE TIENE UNA ROTACION Y UNA TRASLACION POR APOYO:

$$x_s = \sum_{i=1}^{4} \phi_i \delta_i(t) \qquad (8)$$

$\phi_i(z)$ = CONFIGURACION DE LA VIGA DEBIDA A $\delta_i = 1$

INCORPORANDO (8) EN (7):

$$p_{efect} = -\sum_{i=1}^{4} \{m\phi_i \ddot{\delta}_i(t) + c\,\phi_i \dot{\delta}_i(t) + \frac{\partial^2}{\partial z^2}[c_d I(z) \frac{\partial^2 \phi_i(z)}{\partial z^2} \dot{\delta}_i(t)]\} \qquad (9)$$

EN LA MAYORIA DE LOS CASOS EL AMORTIGUAMIENTO INFLUYE POCO EN LA FUERZA EFECTIVA Y LA EC.(9) SE SIMPLIFICA A

$$p_{efect} = -\sum_{i=1}^{4} m\phi_i(z) \ddot{\delta}_i(t)$$

EN EL CASO DE UN VOLADIZO

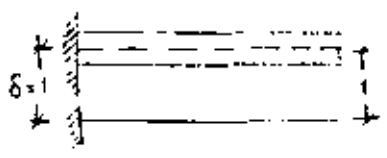

$$\phi_1(z) = 1$$

Y

$$p_{efect} = -\, m(z)\, \ddot{\delta}_1(t)$$

ANALISIS DE VIBRACIONES LIBRES

CONSIDEREMOS UNA VIGA DE SECCION CONSTANTE (EI= CONSTANTE ; $\bar{m}$=MASA POR UNIDAD DE LONGITUD).

DE LA EC.(5): $EI \frac{\partial^4 x}{\partial z^4} + \bar{m} \frac{\partial^2 x}{\partial t^2} = 0$

$$\frac{\partial^4 x}{\partial z^4} = \frac{\bar{m}}{EI} \frac{\partial^2 x}{\partial t^2} = 0 \qquad (10)$$

RESOLVIENDO LA EC. (10) POR SEPARACION DE VARIABLES:

$$x(z,t) = \theta(z)\, Y(t)$$

$$\theta^{IV}(z)\, Y(t) + \frac{\bar{m}}{EI}\, \theta(z)\, \ddot{Y}(t) = 0 \; ; \; \frac{\theta^{IV}(z)}{\theta(z)} + \frac{\bar{m}}{EI} \frac{\ddot{Y}(t)}{Y(t)} = 0$$

POR LO QUE

$$\frac{\theta^{IV}(z)}{\theta(z)} = -\frac{m}{EI} \frac{\ddot{Y}(t)}{Y(t)} = C = a^4 \quad (C = \text{CONSTANTE})$$

POR LO TANTO OBTENEMOS DOS ECUACIONES DIFERENCIALES ORDINARIAS:

$$\theta^{IV}(z) - a^4\, \theta(z) = 0$$

$$\ddot{Y}(t) + \omega^2 Y(t) = 0 \quad \text{DONDE} \quad \omega^2 = \frac{a^4 EI}{\bar{m}}$$

$$\text{O} \qquad a^4 = \frac{\omega^2 \bar{m}}{EI}$$

LA SOLUCION DE LA SEGUNDA DE ESTAS ES:

$$Y(t) = \frac{\dot{Y}(o)}{\omega} \operatorname{sen}\omega t + Y(o) \cos\omega t \qquad (11)$$

i1

LA SOLUCION DE LA PRIMERA ES:

$$\theta(z) = A_1 \text{ sen } az + A_2 \cos az + A_3 \text{ senh} az + A_4 \cosh az \qquad (12)$$

EN DONDE LAS A_i SE CALCULAN EN FUNCION DE LAS CONDICIONES DE FRONTERA DE LA VIGA EN AMBOS EXTREMOS.

EJEMPLO

VIGA SIMPLEMENTE APOYADA

LAS CUATRO CONDICIONES DE FRONTERA SON:

en $z=0$: $\theta(o)=0$, $M(o)= EI\ \ddot{\theta}(o) = 0$

en $z=L$: $\theta(L)=0$, $M(L)= EI\theta''(L) = 0$

SUSTITUYENDO $\theta(o)=0$ Y $\theta''(o)=0$ EN LA EC.(12) Y SU SEGUNDA DERIVADA:

$$\left.\begin{aligned} \theta(o) &= A_2 + A_4 \cosh 0 = 0 \\ \ddot{\theta}(o) &= a^2(-A_2 + A_4 \cosh 0) = 0 \end{aligned}\right\} \Rightarrow A_2 = A_4 = 0$$

HACIENDO LO MISMO CON $\theta(L) = 0$ y $\theta''(L) = 0$:

$$\left.\begin{aligned} \theta(L) &= A_1 \text{ sen } aL + A_3 \text{ senh } aL = 0 \\ \ddot{\theta}(L) &= a^2(-A_1 \text{ sen } aL + A_3 \text{ senh } aL) = 0 \end{aligned}\right\} \rightarrow A_3 = 0$$

POR LO TANTO, $\theta(L) = A_1 \text{ sen } aL = 0$

PUESTO QUE $A_1=0$ ES LA SOLUCION TRIVIAL, SE DEBE TENER QUE A_1 SEA ARBITRARIA Y QUE

$$\text{sen } aL = 0 \rightarrow aL = n\pi; \quad n = 0, 1, 2, \ldots, \infty$$

POR LO TANTO, $a = n\pi/L$. RECORDANDO QUE

$a^4 = \omega^2\bar{m}/EI$, SE TIENE QUE

(12

$$\omega_n^2 = (n\pi/L)^4 EI/\bar{m} \qquad \text{O} \qquad \omega_n = \frac{n^2\pi^2}{L^2}\sqrt{EI/\bar{m}}$$

SON LAS FRECUENCIAS CIRCULARES NATURALES DE VIBRACION DE LA VIGA.

LAS CONFIGURACIONES MODALES SON

$$\theta_n(z) = A_1 \text{ sen } \frac{n\pi}{L} z$$

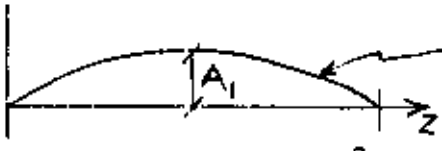

$\theta_1 = A_1 \text{sen } \frac{\pi z}{L}$; $\omega_1 = \frac{\pi^2}{L^2}\sqrt{EI/\bar{m}}$

1er. MODO

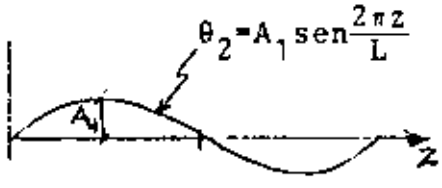

$\omega_2 = \frac{4\pi^2}{L^2}\sqrt{EI/\bar{m}}$

2o. MODO

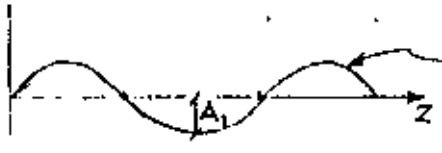

$\theta_3 = A_1 \text{sen } \frac{3\pi z}{L}$; $\omega_3 = \frac{9\pi^2}{L^2}\sqrt{EI/\bar{m}}$

3er. MODO

$$\omega_1 : \omega_2 : \omega_3 :: 1 : 4 : 9$$

$$\omega_i = n^2 \omega_1$$

DIVISION DE EDUCACION CONTINUA
FACULTAD DE INGENIERIA U.N.A.M.

CURSOS DE INGENIERIA CIVIL EN EL

PROYECTO DE PLANTAS HIDROELECTRICAS

INGENIERIA SISMICA

Efectos sísmicos en estructuras en forma de péndulo invertido.

Dr. Octavio Rascón Chávez

Mayo 1981

1

Efectos sísmicos en estructuras en forma de péndulo invertido

Octavio RASCON CH. *

INTRODUCCION

En la práctica se presentan estructuras constituidas por una sola columna la cual sostiene una cubierta que puede ser una losa o un cascarón. Su comportamiento dinámico debe estudiarse considerando el efecto que la inercia rotacional de la cubierta induce en el movimiento total de la estructura.

A principios de este año se presentó en California, EUA un trabajo[1] en el cual se trató este problema desde un punto de vista energético. Se calculó sólo el periodo fundamental y con base en él, la respuesta de la estructura a un determinado temblor. Los periodos calculados para cuatro estructuras de este tipo ya construidas fueron menores que los medidos *in sitn*. La discrepancia fue atribuida a efectos de rotación y traslación de la base.

El objeto de este trabajo es introducir un análisis modal, el cual nos proporcionará los efectos del acoplamiento que existe entre los modos de vibración. También se tomarán en cuenta en forma aproximada los efectos de rotación y traslación de la base.

CALCULO DE FRECUENCIAS Y CONFIGURACIONES MODALES DE VIBRACION

1. *Suelo rígido*

Para el caso en que el centro de gravedad de la cubierta se encuentra localizado en la prolongación del eje de la columna, el movimiento de la estructura podrá estudiarse en dos direcciones perpendiculares entre sí. En tal caso el problema podrá discretizarse como de dos modos de vibración acoplados en cada dirección.

Para el cálculo de las frecuencias de vibración se idealizará la estructura como de comportamiento lineal, constituida por una cubierta infinitamente rígida de masa simétricamente distribuida y soportada por una sola columna. Como primer caso se considerará al suelo infinitamente rígido (fig. 1).

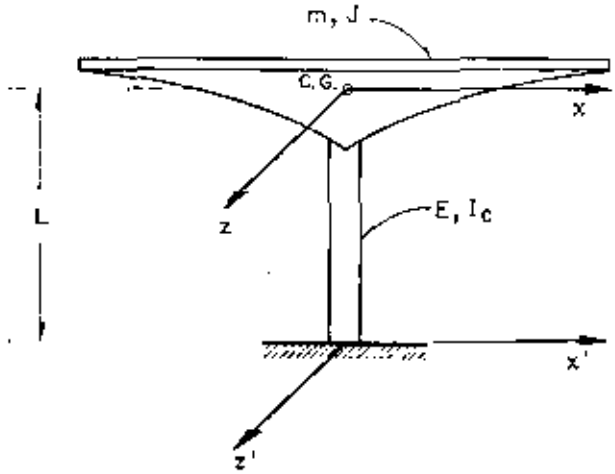

FIG. 1. *Péndulo invertido*

En fig 1

W = peso de la cubierta más la parte tributaria de la columna
J = momento de inercia de la masa de la cubierta respecto al eje z
E = módulo de elasticidad del material de la columna
I_c = momento de inercia de la sección transversal de la columna con respecto al eje z
C.G. = centro de gravedad de la cubierta
L = distancia de C.G. al suelo.

Para la columna mostrada en las figs. 2*a* y 2*b*,

k = rigidez por traslación (fuerza horizontal aplicada en C.G. necesaria para que este se desplace la unidad)
k_r = rigidez por rotación (par aplicado en C.G. necesario para producir un giro unitario a la altura de C.G.
θ = rotación en C.G. debida a la fuerza k
δ = desplazamiento lateral de C.G. debido al momento k_r.

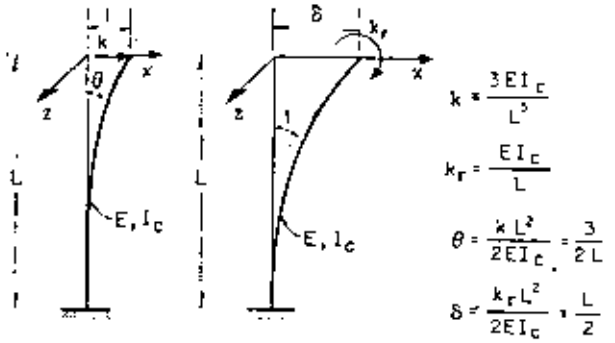

FIG. 2. *Rigideces*

* Asistente de Investigador, Instituto de Ingeniería, UNAM.

Despreciando las deformaciones por cortante, las expresiones para k, k_r, Θ y δ pueden encontrarse por estática y valen

$$k = 3EI_c/L^3; \qquad (1a)$$

$$k_r = EI_c/L; \qquad (2a)$$

$$\Theta = 1.5/L \qquad (1b)$$

$$\delta = L/2 \qquad (2b)$$

Para una fuerza de magnitud αk, el desplazamiento será α y el giro $\alpha\Theta$. Para un par de magnitud βk_r el giro será β y el desplazamiento $\beta\delta$. Al aplicarse ambos simultáneamente, el desplazamiento total de C.G. será x_1 y el giro ε_1 (fig. 3).

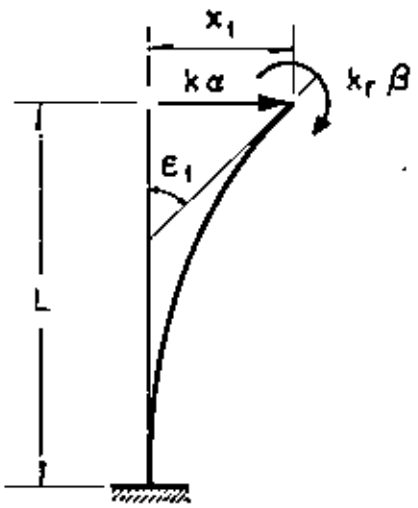

$$x_1 = \alpha + \beta\,\delta$$

$$\varepsilon_1 = \alpha\,\theta + \beta$$

FIG. 3. *Desplazamientos y giros totales*

Por tanto los valores de x_1 y ε_1 quedan dados por

$$x_1 = \alpha + \beta\delta \qquad (3)$$

$$\varepsilon_1 = \alpha\Theta + \beta \qquad (4)$$

Resolviendo el sistema de ecuaciones 3 y 4 para α y β, y utilizando las ecs 1*b* y 2*b* se obtiene

$$\alpha = (x_1 - k_r\gamma\varepsilon_1)/\kappa; \qquad (5a)$$

$$\beta = (\varepsilon_1 - k\gamma x_1)/\kappa \qquad (5b)$$

en las cuales

$$\gamma = L^2/2EI_r; \qquad (6a)$$

$$\kappa = 1 - kL^3/4EI_c = 0.25 \qquad (6b)$$

Para las oscilaciones del péndulo mostrado en la fig 1, el diagrama de cuerpo libre de la cubierta está indicado en la fig 4. Las ecuaciones de movimiento, despreciando efectos gravitacionales, serán

$$m\ddot{x}_1 + k\alpha = 0 \qquad (7)$$

$$J\ddot{\varepsilon}_1 + k_r\beta = 0 \qquad (8)$$

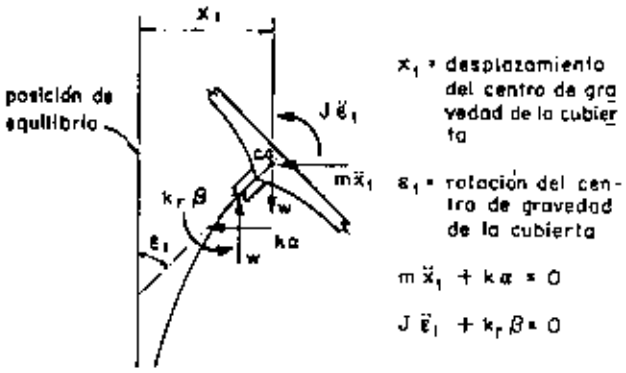

FIG. 4. *Diagrama de cuerpo libre*

Sustituyendo a (5a) y (5b) en (7) y (8) se obtiene

$$m\ddot{x}_1 + (kx_1 - kk_r\gamma\varepsilon_1)/\kappa = 0 \qquad (9)$$

$$J\ddot{\varepsilon}_1 + (k_r\varepsilon_1 - kk_r\gamma x_1)/\kappa = 0 \qquad (10)$$

Las ecs. 9 y 10 se pueden expresar matricialmente en la forma

$$\begin{bmatrix} m & 0 \\ 0 & J \end{bmatrix}\begin{bmatrix} \ddot{x}_1 \\ \ddot{\varepsilon}_1 \end{bmatrix} + \frac{1}{\kappa}\begin{bmatrix} k & -\gamma kk_r \\ -\gamma kk_r & k_r \end{bmatrix}\begin{bmatrix} x_1 \\ \varepsilon_1 \end{bmatrix} = 0 \qquad (11)$$

Utilizando las ecs 1a, 2a y 6a se encuentra que

$$\gamma kk_r = Lk/2 \qquad (12)$$

Puesto que el movimiento es armónico se tiene que

$$\ddot{x}_1 = -\omega^2 x_1 \quad \text{y} \quad \ddot{\varepsilon}_1 = -\omega^2\varepsilon_1 \qquad (13)$$

en donde ω es la frecuencia circular natural de vibración.

Sustituyendo las ecs. 12 y 13 en (11) se obtiene

$$-\begin{bmatrix} m & 0 \\ 0 & J \end{bmatrix}\omega^2\begin{bmatrix} x_1 \\ \varepsilon_1 \end{bmatrix} + \frac{1}{\kappa}\begin{bmatrix} k & -\frac{Lk}{2} \\ -\frac{Lk}{2} & k_r \end{bmatrix}\begin{bmatrix} x_1 \\ \varepsilon_1 \end{bmatrix} = 0 \qquad (14)$$

Factorizando en la ec. 14

$$\left\{\frac{1}{\kappa}\begin{bmatrix} k & -\frac{Lk}{2} \\ -\frac{Lk}{2} & k_r \end{bmatrix} - \omega^2\begin{bmatrix} m & 0 \\ 0 & J \end{bmatrix}\right\}\begin{bmatrix} x_1 \\ \varepsilon_1 \end{bmatrix} = 0 \qquad (15)$$

La ec 15 representa un sistema de ecuaciones homogéneas, el cual, para tener solución diferente de la trivial, necesita que su determinante sea nulo. Por tanto

$$\begin{vmatrix} \frac{k}{\kappa} - m\omega^2 & -\frac{Lk}{2\kappa} \\ -\frac{Lk}{2\kappa} & \frac{k_r}{\kappa} - J\omega^2 \end{vmatrix} = 0 \qquad (16)$$

Desarrollando el determinante se llega a

$$mJ\omega^4 - \frac{1}{\kappa}(kJ + mk_r)\omega^2 + \frac{1}{4\kappa^2}(4kk_r - L^2k^2) = 0 \qquad (17)$$

Dividiendo ambos miembros entre mJ y considerando que $L^2k^2 = 3kk_r$, se obtiene

$$\omega^4 - \frac{kJ + mk_r}{mJ\kappa}\omega^2 + \frac{k\,k_r}{4mJ\kappa^2} = 0 \qquad (18)$$

que es una ecuación de segundo grado en ω^2, cuyas soluciones son

$$\omega^2_{1,2} = \frac{kJ + mk_r}{2mJ\kappa} \pm \sqrt{\frac{(kJ + mk_r)^2}{4m^2J^2\kappa^2} - \frac{k\,k_r}{4mJ\kappa^2}} \qquad (19)$$

Dividiendo numerador y denominador de (19) entre mJ

$$\omega^2_{1,2} = \frac{k/m + k_r/J}{2\kappa} \pm \frac{1}{2\kappa}\sqrt{(k/m + k_r/J)^2 - (k/m)(k_r/J)} \qquad (20)$$

Llamando a

$k/m = p^2 =$ cuadrado de la frecuencia circular natural por traslación

$k_r/J = \Omega^2 =$ cuadrado de la frecuencia circular natural por rotación

se obtiene

$$\omega^2_{1,2} = 2\left(p^2 + \Omega^2 \pm \sqrt{(p^2 + \Omega^2)^2 - p^2\Omega^2}\right) \qquad (21)$$

Dividiendo ambos miembros de (21) entre p^2 y haciendo $\omega^2/p^2 = \lambda$ y $\Omega^2/p^2 = \mu$ se llega a

$$\lambda_{1,2} = 2\left(1 + \mu \pm \sqrt{(1 + \mu)^2 - \mu}\right) \qquad (22)$$

Es interesante notar que si $J = 0$ (masa concentrada) de la ec 17 se obtiene $\omega^2 = k/m = p^2$.

Las configuraciones modales pueden obtenerse de cualquiera de las dos ecuaciones algebraicas contenidas en la ecuación matricial dada en ec 15. La primera de ellas es

$$\left(\frac{k}{\kappa} - m\omega_n^2\right)x_{1,n} - \frac{Lk}{2\kappa}r_{1,n} = 0 \qquad (23)$$

donde el índice n indica el número del modo y de la cual se obtiene

$$x_{1,n}/r_{1,n} = \frac{Lk}{2\kappa}\Big/\left(\frac{k}{\kappa} - m\omega_n^2\right) \qquad (24)$$

dividiendo numerador y denominador de (24) entre m y considerando que $\kappa = 0.25$, $k/m = p^2$ y que $\lambda_n = \omega_n^2/p^2$ se llega a

$$x_{1,n}/r_{1,n} = 2L/(4 - \lambda_n) \qquad (25)$$

Si se desean tomar en cuenta las deformaciones por cortante basta con modificar las rigideces mediante un análisis de estática y partir de nuevo de la ec 17 sin considerar que $L^2k^2 = 3kk_r$. Si existe excentricidad en alguna dirección su efecto podrá tomarse en cuenta introduciendo un grado de libertad adicional.

En las figs 5 y 6 se encuentran representados los resultados de las ecs 22 y 25.

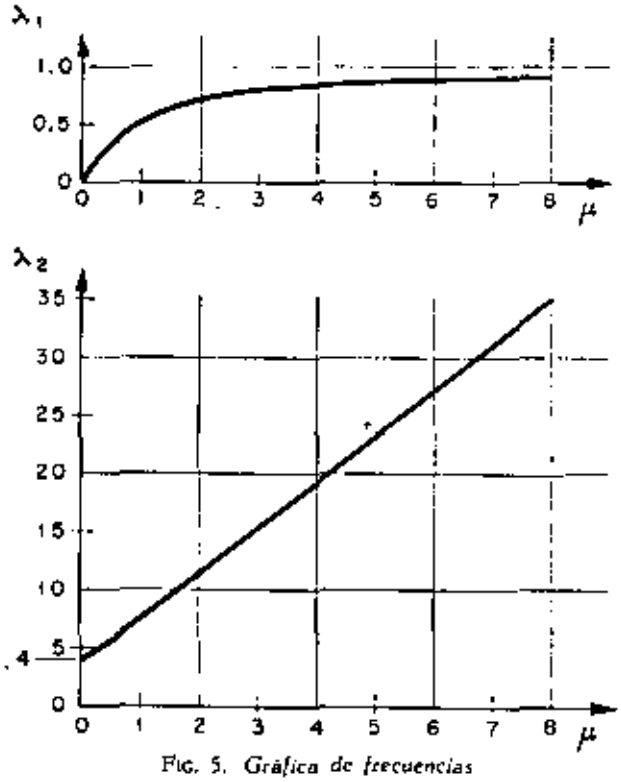

FIG. 5. *Gráfica de frecuencias*

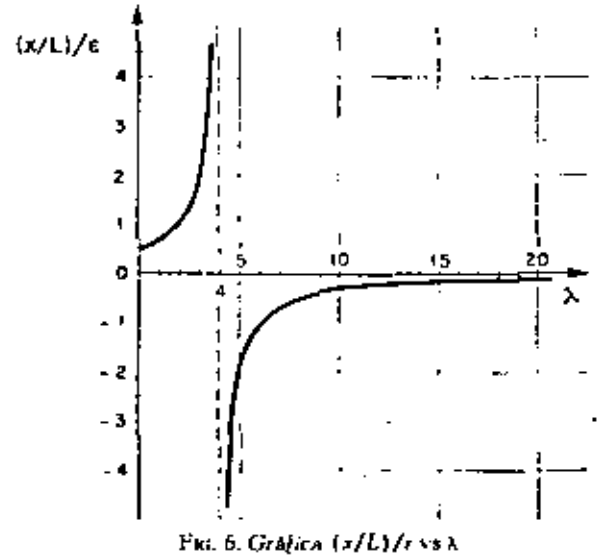

FIG. 6. *Gráfica* $(x/L)/r$ *vs* λ

2. *Suelo flexible*

Al oscilar una estructura cimentada en suelo blando, existe interacción dinámica suelo-estructura que en la mayoría de los casos no debe despreciarse al calcular las frecuencias y los modos de vibración. En lo que sigue se propone la adaptación de un método numérico para tomar en cuenta dicho efecto.

Las restricciones del suelo serán idealizadas mediante resortes de comportamiento lineal; uno para desplazamientos lineales horizontales y otro para deformaciones angulares de cabeceo de la cimentación [3,5].

En la fig. 7 se hace referencia a los parámetros que a continuación se mencionan

K = rigidez del resorte correspondiente a la traslación de la base $= C_v A$
C_v = coeficiente de cortante elástico uniforme del suelo.
A = área de contacto de la cimentación.
R = rigidez del resorte correspondiente a rotación de la base $= C_\varphi I_b - W' y$
C_φ = coeficiente de compresión elástica no uniforme del suelo.
I_b = momento de inercia de área de la base de la cimentación con respecto al eje x'
W' = peso total de la estructura
$\dot{y}$ = altura del centro de gravedad de la estructura sobre el nivel de desplante
$F = m\omega_n^2 x$
x = desplazamiento ~~angular~~ lineal total en C.G.
$M = J\omega_n^2 \varepsilon$
ε = desplazamiento angular total en C.G.
L' = altura de C.G. sobre el nivel de desplante
x_0 = traslación de la base
ε_0 = rotación de la base
$x_1 = \alpha + \beta\delta$
$\varepsilon_1 = \beta + \alpha\phi$
$x_2 = L'\varepsilon_0$
$\alpha = F/k$
$\beta = M/k_r$

J, L, δ, ϕ, k, k_r, x_1, ε_1 y W ya definidos anteriormente.

El problema será resuelto utilizando un procedimiento iterativo y la tabulación propuesta por N. M. Newmark[4]: se despreciarán la variación de la rigidez de la columna debida a la fuerza normal W y los momentos en la misma, causados por la excentricidad del peso debida a deformaciones de la columna.

Sean

F_s = fuerza horizontal en la base de la cimentación $= F$
M_s = momento flexionante en la base de la cimentación $= M + FL'$
$x_s = F_s/K$
$r_s = M_s/R$

A continuación se describe el procedimiento a seguir:

1. Suponer valores para x y ε
2. Calcular F y M usando las expresiones $F = m\omega_n^2 x$ y $\varepsilon = J\omega_n^2 \varepsilon$. En esta etapa el valor de ω_n aún no se conoce: por tanto se llevará como factor común en el resto del cálculo

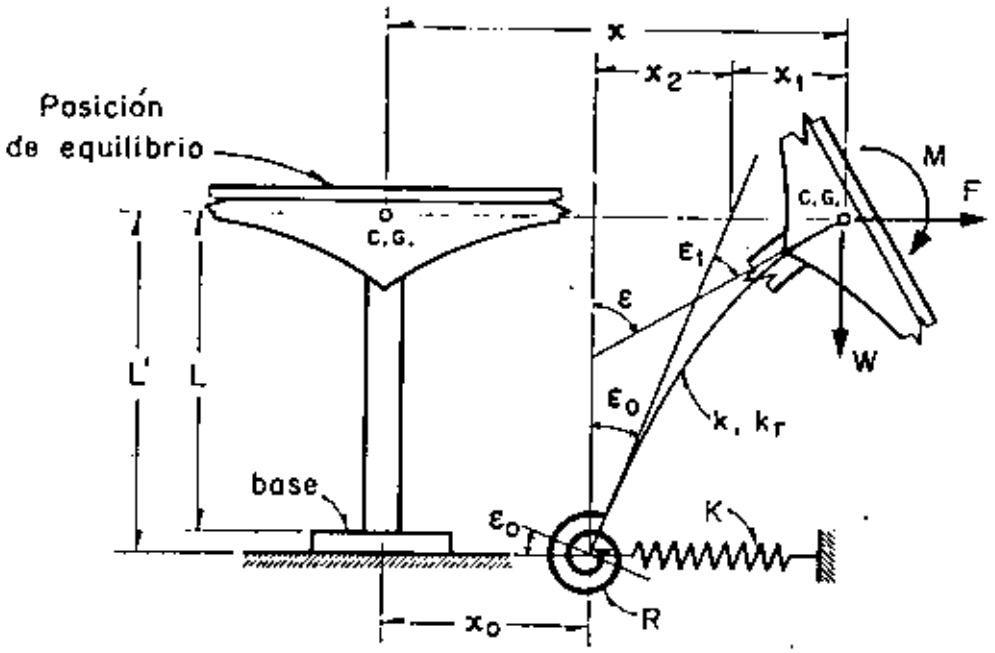

Fig. 7. *Modelo de interacción dinámica suelo-estructura*

3. Calcular la fuerza y el momento en la base mediante las fórmulas
$$F_0 = F \quad \text{y} \quad M_0 = M + FL'$$
4. Encontrar los valores de los desplazamientos $x_0 = F_0/K$ y $\epsilon_0 = M_0/R$
5. Calcular los valores de los parámetros $\alpha = F/k$ y $\beta = M/k_r$
6. Efectuar los productos $\beta\delta$ y $\alpha\phi$
7. Calcular $x_1 = \alpha + \beta\delta$ y $\epsilon_1 = \beta + \alpha\phi$
8. Efectuar el producto $x_2 = L'\epsilon_0$
9. Calcular los desplazamientos lineales y angulares totales de C.G. mediante las expresiones
$$x' = x_0 + x_1 + x_2 \quad \text{y} \quad \epsilon' = \epsilon_0 + \epsilon_1$$
10. Encontrar el valor de ω_0^2 mediante los cocientes x/x' y ϵ/ϵ'
11. Si los valores de ω_0^2 calculados en el paso anterior son aproximadamente iguales, el proceso habrá concluido. En caso contrario repítase la secuela utilizando como valores de partida para x y ϵ los encontrados en etapa 9 o valores cuyo cociente sea igual al de x' entre ϵ'. El proceso deberá continuarse hasta lograr la aproximación deseada.

EJEMPLO DE APLICACION

Con motivo de ilustrar los conceptos enunciados anteriormente se calcularán las frecuencias y modos de vibración de un cascarón ya construido en California, EUA (fig 8). Los datos necesarios han sido extraidos de la ref 1. Se computarán también las respuestas sísmicas suponiendo que esa estructura fuera a construirse en la zona blanda de la ciudad de México. Se utilizarán por tanto los parámetros elásticos de las arcillas del Valle de México y los espectros de diseño propuestos en el reglamento de construcción para el Distrito Federal [3].

Los datos necesarios de la estructura son

L = 419 cm
L' = 480 cm
$\bar{y}$ = 249 cm
W = 20, 450 kg (m = 20.81 kg seg^2/cm)
W' = 43, 600 kg
I_0 = 1.775×10^6cm^4
I_r = 1.065×10^6cm^4
k = 1.266×10^4 kg/cm
k_r = 7.41×10^8 kg cm/rad
J = 1.386×10^9 kg seg^2 cm
ϕ = 0.00358 rad/cm
δ = 208 cm/rad

Las expresiones para C_T y C_φ son las siguientes [2]

$$C_T = F_1 \frac{E'}{1-\nu^2}\frac{1}{\sqrt{A}}; \quad C_\varphi = F_2 \frac{E'}{1-\nu^2}\frac{1}{\sqrt{A}} \quad (26)$$

En ecs 26

E' = módulo de elasticidad del suelo
ν = relación de Poisson del suelo
A = área de contacto de la cimentación
F_1, F_2 = factores de forma de la cimentación

Para el caso de la zona blanda del Valle de México un valor representativo de E' es 50 kg/cm^2 y $\nu = 0.5$ [4]. Para una cimentación cuadrada los valores de F_1 y F_2 son 0.704 y 2.11 respectivamente.

Sustituyendo valores en ecs 26 se obtiene

$$C_T = 0.123 \text{ kg/cm}^3$$
$$C_\varphi = 0.369 \text{ kg/cm}^3$$

CASO 1. SUELO RÍGIDO

a) *Cálculo de frecuencias y modos de vibración*

Para el cálculo de las frecuencias de vibración usaremos la fórmula dada en ec 22. Los valores de los parámetros a sustituir son

$$p^2 = k/m = 608 \text{ (rad/seg)}^2$$
$$\Omega^2 = k_r/J = 535 \text{ (rad/seg)}^2$$
$$\mu = \Omega^2/p^2 = 0.882$$

con los cuales

$$\lambda_{1,2} = 2(1.882 \pm \sqrt{3.55 - 0.882}) = 0.494;\ 7.034$$

Por tanto

$$\omega_1 = \sqrt{0.494 \times 608} = \sqrt{300} = 17.32 \text{ rad/seg}$$

$$\omega_2 = \sqrt{7.034 \times 608} = \sqrt{4260} = 65.30 \text{ rad/seg}$$

Los periodos naturales son

$T_1 = 2\pi/\omega_1 = 0.362$ seg (T_1 obtenido de un registro de vibraciones libres de la estructura y reportado en ref 1 = 0.483 seg)

$T_2 = 2\pi/\omega_2 = 0.096$ seg

Comparando los valores calculado y medido de T_1 se puede ver la importancia de la interacción dinámica suelo-estructura.

Las relaciones modales se obtienen de las ecs. 25 y sus valores son

$$x_1/\epsilon_1 = \frac{2 \times 419}{4 - 0.494} = 238 \text{ cm/rad}$$

$$x_2/\epsilon_2 = \frac{2 \times 419}{4 - 7.034} = -275 \text{ cm/rad}$$

b) *Respuesta sísmica*

Para el cálculo de la respuesta sísmica de sistemas de varios grados de libertad es necesario calcular los coeficientes de participación de cada modo de vibración. Se puede demostrar [7] que para este caso es aplicable la siguiente ecuación

$$C_n = \frac{\bar{X}_n^T \bar{M}\,\bar{I}}{\bar{X}_n^T \bar{M} \bar{X}_n} \quad (27)$$

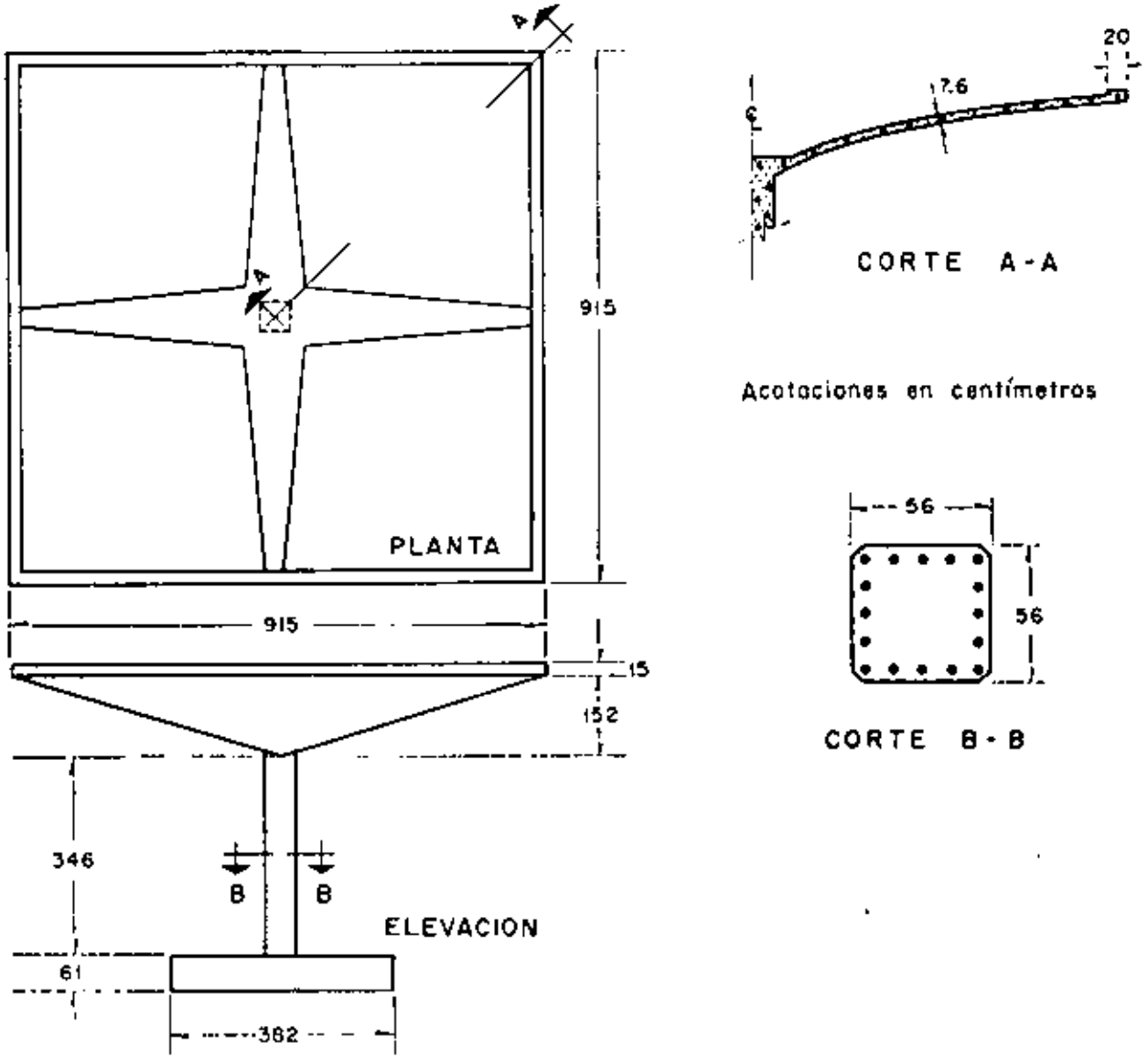

Fig. 8. *Cascarón utilizado para ejemplo.* (Después de R. McLean)

en la cual

$\bar{\Gamma}$ es un vector que representa los desplazamientos estáticos de cada grado de libertad de la estructura inducidos por un desplazamiento estático unitario de la base.

$\bar{X}_n$ es el vector modal para el enésimo modo (n)

$\bar{M}$ es la matriz de inercia y

$\bar{X}_n^T$ es el vector traspuesto de $\bar{X}_n$

Para nuestro caso se tendrá

$$\bar{\Gamma} = \begin{bmatrix} X_{r,1} \\ r_{r,1} \end{bmatrix} = \begin{bmatrix} 1 \\ 0 \end{bmatrix}$$

$$\bar{X}_1 = \begin{bmatrix} 238 \\ 1 \end{bmatrix}, \qquad \bar{X}_2 = \begin{bmatrix} -275 \\ 1 \end{bmatrix}$$

$$\bar{X}_1^T = \begin{bmatrix} 238 & 1 \end{bmatrix}, \qquad \bar{X}_2^T = \begin{bmatrix} -275 & 1 \end{bmatrix}$$

$$\bar{M} = \begin{bmatrix} m & 0 \\ 0 & I \end{bmatrix} = \begin{bmatrix} 20.81 & 0 \\ 0 & 1.386 \times 10^6 \end{bmatrix}$$

Sustituyendo valores en ec 27 y efectuando los productos matriciales en ella indicados se obtiene

$$C_1 = \frac{4.960}{2.566 \times 10^6} = 0.00193$$

$$C_2 = \frac{-5.720}{2.959 \times 10^6} = -0.00193$$

El valor absoluto de la respuesta máxima en cada uno de los modos será [7].

$$\begin{bmatrix} V_n = \text{fuerza cortante} \\ M_n = \text{momento flexionante} \end{bmatrix} = [C_s] \begin{bmatrix} m & 0 \\ 0 & I \end{bmatrix} \times$$

$$\times \begin{bmatrix} x_n \\ r_n \end{bmatrix} S_{an} \qquad (28)$$

donde

S_{an} = ordenada del espectro de aceleraciones afectada por el coeficiente sísmico $C = 0.15$.

El espectro que será utilizado es el propuesto en el reglamento de construcciones del Distrito Federal [5] (fig. 9). Los valores de las ordenadas espectrales correspondientes a T_1 y T_2 son 100 cm/seg² y 80.6 cm/seg² respectivamente.

Sustituyendo valores en ec 28 se llega a

$$\begin{bmatrix} V_1 \\ M_1 \end{bmatrix} = \begin{bmatrix} 957 \text{ kg} \\ 268{,}000 \text{ kg cm} \end{bmatrix} \qquad (29)$$

$$\begin{bmatrix} V_2 \\ M_2 \end{bmatrix} = \begin{bmatrix} 893 \text{ kg} \\ 216{,}000 \text{ kg cm} \end{bmatrix} \qquad (30)$$

El criterio propuesto en ref. 8 será utilizado para el cálculo de la respuesta total (considerando los efectos combinados de los dos modos). Por lo anterior la respuesta total de la estructura valdrá

$$V = \sqrt{V_1^2 + V_2^2} \quad ; \quad M = \sqrt{M_1^2 + M_2^2} \qquad (31a, 31b)$$

En ecs 31a y 31b

V = fuerza cortante total en la columna

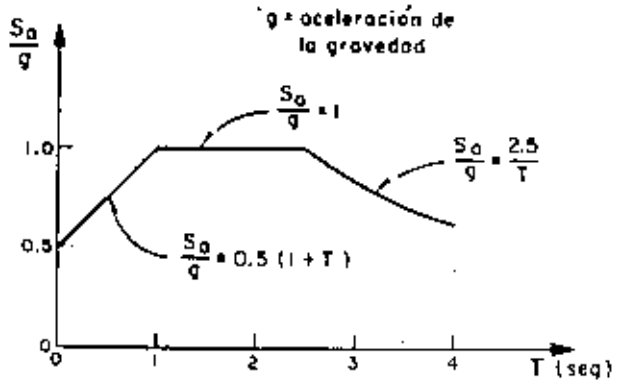

Fig. 9. *Espectro de aceleraciones* (Después de E. Rosenblueth y L. Esteva)

M = momento flexionante total en C. G.

Sustituyendo los valores dados en ecs 29 y 30 en (31) se obtiene

$$V = 1{,}310 \text{ kg} \quad ; \quad M = 344{,}000 \text{ kg cm}$$

El momento en la base de la columna valdrá

$$M_b = 344{,}000 + 1.310 \times 419 = 893{,}000 \text{ kg cm}$$

Los resultados de este caso se resumen en la fig. 10a.

CASO 2. SUELO FLEXIBLE

a) *Cálculo de frecuencias y modos de vibración.*

Para considerar las restricciones del suelo emplearemos el método propuesto anteriormente procediendo en forma tabular. Sustituyendo valores en ecuaciones para K y R se obtienen 1.88×10^4 kg/cm y 6.35×10^6 kg cm/rad respectivamente.

PRIMER MODO

Parámetros	*Valores (1er. ciclo)*		*Factor común*
x, r (supuestos)	$x = 400$ cm	$r = 1$ rad	
$F = m\omega_1^2 x$, $M = I\omega_1^2 r$	$F = 8320$	$M = 1{,}386{,}000$	ω_1^2
$F_0 = F$, $M_0 = M + FL'$	$F_0 = 8320$	$M_0 = 5{,}376{,}000$	ω_1^2
$x_0 = F_0/K$, $r_0 = M_0/R$	$x_0 = 0.4420$	$r_0 = 0.00847$	ω_1^2
$\alpha = F/k$, $\beta = M/k_r$	$\alpha = 0.6570$	$\beta = 0.00187$	ω_1^2
$\beta\delta$, $\alpha\theta$	$\beta\delta = 0.3892$	$\alpha\theta = 0.00235$	ω_1^2
$x_1 = \alpha + \beta\delta$, $r_1 = \beta + \alpha\theta$	$x_1 = 1.0462$	$r_1 = 0.00422$	ω_1^2
$x_2 = r_0 L'$	$x_2 = 4.0650$	———	ω_1^2
$x' = x_0 + x_1 + x_2$, $r' = r_0 + r_1$	$x' = 5.5532$	$r' = 0.01269$	ω_1^2
$\omega_1^2 = x/x'$, $\omega_1^2 = r/r'$	72.0	78.7	

$$x'/r' = 438, \quad X_1^T = [438\ 1]$$

PRIMER MODO

Parámetros	*Valores (2º ciclo)*		*Factor común*
x, r	438	1	
F, M	9130	1,386,000	ω_1^2
F_0, M_0	9130	5,766,000	ω_1^2
x_0, r_0	0.4860	0.00910	ω_1^2
α, β	0.7210	0.00187	ω_1^2
$\beta\delta, \alpha\theta$	0.3892	0.002585	ω_1^2
x_1, r_1	1.1102	0.004455	ω_1^2
x_2, r_2	4.365	———	ω_1^2
$x' r'$	5.961	0.013565	ω_1^2
ω_1^2	73.5	75.8	—

Suponiendo que la aproximación es suficiente resulta

$$x'/r' = 440,\ X_1^T = [440,1],\ \omega_1^2 \doteq 74\ (\text{rad/seg})^2$$

$$T_1 = 0.731\ \text{seg}.$$

El procedimiento para el cómputo de los parámetros del segundo modo es el mismo, sólo que la configuración supuesta deberá "limpiarse", antes de proseguir el cálculo, de las componentes del primer modo que pudiera contener. Se demuestra[7] que si X_2' es el vector de la configuración supuesta, el vector libre de componentes del primer modo queda dado por

$$X_2 = X_2' - \frac{X_1^T M X_2'}{X_1^T M X_1} X_1 \qquad (32)$$

Suponiendo para el primer ciclo

$$X_2' = \begin{bmatrix} -150 \\ 1 \end{bmatrix}$$

y sustituyendo valores en la ecuación matricial 32 se obtiene

$$X_2 = \begin{bmatrix} -151 \\ 1 \end{bmatrix}$$

que nos da los valores de partida para el primer ciclo de cálculo.

SEGUNDO MODO

Parámetros	*Valores (1er. ciclo)*		*Factor común*
x, r	—151	1	
F, M	—3143	1,386,000	ω_2^2
F_0, M_0	—3143	—123,000	ω_2^2
x_0, r_0	—0.1672	—0.0001940	ω_2^2
α, β	—0.2481	0.0018700	ω_2^2
$\beta\delta, \alpha\theta$	0.3892	—0.0008890	ω_2^2
x_1, r_1	0.1411	0.0009810	ω_2^2
x_2, r_2	—0.0930	———	ω_2^2
x', r'	—0.1191	0.0007870	ω_2^2
ω_2^2	1267	1270	—

$x'/r' = -151,\ X_2^T = [-151\ 1],\ T_2 = 0.176$ seg.

En este caso se supuso un valor cercano al real y por tanto sólo se necesitó un ciclo para que se obtuviera la aproximación deseada. Si el valor supuesto no hubiese sido ese sino otro cualquiera seguramente no hubiera sido suficiente un ciclo de cálculo. En los ciclos subsiguientes se procedería en igual forma que antes: suponer inicialmente la configuración obtenida en el ciclo anterior; limpiarla de las componentes del primer modo; etc.

b) Respuesta sísmica

Los valores de los coeficientes de participación y de las ordenadas espectrales para este caso son:

$$C_1 = 0.001689, \qquad C_2 = -0.001689$$

$$S_{a1} = 127.4\ \text{cm/seg}^2, \qquad S_{a2} = 86.6\ \text{cm/seg}^2$$

Las respuestas máximas para cada modo valen

$$\begin{bmatrix} V_1 \\ M_1 \end{bmatrix} = \begin{bmatrix} 1,970\ \text{kg} \\ 298,200\ \text{kg cm} \end{bmatrix}$$

$$\begin{bmatrix} V_2 \\ M_2 \end{bmatrix} = \begin{bmatrix} 461\ \text{kg} \\ 203,000\ \text{kg cm} \end{bmatrix}$$

Las respuestas máximas totales serán (fig 10b)

$$V = 2,030\ \text{kg}$$

$$M = 361,000\ \text{kg cm}$$

$$M_t = 1,209,000\ \text{kg cm}$$

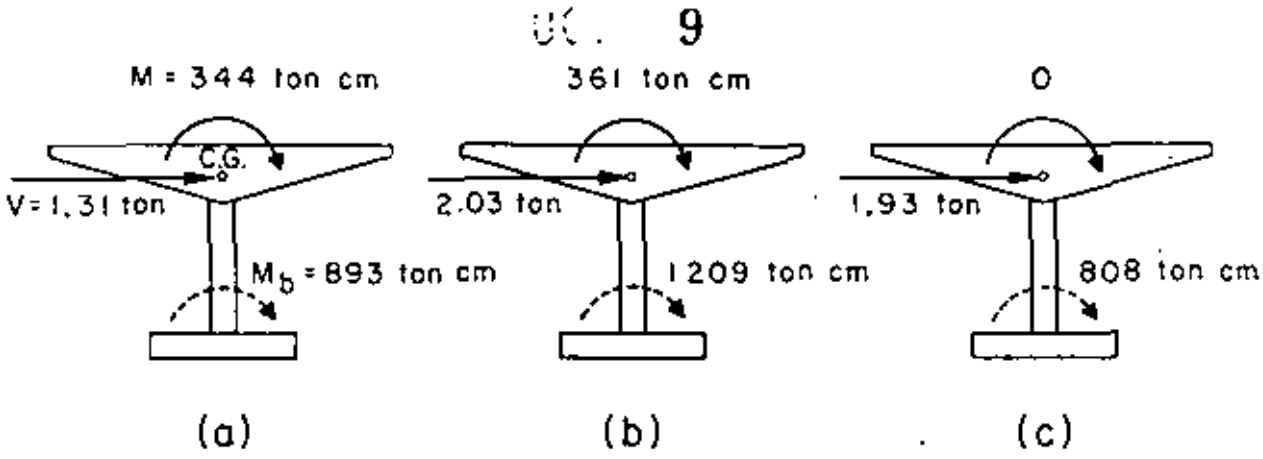

FIG. 10. *Respuestas sísmicas*

CASO 3. BASE RÍGIDA Y MASA CONCENTRADA

Para comparación de resultados se verá cuál es el valor de la respuesta máxima en el caso de despreciar la inercia rotacional y la interacción suelo-estructura.

Para este caso $p^2 = 608$ (rad/seg)^2, $T = 0.325$ seg, $0.15S_a = 92.6$ cm/seg^2, $V = mS_a = 1{,}930$ kg y $M_b = 808{,}000$ kg cm (fig 10c).

CONCLUSIONES

En la siguiente tabla se resumen los resultados de los tres casos, indicados como porcentajes del segundo caso.

Concepto	*Caso 1*	*Caso 2*	*Caso 3*
V	64.4%	100%	95.0%
M	95.2%	100%	0 %
M_b	73.8%	100%	66.7%

Los resultados de la tabla anterior dan una idea clara de la importancia que tiene el considerar la inercia rotacional de la cubierta y la interacción suelo-estructura. La importancia del primer concepto aumentará conforme mayor sea el momento de inercia de masa de la cubierta con respecto al eje z. El último concepto es tanto más importante cuanto más blando sea el suelo de cimentación. En particular puede observarse que en el tipo de solución 3 no se obtiene momento flexionante a la altura de C.G. Esto puede traer consigo serios errores en la cuantía del acero de refuerzo necesario en la unión columna-cubierta que es donde más ductilidad necesita desarrollarse.

AGRADECIMIENTO

El autor manifiesta su agradecimiento a los doctores E. Rosenblueth y J. A. Nieto, así como al Ing. E. del Valle por sus valiosos comentarios y sugerencias.

REFERENCIAS

1. McLean, R. S., "Inverted pendulum structures", technical report of *Consulting Civil and Structural Engineers*, Fullerton, Cal. (ene. 1965).
2. Barkan, D. D., "Dynamics of bases and foundations", McGraw Hill Book Co. Inc. (1962).
3. Jacobsen, L. S., y Ayre, R. S., "Engineering vibrations", McGraw Hill Book Co. Inc. (1958).
4. Newmark, N. M., "Numerical procedure for computing deflections, moments and buckling loads", *Transactions ASCE*, Vol. 108 (1943), pp. 1161-1234.
5. Rosenblueth, E. y Esteva, L., *"Proyecto de reglamento de las construcciones en el Distrito Federal. "Folleto complementario. Diseño sísmico de edificios"*, Ediciones Ingeniería, México (1962).
6. Marsal, R., y Mazari, M., *"El subsuelo de la Ciudad de México"*, Publicación del Instituto de Ingeniería, UNAM (1962).
7. Newmark, N. M., y Rosenblueth, E., *"Earthquake Engineering"*, será publicado por Prentice-Hall, Inc.
8. Rosenblueth, E., "Some applications of probability theory in aseismic design", *Proceedings, 1st World Conference on Earthquake Engineering*, Berkeley, Cal. (1956), paper 8.

Ejemplo: Calcular las frecuencias circulares y los modos de vibración de la siguiente estructura:

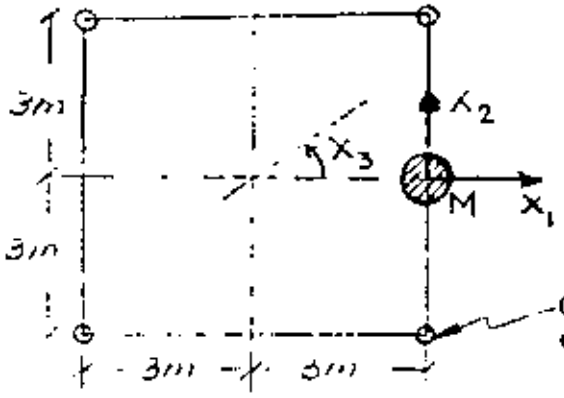

$K = 4k$

Columnas de rigidez k en cualquier dirección

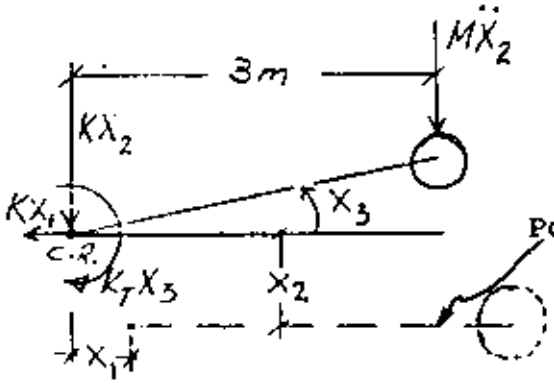

$X_2 = x_2 + 3X_3$

$\therefore \quad x_2 = X_2 - 3X_3$

Posición de equilibrio estático

En la dirección de X_1: $M\ddot{X}_1 + KX_1 = 0 \rightarrow \omega_1^2 = \frac{K}{M}$

(movimiento desacoplado con X_2 y X_3)

$$\underline{z}_1^T = [1,0,0]$$

En la dirección X_2: $M\ddot{X}_2 + Kx_2 = 0$

$$M\ddot{X}_2 + KX_2 - 3KX_3 = 0 \qquad (1)$$

En la dirección X_3: $M\ddot{X}_2 \times 3 + K_T X_3 = 0 \qquad (2)$

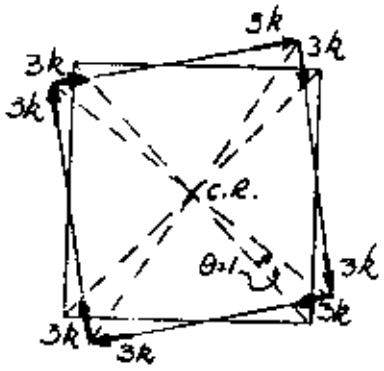

Momento respecto a C.R.= 8 x 3k x 3 = 72k

= 18K

Sustituyendo K_T en la ec. (2):

$$3M\ddot{X}_2 + 18K\,X_3 = 0 \qquad (3)$$

$$M\ddot{X}_2 + 6K\,X_3 = 0 \qquad (4)$$

Restando la ec. (4) a la ec. (1) se obtiene:

$$KX_2 - 9KX_3 = 0 \quad \therefore \quad X_2 = 9X_3 \quad \rightarrow \quad \ddot{X}_2 = 9\ddot{X}_3$$

Sustituyendo esto último en la ec. (4): $\ddot{X}_3 + \frac{6K}{9M} X_3 = 0$

$$\therefore \quad \omega_2^2 = \frac{2}{3}\frac{K}{M} \quad ; \quad \underline{Z}_2^T = [0,9,1]$$

centro de educación continua
división de estudios de posgrado
facultad de ingeniería unam

CURSOS DE INGENIERIA CIVIL EN EL PROYECTO DE PLANTAS HIDROELECTRICAS.

INGENIERIA SISMICA.

VIBRACION DE SISTEMAS DISCRETOS DE VARIOS GRADOS DE LIBERTAD.

JORGE PRINCE ALFARO.

JUNIO, 1981.

VIBRACION DE SISTEMAS DISCRETOS DE VARIOS GRADOS DE LIBERTAD

Ejemplos de sistemas de n GL

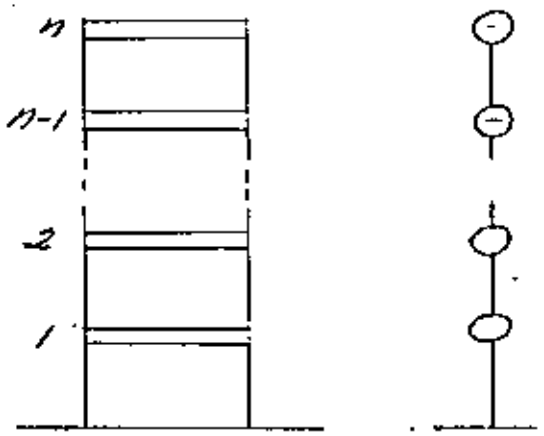

Características:

- masas { concentradas / rígidas / constantes
- columnas solo se deforman lateralmente
- con una coordenada por masa queda definida la configuración del sistema
- equivale a:

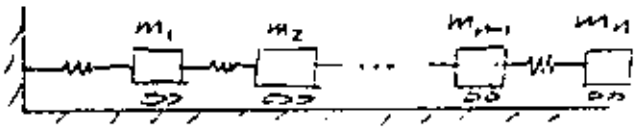

Además, la consideramos elástica, lineal

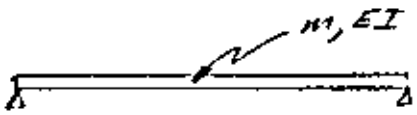

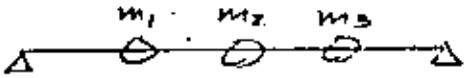

Supongamos:

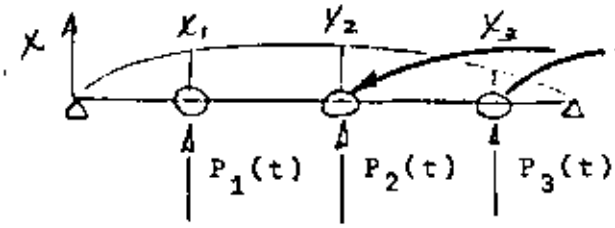

masas concentradas

fuerzas concentradas exteriores .

aislemos una masa:

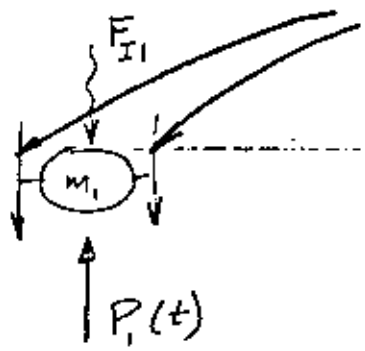

F_{r1} = Σ fuerzas resistencia elástica a la deformación

F_I = Fuerza de inercia

Las ecuaciones condensadas de movimiento serán:

$$F_{I1} + F_{r1} = P_1(t)$$

$$F_{I2} + F_{r2} = P_2(t)$$

$$F_{I3} + F_{r3} = P_3(t)$$

Fuerzas asociadas al desplazamiento, NO al movimiento

∴ la determinación de estas fuerzas es un problema estático.

Coeficientes de influencia

1. De flexibilidad

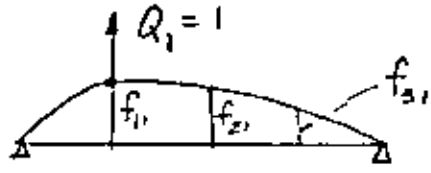

f_{ij} = despl. de la coord. i debido a una carga unitaria en coord. j (desplazamiento y fuerza en = dirección)

Por superposición

$$X_1 = f_{11}\,Q_1 + f_{12}\,Q_2 + f_{13}\,Q_3$$

$$X_2 = f_{21}\,Q_1 + f_{22}\,Q_2 + f_{23}\,Q_3 \qquad \text{inv. (1)}$$

$$X_3 = f_{31}\,Q_1 + f_{32}\,Q_2 + f_{33}\,Q_3$$

2. De rigidez:

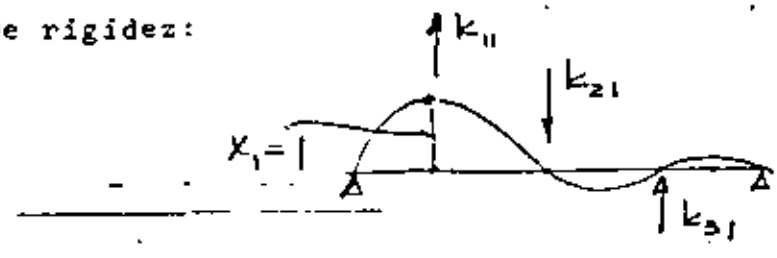

K_{ij} = fuerza en coordenada i por un desplazamiento unitario en coordenada j.

Por superposición

$$Q_1 = K_{11} X_1 + K_{12} X_2 + K_{13} X_3$$

$$Q_2 = K_{21} X_1 + K_{22} X_2 + K_{23} X_3 \qquad (2)$$

$$Q_3 = K_{31} X_1 + K_{32} X_2 + K_{33} X_3$$

Desde luego $K_{ij} = K_{ji}$ (y $f_{ij} = f_{ji}$) (Maxwell-Mohr)

La ecuación 2 también puede escribirse:

$$Q_i = \sum_{j=1}^{3} K_{ij} X_j$$

o bien, en notación matricial

$$\begin{Bmatrix} Q_1 \\ Q_2 \\ Q_3 \end{Bmatrix} = \begin{bmatrix} K_{11} & K_{12} & K_{13} \\ K_{21} & K_{22} & K_{23} \\ K_{31} & K_{32} & K_{33} \end{bmatrix} \begin{Bmatrix} X_1 \\ X_2 \\ X_3 \end{Bmatrix} \qquad (3)$$

matriz de rigideces

Ponemos:

$$\{Q\} = [K] \{X\}$$

Claro que $[K]^{-1} = [F] = [f_{ij}]$

Sustituyendo (2) o (3) en ecuaciones de movimiento:

$$m_1 \ddot{X}_1 + K_{11} X_1 + K_{12} X_2 + K_{13} X_3 = P_1(t)$$
$$m_2 \ddot{X}_2 + K_{21} X_1 + K_{22} X_2 + K_{23} X_3 = P_2(t)$$
$$m_3 \ddot{X}_3 + K_{31} X_1 + K_{32} X_2 + K_{33} X_3 = P_3(t)$$

o bien:

$$\begin{bmatrix} m_1 & 0 & 0 \\ 0 & m_2 & 0 \\ 0 & 0 & m_3 \end{bmatrix} \begin{Bmatrix} \ddot{X}_1 \\ \ddot{X}_2 \\ \ddot{X}_3 \end{Bmatrix} + \begin{bmatrix} K_{11} & K_{12} & K_{13} \\ K_{21} & K_{22} & K_{23} \\ K_{31} & K_{32} & K_{33} \end{bmatrix} \begin{Bmatrix} X_1 \\ X_2 \\ X_3 \end{Bmatrix} = \begin{Bmatrix} P_1(t) \\ P_2(t) \\ P_3(t) \end{Bmatrix}$$

o también:

$$[M] \{\ddot{X}\} + [K] \{X\} = \{P(t)\} \quad \text{(vibración forzada)}$$

$$= \{0\} \quad \text{(vibración libre)}$$

1. VIBRACION LIBRE

$$[M] \{\ddot{X}\} + [K] \{X\} = \{0\} \qquad (1.1)$$

Supongamos la solución

$$\{X\} = \underbrace{\{r\}}_{\text{constante con t}} \underbrace{(A \text{ sen } pt + B \text{ sen } pt)}_{\text{escalar}} = \{r\} \; Y(t)$$

define:
- variación armónica
- amplitud

tenemos:

$$\{X\} = \{r\} (A \text{ sen } pt + B \cos pt) = r \; Y(t)$$

$$\{\dot{X}\} = \{r\} (Ap \cos pt - B p \text{ sen } pt) \qquad (1.2)$$

$$\{\ddot{X}\} = \{r\} (-Ap^2 \text{ sen } pt - B p^2 \cos pt) = - p^2 \{r\} Y(t)$$

Sustituyendo 1.2 en 1.1 y dividiendo entre Y(t) nos queda:

$$- p^2 [M] \{r\} + [K] \{r\} = \{0\}$$

o sea:

$$\underbrace{\left[[K] - p^2 [M]\right]}_{[E]} \{r\} = \{0\} \qquad (1.3)$$

$$[K]\{r\} = p^2 [M] \{r\} \qquad [K]\{r\} = p^2 [M]\{r\}$$

pre x $[M]^{-1}$ pre x $[K]^{-1}$. $\frac{1}{p^2}$

$$[M]^{-1} [K]\{r\} = p^2 \{r\} \qquad \frac{1}{p^2}\{r\} = [K]^{-1}[M]\{r\}$$

En las dos formas llegamos a un problema de VAC

$$[L] \{u\} = \lambda \{u\}$$

Problema de valores característicos:

- Dada una matriz cuadrada de orden (nxn) $[L]$, que representa una transformación lineal de vectores n-dimensionales, debe encontrarse un vector $\{u\}$ que transformado por $[L]$ resulte en otro vector $\lambda \{u\}$ en la misma "dirección". O sea, $[L]$ solo cambia la magnitud de $\{u\}$ sin cambiar la dirección.
  El vector es un vector característico (o eigenvector) de $[L]$. λ(escalar) representa la relación entre las "longitudes" antes y después de la transformación y para llegar a los VEC debe tomar valores de un conjunto de valores característicos (VAC) (o eigenvalores).
  El problema de encontrar frecuencias y modos naturales puede considerarse un problema de VAC. - (STD)

Tenemos

$$\left[[K] - p^2 [M]\right] \{r\} = \{0\} \qquad (1.3)$$

Si en el sistema de ecuaciones

$$[A] \{x\} = \{0\}$$

$[A]$ es no singular, la solución única es la trivial $\{x\} = \{0\}$, de donde nos interesa el caso en que $[A]$ es singular. En este caso la adjunta* $[\hat{A}]$ existe y puede pre X por ella, con el resultado

$$|A| \{X\} = \{0\}$$

porque $[\hat{A}] [A] = |A| [I] \quad \forall [A]$ (nxn)

Puesto que $|A| = 0$, $\{x\}$ no necesariamente es nulo, pero si se asigna un valor dado a uno de sus elementos los demás quedan determinados en forma única.

También notamos que si $\{X\}$ es solución de $[A] \{X\} = \{0\}$ y α es una constante, entonces $\alpha\{X\}$ es también solución. Por lo tanto, hay un número infinito de soluciones. Todos estas se considerarán juntas y hablaremos de una "solución" como un conjunto de relaciones entre los elementos de $\{x\}$.

Volvemos a $\underbrace{\left[[K] - p^2 [M]\right]}_{[E]} \{r\} = \{0\}$ (1.3)

Al desarrollar $|E| = 0$ llegamos a una ecuación de grado n en p^2, cuyas raíces son los VAC.

- Como $[K]$ y $[M]$ son simétricas y positivas definidas*,

---

*Transpuesta de la matriz de cofactores.

**$[A]$ es POS. DEF. si $\{\dot{q}\} [A] \{\dot{q}\} > 0$ para todo $\{\dot{q}\}$ no nulo

puede demostrarse que las raíces de la ecuación característica son reales y positivas. Las llamamos p_1^2, p_2^2, ..., p_n^2.

Las n frecuencias naturales son los términos positivos de las raíces y la más baja es llamada <u>frecuencia fundamental</u>.

- Para la gran mayoría de los casos de interés las frecuencias son diferentes entre sí.
- Para cada frecuencia p_i existe una VEC asociado:

$$[K] \{r\}_i = p_i^2 [M] \{r\}_i \qquad i = 1, \ldots, n$$

o sea para cada p_i existe una solución $\{r\}$ no trivial

- Normalización (solo conveniencia, sin significado físico)

Varias formas:

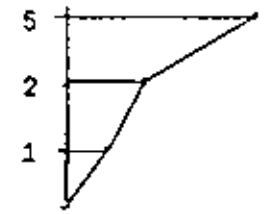

$\{r\}_i' [M] \{r\}_i = 1$

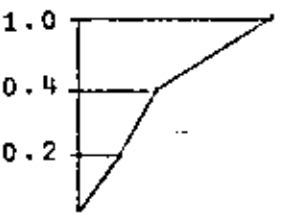

(modos normales)

- Los modos y frecuencias naturales del sistema son propiedades características derivadas de las propiedades de inercia y rigidez expresadas por los elementos de $[M]$ y $[K]$.
- Llamaremos <u>matriz modal</u> $[R]$ a la que tiene los VEC, o vectores modales, como columnas.

ORTOGONALIDAD DE MODOS DE VIBRACION

Se dice que dos vectores $\{a\}$ y $\{b\}$ son ortogonales con respecto a la matriz simétrica $[J]$ si

$$\{a\}' [J] \{b\} = \{b\}' [J] \{a\} = 0$$

Demostremos que dos vectores modales $\{r\}_i$ y $\{r\}_j$, asociados a frecuencias diferentes ($p_i \neq p_j$) son ortogonales con respecto a las matrices de inercia y elástica.

- Cada uno de estos vectores satisface la ecuación 1.3

$$p^2 [M] \{r\} = [K] \{r\} \qquad [M] \{r\} = \frac{1}{p^2} [K] \{r\}$$

es decir:

$$p_i^2 [M] \{r\}_i = [K] \{r\}_i \qquad [M] \{r\}_i = \frac{1}{p_i^2} [K] \{r\}_i$$

$$p_j [M] \{r\}_j = [K] \{r\}_j \qquad [M] \{r\}_j = \frac{1}{p_j^2} [K] \{r\}_j$$

pre X i y j por $\{r\}'_j$ y $\{r\}'_i$ respectivamente

$$\left.\begin{array}{l} p_i^2 \{r\}'_j [M] \{r\}_i = \{r\}'_j [K] \{r\}_i \\ p_j^2 \{r\}'_i [M] \{r\}_j = \{r\}'_j [K] \{r\}_j \end{array}\right\} \quad \left.\begin{array}{l} \{r\}_j [M] \{r\}_i = \frac{1}{p_i^2} \{r\}'_j [K] \{r\}_i \\ \{r\}'_i [M] \{r\}_j \quad \frac{1}{p_j^2} \{r\}'_i [K] \{r\}_j \end{array}\right. \qquad (a)$$

pero como $[M]$ y $[K]$ son simétricas:

$$\{r\}'_j [K] \{r\}_i = \{r\}'_i [K] \{r\}_j$$
$$\{r\}'_j [M] \{r\}_i = \{r\}'_i [M] \{r\}_j$$

∴, restando miembro a miembro en ecuaciones (a):

$$(p_i^2 - p_j^2)\left(\{r\}_i' [M] \{r\}_j\right) = 0 \qquad 0 = \left(\frac{1}{p_i^2} - \frac{1}{p_j^2}\right)\{r\}_i' [K] \{r\}_j$$

y como $p_i^2 \neq p_j^2$

$$\{r\}_i' [M] \{r\}_j = 0 \qquad \{r\}_i' [K] \{r\}_j = 0$$

Tenemos ecuaciones de ortogonalidad:

$$\{r\}_i' [M] \{r\}_j = 0$$
$$\{r\}_i' [K] \{r\}_j = 0 \qquad \text{si } i \neq j$$

La ec

$$[M] \{\ddot{x}\} + [K] \{x\} = \{0\} \tag{a}$$

y la matriz modal $[R]$

Hagamos:

$$\{x\} = [R] \{y\}$$

y sustituyendo en (a):

$$[M] [R] \{\ddot{y}\} + [K] [R] \{y\} = \{0\}$$

premultiplicando por $[R]'$:

$$\underbrace{[R]' [M] [R] \{\ddot{y}\}}_{\text{diagonales}} + \underbrace{[R]' [K] [R] \{y\}}_{\text{diagonales}} = \{0\} \tag{b}$$

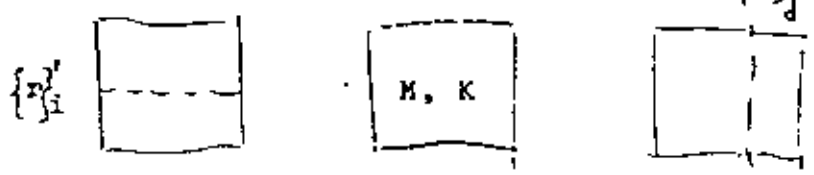

$i \neq j$

Llamemos

$$[R]' [M] [R] = [M^*]$$
$$[R]' [K] [R] = [K^*]$$

∴ la ec (b) (p. 14) puede ponerse:

$$[M^*] \{\ddot{y}\} + [K^*] \{y\} = \{0\}$$

que equivale a:

$$m_{11}^* \ddot{y}_1 + k_{11}^* y_1 = 0$$
$$m_{22}^{**} \ddot{y}_2 + k_{22}^* y_2 = 0$$
$$\cdots\cdots\cdots\cdots$$
$$m_{nn}^* \ddot{y}_n + k_{nn} y_n = 0$$

de las que

$$p_1^2 = \frac{k_{11}^*}{m_n^*}, \ldots\ldots, \quad p_n^2 = \frac{k_{nn}^*}{m_{nn}^*}$$

Recordar que para → 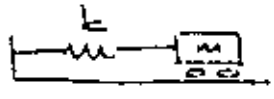

$$m\ddot{x} + kx = 0$$
$$\ddot{x} + p^2 x = 0 \quad y \quad p^2 = \frac{k}{m}$$

O sea, con la transformación

$$\{x\} = [R] \{y\}$$

aplicada a la ecuación

$$[M] \{\ddot{x}\} + [K] \{x\} = \{0\}$$

hemos descompuesto un sistema de nGL en n sistemas de 1GL independientes.

Consideremos el producto

$$[M^*]^{-1}[K^*] = ([R]'[M][R])^{-1} [R]' [K] [R] = [K^*] [M^*]^{-1}$$

$$= [R]^{-1} [M]^{-1} [R]^{'-1} [R]' [K] [R]$$

$$= [R]^{-1} [M]^{-1} [K] [R] = [\Phi]$$

$[\Phi]$ contiene las frecuencias naturales en la diagonal principal

∴ El problema de encontrar frecuencias y modos naturales equivale al de encontrar la matriz $[R]$ que diagonalice $[M]$ y $[K]$ de acuerdo con

$$[R]' [M] [R] = [M^*]$$
$$[R]' [K] [R] = [K^*]$$

Las frecuencias naturales se obtendrán de

$$[M^*]^{-1} [K^*] = [K^*] [M^*]^{-1} = [\Phi]$$

Veámoslo en otra forma

$$[M] \{\ddot{x}\} + [K] \{x\} = \{P(t)\}$$

Sustituyendo $\{x\} = [R] \{y\}$

$$[M] [R] \{y\} + [K] [R] \{y\} = \{P(t)\}$$

premultiplicando por $\{r\}_j^t$

$$\underbrace{\{r\}_j^t [M] [R]}_{(a)} \{\ddot{y}\} + \underbrace{\{r\}_j^t [K] [R]}_{(b)} \{y\} = \underbrace{\{r\}_j^t \{P(t)\}}_{\text{escalar}}$$

En los productos (a) y (b) solo queda (por ortogonalidad):

$$\underbrace{\{r\}_j^t [M] \{r\}_j}_{M_j^*} \ddot{y}_j + \underbrace{\{r\}_j^t [K] \{r\}_j}_{K_j^* = p_j^2 M_j^*} y_j = \underbrace{\{r\}_j^t \{P(t)\}}_{P_j^* = \sum_i P_i r_{ij}}$$

y para el modo j tenemos:

$$M_j^* \ddot{y}_j + p_j^2 M_j^* y_j = P_j^*(t)$$

o bien (1.5)

$$M_j^* \ddot{y}_j + K_j^* y_j = P_j^*(t)$$

análoga a la ecuación de movimiento para 1 GL:

$$m \ddot{x} + k x = P(t)$$

En (1.5) tenemos:

n ecuaciones independientes para nGL

1 ecuación independiente para cada modo

Para vibración libre (1GL)

$$\ddot{x} + p^2 x = 0 \qquad p^2 = \frac{k}{m}$$

la solución es:

$$x = A \cos pt + B \operatorname{sen} pt \qquad (c)$$

y para el modo j tendremos ($P_j(t) = 0$)

$$y_j = A_j \cos p_j t + B_j \operatorname{sen} P_j t \qquad (d)$$

Si en (c) hacemos

$$x\big]_{t=0} = X_o \qquad \dot{x}\big]_{t=0} = \dot{X}_o$$

llegamos a

$$x(t) = X_o \cos pt + \frac{\dot{X}_o}{p} \operatorname{sen} pt$$

y ∴ en (d):

$$y_j = y_{oj} \cos p_j t + \frac{\dot{y}_{oj}}{P_j} \operatorname{sen} P_j t$$

Cualquier configuración del sistema puede expresarse como una suma de formas modales multiplicadas por ciertos coeficientes. Esquemáticamente:

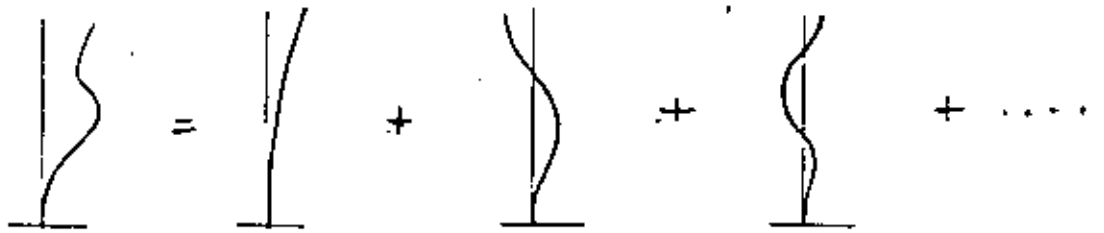

$$\underset{\substack{\text{estática}\\ \text{o}\\ \text{dinámica}}}{\{X\}} = \{r\}_1 Y_1 + \{r\}_2 Y_2 + \{r\}_3 Y_3 + \ldots$$

$(Y = Y(t))$

$$\left(\{X\} = \{X(t)\}\right)$$

En nuestra expresión

$$\{x\} = [R]\ \{y\} \qquad 1.4$$

$\{x\}$ puede no ser función de t, por ejemplo:

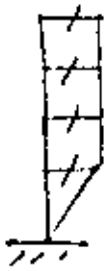

$$\{1\} = [R]\ \{c\} \qquad (e)$$

donde $\{c\}$ es el vector de constantes que prex $[R]$ nos da la configuración $\{1\}$

De la ec. (e):

$$\{c\} = [R]^{-1}\ \{1\} \qquad \left([R]\ \text{NOSING}\right)$$

En 1.4 también podríamos hacer

$$\{Y\} = [R]^{-1}\ \{x\}$$

pero sigamos otro camino, premultiplicando por $\{r\}_j^t\ [M]$ o por $\{r\}_j^t\ [K]$

$$\{r\}_j^t\ [M]\ \{x\} = \{r\}_j^t\ [M][R]\ \{y\} = \{r\}_j^t\ [M]\ \{r\}_1\ y_1 +$$

$$+ \{r\}_j^t\ [M]\ \{r\}_2\ y_2 + \cdots$$

$$\cdots + \{r\}_j^t\ [M]\ \{r\}_n\ Y_n$$

Por ortogonalidad todos estos productos son nulos excepto el término

$$\{r\}_j^t\ [M]\ \{r\}_j\ Y_j$$

de donde tenemos

$$\{r\}_j' \cdot [M]\{x\} = \{r\}_j' [M]\{r\}_j \; y_j$$

de donde:

$$y_j = \frac{\{r\}_j' [M]\{x\}}{\{r\}_j' [M]\{r\}_j} = \frac{\{r\}_j [M]\{x\}}{M_j^*} = \frac{\{r\}_j' [K]\{x\}}{K_j^*} = \frac{\{r\}_j [K]\{x\}}{p_j^2 M_j^*}$$

(coeficiente de participación)

Ejemplo (vigas rígidas)

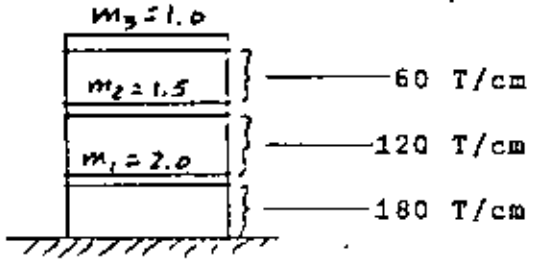

$$[M] = \begin{bmatrix} 2.0 & 0 & 0 \\ 0 & 1.5 & 0 \\ 0 & 0 & 1.0 \end{bmatrix} \frac{\text{ton seg}^2}{\text{cm}}$$

Matriz de rigideces

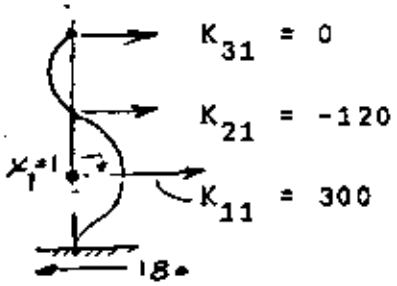

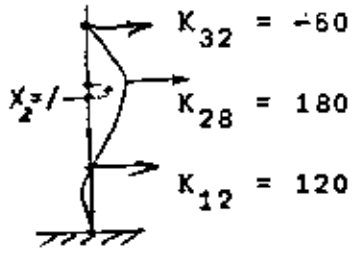

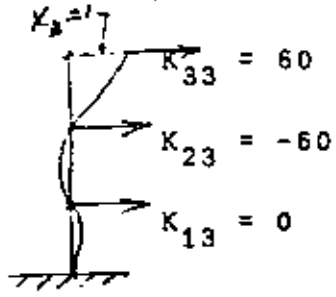

$$\therefore [K] = \begin{bmatrix} 300 & -120 & 0 \\ -120 & 180 & -60 \\ 0 & -60 & 60 \end{bmatrix} = 60 \begin{bmatrix} 5 & -2 & 0 \\ -2 & 3 & -1 \\ 0 & -1 & 1 \end{bmatrix} \quad \text{(T/cm)}$$

$$[E] = \left[[K] - p^2\,[M]\right] \qquad M = \begin{bmatrix} 2 & 0 & 0 \\ 0 & 1.5 & 0 \\ 0 & 0 & 1 \end{bmatrix}$$

$$= 60 \begin{bmatrix} (5 - \frac{2}{60} p^2) & -2 & 0 \\ -2 & (3-\frac{1.5}{60} p^2) & (-1) \\ 0 & (-1) & (1-\frac{1}{60} p^2) \end{bmatrix}$$

si $d = p^2/60$:

$$[E] = 60 \begin{bmatrix} (5-2d) & -2 & 0 \\ -2 & (3-1.5\,d) & -1 \\ 0 & -1 & (1-d) \end{bmatrix}$$

$$|E| = 0 = 60\,(d^3 - 5.5\,d^2 + 7.5\,d - 2) = 0$$

$$d_1 = 0.35$$

$$d_2 = 1.61$$

$$d_3 = 3.54$$

$p^2 = 60\,d$:

$$p_1^2 = 21.0 \qquad p_1 = 4.58$$
$$p_2^2 = 96.5 \qquad p_3 = 9.82$$
$$p_3^2 = 212.4 \qquad p_3 = 14.56$$

} frecuencias naturales

Modos:

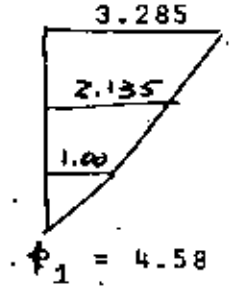

$p_1 = 4.58$

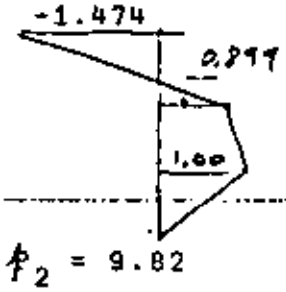

$p_2 = 9.82$

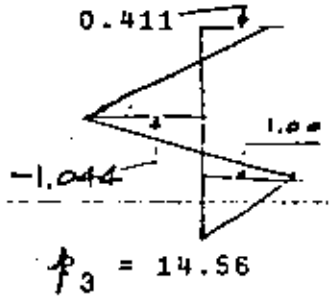

$p_3 = 14.56$

$$[R] = \begin{bmatrix} 1.000 & 1.000 & 1.000 \\ 2.135 & 0.899 & -1.044 \\ 3.285 & -1.474 & 0.411 \end{bmatrix}$$

$$[M^*] = [R]' [M] [R] = \begin{bmatrix} 19.629 & 0.038 & 0.007 \\ 0.037 & 5.386 & -0.014 \\ 0.006 & -0.014 & 3.804 \end{bmatrix}$$

Ej:

$$19.6296 = \{r\}_1' [M] \{r\}_1 = M_1^* = \sum_i r_{i1}^2 m_i$$

$$[K^*] = [R]' [K] [R] = 60 \begin{bmatrix} 6.899 & 0.042 & 0.034 \\ 0.042 & 8.651 & -0.040 \\ 0.034 & -0.040 & 13.473 \end{bmatrix}$$

Comprobación con $[K^*] = [p^2 M^*] =$

$$= \begin{bmatrix} 412.209 & 0 & 0 \\ 0 & 519.749 & 0 \\ 0 & 0 & 807.970 \end{bmatrix} = [\phi^2 M^*]$$

$$[K^*] = \begin{bmatrix} 413.940 & 0\cdots & 0\cdots \\ 0\cdots & 519.060 & 0\cdots \\ 0\cdots & 0\cdots & 808.380 \end{bmatrix}$$

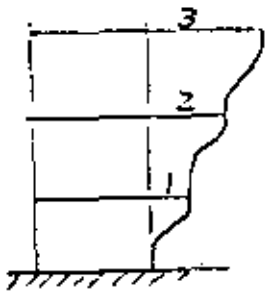

$X_{30} = 3$ cm

$X_{20} = 2$ cm

$X_{10} = 1$ cm

$$\{X_o\} = \begin{Bmatrix} 1 \\ 2 \\ 3 \end{Bmatrix}$$

$$Y_{01} = \frac{\{r\}_1^{'} [M] \{x_o\}}{M_1^*} = \frac{2.0 + 6.405 + 9.855}{19.629} = 0.9303 \text{ cm}$$

$$Y_{02} = \frac{\{r\}_2 [M] \{x_o\}}{M_2^*} = \frac{2.0 + 2.697 - 4.422}{5.386} = 0.0511$$

$$Y_{03} = \frac{\{r\}_3 [M] \{x_o\}}{M_3^*} = \frac{2.0 - 3.132 + 1.233}{3.804} = 0.0266$$

Modo $Y_1(t)$

$P_1 = 4.58$

$P_2 = 9.82$

$P_3 = 14.56$

En p.

0.930 cm
0.051 cm
0.026 cm

son amplitudes de los modos

Para obtener los desplazamientos de las masas debemos multiplicar por las configuraciones modales:

$$x_{i1} = \{r\}_1 \quad Y_1(t) = \begin{Bmatrix} 1.0 \\ 2.135 \\ 3.285 \end{Bmatrix} \quad 0.93 \cos 4.58\ t$$

$$x_{i2} = \{r\}_2 \quad Y_2(t) = \begin{Bmatrix} 1.0 \\ 0.899 \\ -1.474 \end{Bmatrix} \quad 0.051 \cos 9.82\ t$$

$$x_{i3} = \{r\}_3 \quad Y_3(t) = \begin{Bmatrix} 1.00 \\ -1.044 \\ 0.411 \end{Bmatrix} \quad 0.0266 \cos 14.56\ t$$

y sumar. O sea los desplazamientos $x_i(t)$ de las masas serán

$$\{x(t)\} = [R]\{y(t)\}$$

$$x_1(t) = r_{11} Y_1(t) + r_{12} Y_3(t) + r_{13} Y_3(t)$$
$$x_2(t) = r_{21} Y_1(t) + r_{22} Y_2(t) + r_{23} Y_3(t)$$
$$x_3(t) = r_{31} Y_1(t) + r_{32} Y_2(t) + r_{33} Y_3(t)$$

Otro ejemplo

Para 1GL teníamos

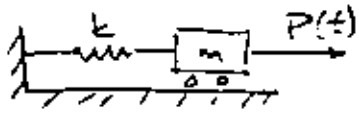

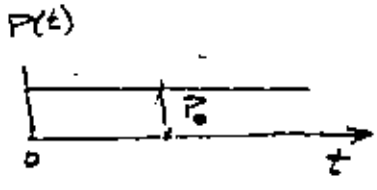

La ec:

$$\ddot{x} + P^2 x = \frac{P(t)}{m} = \frac{P_o}{m}$$

y para CI = 0 la solución

$$x = \frac{P_o}{K}\left(1 - \cos pt\right)$$

Tenemos ahora el problema de encontrar la respuesta de

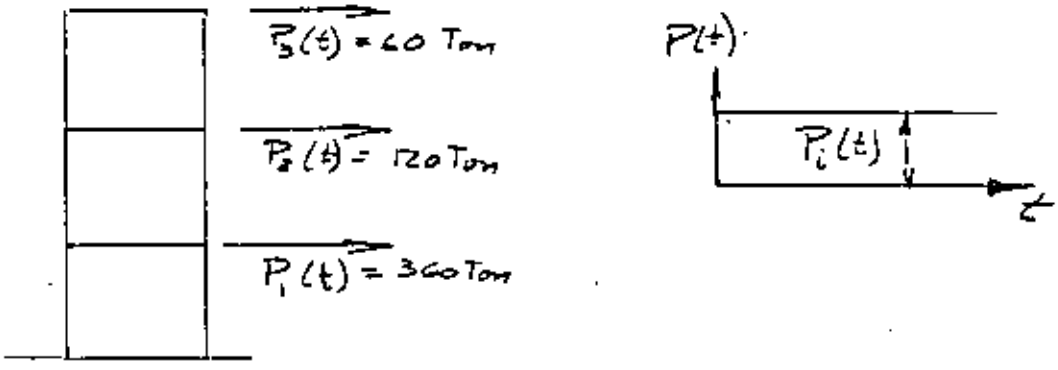

Para el modo j:

$$\ddot{Y}_j + p^2 Y_j = \frac{P_j^*(t)}{M_j^*} = \frac{P_{jo}^*}{M_j^*} \quad \text{cuya solución es:}$$

$$Y_j = \frac{P_{jo}^*}{K_j^*} \left(1 - \cos p_j t\right) = \frac{P_{jo}^*}{p_j^2 M_j^*} \left(1 - \cos p_j t\right)$$

Cálculo de P_j^*

$$P_j^* = \{r\}_j' \{P(t)\} = \{r\}_j' \begin{Bmatrix} 360 \\ 120 \\ 60 \end{Bmatrix}$$

modo ↓

1) $P_1^* = P_1 r_{11} + P_2 r_{21} + P_3 r_{31} = 360+256.2+197.1 = 813.3$

2) $P_2^* = P_1 r_{12} + P_2 r_{22} + P_3 r_{32} = 360+107.88-88.4 = 379.48$

3) $P_3^* = P_1 r_{13} + P_2 r_{23} + P_3 r_{33} = 360-125.28+24.66 = 259.98$

Ahora bien,

$$Y_{j(st)} = \frac{P_j^*}{p_j^2 M_j^*} = \frac{P_j^*}{K_j^*}$$

$$\therefore \quad Y_{1(st)} = \frac{813.30}{21 \times 19.629} = 1.973 \text{ cm}$$

$$Y_{2(st)} = \frac{379.48}{965 \times 5.386} = 0.730 \text{ cm}$$

$$Y_{3(st)} = \frac{259.38}{212.4 \times 3.804} = 0.321 \text{ cm}$$

de donde

$$Y_j = \frac{P_j^*}{p_j^2 M_j^*} \left(1 - \cos P_j t\right), \text{ y tenemos:}$$

$$Y_1(t) = Y_{1(st)} \left(1 - \cos p_1 t\right)$$

$$Y_2(t) = Y_{2(st)} \left(1 - \cos p_2 t\right)$$

$$Y_3(t) = Y_{3(st)} \left(1 - \cos p_3 t\right)$$

y, finalmente:

$$\{x(t)\} = \{r_1\} Y_1(t) + \{r_2\} Y_2(t) + \{r_3\} Y_3(t) = [R] \{Y\}$$

$$\begin{Bmatrix} X_1(t) \\ X_2(t) \\ X_3(t) \end{Bmatrix} = \begin{Bmatrix} 1.000 \\ 2.135 \\ 3.285 \end{Bmatrix} 1.973 \left(1 - \cos p_1 t\right) + \ldots + \begin{Bmatrix} 1.000 \\ -1.044 \\ 0.411 \end{Bmatrix} 0.321 \left(1 - \cos p_3 t\right) -$$

EXCITACION SISMICA

A. Sistemas 1GL

$$m\ddot{x} + kx + P(t) \qquad (a)$$

Para P(t) cualquiera y para CI $\neq 0$ la solución de (a) es:

$$x(t) = x_o \cos pt + \frac{\dot{x}_o}{p} \operatorname{sen} pt + \frac{1}{mp}\int_0^t P(\zeta) \operatorname{sen} p(t-\zeta)d\zeta$$

Para excitación sísmica:

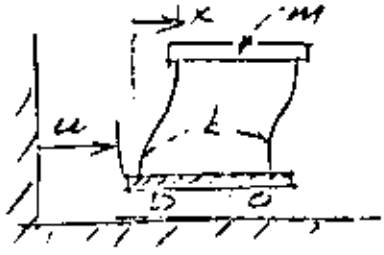

$$m(\ddot{x} + \ddot{u}) + k\,x = 0$$

o sea,

$$m\ddot{x} + k\,x = -m\ddot{u} \qquad (b)$$

De la comparación de (a) y (b), la solución completa de ésta es:

$$x(t) = x_o \cos pt + \frac{\dot{x}_o}{p} \operatorname{sen} pt - \frac{1}{p}\int_0^t \ddot{u}(\zeta) \operatorname{sen} p(t-\zeta)\, d\zeta$$

B. Sistemas de nGL:

$$[M]\{\ddot{x}\} + [k]\{x\} = \{P(t)\} = \begin{Bmatrix} P_1(t) \\ P_2(t) \\ \vdots \\ P_n(t) \end{Bmatrix} = \begin{Bmatrix} -m_1\ddot{u} \\ -m_2\ddot{u} \\ \vdots \\ -m_n\ddot{u} \end{Bmatrix}$$

$$= -\begin{Bmatrix} m_1 \\ m_2 \\ \vdots \\ m_n \end{Bmatrix} \ddot{u} \qquad \ddot{u} = -\{m\}\ddot{u}$$

Es decir, tenemos:

$$[M]\{\ddot{x}\} + [K]\{x\} = \{P(t)\} = -\{m\}\ \ddot{u}$$

sust. $\{x\} = [R]\{y\}$

$$[M][R]\{\ddot{y}\} + [K][R]\{y\} = \{P(t)\} = -\{m\}\ \ddot{u}(t)$$

pre x $\{r\}_j^t$

$$\{r\}_j^t [M][R]\{\ddot{y}\} + \{r\}_j^t [K][R]\{y\} = \underbrace{\{r\}_j^t \{P\}}_{P_j^*} = -\underbrace{\{r\}_j^t \{m\}}_{m_j^*}\ \ddot{u}$$

U_j^*

por ortogonalidad:

$$\{r\}_j^t [M]\{r\}\ \ddot{y}_j + \{r\}_j^t [K]\{r\}_j\ y_j = P_j^* = U_j^*$$

y queda:

$$M_j^*\ \ddot{y}_j + K_j^*\ y_j = P_j^* = U_j^* = -\ m_j^*\ \ddot{u}$$

∴ la solución (CI = 0) de esta ecuación es:

Para P_j^* :

$$y_j(t) = \frac{1}{\phi_j M_j^*} \int_0^t P_j^*(\tau)\ \text{sen}\ \phi_j(t-\tau)d\tau$$

Para U_j^*:

$$y_j(t) = \frac{1}{\phi_j M_j^*} \int_0^t U_j^*(\tau)\ \text{sen}\ \phi_j(t-\tau)d\tau$$

que puede escribirse:

$$y_j(t) = -\frac{m_j^*}{\omega_j M_j^*}\int_0^t \ddot{u}(Z)\,\text{sen}\,\omega_j(t-Z)\,dZ$$

$$+ y_{oj}\cos\omega_j t + \frac{\dot{y}_{oj}}{\omega_j}\,\text{sen}\,\omega_j t \qquad \begin{matrix}\text{término a}\\ \text{para}\\ CI \neq 0\end{matrix}$$

Una vez obtenidos los elementos de $\{y\}$ solo falta premultiplicar por $[R]$ para obtener $\{x\}$:

$$\{x(t)\} = [R]\,\{y(t)\}$$

GENERALIZACION DE LAS CONDICIONES DE ORTOGONALIDAD

Tenemos la ecuación:

$$\left[[K] - p^2\,[M]\right]\{x\} = \{0\}$$

que convenimos en escribir en la forma:

$$(K - p^2 M)\,x = 0$$

como los vectores modales la satisfacen:

$$K\,r_j = \omega_j^2\,M\,r_j \qquad (a)$$

y premultiplicando por: $r_i'\,MM^{-1}$ tenemos:

$$r_i'\,M\,M^{-1}\qquad K\,r_j = p_j^2\,M\,M^{-1}\qquad M\,r_j = p_j^2\,M\,M^{-1}K\,r_j = 0$$

que puede escribirse

$$r_i' \; M \; (M^{-1} K)^2 \; r_j = 0$$

y así podría seguirse para llegar a:

$$r_i' \; M \; (M^{-1}K)^{\ell} \; r_j = 0 \quad - \begin{cases} \ell \text{ entero} \\ -\infty < \ell < \infty \end{cases}$$

$$r_i' \; M \; (M^{-1} \; K)^{\ell} \; r_j = 0 \qquad (b)$$

en forma análoga podemos obtener

$$r_i' \; (MF)^{\ell} \; M \; r_j = 0 \qquad (c)$$

o

$$r_i' \; (K \; M^{-1})^{\ell} \; K \; r_j = 0$$

En (b):

$\ell = -2$ $\quad M \; (M^{-1}K)^{-2} = M \; (M^{-1}K)^{-1} \; (M^{-1}K)^{-1}$

(en (c), con $\ell=2$) $\quad = M \; K^{-1} \; M \; K^{-1} \; M = \underline{M \; F \; M \; F \; M}$

$\ell = -1$ $\quad M(M^{-1}K)^{-1} = M \; K^{-1} \; M = \underline{M \; F \; M}$

$\ell = 0$ $\quad M \; (M^{-1}K)^{0} = \underline{M}$

$\ell = 1$ $\quad M \; (M^{-1}K)^{1} = M \; M^{-1} \; K = \underline{K}$

$\ell = 2$ $\quad M \; (M^{-1}K)^{2} = M \; M^{-1} \; K \; M^{-1} \; K = \underline{K \; M^{-1} \; K}$

$\ell = 3$ $\quad M \; (M^{-1}K)^{3} = M \; M^{-1} \; K \; M^{-1} \; K \; M^{-1}K = \underline{K \; M^{-1} \; K \; M^{-1} \; K}$

VIBRACION LIBRE Y FORZADA DE SISTEMAS DE N GL CON AMORTIGUAMIENTO

Las ecuaciones de equilibrio dinámico son:

$$\{F_I\} + \{F_a\} + \{F_r\} = \{P(t)\}$$

Ya tenemos:

$$\{F_I\} = [M] \{\ddot{x}\}$$

$$\{F_r\} = [K] \{x\}$$

y ahora hacemos

$$\{F_a\} = [c] \{\dot{x}\}$$

donde

$$[c] = [c_{ij}]$$

y c_{ij} = fuerza de amortiguamiento en la coordenada i debido a una velocidad unitaria en la coordenada j.

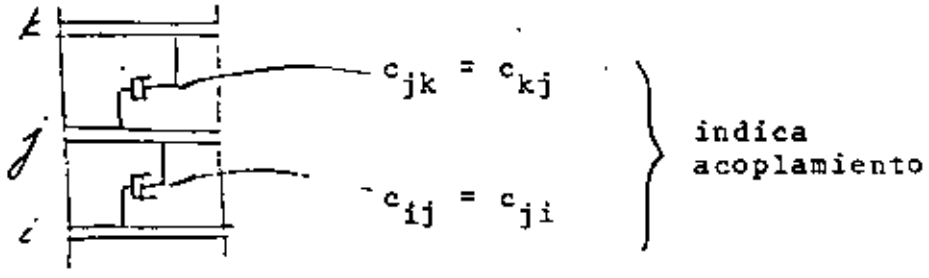

La ecuación de movimiento es

$$[M] \{\ddot{x}\} + [c] \{\dot{x}\} + [K] \{x\} = \{P(t)\}$$

Hagamos: $\{X\} = [R]\{y\}$ premultiplicando por $\{r\}_j'$

$$\{r\}_j'[M][R]\{\ddot{y}\} + \{r\}_j'[C][R]\{\dot{y}\} + \{r\}_j'[K][R]\{y\} = \{r\}_j'\{P(t)\}$$

Para desacoplar estas ecuaciones debemos tener

$$\left.\begin{aligned} \{r\}_j'[M]\{r\}_i &= 0 \quad i \neq j \\ \{r\}_j'[K]\{r\}_i &= 0 \quad i \neq j \end{aligned}\right\} \text{ cierto por ortogonalidad}$$

$$\{r\}_j'[C]\{r\}_i = 0 \quad i \neq j \qquad \text{¿pero ésta?} \quad (a)$$

1° <u>admitamos</u> que se cumple:

Ya definimos

$$\{r\}_j'[M]\{r\}_j = M_j^* \qquad \{r\}_j'\{P(t)\} = P_j^*$$

$$\{r\}_j'[K]\{r\}_j = K_j^*$$

y ahora

$$\{r\}_j'[C]\{r\}_j = C_j^* = 2\beta_j p_j M_j^*$$

y nuestra ecuación para el modo j queda:

$$M_j^*\ddot{y}_j + 2\beta_j p_j M_j^*\dot{y}_j + p_j^2 M_j^* y_j = P_j^*$$

o bien:

$$\ddot{y}_j + 2\beta_j p_j \dot{y}_j + p_j^2 y_j = \frac{P_j^*}{M_j^*}$$

Como las soluciones para un sistema de 1GL (cuya ec. es $\ddot{x}+2\beta p\dot{x}+p^2x = \frac{P(t)}{m}$) ya las conocemos, solo nos falta saber cómo debe ser $[C]$ para que se cumpla

$$\{r\}_i' [C] \{r\}_j = 0 \qquad i \neq j \qquad \text{(a)}$$

además, claro, de

$$\left.\begin{aligned} \{r\}_i' [M] \{r\}_j &= 0 \\ \text{y} \qquad \{r\}_i' [K] \{r\}_j &= 0 \end{aligned}\right\} \; i \neq j$$

La ec. (a) se satisface si

i) $[C]$ es proporcionala $[M]$ o a $[K]$

ii) $[C]$ es una combinacion lineal de $[M]$ y $[K]$, o sea:

$$[C] = a_0 [M] + a_1 [K]$$

esto es muy restringido.

iii) En forma más general:

$$[C] = [M] \sum_l a_l [M^{-1}K]^l = \sum_l [C_l] \qquad (38.1)$$

pues ya sabemos que todas las posibles formas $[M] [M^{-1}K]^l$ son satisfactorias y (38.1) es una C. L de matrices de este tipo.

La selección adecuada de a_1 dará a $[C]$ las propiedades deseadas, o sea, podremos dar valores específicos a los elementos de $[C]$. ¿Cuáles le damos?

Asignamos un cierto valor de β a cada modo.

$$C_j^* = \{r\}_j' [C] \{r\}_j = 2\beta_j \not{p}_j M_j^* = \sum_1 \{r\}_j' [C_1] \{r\}_j = \sum_1 C_{j1}^* \quad (38.2)$$

(A)

De 38.1 y A

$$C_{j1}^* = \{r\}_j' [M] [M^{-1}K]^1 \{r\}_j a_1 \quad (38.3)$$

Por otra parte, para vibración libre:

$$(K - \not{p}_j^2 M) r_j = 0$$

$$Kr_j = \not{p}_j^2 M r_j \rightarrow \frac{1}{\not{p}_j^2} r_j = FMr_j$$

premultiplicando por $r_j' M$:

$$\frac{1}{\not{p}_j^2} r_j' M r_j = r_j' MFMr_j$$

es decir

$$(\not{p}_j^2)^{-1} M_j^* = r_j' M (M^{-1}K)^{-1} r_j$$

y así podríamos llegar a que, para cualquier 1:

$$(\not{P}_j^2)^1 M_j^* = r_j' M (M^{-1}K)^1 r_j = \underbrace{\frac{C_{j1}^*}{a_1}}_{\text{por } 38.3} \qquad 39.1$$

De 39.1:

$$C_{j1}^* = (\not{P}_j^2)^1 M_j^* a_1$$

$$C_{j1}^* = (\not{P}_j^2)^1 M_j^* a_1$$

y sumando sobre 1:

$$\sum_1 C_{j1}^* = \sum_1 (\not{P}_j^2)^1 M_j^* a_1$$

pero ya teníamos que

$$\sum_1 C_{j1}^* = 2\beta_j \not{P}_j M_j^*$$

$$\therefore \quad 2\beta_j \not{P}_j M_j^* = \sum_1 (P_j^2)^1 M_j^* a_1$$

de donde:

$$\beta_j = \frac{1}{2P_j} \sum_1 (\not{P}_j^2)^1 a_1$$

Con los n valores de β_j para los n modos podemos resolver para los n valores de a_1 y formar nuestra $[C]$ con la ecuación

$$[C] = [M] \sum_{1} a_1 [M^{-1}K]^1$$

Por ejemplo para nuestra estructura de 3GL asignemos:

$$\beta_1 = 0.10, \qquad \beta_2 = 0.05, \qquad \beta_3 = 0.02$$

$$\beta_1 = 0.10 = \frac{1}{2\omega_1}\left[a_1(\omega_1^2)^{-1} + a_0(\omega_1^2)^0 + a_1(\omega_1^2)^1\right]$$

$$\beta_2 = 0.05 = \frac{1}{2\omega_2}\left[a_{-1}(\omega_2^2)^{-1} + a_0(\omega_2^2)^0 + a_1(\omega_2^2)^1\right]$$

$$\beta_3 = 0.02 = \frac{1}{2\omega_3}\left[a_{-1}(\omega_3^2)^{-1} + a_0(\omega_3^2)^0 + a_1(\omega_3^2)^1\right]$$

o, en forma matricial:

$$\begin{Bmatrix} 0.10 \\ 0.05 \\ 0.02 \end{Bmatrix} = \frac{1}{2}\begin{bmatrix} 1/\omega_1^3 & 1/\omega_1 & \omega_1 \\ 1/\omega_2^3 & 1/\omega_2 & \omega_2 \\ 1/\omega_3^3 & 1/\omega_3 & \omega_3 \end{bmatrix}\begin{Bmatrix} a_{-1} \\ a_0 \\ a_1 \end{Bmatrix}$$

al resolver para a_1 resulta

$$\underline{[C] = a_{-1}[MFM] + a_0[M] + a_1[K]}$$

En p. tenemos que para CI = 0. y $\beta = 0$, para excitación sísmica

$$y_j(t) = -\frac{m_j^*}{P_j M_j^*}\int_0^t \ddot{u}(\tau)\,\text{sen}\,P_j(t-\tau)d\tau$$

$$\underline{\text{coeficiente de participación} = \frac{m_j^*}{M_j^*}}$$

$$C_j = \frac{m_j^*}{M_j^*} = \frac{\{r\}_j' \{m\}}{\{r\}_j' [M] \{r\}_j} = \frac{\sum_{i=1}^{m} m_i r_{ij}}{\sum_{i=1}^{m} m_i r_{ij}^2}$$

y ∴ podemos poner:

$$y_j(t) = C_j z_j(t)$$

en la que C_j está definida arriba y

$$z_j(t) = -\frac{1}{p_j}\int_0^t \ddot{u}(\tau)\,\mathrm{sen}\, p_j(t-\tau)\,d\tau$$

(y semejante si $\beta \neq 0$)

$$y_j(t) = C_j z_j(t)$$

Además, tenemos

$$\{X\} = [R]\{y\}$$

o sea

$$\begin{Bmatrix} X_1 \\ X_2 \\ \vdots \\ X_i \\ \vdots \\ X_n \end{Bmatrix} = \begin{bmatrix} r_{11} & r_{12} \cdots\cdots r_{1j} \cdots\cdots r_{1n} \\ r_{21} & r_{22} \cdots\cdots r_{2j} \cdots\cdots r_{2n} \\ \vdots & \vdots \quad\quad \vdots \quad\quad \vdots \\ r_{n1} & r_{n2} \cdots\cdots r_{nj} \cdots\cdots r_{nn} \end{bmatrix} \begin{Bmatrix} Y_1 \\ Y_2 \\ \vdots \\ Y_n \end{Bmatrix}$$

††
∴

$$x_i = \sum_{j=1}^{n} r_{ij} y_j = \sum_{j=1}^{n} r_{ij} C_j z_j(t)$$

De aquí (sin sumar para todos los modos)

$$\left.\begin{aligned} |X_{ij}|_{max} = r_{ij} C_j |z_j(t)|_{max} &= r_{ij} C_j S_d \\ &= r_{ij} C_j \frac{S_a}{p_j^2} \end{aligned}\right\} S_a = p S_v = p^2 S_d$$

De esta ec. pasamos a:

$$|X_i|_{\substack{max \\ ABS}} = \sum_{j=1}^{n} r_{ij} C_j S_d = \sum_{j=1}^{n} r_{ij} C_j \frac{S_a}{p_j^2}$$

$$|x_i|_{\substack{max \\ PROB}} = \sqrt{\Sigma (|X_{ij}|_{max})^2}$$

DIVISION DE EDUCACION CONTINUA
FACULTAD DE INGENIERIA U.N.A.M.

CURSOS DE INGENIERIA CIVIL EN EL PROYECTO
DE PLANTAS HIDROELECTRICAS

CFE

INGENIERIA SISMICA

M. en C. Jorge Prince Alfaro

Mayo 1981

THE INTERIOR OF THE EARTH

K. E. BULLEN

September 1955

Each year 10 or more major earthquakes shake the earth. The smallest of them releases about a thousand times more energy than an atomic bomb; the Assam earthquake of August, 1950, had about 100,000 times that energy. The waves set up by these convulsions travel through the whole interior of the earth, including the core, and their paths are bent and shaped by the shells of the earth's internal structure. Thus the seismic waves bear clues of the regions they traverse, and from the story they tell when they are received at our seismological stations on the surface it is possible to infer a picture of the interior. In effect the seismologist X-rays the earth, even if at times he sees through a glass, darkly.

Seismology has lifted our notions about the interior of our planet from the realm of wild speculation to the stage of scientific measurement and well-reasoned inferences. Combined with geological information about surface rocks, laboratory experiments on rocks at high pressures and certain astronomical observations, it gives us a basis for learning something about the various conditions in the deep interior—its layered structure, the materials, their physical state, the pressures and so on.

The study of earthquakes is a fairly new science. In 1750 a writer on the subject in the *Philosophical Transactions* of the Royal Society of London apologized to "those who are apt to be offended at any attempts to give a natural account of earthquakes." But observations of earthquake effects accumulated, and late in the 19th century seismology began to emerge as a real quantitative science when the Englishman John Milne constructed in Japan a seismograph suitable for world-wide use. The seismograph was later developed further, notably by E. Wiechert in Germany, by Prince Galitzin in Russia and recently by Hugo Benioff of the California Institute of Technology.

The release of elastic strain-energy at the source, or "focus," of an earthquake produces waves which begin to radiate in all directions from the focus. In 1897 R. D. Oldham of England identified on seismograms three main types of seismic waves: (1) primary (P) waves, which are compression-and-expansion waves like those of sound; (2) secondary (S) waves, which vibrate at right angles to the direction of travel, as

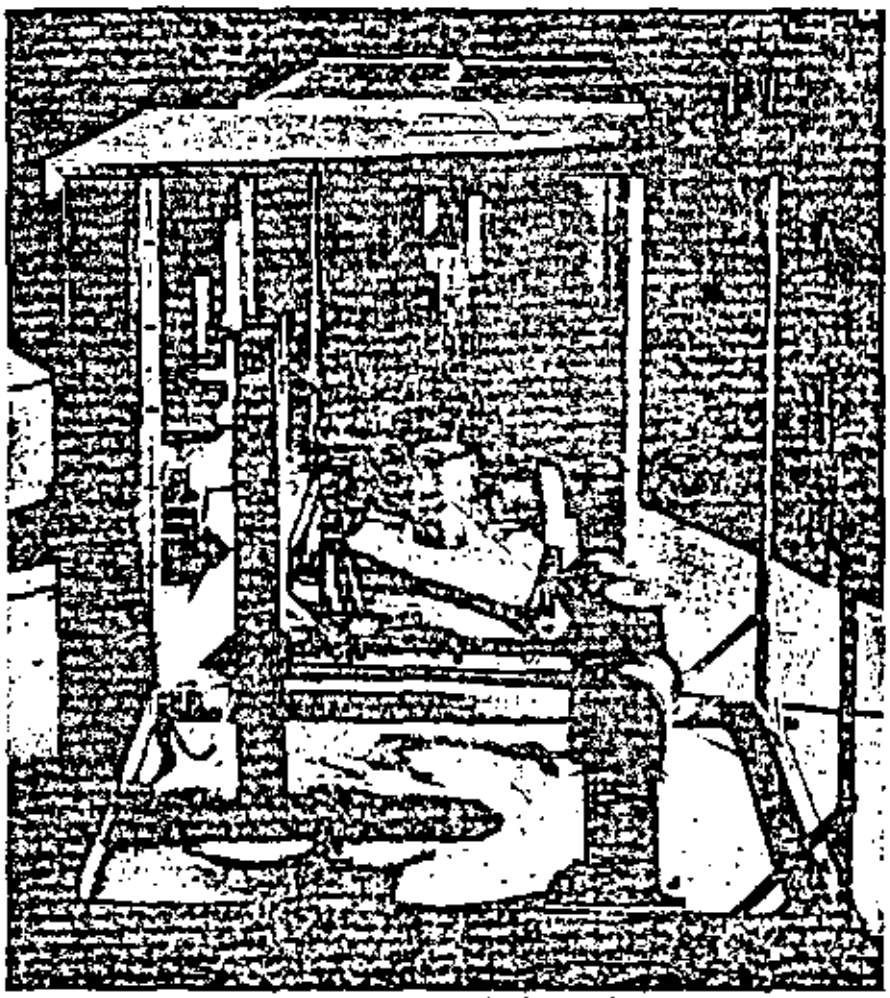

TWO SEISMOMETERS are photographed at the Lamont Geological Observatory of Columbia University. They consist essentially of three pendulums: one for each dimen-

light waves do; (3) surface waves, which appear in the upper 20 miles or so near the earth's surface. The P waves travel through both solid and liquid parts of the earth; the S waves only through solid.

S waves travel at about two thirds of the speed of P waves. The speed of both varies with depth in the earth; for example, the P waves travel at 8¼ miles per second, their maximum speed, at a depth of 1,800 miles and at about three miles per second in rocks near the earth's surface. Because of the change of speed, the path of the waves' travel usually curves upward. When they arrive at a boundary between layers they may be refracted or reflected, and on reaching the earth crust they are reflected downward again. At a boundary either a P or an S wave may give rise to both P and S waves. Thus any one seismogram from a particular earthquake may show many distinct phases, signifying the stages of the waves' routes and their changes of form. A typical seismogram illustrating several phases is shown on the next two pages.

With this kind of evidence Oldham proved in 1906 that the earth has a large central core, and in 1914 Beno Gutenberg, then in Germany, located the boundary of the core at 1,800 miles below the earth's surface. Since the radius of the whole earth is about 3,960 miles, the central core has a radius of some 2,160 miles.

The discovery of the core came about from the observation of shadow zones where relatively few P waves were recorded. Consider P waves issuing from a major earthquake with its focus at the South Pole. These waves would be observed at the surface throughout the Southern Hemisphere and up to 15 degrees above the equator (*i.e.*, the latitude of Guatemala) in the Northern Hemisphere. But between the latitudes of Guatemala and Winnipeg little indication of P waves would be received. Then, from a latitude of 52 degrees north to the North Pole, the waves would come in again strongly. The whole of the U. S. would thus be part of a "shadow zone" for that earthquake. On examination, it was seen that the existence of such shadow zones required the presence of a central core which would bend sharply downwards the seismic rays striking it from above, somewhat after the manner in which light rays from a stick in water are bent by the water surface.

One of the great labors of seismologists during the first 40 years of this century was to evolve reliable tables for the times of travel of P and S waves along the various phases of their routes. In 1930 Sir Harold Jeffreys of the University of Cambridge, suspecting that the existing "travel-time tables" contained large errors, began a long series of studies to correct them. The author of this article was associated with Jeffreys in this work from 1931 to 1939.

The Jeffreys-Bullen tables of 1940 are now used internationally. They agree closely, in the main, with travel times derived about the same time by Gutenberg and Charles F. Richter at the California Institute of Technology. The travel-time tables are of cardinal importance for charting the structure of the earth's

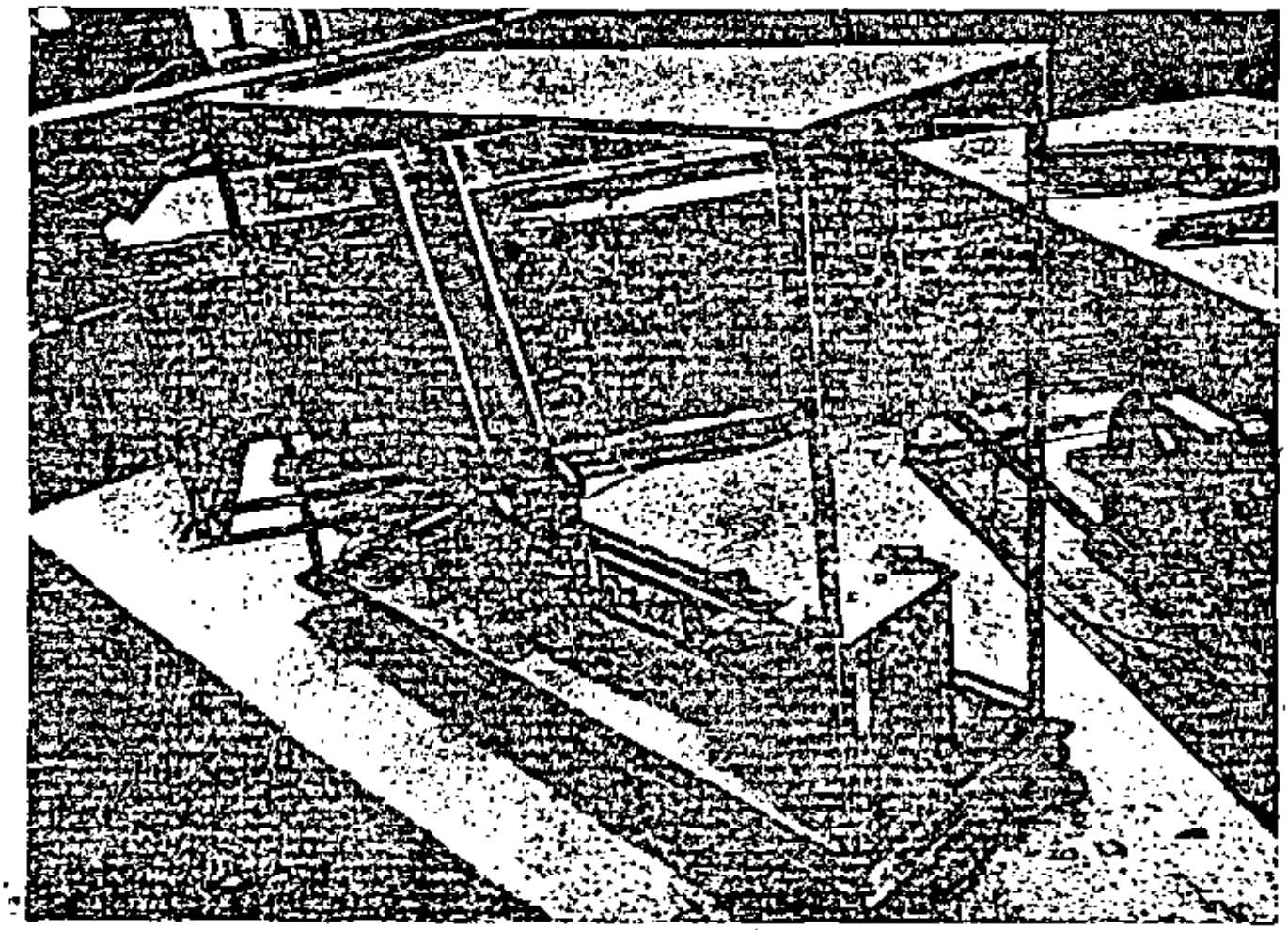

sion. When the earth shakes, the pendulums tend to stand still. Their apparent motion is then recorded by a pen or a beam of light. One of the pendulums, suspended by a horizontal arm and two diagonal wires, is visible at right in the photograph at left.

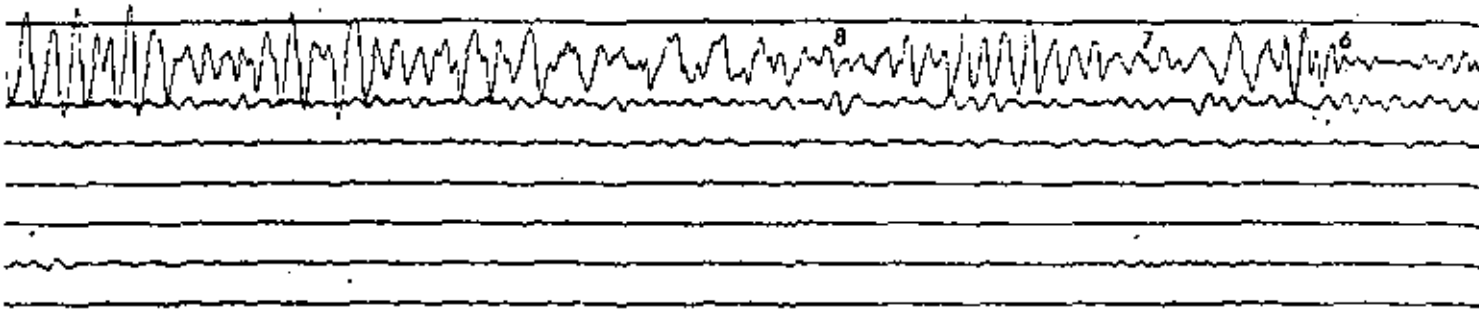

SEISMOGRAM of an earthquake on the Kamchatka Peninsula in Siberia was recorded at the Lamont Geological Observatory. The separate lines are actually part of a continuous spiral trace, going from right to left, on a circular drum. The interval between succes-

interior. It is possible to deduce from the tables the velocities of P waves and S waves in various parts of the interior. Studying the variations of velocity with depth, one can chart different layers and locate boundaries.

With the new tables Jeffreys calculated that Gutenberg's measurement, placing the boundary of the central core at 1,800 miles below the earth's surface, is correct within three or four miles.

At least the outer part of the core is judged to be molten. S waves do not pass through it, and its fluid character is established by other evidence, including data on the tidal deformation of the solid earth and astronomical data on the movements of the earth's poles. H. Takeuchi of Japan has calculated that this region is at most one 300th as rigid as the next outward layer.

The use of the terms "solid" and "fluid" in connection with the huge pressures prevailing in the earth's interior is sometimes questioned. What a geophysicist means by the term "solid" in this context is simply that the elastic behavior of the material in question can be described by equations which match those applying to ordinary solids in normal laboratory conditions. These equations involve the use of two coefficients: "incompressibility," which is the measure of resistance to pressure, and "rigidity," signifying resistance to shearing stress. In the case of a fluid, the resistance to shear is much smaller than the resistance to compression. This is why a fluid does not transmit S waves.

All the earth outside the core is called the mantle. The whole of the mantle (apart from the oceans and pockets of magma in volcanic regions) is now known to be essentially solid: both S and P waves travel through every part of it.

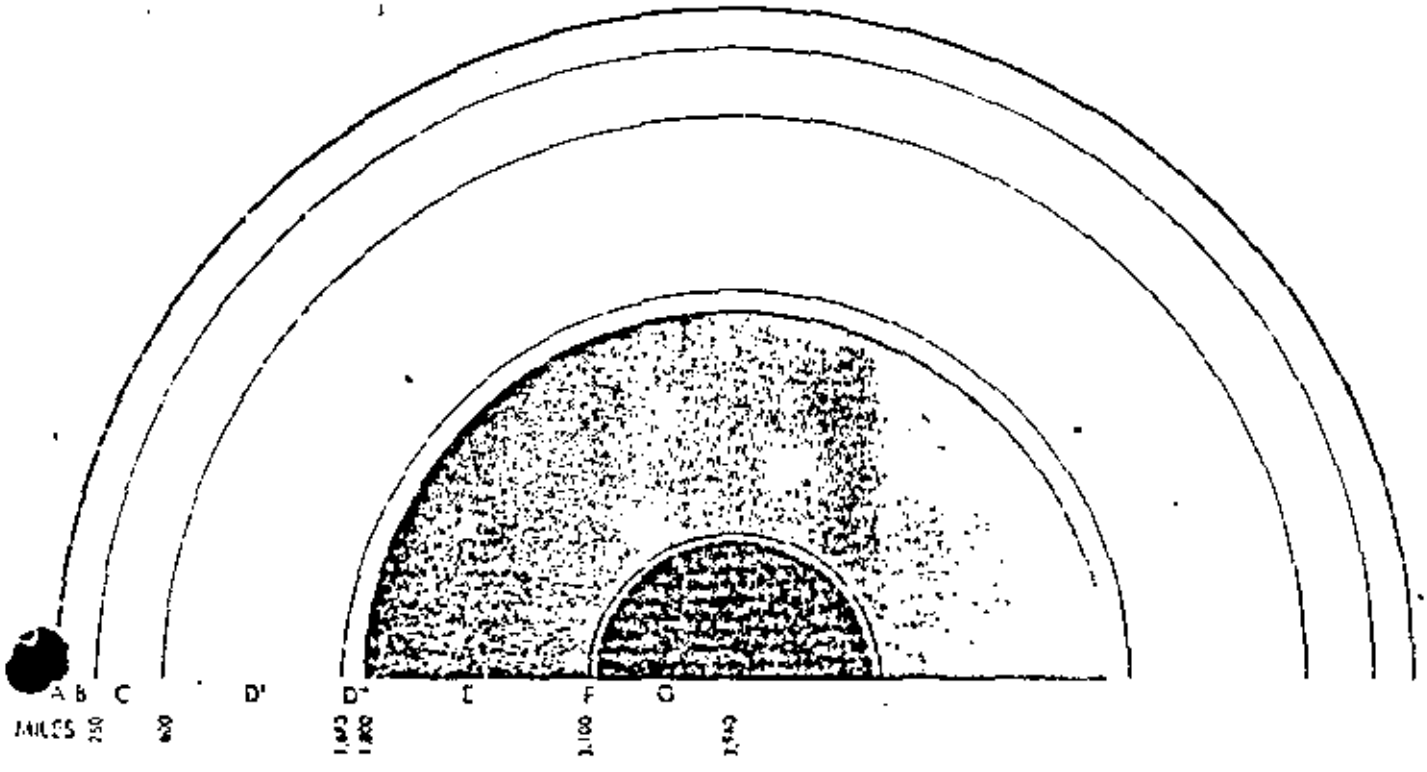

EARTH'S CROSS SECTION is divided into distinct layers through which seismic waves travel at different speeds. The outer core is indicated by the lighter tone of color; the inner core, by the darker tone of color. Layer A is the thin crust of the earth.

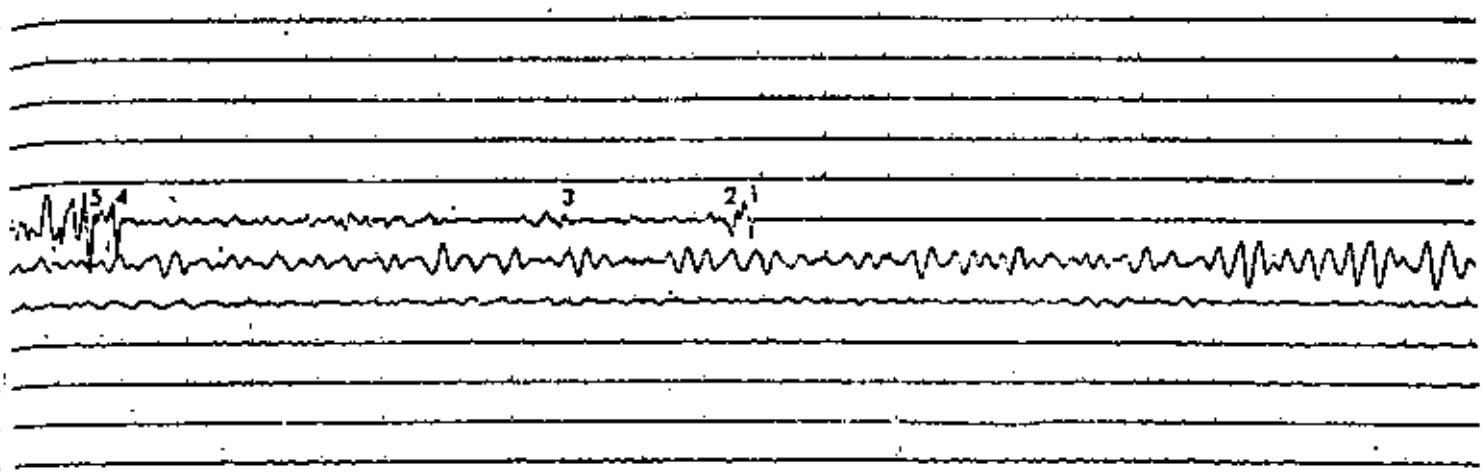

sive dots is one minute. The first disturbance recorded was the P wave designated by the number 1. Then followed the multiply reflected P waves 2 and 3. S waves begin at position 4, followed by multiply reflected waves at 5, 6 and 7. Surface waves start at 8.

In 1909 the Croatian seismologist A. Mohorovicic, studying the seismograph of a Balkan earthquake, discovered an important discontinuity (boundary) now known to be some 20 miles below the earth's surface. The part of the earth above the Mohorovicic discontinuity has come to be called the crust. But nowadays the term "crust" has only a conventional meaning. According to seismic evidence the crust is not more rigid than the material just below it.

Seismologically speaking, the crust differs from the underlying part of the mantle in the fact that P and S waves travel in it more slowly and with more variable speed. This irregularity of travel velocity makes detailed charting of the crust difficult. The work is being pursued vigorously, however, by the study of surface waves, of P and S waves from near earthquakes (near the recording station), of waves from large man-made explosions (such as the one on Helgoland in 1947) and by seismic probings with dynamite, as in oil prospecting. One important discovery has been that the crust is much thinner under the oceans than under the continents.

Seven distinct regions or shells have now been identified in the earth. In 1936 Miss I. Lehmann of Denmark discovered that the core was not uniform but seemed to consist of at least two different parts. Looking closely at the relatively minor P waves that emerge in the shadow zone on the surface, she concluded that these waves might come to the surface because they were bent sharply upward by an inner core where P waves traveled faster than in the outer core. Her proposal later received support from work by Gutenberg, Richter and Jeffreys. The inner core has a radius of some 800 miles, so the thickness of the

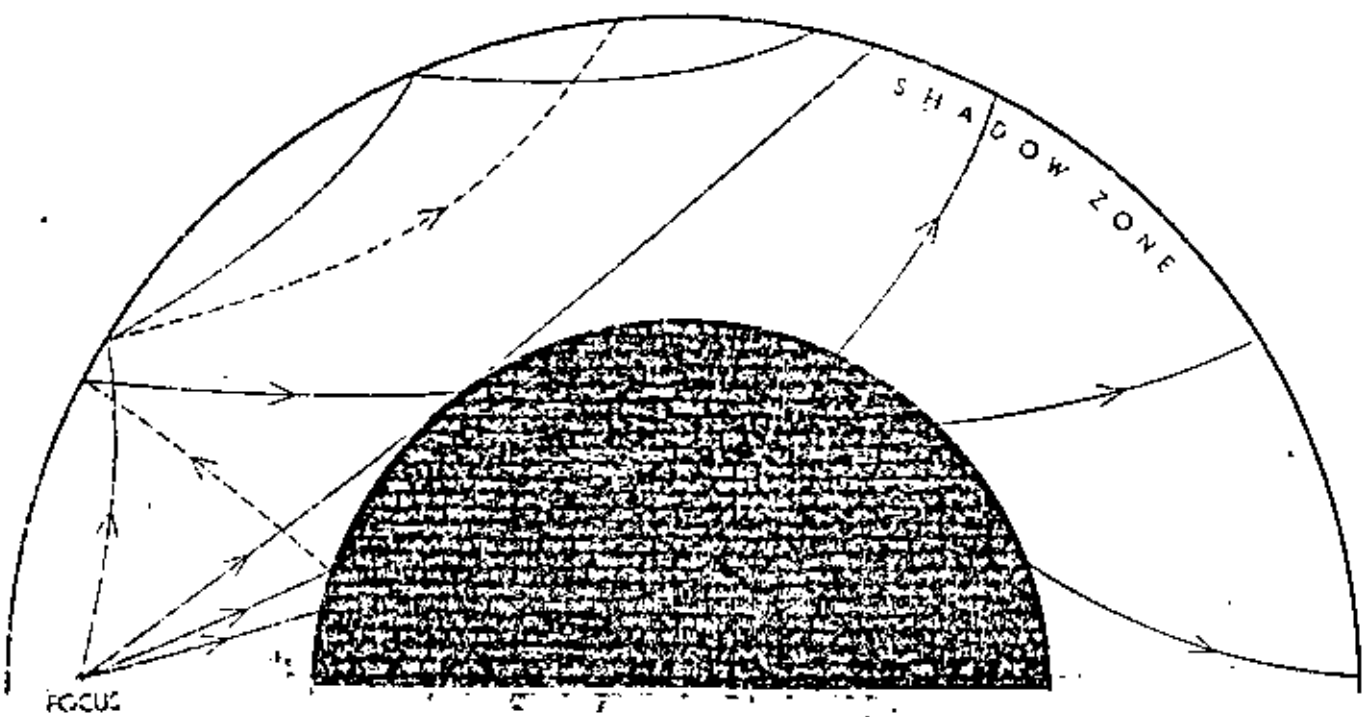

EARTHQUAKE WAVES are bent and reflected as they travel from their source. Solid lines represent P waves, dotted lines are S waves formed by reflection. The only P waves that can get into the shadow zone are those which enter the inner core and are sharply bent.

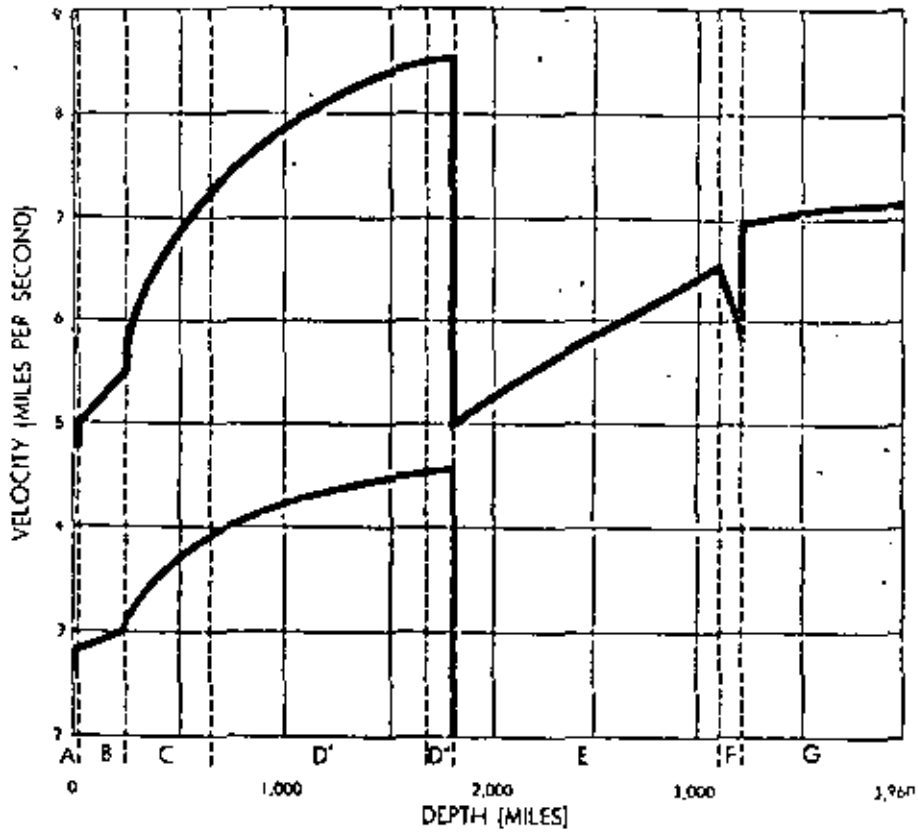

SEISMIC WAVE SPEEDS vary with depth. The black line gives velocities of P waves; the gray line, of S waves. Both change abruptly at core, or E layer, and the S wave disappears.

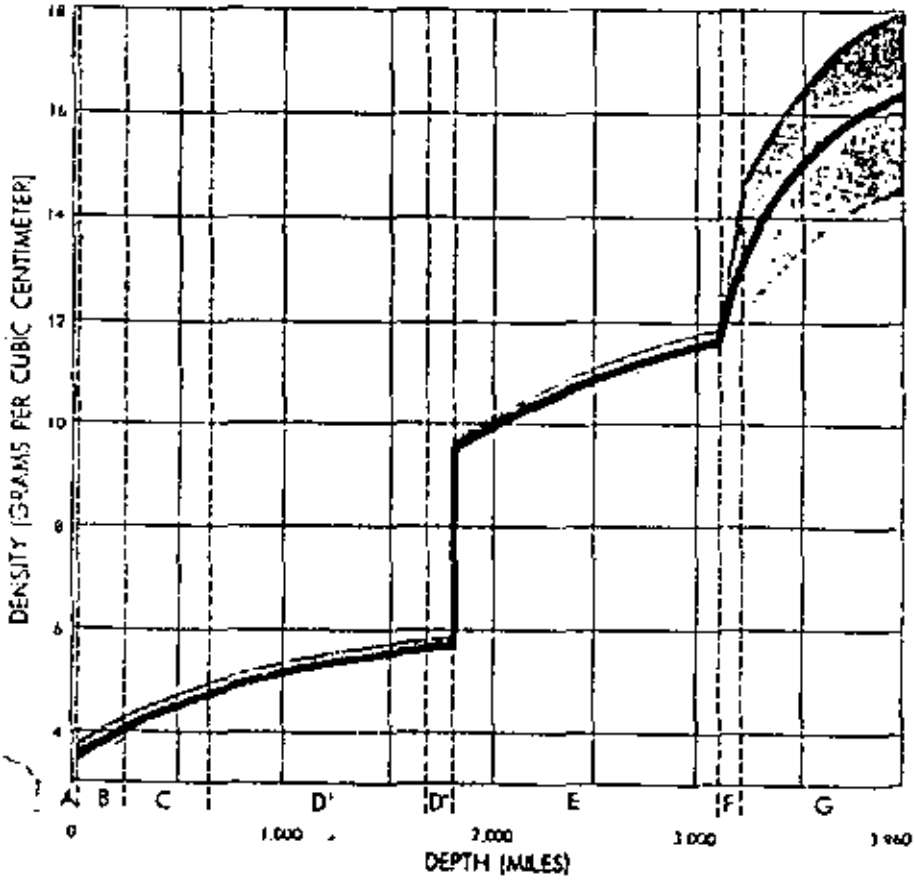

DENSITY of the earth's material increases with depth. The solid line shows the most probable value at each depth and the gray region outlines the probable range of uncertainty.

outer core would be about 1,300 miles.

On the basis of density variations the writer has divided the body of the earth into seven regions, called A, B, C, D, E, F and G [*see diagram on page 24*]. The A region is the crust. The rest of the mantle below is divided into B, C and D, with D subdivided into D' and D''. These divisions are still tentative because of certain uncertainties in estimates of velocity gradients. The outer part of the core is called E, and the inner part, G. Between the inner and outer core Jeffreys finds a layer F, some 80 miles thick, where the velocity of P waves declines sharply. Gutenberg has not found this layer, but has said that his data do not exclude its existence.

How can we estimate the pressures and physical characteristics of matter at these various depths in the body of the earth? The velocities of P and S waves are determined by the density, compressibility and rigidity of the material through which they pass, but they do not provide enough information to solve exact equations for those values. There are, however, indirect clues which help us to arrive at estimates—information on the earth's mass and moment of inertia, field observations and laboratory experiments on rocks, mathematical theories of elasticity and gravitational attraction.

By such means the writer has estimated that the earth's density increases gradually from 3.3 grams per cubic centimeter just below the crust to 5½ grams per c.c. at the bottom of the mantle, then jumps suddenly to 9½ grams at the top of the core and thereafter increases steadily to 11½ grams at the bottom of the outer core.

A related calculation gave the increase in pressure with depth in the earth. At the bottom of the Pacific Ocean the pressure is about 800 atmospheres. Only 200 miles down in the mantle the pressure is already 100,000 atmospheres—as great as the highest pressure Percy W. Bridgman of Harvard University has been able to produce in the laboratory. At the base of the mantle, 1,800 miles down, the pressure reaches the immense figure of 1½ million atmospheres, and at the center of the earth it is nearly four million atmospheres.

Next the calculations yielded the surprising finding that the rigidity of the material in the mantle increases with depth until, at the mantle's base, it is nearly four times that of steel in ordinary conditions. Below this, in the outer core, the seismic evidence shows that the rigidity sinks to practically zero, meaning that the material is essentially fluid.

Perhaps the most important fruits of this series of calculations have been the findings on compressibility. In spite of the sharp changes in density and in rigidity at the boundary between the mantle and the core, the compressibility of the material does not change substantially at the boundary, according to the calculations. This finding led the writer to examine the theoretical effect of pressures of a million atmospheres or more on materials likely to be present in the core. Taking into account a variety of evidence, the conclusion was that bounds could be set to the compressibilities of materials in the core.

Following this line of argument, it seems highly probable that the inner core, unlike the outer core, is solid in the sense defined. The idea that the inner core is solid, suggested by the writer in 1946 and since developed, would explain the speeding up of P waves when they penetrate into the inner core. Calculation indicates that the inner core is probably at least twice as rigid as steel at ordinary pressures.

On the same line of evidence we can also estimate, as we could not before, the density of the inner core. Apparently at the center of the earth the density is between 14½ and 18 grams per cubic centimeter. Yet another inference is that the increase of density with depth in the inner core (and at the base of the mantle) is greater than average, implying some variability in the composition of that region.

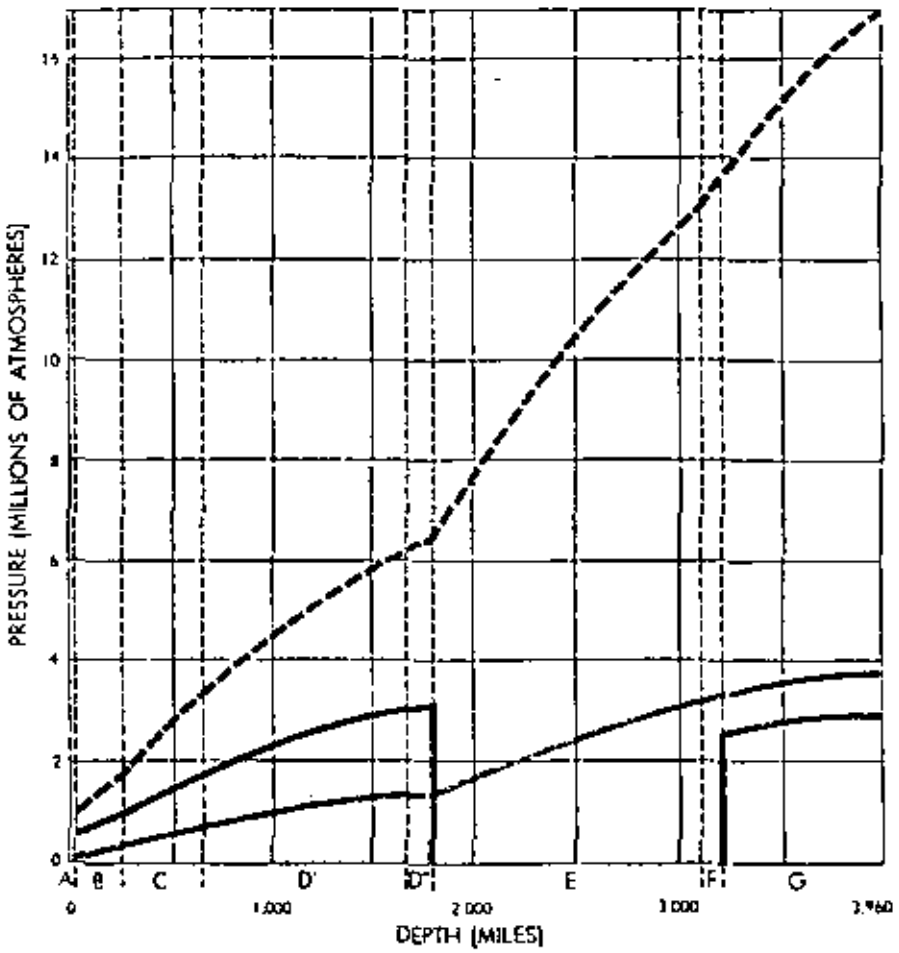

ELASTICITY of the earth's interior is shown graphically above. The gray line measures pressure. Incompressibility is indicated by dotted black line; rigidity, by solid black line.

What is the deep interior of the earth made of? For many years there have been good grounds for believing that much of the mantle below the crust consists of ultrabasic rock such as magnesium-iron silicate. The region B seems to be composed of a material like the known mineral olivine, C appears to be a transition region where the composition changes, perhaps only from one geometric form of olivine to another. The region D′ may contain several distinct phases, such as silica, magnesia and iron oxide. The bottom of the mantle, D″, is probably of variable composition, but there is as yet no widely accepted agreement on what materials would have gravitated to this depth.

The composition of the central core has lately become the subject of extremely interesting new conjectures. It had long been assumed that the core consists largely of iron or nickel-iron, and this view was supported by analysis of meteorites, believed to be pieces of an exploded planet resembling the earth. But in 1941 W. Kuhn and A. Rittmann of Germany put forward the radical idea that compressed hydrogen made up the core. This theory, while contradicted by weighty arguments, gave rise to new investigations based on the idea that under increasingly high pressures the material at the base of the earth's mantle might suddenly jump in density. Thus the outer core may consist not of uncombined iron or nickel but of a high-density modification of the rocky material in the mantle just above it. This theory is highly controversial. On balance of probability the present evidence appears to favor a compromise: namely, that the outer core contains both uncombined iron and some material of appreciably smaller atomic number.

An interesting aspect of the new theory is that it makes plausible the idea that the planets Mars, Venus, Mercury and Earth are all of the same primitive over-all composition. Jeffreys has shown that the earth cannot have the same elemental composition as the other planets if its core is completely different from the mantle in composition. According to calculations by W. H. Ramsey of England and the writer, the observed masses and diameters of Mars and Venus, and the oblateness of Mars, would be accounted for fairly well by the theory that they are composed of terrestrial materials modified by pressure at depth.

As regards the earth's inner core, it probably consists of nickel and iron with perhaps some denser materials as well.

Estimates of the temperatures in the interior of the earth are much less certain than estimates of pressure. In deep mines the temperature rises at the rate of about 30 degrees Centigrade per mile as one descends. If it rose at this rate all the way down to the core the temperature in the center of the earth would exceed 100,000 degrees. Actually it is practically certain that the rate of increase is very much less in the depths of the earth. Present estimates are that the temperature at the center is no more than 2,000 to 6,500 degrees. In any case, it is fairly clear that the increase of temperature in the earth's interior is dwarfed by the increase in pressure.

5

THE PLASTIC LAYER OF THE EARTH'S MANTLE

DON L. ANDERSON

July 1962

Earth scientists have often pointed out that physical conditions inside our own planet are less well understood than those in stars light-years away. Even more paradoxical is the fact that the region within a few hundred miles of the surface presents more problems and gives rise to more technical controversy than the region below. One long-standing item of debate is the zone called the low-velocity layer.

In 1926 the seismologist Beno Gutenberg suggested that earthquake waves slow down when they travel through a zone roughly 100 to 200 kilometers (60 to 120 miles) below the surface. He attributed the effect to a decrease in the rigidity of the material in the zone compared with that above and below it. Most authorities considered his evidence to be dubious at best, and for 30 years they largely ignored his proposal. Recently a mass of data has accumulated that strongly supports the concept of a low-velocity, low-rigidity layer. Its existence has important implications for all theories concerned with structural changes in and near the earth's surface.

The idea that the earth becomes plastic—if not, indeed, liquid—at moderate depths goes back to the earliest days of geology. Volcanic lava flows pointed to a molten interior not too far below the surface. Observations on the rate of increase of temperature in deep mines indicated that if the temperature continues to increase at the same rate, rocks should be molten at depths of less than 100 kilometers. The enormous cracks and folds found in the earth's crust suggested upheavals in a mobile substratum. All this agreed with prevailing views of the origin of the solar system, which held that the earth and other planets had been torn loose from the sun and had had time to solidify only at the surface.

One of the most compelling arguments for some degree of fluidity in the interior came from the principle of isostatic equilibrium. As long ago as 1854 gravity measurements led geologists to suspect that the earth's crust floats on a denser material. Like other floating bodies, the crust seeks an equilibrium, riding deeper where it is heavier and rising higher where it is lighter. Subsequent studies, of both the strength of gravity and the propagation of earthquake waves, confirmed the notion, indicating that mountains have deep roots that support them just as the submerged portion of an iceberg supports the part above water, whereas plains resemble ice floes, having smooth upper and lower surfaces. Moreover, when the load on a part of the crust changes suddenly (on the geological time scale), the surface can be observed to respond by rising or sinking to restore equilibrium. For example, land covered by ice during the last glaciation is still rising at the rate of about a meter per century. Obviously this behavior implies that the material under the crust can flow, if only slowly.

On the other hand, several facts appeared to rule out the idea of widespread fluid material anywhere near the surface. From the tidal distortions of the solid earth in response to the pulls of the sun and moon, Lord Kelvin calculated that the earth is more rigid than steel. Studies of earthquake waves indicated that at depths down to thousands of kilometers the earth transmits not only compression waves (*P* waves) but also transverse, or shear, waves (*S* waves). Shear waves, which oscillate at right angles to their direction of motion, cannot propagate through liquids because liquids have no shear strength. When liquids are subjected to shearing forces, they simply flow. Finally, seismologists discovered that earthquakes originate as deep as 700 kilometers below the surface. Since an earthquake represents the abrupt yielding of rock to accumulated stress, it characterizes brittle, not plastic, material.

The answer to this apparent contradiction is suggested by the properties of noncrystalline materials such as glass and pitch, which behave like solids in

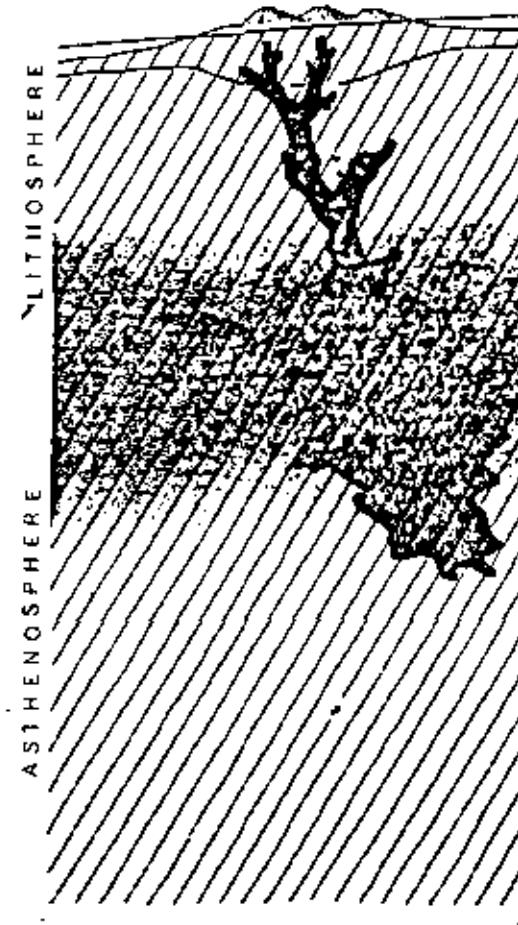

PLASTIC ZONE of earth's mantle (color) occupies an ill-defined region some 60 to perhaps 250 kilometers below the surface. In the plastic or low-velocity zone the tem-

the short run and like fluids over longer periods. They transmit shear waves and can support loads for a short time, but under a steady, long-lasting force they are plastic; that is, they flow and change their shape permanently. Under conditions of high temperature and high pressure the rock under the crust could also behave plastically. It would respond like a rigid solid to the relatively short-lived stresses that build up to cause earthquakes and the even briefer stresses involved in earthquake waves, while flowing slowly to adjust to the long-term stresses caused by changes in the weight of overlying material. Some geologists believe that the plastic substance under the crust is a glassy basalt. Recent evidence suggests, however, that it is crystalline. At high temperature even a crystalline material can flow easily, because melting at the boundaries of individual crystal grains allows them to slide over one another.

In 1909 the Yugoslav seismologist Andrija Mohorovičić proposed that at some distance below the surface there is a discontinuity where the velocity of earthquake waves jumps from about seven kilometers per second to eight. Subsequent measurements placed the Mohorovičić discontinuity, or Moho, at an average depth of 35 kilometers below the surface of the continents and only about five kilometers below the ocean floor. Under high mountains the Moho is as deep as 65 kilometers. Geologists saw in the Moho the lower boundary of the rigid, floating crust. The material between the Moho and the presumably liquid core of the earth they named the mantle. Yet the fact that seismic waves travel faster below the Moho than they do above it implies a greater rigidity at the top of the mantle than in the crust. It now seems clear that the Moho marks a change in chemical composition or crystal structure rather than an abrupt transition from strong to weak material.

The first seismic evidence for this transition was not forthcoming until Gutenberg announced the low-velocity zone. Actually what he had found was a decrease in the amplitude of compressional waves reaching the surface at a distance between 100 and 1,000 kilometers from an earthquake. At 1,000 kilometers the amplitudes were only a hundredth as great as they were at 100 kilometers. Beyond 1,000 kilometers the amplitudes increased sharply.

Gutenberg explained the effect by assuming a subsurface layer in which the earthquake waves travel slower than they do in the regions above or below. A wave entering this layer obliquely from above would be refracted downward, away from the surface, as light is bent downward when it passes from air to water. On leaving the bottom of the layer the wave would be refracted upward again [*see illustration on page 31*]. The result is that the wave would arrive at the surface farther away from its source than it would if there had been no decrease in velocity. Hence a gap would appear between the last "ray" that had missed the low-velocity layer and the first one to enter it. As the illustration shows, the gap, or shadow zone, is great-

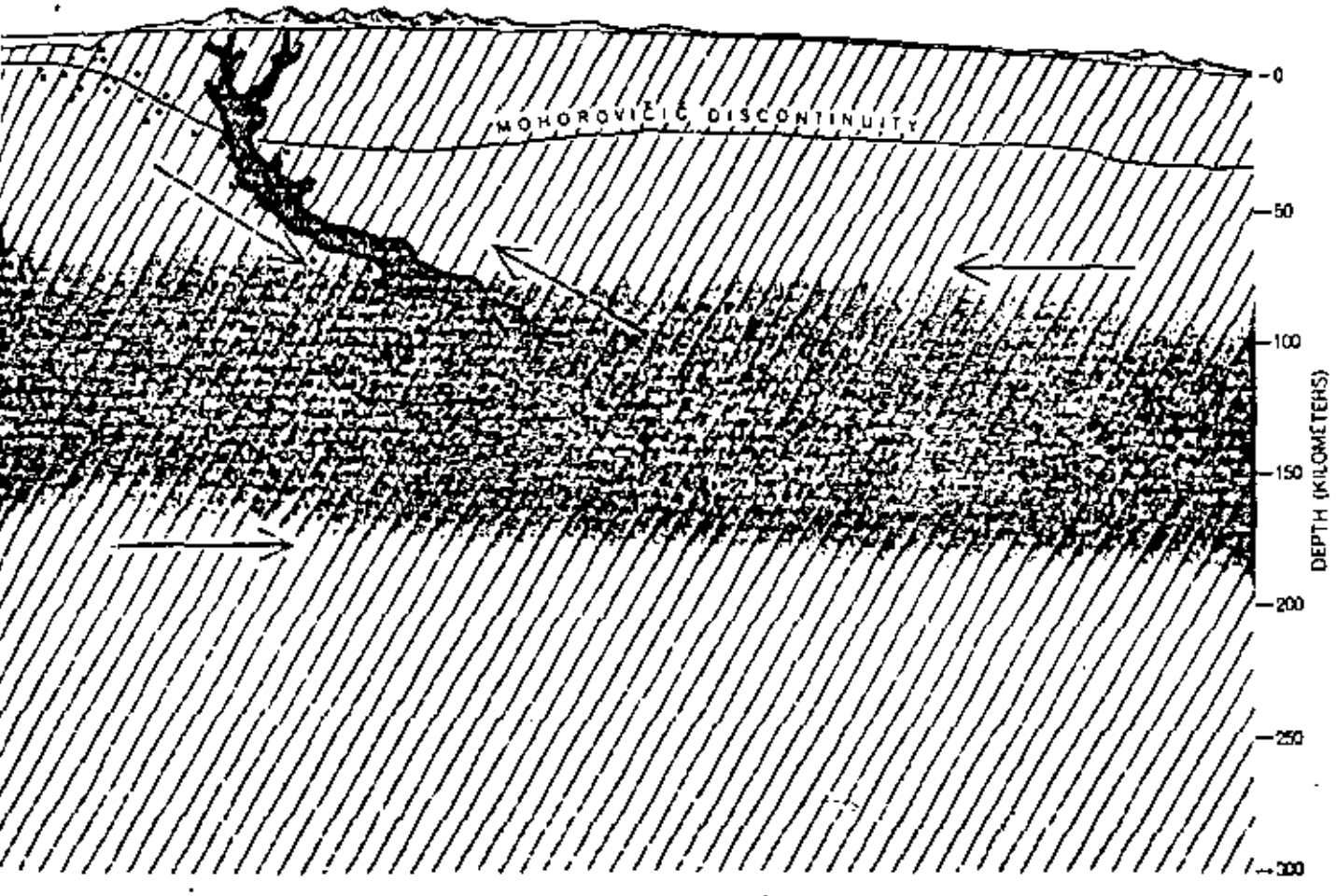

perature approaches the melting point of the rock. The lithosphere is very elastic or brittle rock; the asthenosphere, extending down to earth's core, can flow and relieve stress. In this highly schematic cross section of upper portion of earth, ocean and islands are at left. Dots denote earthquake foci. Broken arrows indicate possible movement of continents over ocean basin. Solid arrows mark hypothetical slippage of whole lithosphere over asthenosphere. The two solid-color regions represent magma, or molten rock.

rest for an earthquake originating just above the top of the layer. Those coming from deeper levels evince no gap. From the extent of the shadow zone for different earthquakes, Gutenberg calculated that the layer is centered at a depth of about 150 kilometers, and that between 100 and 200 kilometers the velocity is some 6 per cent less than it is just under the Moho. Such a decrease in velocity means that the rock within the layer must be substantially less rigid than the material above and below it. The velocity does not reach the value it had at the base of the crust until some 250 or 300 kilometers below the surface.

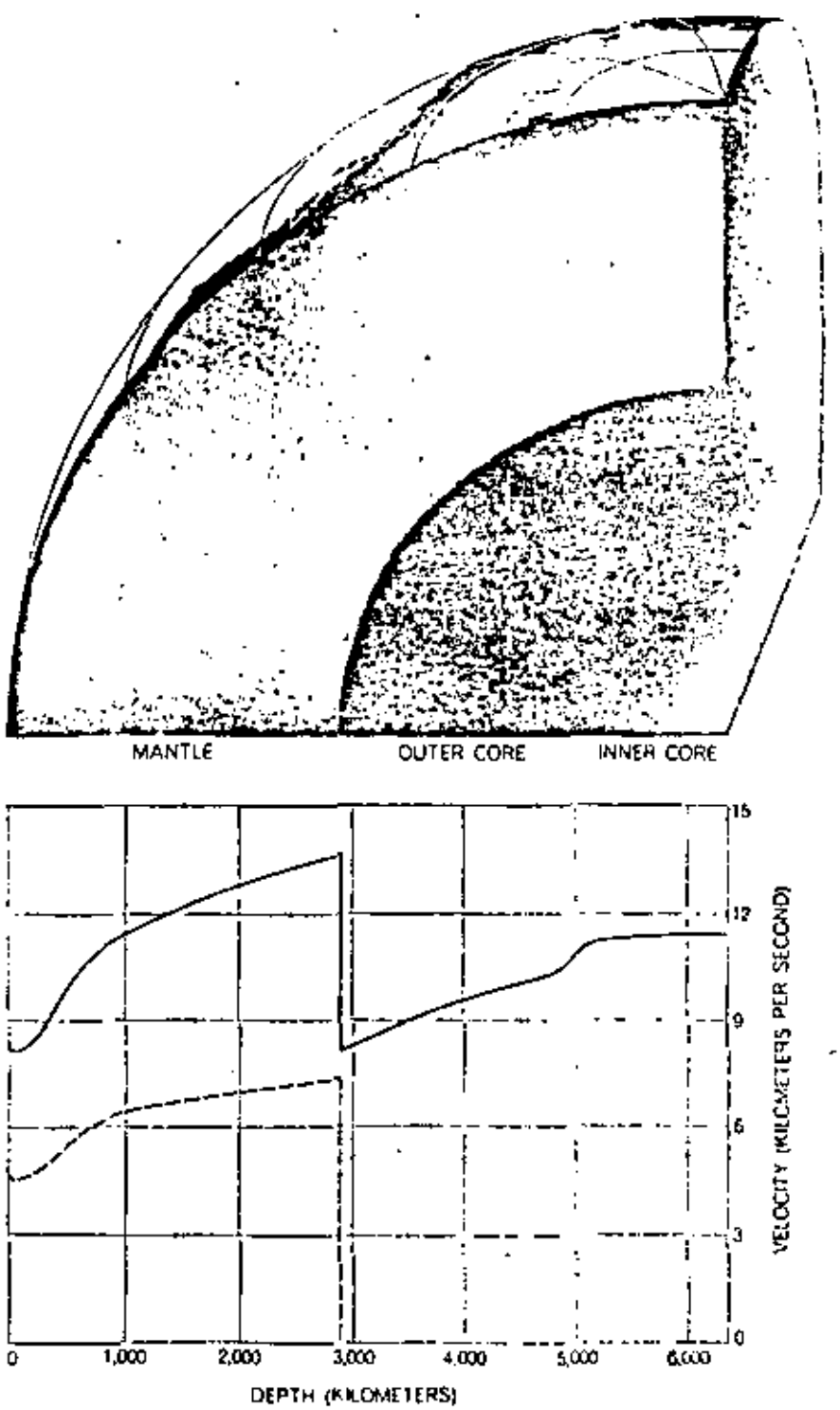

INTERNAL STRUCTURE OF THE EARTH is deduced from travel times of seismic waves. Solid line represents compressional, or P, waves; broken line represents shear, or S, waves. The latter disappear entirely at the outer core, indicating that this region is liquid. Low-velocity zone causes dip in curves at far left. Hatching on block diagram near surface marks low-velocity zone. It also marks transition zone above inner core at depth of 5,000 kilometers.

If the low-velocity layer were perfectly uniform, and if the waves really traveled as rays, the shadow zone at the surface would be completely "black." No waves at all would emerge within its limits. Actually the layer is full of inhomogeneities, and seismic waves do not travel strictly along classical ray paths. Like all waves, they bend around corners by diffraction, thereby leaking into shadowed regions. Both effects contribute to the energy that is found in the shadow zone.

It was partly this energy leak that made other workers reluctant to accept Gutenberg's conclusion. In those days seismologists paid little attention to the comparative amplitudes of earthquake waves. They were primarily interested in travel times, and they tended to accept any signal, weak or strong, if it appeared in their records at a time when readings at other seismographic stations led them to expect it.

Moreover, the evidence for the low-velocity layer was by no means clear-cut. The statistics were assembled from many earthquakes, large and small, shallow and deep. The data came from seismographs of different designs. In his calculations Gutenberg could make only approximate corrections for these variations as well as for the local irregularities, mostly unmapped, in the rock through which different waves traveled.

Underground nuclear explosions finally made possible a controlled experimental test of Gutenberg's analysis. The time, strength and location of these events is known so precisely that a single blast provides excellent data. Furthermore, seismographs today are more numerous, more sensitive and more standardized than they were in 1926. Studies of several explosions have confirmed the conclusions Gutenberg extracted so tediously from earthquake records [*see illustration on page 33*]. Seen in sharper detail, the low-velocity layer extends from about 60 kilometers to about 250 kilometers. (It is interesting to note that the layer damps blast waves so effectively that many seismologists think it poses a major difficulty for the detection of underground nuclear tests.)

Several independent pieces of evidence now support the idea of a low-velocity plastic layer. One is furnished by surface waves. These are seismic disturbances that follow the curved surface of the earth [*see bottom illustration on page 32*] instead of passing through its body. Although the waves travel along the surface, they "feel" the elastic properties of the underlying material to a

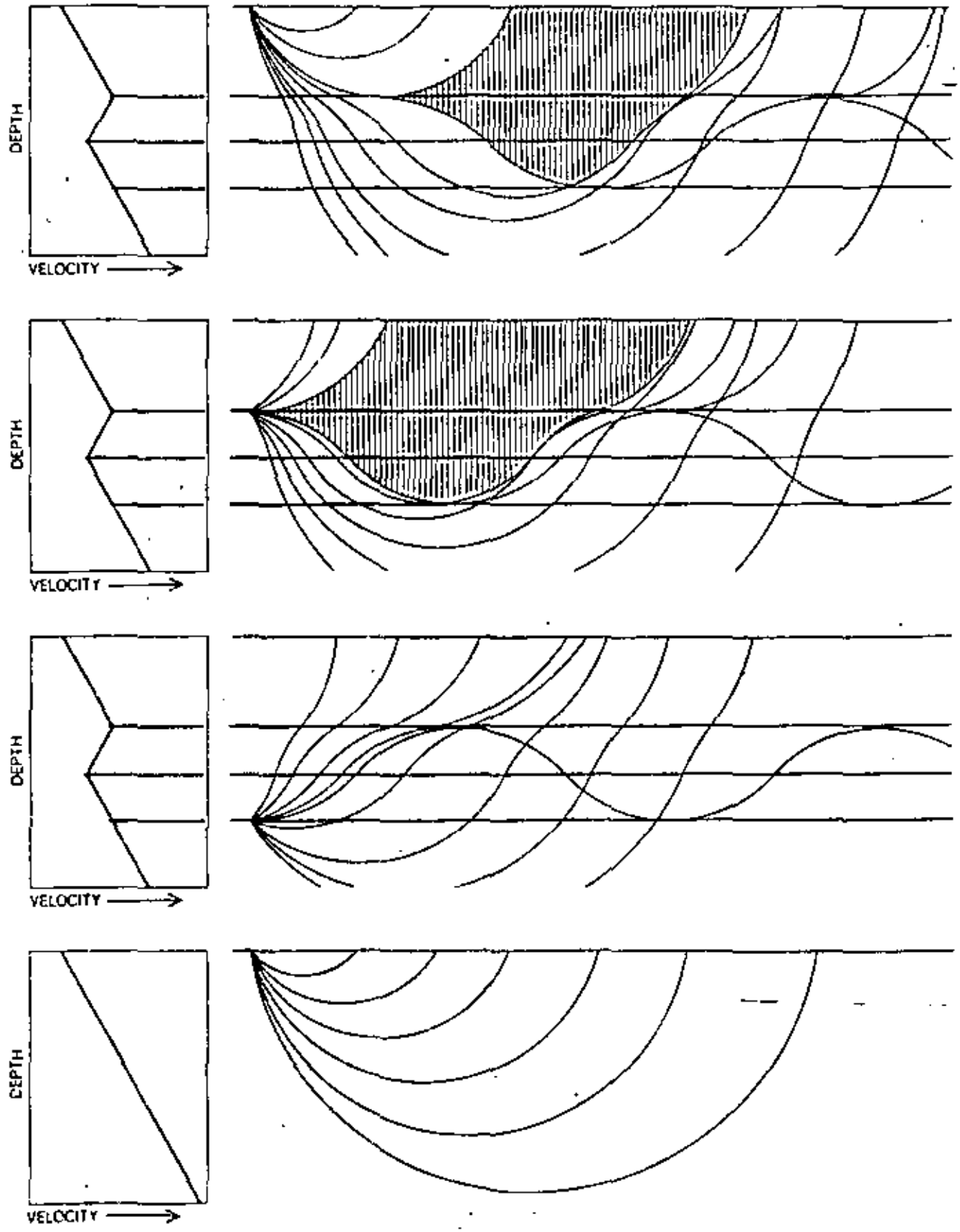

PATHS OF EARTHQUAKE WAVES bend in various ways in response to the low-velocity zone, depending on whether the earthquake occurs at the surface of the earth (*top*), at the top of the low-velocity zone (*second from top*) or below the zone (*third from top*). In the first two cases, refraction of waves by the zone creates a "shadow zone" (*hatching*), where direct waves from the earthquake do not appear. The bottom diagram shows how waves from an earthquake at the surface would travel if there were no low-velocity zone to bend them down. The graphs at left show changes in the velocity of earthquake waves with increasing depth.

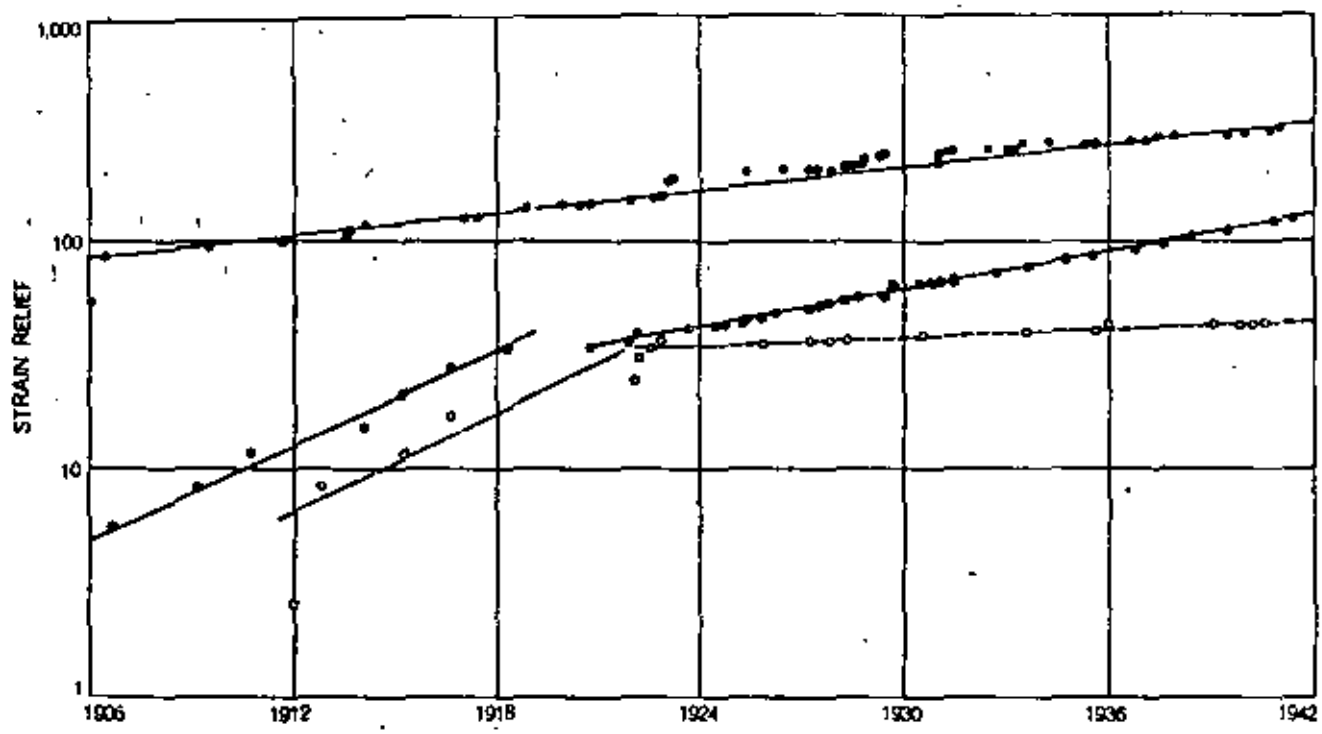

SEQUENCE OF EARTHQUAKES between 1906 and 1943 along west coast of South America falls into three groups: those occurring down to a depth of 70 kilometers (*colored dots, colored line*), those from 70 to 250 or 300 kilometers (*black dots, black line*) and those from 300 to 600 kilometers (*open dots, broken line*). The vertical scale shows relative amount of strain relieved by the quakes. Break in two lower groups around 1921 shows that they are mechanically coupled and are quite separate from the upper group.

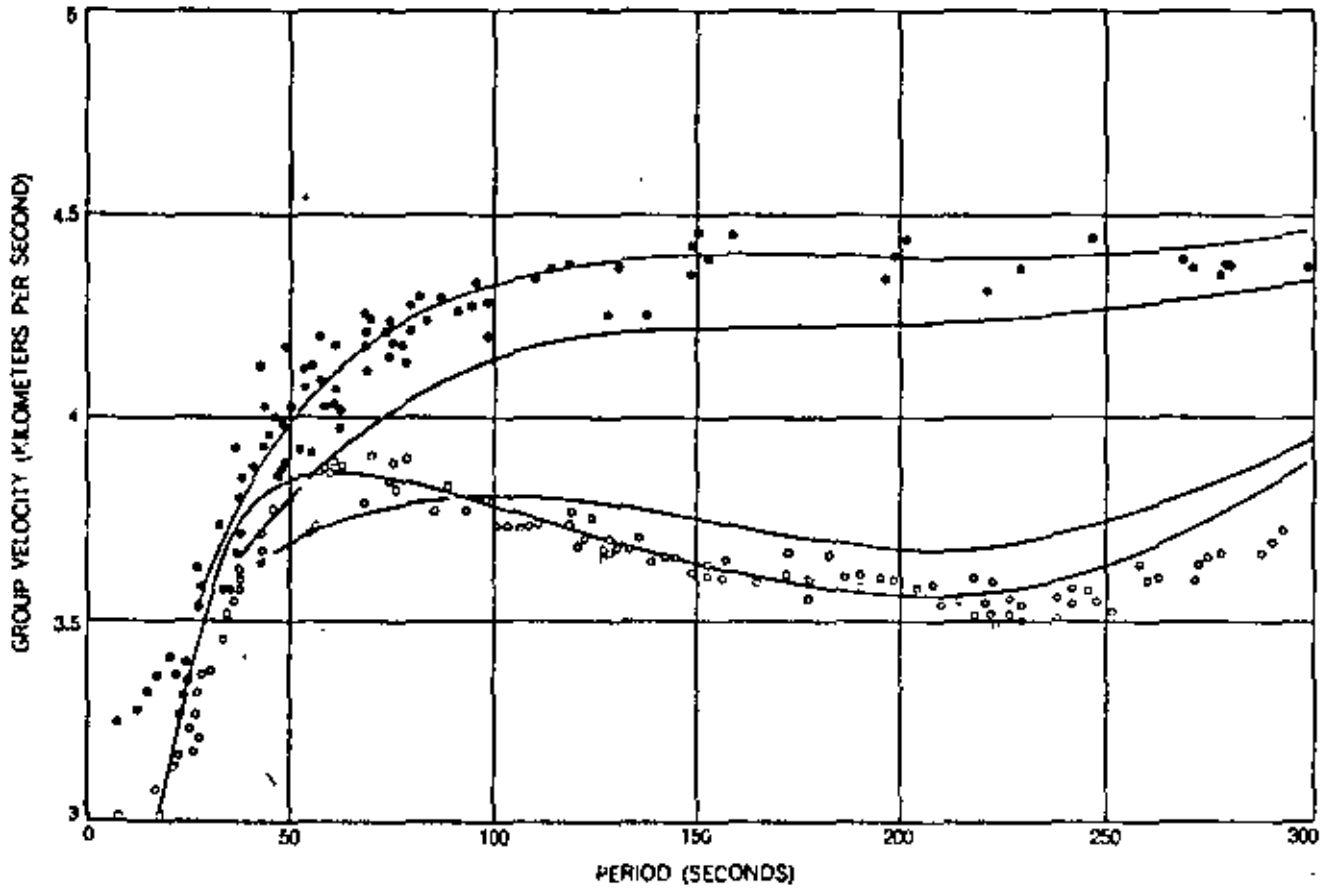

SURFACE-WAVE DATA reflect existence of low-velocity zone. The two types of dot represent actual observations of velocity of two kinds of surface waves plotted against wave period or length. Theoretical curves for an earth with a low-velocity zone (*colored lines*) fit observational data far more closely than do theoretical curves for an earth without a low-velocity zone (*black lines*).

depth that depends on their wavelength; the longer the wave, the deeper it feels [see "Long Earthquake Waves," by Jack Oliver; SCIENTIFIC AMERICAN Offprint 827]. Since in general elasticity increases with depth, longer waves travel faster than shorter ones, and waves that start out together are dispersed, or spread out. Detailed analyses of the dispersion patterns show that elasticity does not increase continuously with depth but falls off in the region of the low-velocity layer.

Body waves, which pass through the deep interior, provide only a point-by-point sampling of the outer regions of the earth. Surface waves, on the other hand, contain information about these regions over their entire path. Recent studies of surface waves in our laboratory at the California Institute of Technology and at Columbia University have demonstrated for the first time that the low-velocity layer is present below the oceans as well as below the continents. Some of the waves used in the analysis had traveled around the earth as many as seven times. They indicate that the layer is in fact a world-wide phenomenon. Comparison of oceanic and continental paths shows that the waves are slowed more under the oceans. Evidently the geological differences between ocean basins and land masses are not limited to the crust but extend several hundred kilometers into the mantle.

Conclusive proof of the world-wide extent of the low-velocity layer came from the great Chilean earthquake of May 22, 1960. It was so violent that it set the earth as a whole into vibration, making it "ring" like a bell. The tone of a bell—that is, the frequencies at which it vibrates—depends on its elastic properties; a steel and a bronze bell emit different sounds. From records of the free vibrations following a big earthquake it is possible, with enormous mathematical labor, to deduce the elastic structure of the earth. The labor has been performed. It shows that the low-velocity zone is necessary to account for the observed frequencies.

In an attempt to construct a model of the earth that fits the current seismic data, I have been obliged to conclude that the low-velocity zone transmits the horizontal and vertical vibrations in shear waves at different speeds. A crystalline material in which the crystal grains were aligned in one direction would behave this way. One mechanism that could bring about such an alignment is a flow of the material. Others are directional heat flow and differential stress.

In addition to the purely seismic data, several other phenomena attest to a lowered rigidity in the material near the top of the mantle. Variations in atmospheric pressure cause measurable deflections of the earth's surface. The amount of deflection is much greater than it would be if the crust and mantle had the same strength. By assuming a weak layer in the upper mantle the observations can be explained quite well. Moreover, most earthquakes originate in the first 60 kilometers below the surface, at an average depth of 25 kilometers. At a depth of more than 60 kilometers the number falls abruptly, indicating a sudden drop in the strength of the rock.

From 60 kilometers down the frequency of earthquakes decreases steadily, dying away to zero at about 700 kilometers. This distribution implies that the rock becomes less brittle all the way from 60 to 700 kilometers and that it does not regain its strength at any deeper

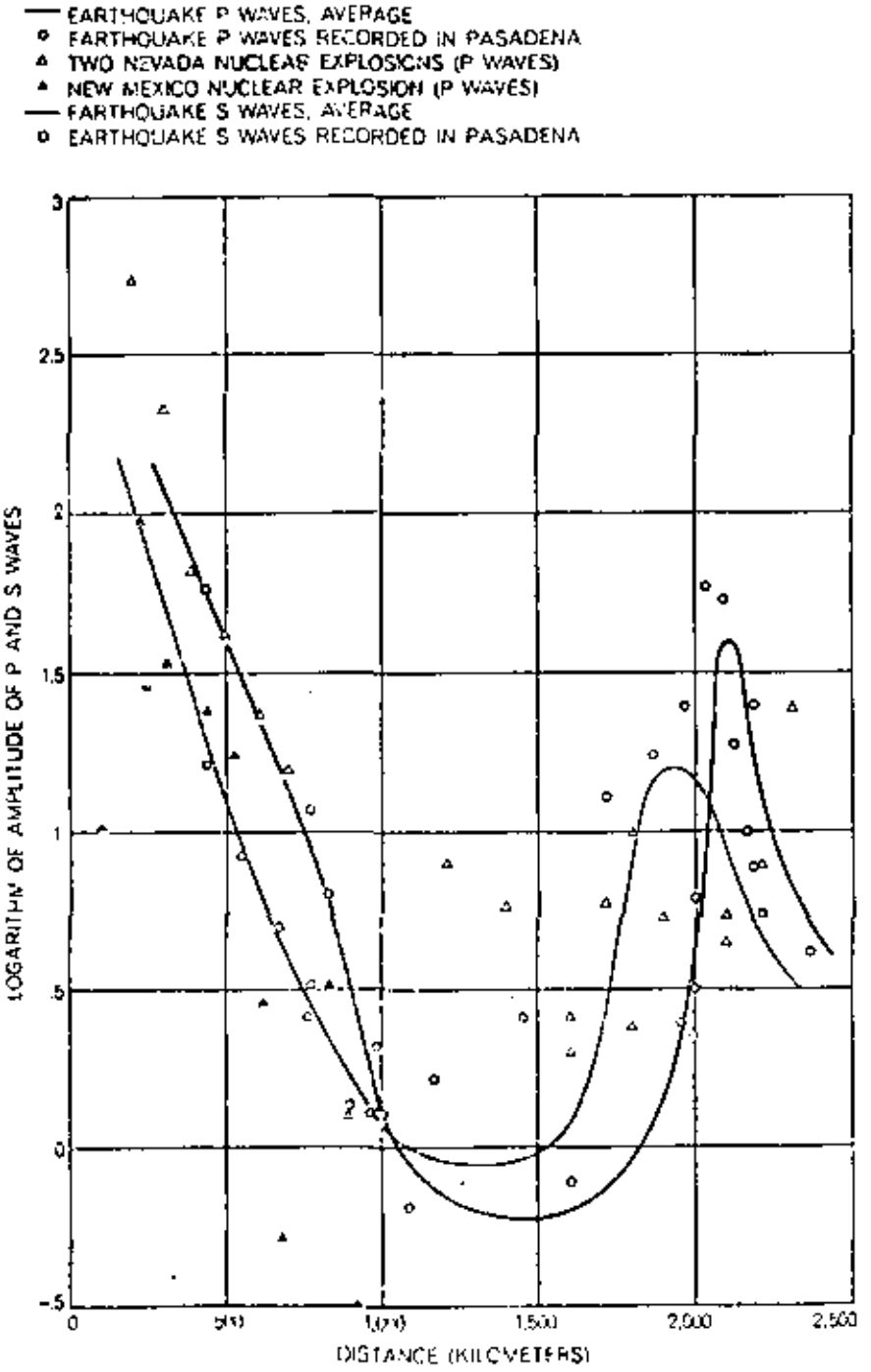

SHARP DROP IN AMPLITUDE of earthquake and nuclear-explosion waves between about 100 kilometers and 1,000 kilometers from the event is caused by low-velocity zone. The two curves of averages for earthquake P and S waves were drawn by Beno Gutenberg on basis of data from many earthquakes and observatories and represent world-wide averages.

level. The picture agrees with a nomenclature first proposed in 1914 by the U.S. geologist Joseph Barrell. He spoke of an upper, rigid "lithosphere" (from the Greek word *lithos*, meaning stone) and a lower, more plastic "asthenosphere" (from the Greek word *asthenes*, meaning weak). Barrell placed the boundary between the two at a depth of 100 kilometers. Now it appears to be not a sharp boundary but a transition zone starting at some 60 kilometers.

The concept of strength and weakness in the foregoing discussion applies to the time in which stresses build up to cause earthquakes. Viewed on this temporal scale the mantle undergoes a transition from a brittle to a plastic state at about 60 kilometers and thereafter increases in plasticity. On the much shorter time scale of earthquake-wave vibrations, however, the material reverts to a stronger, or more elastic, condition at a depth of more than 250 kilometers. The decrease in velocity at the top of the mantle is gradual; it is not yet clear whether the base of the low-velocity zone is characterized by a gradual or an abrupt increase in velocity.

Almost certainly the short-term properties that set apart the low-velocity layer are determined by the temperature and pressure of the mantle in relation to its melting point at different depths. In general the elasticity of any material decreases as its temperature approaches the melting point. But an increase in pressure raises the melting point and elasticity. Below the surface of the earth both temperature and pressure increase with depth, and so the two have opposing effects on the proximity to the melting point as well as on the elastic strength of rock. Presumably at a depth of about 60 kilometers temperature takes the upper hand and the rock begins to approach its melting point, growing weaker as the depth increases. This trend continues down to some 200 kilometers, where it reverses. Then pressure raises the melting point faster than the temperature increases and the material becomes more elastic (until the liquid outer core is reached). A few laboratory experiments on rock under high temperature and pressure seem to confirm this picture. Extrapolating the rather scanty data indicates a very low strength at a depth of somewhat more than 100 kilometers.

Hugo Benioff of the California Institute of Technology has discovered a remarkable indication of discontinuity at the level of the top of the low-velocity zone. In studying a large number of earthquakes in the Pacific Ocean earthquake belt he was able to connect certain sequences of earthquakes to single fault structures. One sequence that occurred in South America between 1908 and 1942 delineates a great fault off the west coast of the continent. The fault is some 4,500 kilometers long and goes down 600 kilometers—a tenth of the distance to the center of the earth. The earthquakes related to the fault fall naturally into three groups: (1) those shallower than 70 kilometers, (2) those from 70 to 250 or 300 kilometers and (3) those from 300 to 600 kilometers [*see top illustration on page 32*]. Analysis of the earth motions in the quakes showed a marked similarity between the intermediate and deep groups but no resemblance of these to the shallower group. In particular the motions of the two deeper groups changed suddenly, and in the

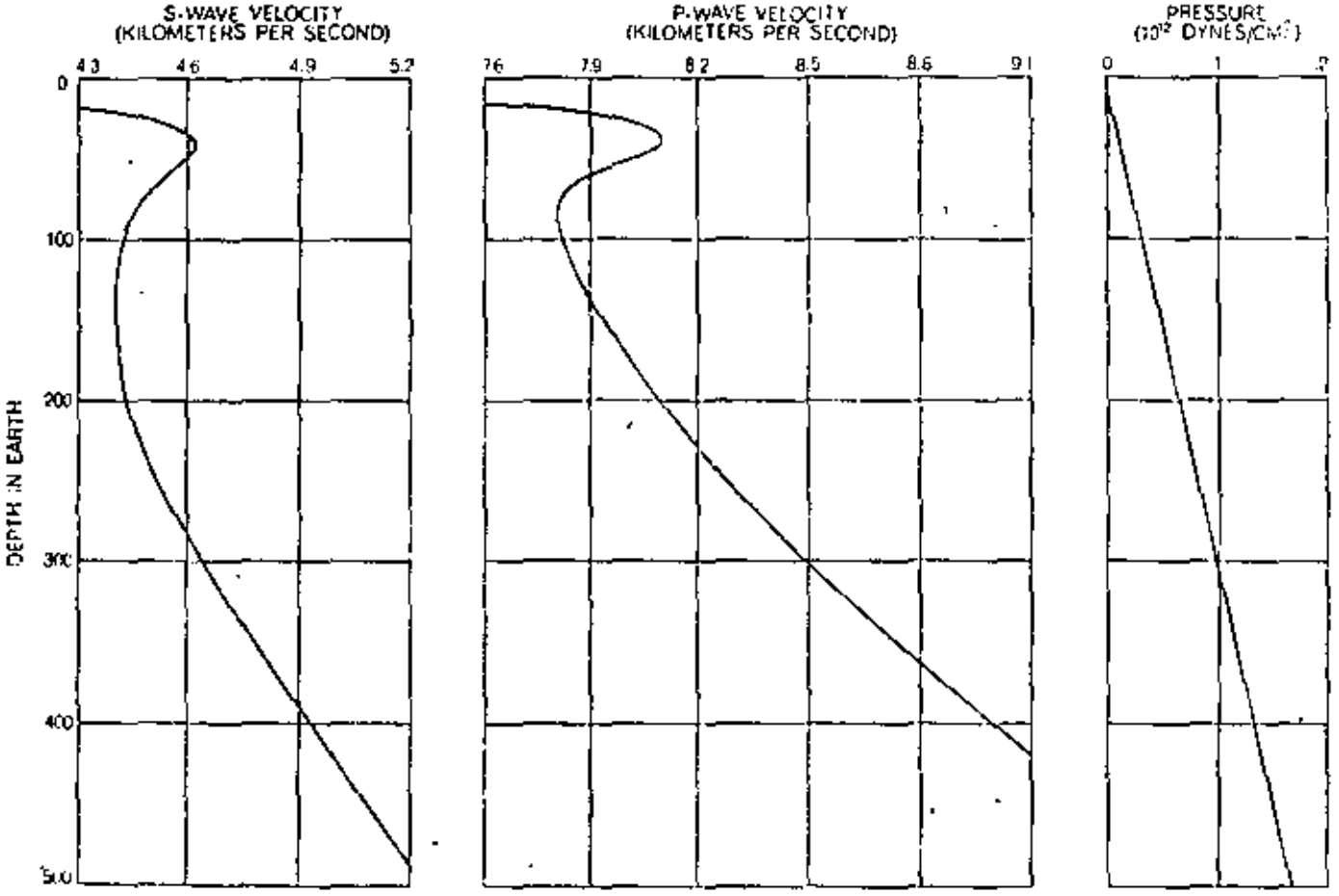

DATA FOR UPPER MANTLE reflect existence of plastic or low-velocity zone. The seismic-wave velocities and the number of earthquakes are the only curves made from direct measurements in the earth. Pressure is derived directly from depth. Temperature curve

same way, in 1921. There was no corresponding change in the shallower earthquakes. Evidently there is some mechanical coupling between the lower layers, but these are sharply decoupled from the region above 70 kilometers. Other areas of the circum-Pacific tectonic belt show similar phenomena.

When the earthquake foci are plotted in three dimensions, those down to 250 kilometers fall in a plane about 900 kilometers wide, dipping about 33 degrees under the continents with respect to the surface of the earth. The deep earthquakes, on the other hand, are on a plane tilted at 60 degrees. Thus, although they are mechanically connected, the intermediate and deep layers are spatially discontinuous. The dimensions and location of the intermediate layer correspond closely to those of the low-velocity zone.

An interesting clue to the state of the material in the upper mantle was furnished by the Soviet volcanologist G. S. Gorshkov in 1957. He found that shear waves from Japanese earthquakes do not reach the Kamchatka Peninsula when their paths cross the volcanic belt between Japan and the peninsula. Gorshkov concluded that there must be pockets of liquid magma at a depth of 55 kilometers that absorb the waves. Apparently in certain regions the temperature not only approaches the melting point but even exceeds it. Many seismologists have remarked on the fact that the average wavelength of shear waves is many times longer than that of compressional waves. The observation could be accounted for by a weak, perhaps partially molten, layer that absorbs the shorter S waves more than the longer S waves.

Volcanoes are concentrated in parts of the world where earthquakes are most common, and the earthquakes actually associated with volcanism mostly originate at depths between 60 and 200 kilometers. This suggests that volcanoes are connected with disturbances in the region of the low-velocity zone. Therefore the distribution of volcanoes constitutes direct evidence for the temperature-melting point relation inferred from laboratory measurements and suggests that the low-velocity layer may be the source of primary basaltic magma.

Volcanism and the postglacial uplift of the crust constitute the only dynamic, as opposed to static, geological "experiments." Both indicate fluidity, and some degree of actual flow, in the material below the crust. Moreover, they are consistent with the idea of a layer of maximum plasticity in the upper mantle.

Almost all present theories of isostasy and tectonics, including those concerned with mountain building, faulting and the possible drifting of the continents, focus attention on the Mohorovičić discontinuity, which divides the crust of the earth from the mantle. If the picture I have tried to outline in this article is correct, the important discontinuity is farther down, at the ill-defined boundary of the rigid lithosphere and the weaker asthenosphere. Most of the activity responsible for the broad-scale features of the earth's surface probably takes place in a low-velocity or plastic layer at the top of the asthenosphere, extending roughly from 60 to 250 kilometers in depth. In particular the existence of such a plastic layer makes the idea of continental drift much more plausible than it has seemed heretofore.

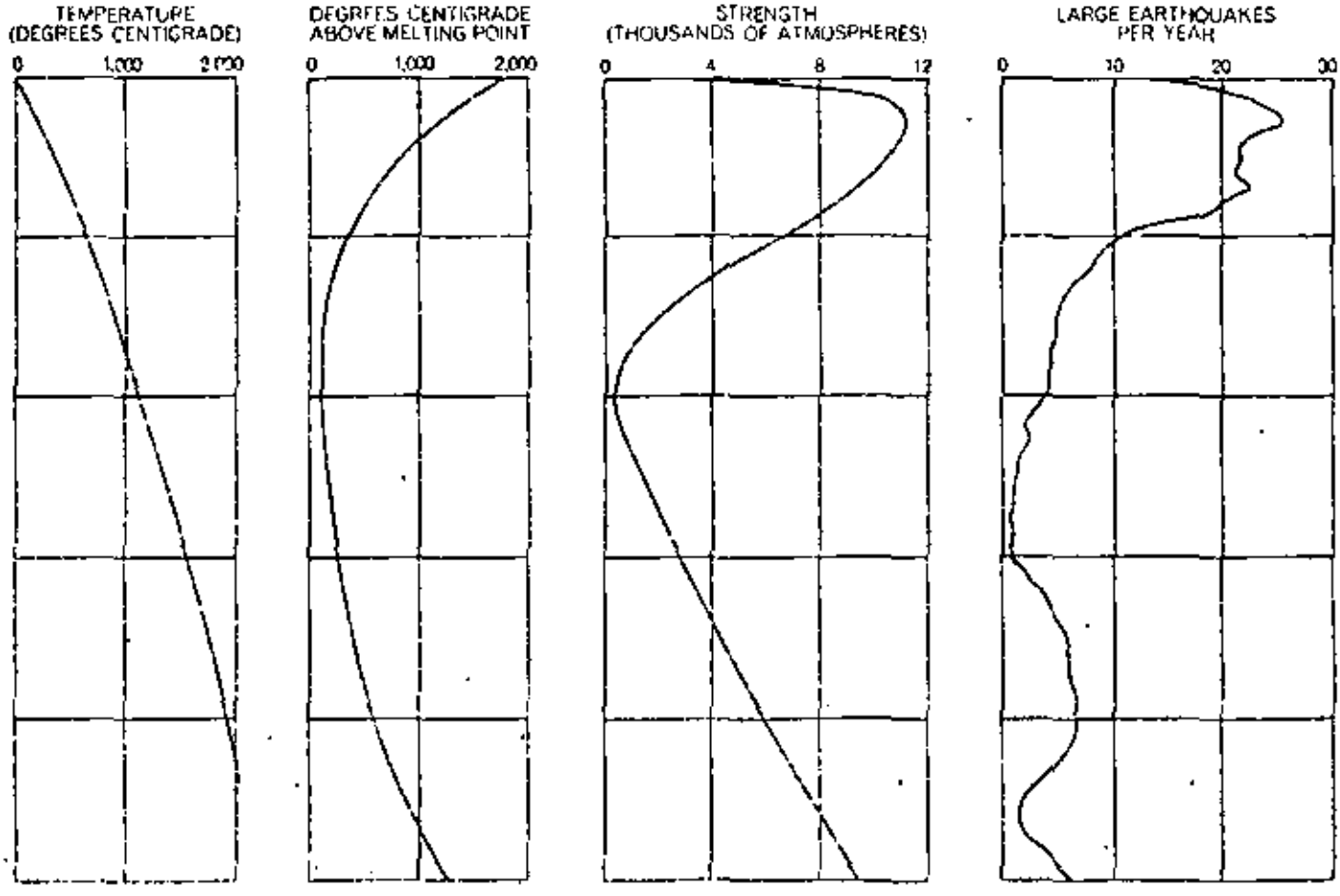

is based largely on theoretical considerations. Temperature above melting point is calculated from pressure and temperature curves. Strength, down to 50-kilometer depth, is derived indirectly from laboratory measurements; below that it is an extrapolation.

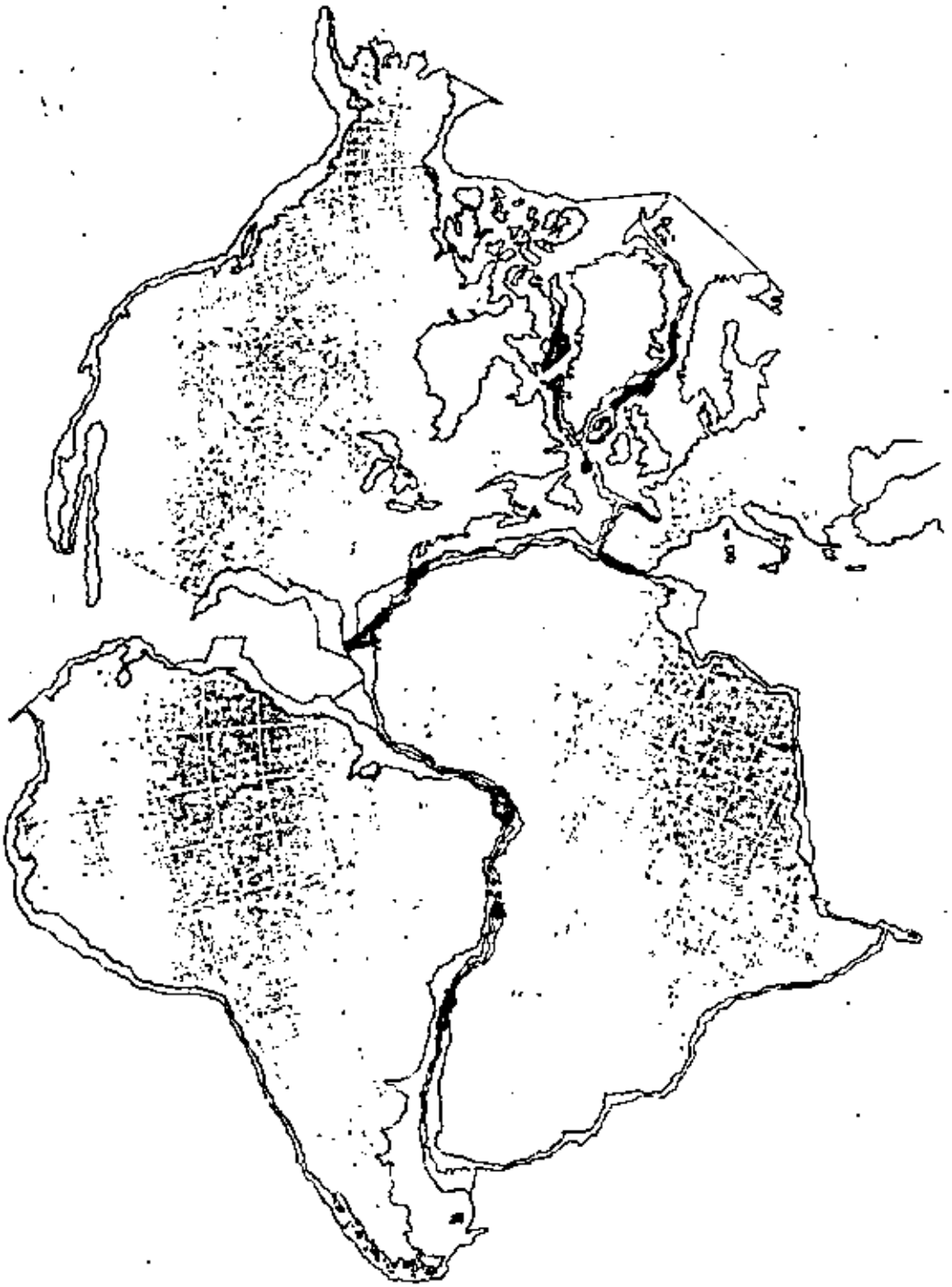

THE CONFIRMATION OF CONTINENTAL DRIFT

PATRICK M. HURLEY

April 1968

As recently as five years ago the hypothesis that the continents had drifted apart was regarded with considerable skepticism, particularly among American investigators. Since then, as a result of a variety of new findings, the hypothesis has gained so much support that its critics may now be said to be on the defensive. The slow acceptance of what is actually a very old idea provides a good example of the intensive scrutiny to which scientific theories are subjected, particularly in the earth sciences, where the evidence is often conflicting and where experimental demonstrations are usually not possible.

As long ago as 1620 Francis Bacon discussed the possibility that the Western Hemisphere had once been joined to Europe and Africa. In 1668 P. Placet wrote an imaginative memoir titled *La corruption du grand et du petit monde, où il est montré que devant le déluge, l'Amérique n'était point séparée des autres parties du monde* ("The corruption of the great and little world, where it is shown that before the deluge, America was not separated from the other parts of the world"). Some 200 years later Antonio Snider was struck by the similarities between American and European fossil plants of the Carboniferous period (about 300 million years ago) and proposed that all the continents were once part of a single land mass. His work of 1858 was called *La Création et Ses Mystères Dévoilés* ("The Creation and Its Mysteries Revealed").

By the end of the 19th century geology had come seriously into the discussion. At that time the Austrian geologist Eduard Suess had noted such a close correspondence of geological formations in the lands of the Southern Hemisphere that he fitted them into a single continent he called Gondwanaland. (The name comes from Gondwana, a key geological province in east central India.) In 1908 F. B. Taylor of the U.S. and in 1910 Alfred L. Wegener of Germany independently suggested mechanisms that could account for large lateral displacements of the earth's crust and thus show how continents might be driven apart. Wegener's work became the center of a debate that has lasted to the present day.

Wegener advanced a remarkable number of detailed correlations, drawn from geology and paleontology, indicating a common historical record on the two sides of the Atlantic Ocean. He proposed that all the continents were joined in a single vast land mass before the start of the Mesozoic era (about 200 million years ago). Wegener called this supercontinent Pangaea. Today the evidence favors the concept of two large land masses: Gondwanaland in the Southern Hemisphere and Laurasia in the Northern.

In the Southern Hemisphere an additional correlation was found in a succession of glaciations that took place in the Permian and Carboniferous periods. These glaciations left a distinctive record in the southern parts of South America, Africa, Australia, in peninsular India and Madagascar and, as has been discovered recently, in Antarctica. The evidence of glaciations is compelling: Beds of tillite—old, consolidated glacial rubble—have been studied in known glaciated regions and are unquestioned evidence of the action of deep ice cover. In addition many of the tillites rest on typically glaciated surfaces of hard crystalline rock, planed flat and grooved by the rock-filled ice moving over them.

This kind of evidence has been found throughout the Southern Hemisphere. In all regions the tillites are found not only in the same geological periods but also in a sequence of horizontal beds bearing fossils of identical plant species. This sequence, including the geological periods from the Devonian to the Triassic, is called the Gondwana succession. The best correlations are apparent in the Permocarboniferous beds, where two distinctive plant genera, *Glossopteris* and *Gangamopteris*, reached their peak of development. These plants were so abundant that they gave rise to the Carboniferous coal measures, which are commonly interbedded in the Gondwana succession [*see top illustration on next two pages*].

The South African geologist Alex L. du Toit and others have sought out and mapped these Gondwana sequences so diligently that today they provide the strongest evidence not only that these continental areas were joined in the past but also that they once wandered over or close to the South Pole. It is inconceivable that the complex speciation of the Gondwana plants could have evolved in the separate land masses we see today. It takes only a narrow strip of water, a few tens of miles wide at the most, to stop the spread of a diversified plant regime. The Gondwana land mass was apparently a single unit until the Mesozoic era, when it broke into separate parts. Thereafter evolution proceeded on divergent paths, leading to the biological diversity we observe today on the different continental units.

Wegener and Du Toit published their work in the 1920's and 1930's. The de-

FIT OF CONTINENTS (*opposite page*) was optimized and generated on a computer by Sir Edward Bullard, J. E. Everett and A. G. Smith of the University of Cambridge. Over most of the boundary the average mismatch is no more than a degree. The fit was made along the continental slope (*black*) at the 500-fathom contour line. The regions where land masses, including the shelf, overlap are black; gaps are white.

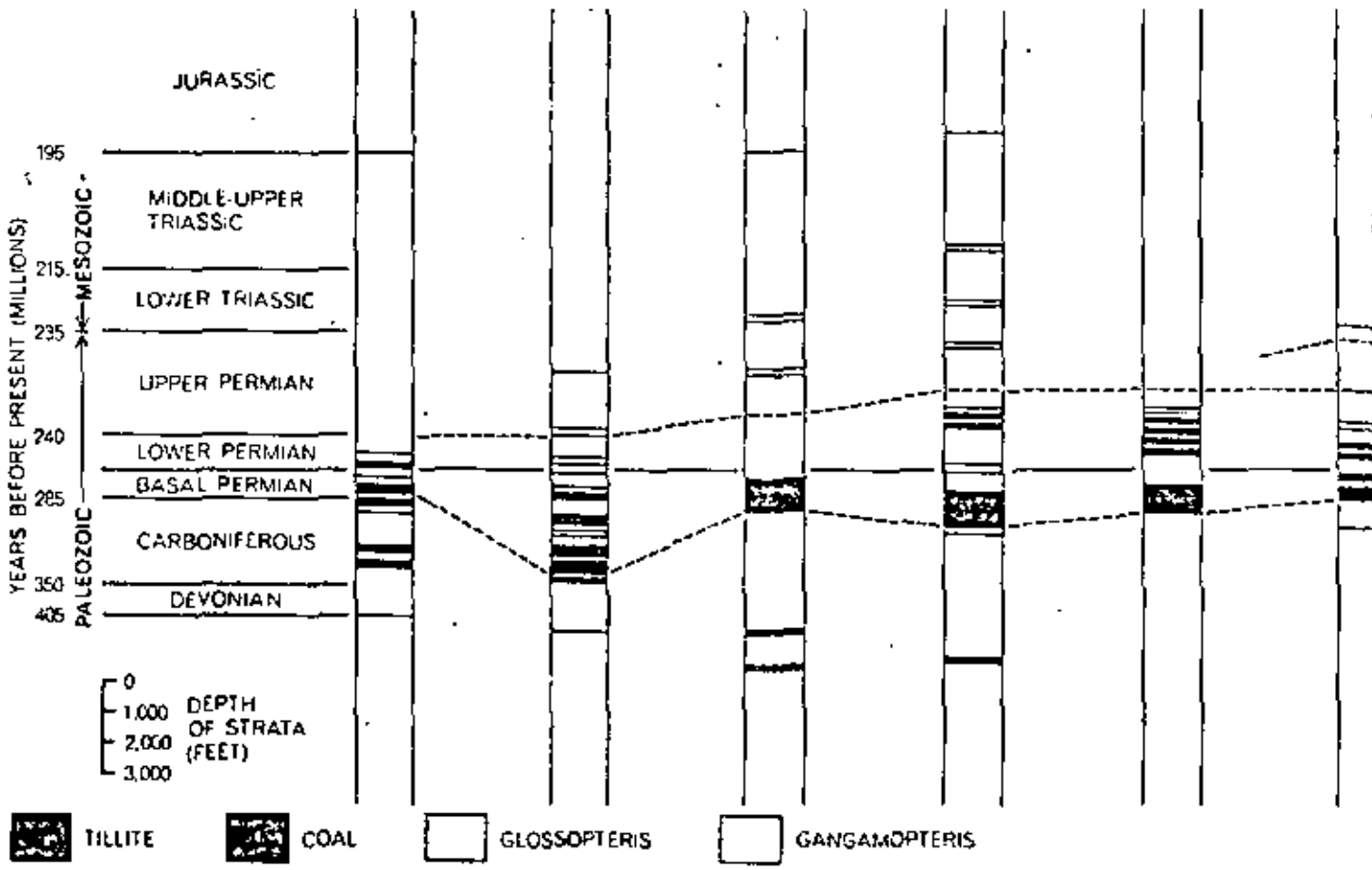

CONDWANA SUCCESSION is the name given to a late Paleozoic succession of land deposits found in South America, Africa, Antarctica, India and Australia. The succession contains beds of tillite (glacial rubble), coal deposits and a diversity of plants arranged in such a way that perhaps 200 million years ago the different areas must have been a single land mass known as Gondwanaland, or at

bate for and against drift became polarized largely between geologists of the Southern Hemisphere and the leaders of geophysical thought in the Western Hemisphere. Eminent geophysicists such as Sir Harold Jeffreys of the University of Cambridge voiced strong opposition to the hypothesis on the grounds that the earth's crust and its underlying mantle were too rigid to permit such large motions, considering the limited energy thought to be available.

Not all felt this way, however. In the late 1930's the Dutch geophysicist F. A. Vening Meinesz proposed that thermal convection in the earth's mantle could provide the mechanism. His ideas were supported by his gravity surveys over the deep-sea trenches and the adjacent island arcs of the western Pacific. The results implied that some force was maintaining the irregular shape of the earth's surface against its natural tendency to flatten out. Presumably the force was somehow related to thermal convection. Arthur Holmes of the University of Edinburgh added his weight to the argument in favor of the hypothesis, and he was followed by S. W. Carey of Tasmania, Sir Edward Bullard and S. K. Runcorn of Britain, L. C. King of South Africa, J. Tuzo Wilson of Canada and others [see the article "Continental Drift," by J. Tuzo Wilson, beginning on page 41]. The historical and dynamical characteristics of the earth now engaged the attention of many more geophysicists, and today the interplay of all branches of geology and geophysics generates the excitement of a new frontier area.

Continents and Oceans

Although the general nature of the earth's crust is familiar to most readers of *Scientific American*, it is worth reviewing and summarizing some of its major features while asking: How do these features look in the context of continental drift? The earth's topography has two principal levels: the level of the continental surface and the level of the oceanic plains. The elevations in between represent only a small fraction of the earth's total surface area. What maintains these levels? Left alone for billions of years, they should reach equilibrium at an average elevation below the present sea level, so that the earth would be covered with water. Instead we see sharp continental edges, new mountain belts, deep trenches in the oceans—in short, a topography that appears to have been regularly rejuvenated.

The continental areas are a mosaic of blocks that are roughly 1,000 kilometers across and have ages ranging from about 3,000 million years to a few tens of millions. In Africa there appear to be several ancient nuclear areas, or cratons, surrounded by belts of younger rocks. Most of the younger belts have an age of 600 million years or less, contrasting sharply with an age of 2,000 million to 3,000 million years for the cratons.

A closer look at the younger belts tells us that although much of the material is

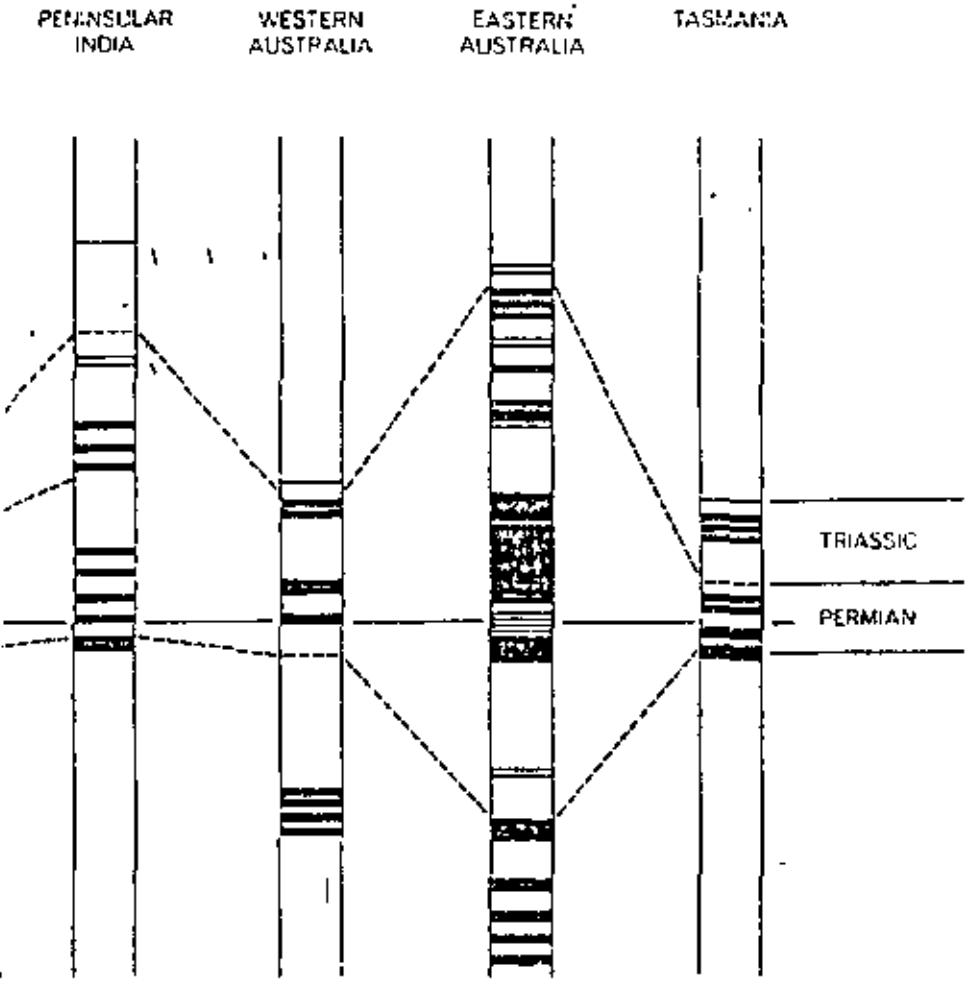

the very least a closely associated mass connected by land bridges. Only two of several major plant genera are plotted here: *Glossopteris* and *Gangamopteris*. The depths of the various deposits have been arbitrarily aligned between the lower and the basal Permian.

apparently new, there are large blocks that have the same age as the cratons. It looks as if the earth's surface has been warped and folded around the ancient continental masses, catching up segments of the crust and intruding younger igneous rocks into the folds. In some places the ancient material has been altered beyond recognition, but elsewhere it has been left fairly undisturbed and its antiquity can be determined by radioactive-dating methods. These composite belts are termed zones of rejuvenation. When they are eroded down to sea level, all we see, as far as topography is concerned, is another part of the continental platform. Geological mapping, however, reveals the belt structure clearly. A closer look at the cratons shows us that they too have the structure of preexisting mountain belts that have been carved into segments, with the younger material always cutting across the older structural pattern.

We see the process in action today. Our young mountain belts have not been eroded to sea level but show high elevations that are clearly apparent; we do not need geological surveys to observe them. It is only when we see the global distribution of these mountain belts on land areas, together with the distribution of rifts and their associated ridges under the oceans, that we begin to perceive the possibility that vast motions of the earth's surface may be their cause [*see illustration on next two pages*].

The earth is also encircled by belts of geological activity in the form of volcanoes, earthquakes and high heat flow, and observable motions in the form of folded rocks and the large displacements known as faults. In recent years the direction of displacements that are not observable on the surface has been deduced by the study of seismic waves arriving at various points on the earth's surface from earthquakes. It is now possible to tell the direction of slippage in the zones of rupture within the solid rocks of the earth's near-surface regions, so that the directions of the forces can be obtained.

If one looks at a map such as the one on the next two pages, one is immediately struck by the large scale and systematic distribution of these lines of geologic activity. Some of the systems are coherent over distances of several thousand kilometers. This immediately suggests the large-scale motion of material in the earth's interior. It does not, however, necessarily imply motions extending a similar distance into the interior. It is

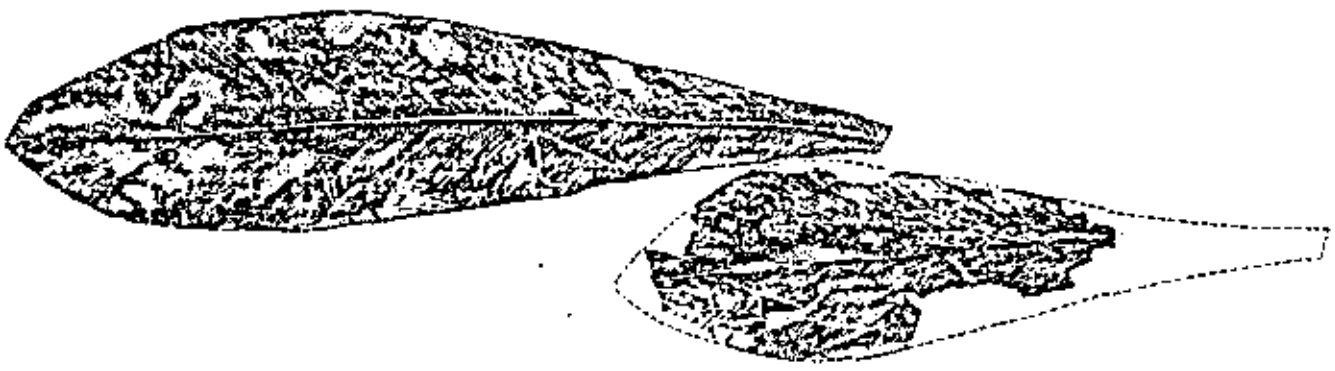

TYPICAL GONDWANA FLORA are *Glossopteris communis* (*leaf at left*) and *Gangamopteris cyclopteroides* (*right*), two species of fern that are identified in the Gondwana succession illustrated at the top of these two pages. The fossils from which these drawings were made were uncovered in the central part of Antarctica in 1961–1962 by William E. Long of Alaska Methodist University.

possible to have sheets of rigid material supporting stresses and fracturing over great distances if the underlying material is less rigid.

The topography of the ocean floors has been rapidly revealed in the past two decades by the sonic depth recorder. The principal systems of ridges and faults have been mapped in considerable detail by such oceanographers as Bruce C. Heezen and Maurice Ewing of Columbia University and H. W. Menard of the Scripps Institution of Oceanography. The layers of sediment on the sea floor have also been explored by such methods as setting explosive charges in the water and recording the echoes. It became a great puzzle how in the total span of the earth's history only a thin veneer of sediment had been laid down. The deposition rate measured today would extend the process of sedimentation back to about Cretaceous times, or 100 to 200 million years, compared with a continental and oceanic history that goes back at least 3,000 million years. How could three-quarters of the earth's surface be wiped clean of sediment in the last 5 percent of terrestrial time? Furthermore, why were all the oceanic islands and submerged volcanoes so young? The new oceanographic investigations were presenting questions that were awesome to contemplate.

In the early 1960's Harry H. Hess of Princeton University and Robert S. Dietz of the U.S. Coast and Geodetic Survey independently proposed that the oceanic ridge and rift systems were created by rising currents of material which then spread outward to form new ocean floors. On this basis the ocean floors would be rejuvenated, sweeping along with them the layer of sedimentary material. If such a mechanism were at work, no part of the ocean basins would be truly ancient. Although this radical hypothesis had much in its favor, it appeared farfetched to most.

Tracking the Shifting Poles

During this time a group of physicists and geophysicists were studying the directions of magnetism "frozen" into rocks in the hope of tracing the history of the earth's magnetic field. When an iron-bearing rock is formed, either by crystallization from a melt or by precipitation from an aqueous solution, it is

WORLDWIDE GEOLOGICAL PATTERNS provide evidence that the major land masses have been driven apart by a slow convection process that carries material upward from the mantle below the earth's crust. The dark-colored lines identify the crests of oceanic ridges that are now believed to coincide with upwelling regions. These ridges are crossed by large transcurrent fracture zones. The broken lines show the approximate limits of the oceanic rises. The light gray areas identify the worldwide pattern of recent mountain belts, island arcs, deep trenches, earthquakes and volcanism that apparently mark the downwelling of crustal material. The

slightly magnetized in the direction of the earth's magnetic field. Unless this magnetism is disturbed by reheating or physical distortion it is retained as a permanent record of the direction and polarity of the earth's magnetic field at the time the rock was formed. By measuring the magnetism in rocks of all ages from different continents, it has been possible to reconstruct the position of the magnetic pole in the past history of the earth. Great impetus was given to this study by P. M. S. Blackett and Runcorn, who with others soon found that the position of the pole followed a path going backward in time that was different for each continent [*see top illustration on next page*].

The interpretation of this effect was that the continents had moved with respect to the present position of the magnetic pole, and that since the paths were different for each land mass, they had moved independently. Because it was unlikely that the magnetic pole had wandered very far from the axis of the earth's rotation, or that the axis of rotation had changed position with respect to the principal mass of the earth, it was concluded that the continents had moved over the surface of the earth. Moreover, since the shift in latitude of the southern continents was generally southward going backward in time, the motions were in accord with the older evidence pointing toward a Gondwanaland in the south-polar regions. In short, the magnetic evidence supported not only the notion of continental drift but also the general locations from which the continents had moved within the appropriate time span.

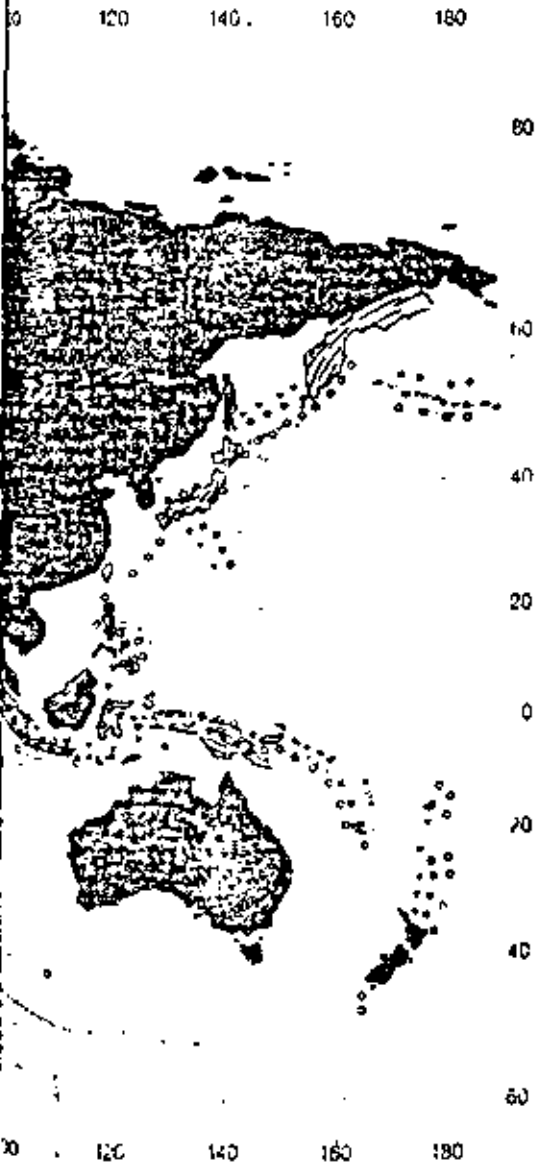

Downwelling seems to coincide with the occurrence of deep earthquakes (*triangles*) and earthquakes of intermediate depth (*solid dots*). Upwelling zones seem to coincide only with shallow earthquakes (*open dots*).

This was still not enough to sway the preponderance of American scientific opinion. Finally, at the annual meeting of the Geological Society of America in San Francisco in 1966, came the blows that broke the back of the opposition. Several papers put forward startling new evidence that related the concepts of ocean-floor spreading and continental drift, the cause of the oceanic-ridge and fault systems and the direction and time scale of the drift motions. In addition, the development of new mechanisms explaining displacement along faults brought into agreement some of the formerly contradictory seismic evidence.

In the study of rock magnetism it was observed that the earth's magnetic field not only had changed direction in the past but also had reversed frequently. In order to study how frequently and when the reversals occurred three workers in the U.S. Geological Survey—Allan Cox, G. Brent Dalrymple and Richard R. Doell—carefully measured the magnetism in samples of basaltic rocks that they dated by determining the amount of argon 40 in the rocks formed by the decay of radioactive potassium 40. They noted a distinct pattern of reversals over some 3.6 million years [see "Reversals of the Earth's Magnetic Field," by Allan Cox, G. Brent Dalrymple and Richard R. Doell; SCIENTIFIC AMERICAN, February, 1967]. Their finding was soon confirmed when Neil D. Opdyke and James D. Hays of Columbia University found the same pattern in going downward into older layers in oceanic sediments. It was thus established that the polarity of the magnetic field had universally reversed at certain fixed times in the past.

Meanwhile an odd pattern of magnetism in the rocks of the ocean floors had been detected by Ronald G. Mason and Arthur D. Raff of the Scripps Institution of Oceanography. Using a shipborne magnetometer, they found that huge areas of the ocean floor were magnetized in a stripelike pattern. Putting together these patterns, the discovery of magnetic reversals and Hess's idea that the oceanic ridges and rifts were the site of rising and spreading material, F. J. Vine, now at Princeton, and D. H. Matthews of the University of Cambridge proposed that the hypothesis of the continuous creation of new ocean floors might be tested by examining the magnetic pattern on both sides of an oceanic ridge. The extraordinary discovery that the pattern was symmetrical with the ridge was demonstrated by Vine and Tuzo Wilson, who studied the two sides of a ridge next to Vancouver Island.

The history of the magnetic field going back into the past was laid out horizontally in the magnetism of the rocks of the sea floor going away from the ridge in both directions. It appeared that new hot material was rising from the rift in the center of the ridge and becoming magnetized in the direction of the earth's field as it cooled; it then moved outward, carrying with it the history of magnetic reversals. Since the dates of the reversals were known, the distance to each reversed formation gave the rate of spreading of the ocean floor [*see bottom illustration on next page*].

This important piece of work was quickly followed up by James R. Heirtzler, W. C. Pitman, C. O. Dickson and Xavier Le Pichon of Columbia, who have now shown that the ridges of the Pacific, Atlantic and Indian oceans all exhibit similar patterns. In fact, these workers have detected recognizable points in the history of magnetic reversals back about 80 million years, or in the Cretaceous period, and have drawn isochron lines, or lines of equal age, over huge strips of the ocean floors. Hence it is now possible to date the ocean floors and perceive the direction and rate of their lateral motion simply by conducting a magnetic survey over them. The implications for the study of drifting continents are immediately apparent.

These and other new findings do not unequivocally call for continental drift. It might be possible to have sea-floor spreading without drifting continents. Nonetheless, the directions and rates of motion for both sea-floor spreading and continental drift are entirely compatible. Above all, the principal objection to a hypothesis of continental movement has been removed.

Looking back, it is interesting to ob-

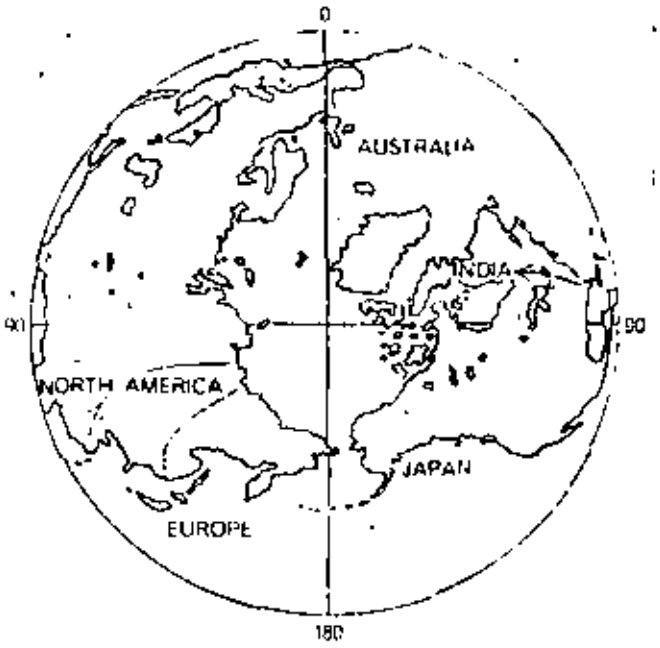

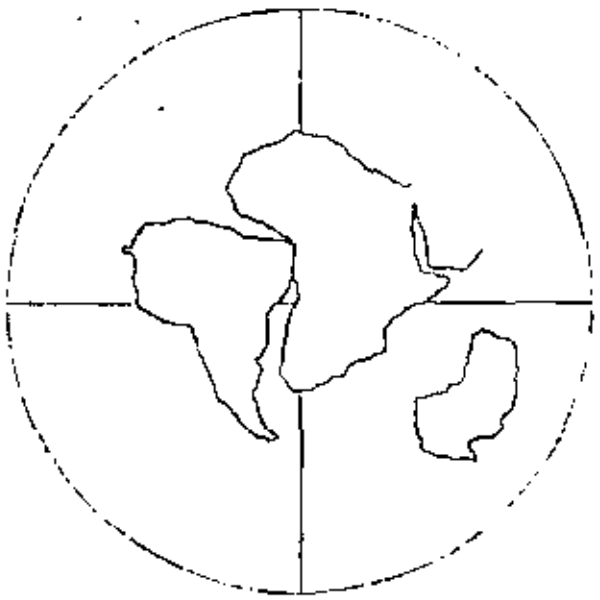

NORTH MAGNETIC POLE would appear to have wandered inexplicably during the past few hundred million years (*colored lines at left*), on the basis of "fossil" magnetism measured in rocks of various ages in various continents. The diagram is based on one by Allan Cox and Richard R. Doell of the U.S. Geological Survey. The pole could hardly have followed so many different tracks simultaneously; evidently it was the continents that wandered. K. M. Creer of the University of Newcastle upon Tyne found that the tracks could be brought together if South America, Africa and Australia were grouped in the late Paleozoic as shown at the right.

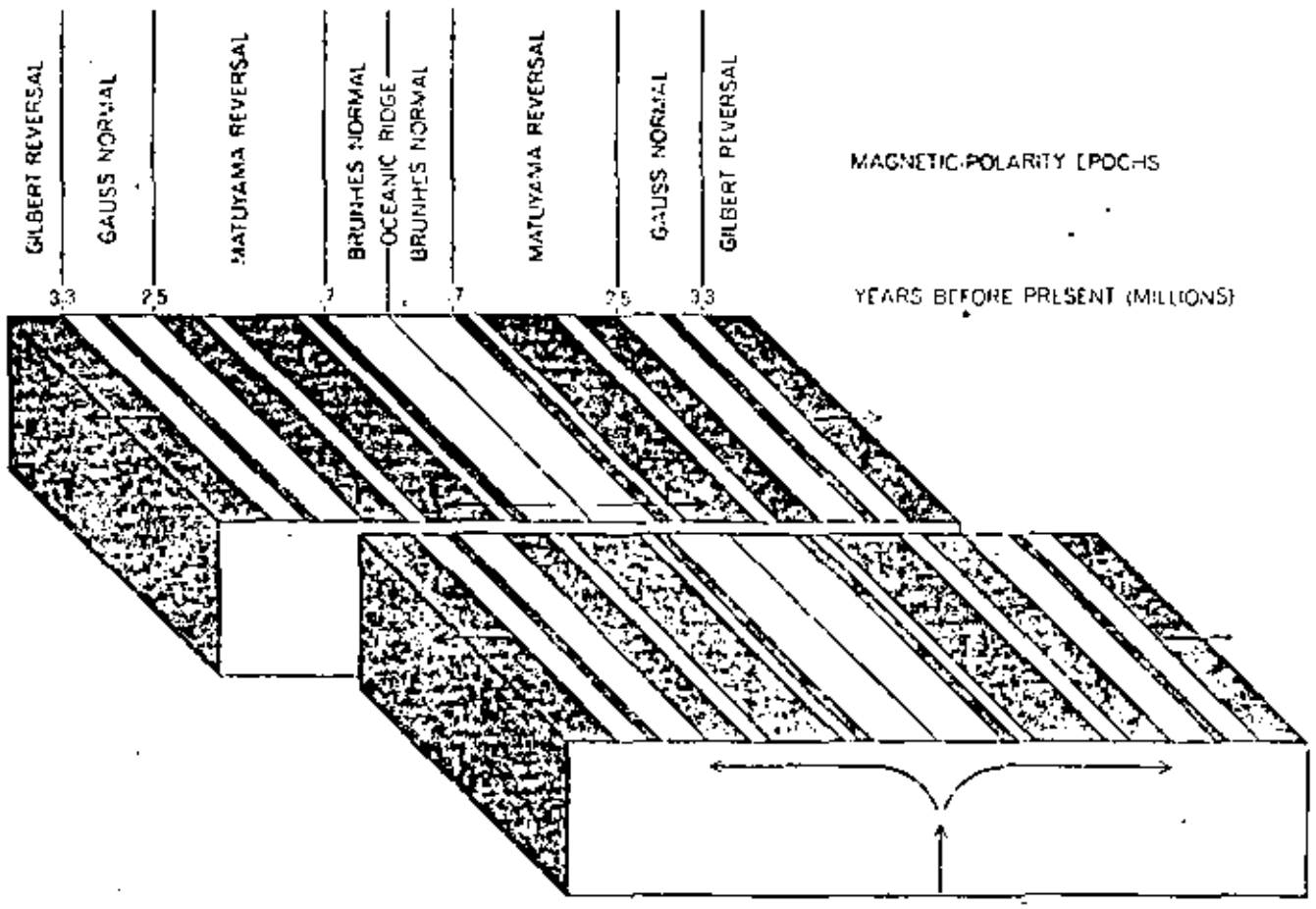

EVIDENCE FOR SEA-FLOOR SPREADING has been obtained by determining the polarity of fossil magnetism in rocks lying on both sides of oceanic ridges. In the diagram rocks of normal, or present-day, polarity are shown in color; rocks of reversed polarity are in gray. The displacement of the two blocks represents a transcurrent fracture zone. The symmetry suggests that the rocks welled up in a molten or semimolten state and gradually moved outward. The diagram is based on studies by a number of workers.

serve how each new piece of evidence presented in the past was met by counterevidence. Wegener's reconstruction, for example, was countered by numerous geologists who took exception to his detailed arguments. The arguments for the Permocarboniferous Gondwana glaciations were countered by Daniel I. Axelrod of the University of California at Los Angeles and others in this country. They contended that most species of fossil plant tend to be restricted to zones of latitude that hold for the continents in their present position, a fact that is hard to reconcile with the presumed pattern of glaciation. The idea that the great Gondwana land masses drifted in latitude has also been opposed by F. G. Stehli of Case Western Reserve University; his studies suggest that ancient fauna were most diverse at the Equator, and that the Equator defined in this way has not shifted.

Another Test of the Hypothesis

Any hypothesis must be tested on all points of observational fact. The balance of evidence must be strongly in its favor before it is even tentatively accepted, and it must always be able to meet the challenge of new observations and experiments. My own interest in the problem of continental drift was stimulated at a 1964 symposium in London sponsored by the Royal Society and arranged by Blackett, Bullard and Runcorn. At that time Bullard and his University of Cambridge associates J. E. Everett and A. G. Smith presented an elegant study of the geographic matching of continents on both sides of the North and South Atlantic. They had employed a computer to produce the best fit by the method of least squares. Instead of using shorelines, as had been done in earlier attempts, they followed the lead of S. W. Carey; he had chosen the central depth of the continental slope as representing the true edge of the continent.

The fit was remarkable [*see illustration on page 56*]. The average error was no greater than one degree over most of the boundary. My colleagues and I at the Massachusetts Institute of Technology now began to think of further testing the fit by comparing the sequence and age of rocks on opposite sides of the Atlantic.

Radioactive dating techniques for determining the absolute age of rocks had reached a point where much could be learned about the age and history of both the ancient cratonic regions and the younger rejuvenated ones. For such purposes two techniques can be used in combination: the measurement of strontium 87 formed in the radioactive decay of rubidium 87 in a total sample of rock, and the measurement of argon 40 formed in the decay of potassium 40 in minerals separated from the rock. A collaborative effort was arranged between our geochronology laboratory and the University of São Paulo in Brazil (in particular with G. C. Melcher and U. Cordani of that institution). We also enlisted the aid of field geologists who had been working on the west coast of Africa (in Nigeria, the Ivory Coast, Liberia and Sierra Leone) and on the east coast of Brazil and Venezuela. The São Paulo group made the potassium-argon measurements of the Brazilian rock samples; we did the rubidium-strontium analyses on samples from all locations.

European geochronologists (notably M. Bonhomme of France and N. J. Snelling of Britain) had done pioneering work on the Precambrian geology of former French and British colonies and protectorates in West Africa. Of special interest to us at the start was the sharp boundary between the 2,000-million-year-old geological province in Ghana, the Ivory Coast and westward from these countries, and the 600-million-year-old province in Dahomey, Nigeria and east. This boundary heads in a southwesterly direction into the ocean near Accra in Ghana. If Brazil had been joined to Africa 600 million years ago, the boundary between the two provinces should enter South America close to the town of São Luís on the northeast coast of Brazil. Our first order of business was therefore to date the rocks from the vicinity of São Luís.

To our surprise and delight the ages fell into two groups: 2,000 million years on the west and 600 million years on the east of a boundary line that lay exactly where it had been predicted. Apparently a piece of the 2,000-million-year-old craton of West Africa had been left on the continent of South America.

In subsequent work on both sides we have found no incompatibilities in the age of many geological provinces on both sides of the South Atlantic [*see illustration on next page*]. Furthermore, the structural trends of the rocks also agree, at least where they are known. Minerals characteristic of individual belts of rocks are also found in juxtaposition on both sides; for example, belts of manganese, iron ore, gold and tin seem to follow a matching pattern where the coasts were joined.

Can such comparisons be made elsewhere? To some extent, yes. Unfortunately the rifting process by which a continent breaks up seems to be guided by zones of rejuvenation between cratons, as if these zones were also zones of weakness deep in the crust. It is necessary for the break to have transected the structure of the continent, cutting across age provinces, if one is to get a close refitting of the blocks. In the North Atlantic this is not the case, but the continental areas on both sides were simultaneously affected by an unmistakable oblique crossing of a Paleozoic belt of geological activity [*see illustration on page 65*]. Actually the belt covers the region of the Appalachian Mountains and the Maritime Provinces of North America, with an overlap along the coast of West Africa, and then splits into two principal belts: one extending through the British Isles and affecting the Atlantic coast of Scandinavia and Greenland and the other turning eastward into Europe. There is a superposition of at least four periods of renewed activity affecting the various parts of this complex. All four are represented on both sides of the North Atlantic, making this correlation extremely difficult to explain unless the continents were once together.

My colleagues H. W. Fairbairn and W. H. Pinson, Jr., and I, as well as other workers, have made age measurements in the northern Appalachians and Nova Scotia for many years, and we have found all four periods well represented in New England. The earliest period of activity (which Fairbairn has named Neponset) is dated about 550 million years ago. It is seen in some of the large rock bodies in eastern Massachusetts and Connecticut, in the Channel Islands off the northern coast of France, in Normandy, Scotland and Norway. The next-oldest period (the Taconic) was about 450 million years ago and is found on the western edge of New England and in parts of the British Isles. The next period, going back about 360 million years, is strongly represented in the entire span of the Appalachians and Nova Scotia (where it is called the Acadian) and in England and Norway (where it is called the Caledonian). Finally, about 250 million years ago, the activity seemed to move into southern Europe and North Africa, where it has been called the Hercynian. This activity, however, also extended into New England; much of southern Maine, eastern New Hampshire, Massachusetts and Connecticut show rocks of this age. Here the event is called the Appalachian.

Farther south the Lower Paleozoic section of the northwest coast of Africa (Senegal) appears to continue under the younger coastal sediments of Florida.

23

This African belt shows large rock units with ages equivalent to the Nipanset, and also evidence of the younger events.

The Fitting of Antarctica

The recent extensive geological surveys in Antarctica have been highly rewarding in reconstructing Gondwanaland. Prior to the end of the Permian period the younger parts of western Antarctica were not yet formed. Only eastern Antarctica was present, including the great belts of folded rocks that form the Transantarctic Mountains. These consist of two geosynclines, or sediment-filled troughs: the inner Eopaleozoic and the outer Paleozoic *[see illustration on page 66]*. The inner belt includes late Precambrian and early Cambrian sediments, which were folded and invaded by igneous rocks during late Cambrian or early Ordovician times (about 500 million years ago). Thus the inner belt is similar in age to the widespread event in the rest of Gondwanaland. It is marked by the Cambrian fossil Archaeocyatha, an organism that formed barrier reefs. These coral-like structures are found transecting sediments in bodies known as bioherms. The outer belt, farther within western Antarctica, is a geosyncline filled with Lower Paleozoic sediments. Like the southern Appalachians, it was deformed and invaded by igneous rocks in the middle and late Paleozoic. Later it was covered with a quite representative Gondwana succession, with its glacial deposits, coal and diverse plants.

There seems to be a similar record of events in eastern Australia. The late terms of the Cambrian Archaeocyatha are found in a belt extending northward from Adelaide and mark the edge of an early geosyncline filled with sediments including late Precambrian and Cambrian ones. Later in time, and farther to the east, great thicknesses of Silurian and Lower Devonian sediments accumulated in the Tasman trough. Compression and igneous intrusion occurred in this Tasman geosyncline mostly in the late Lower Devonian period to the middle Devonian (about 350 million years

TENTATIVE MATCHING of geological provinces of the same age shows how South America and Africa presumably fitted together some 200 million years ago. Dark-colored areas represent ancient continental blocks, called cratons, that are at least 2,000 million years old. Lighter-colored areas are younger zones of geological activity: mostly troughs filled with sediments and volcanic rocks that were folded, compressed and intruded by hot materials, forming granites and other rock bodies. Much of this activity was 450 million to 650 million years ago, but some of it goes back 1,100 million years. The dots show the sites of rocks dated by many laboratories, including the author's at the Massachusetts Institute of Technology. Solid dots denote rocks older than 2,000 million years; open dots denote younger rocks. The region near São Luís is part of an African craton left stranded on the coast of Brazil.

ago). The later cover of sediments includes a Gondwana succession similar to the one in Antarctica.

There is also strong evidence for a juncture between Australia and India, particularly in the Permian basins of sedimentation of the two continental blocks and in Gondwana sequences of coal and plants. Limestone beds containing the same Productid shells are found in the upper layers of the sequence on both sides. A correlation also exists between the banded iron ores of Yampi Sound in northwestern Australia and the similar ores of Singhbhum in India.

The illustration on page 66 is a reconstruction of Gondwanaland based on the evidence we have discussed so far. The three land masses—Antarctica, Australia and India—have been fitted together not at their present shorelines but where the depth of the surrounding ocean reaches 1,000 meters. As can be seen, the fit of the edges is good. The detailed fit of this assemblage into the southeastern part of Africa is still debated because most of the edges lack structures that cut across them. Nevertheless, I have included the edge of Africa in the map to show how it might possibly fit on the basis of limited age data from Antarctica.

This arrangement of land masses in the late Paleozoic is extremely tentative. It is now up to the geochronologists to test each juncture more closely for correlations in geologic age, and up to the field geologists to match structure and rock type. One particularly interesting fit may be forthcoming in a study of the boundaries of shallow and deep marine glacial deposits, and of the land tilting around what appears to be the start of an oceanic basin at the time Antarctica was breaking away. This attempt to establish the former position of Antarctica, which is being made by L. A. Frakes and John C. Crowell of the University of California at Los Angeles, may set in place the key piece in the puzzle. A detailed correlation of fossil plants in Antarctica with those of the adjacent land masses, which has been undertaken by Rose Bronstead of the University of Witwatersrand, is similarly limiting the possible position of the blocks.

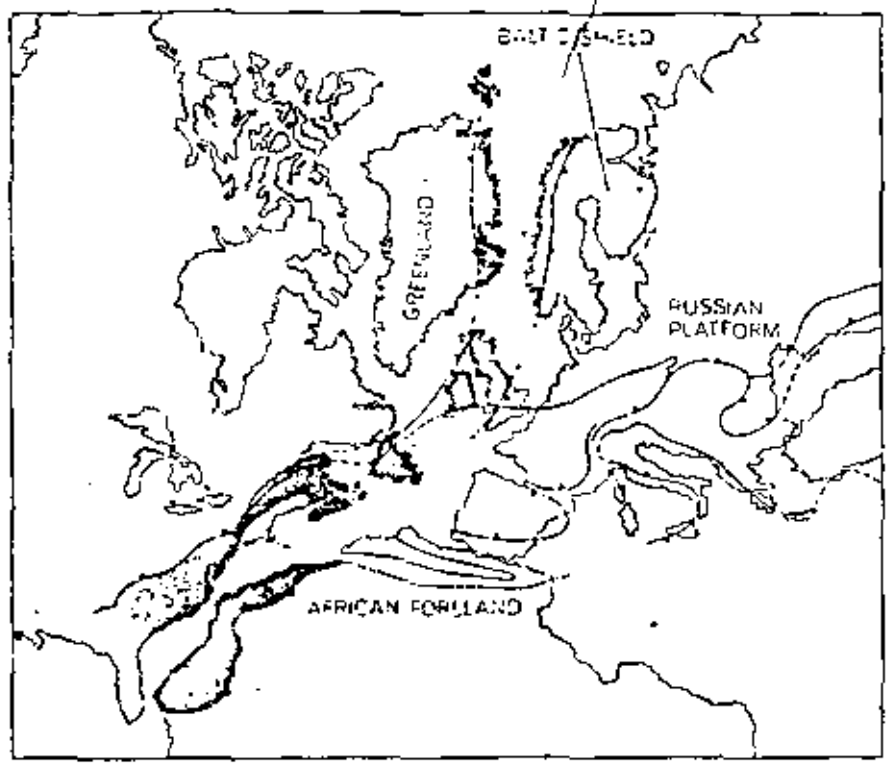

MATCHING OF NORTH ATLANTIC REGIONS is more difficult than in the South Atlantic. This tentative, predrift reconstruction of a portion of Laurasia depends on matching ancient belts of similar geological activity. The dark gray belt represents the formation of sediment-filled troughs and folded mountains in the early and middle Paleozoic (470 million to 350 million years ago). The medium gray belt was formed in the late Paleozoic (350 million to 200 million years ago). The latter belt overlapped the region of the former in the northern Appalachians and in southern Ireland and England, but diverged eastward in Europe. Four distinct and superimposed periods of geological activity occur on both sides of the present North Atlantic, providing strong evidence for a previous juncture.

The Age of the Atlantic

When did Gondwanaland begin to break up? One of the best pieces of evidence for the start of the opening of the South Atlantic is the age of offshore sediments along the west coast of Africa. Drilling through these sediments down to the ancient nonsedimentary rocks shows that the layer of sediments is quite young: not older than the middle Mesozoic (about 160 million years ago). If the South Atlantic had been in existence for a major part of geologic time, the continent of Africa would unquestionably have developed a large shelf of sediments along the entire length of its western margin. The continental shelf would consist of sediments dating all the way back to the time of the ancient cratons. This is not the case. It looks as though the rift started from the northern edge of western Africa in the middle Triassic and slowly opened to the south until the final separation occurred in the Cretaceous. The east coast of Africa, on the other hand, apparently started to open earlier, in the Permian.

With the acceptance of sea-floor spreading and continental drift the global problems of geology are beginning to be solved. Although the train of thought on such matters is not universally accepted in detail, it is something like the following. Continental areas appear to have greater strength, to a depth of 100 kilometers or so, than ocean basins do, so that they tend to maintain themselves as buoyant masses that are not destroyed by sinking motions. They can, however, be ruptured. Rising material pushes the surface apart; sinking material pulls the surface together and toward the region of sinking. Therefore if a sinking zone is established in an oceanic region, the continents will move toward the zone, and if a rising zone is established under a continent, the continent will split apart and the parts will move away from the zone. When the ocean floor moves toward a sinking zone in an oceanic region, it forms a deep trench bordered by volcanoes, chains of islands or elongated land masses such as the Philippines and Japan. When an ocean floor moves toward a continent, it appears to pass under the continental border, forming a great mountain chain. The mountain chain may be in part piled-up material that was already present and in part volcanic material that rose as the ocean swept its load of sediment, underlying volcanic rock and the continental shelf itself toward and under the edge of the continent. The process leads to a melting of underlying rock and to the intrusion of new volcanic material. The west coast of South America is a good example.

Another example is the thrust of India into Eurasia that formed the Himalayas. It has long been known that there was a large body of water between Africa and Eurasia and that a great thickness of sediments was deposited there at some time during the past 200 million years. This body is known as the Tethys Sea. It was located north of Arabia and extended from the former location of the Atlas Mountains to east of the Himalayas. As I have mentioned, it appears that Gondwanaland not only broke up but also moved northward, with India and Africa pushing up into Eurasia. This motion apparently caused the buckling up of sediments in the Tethys Sea, giving rise to the mountain ranges that now form a contorted chain from the western Atlas range through the Mediterranean, the western Alps, the Caucasus and the Himalayas.

The way the present mountain systems of the earth fall along great circles suggests that the motions in the earth's interior have a large-scale coherence, of the order of the dimensions of the earth itself. The prevailing explanation stems from a new lead in seismology: a zone in the earth at a depth of 100 or 200 kilom-

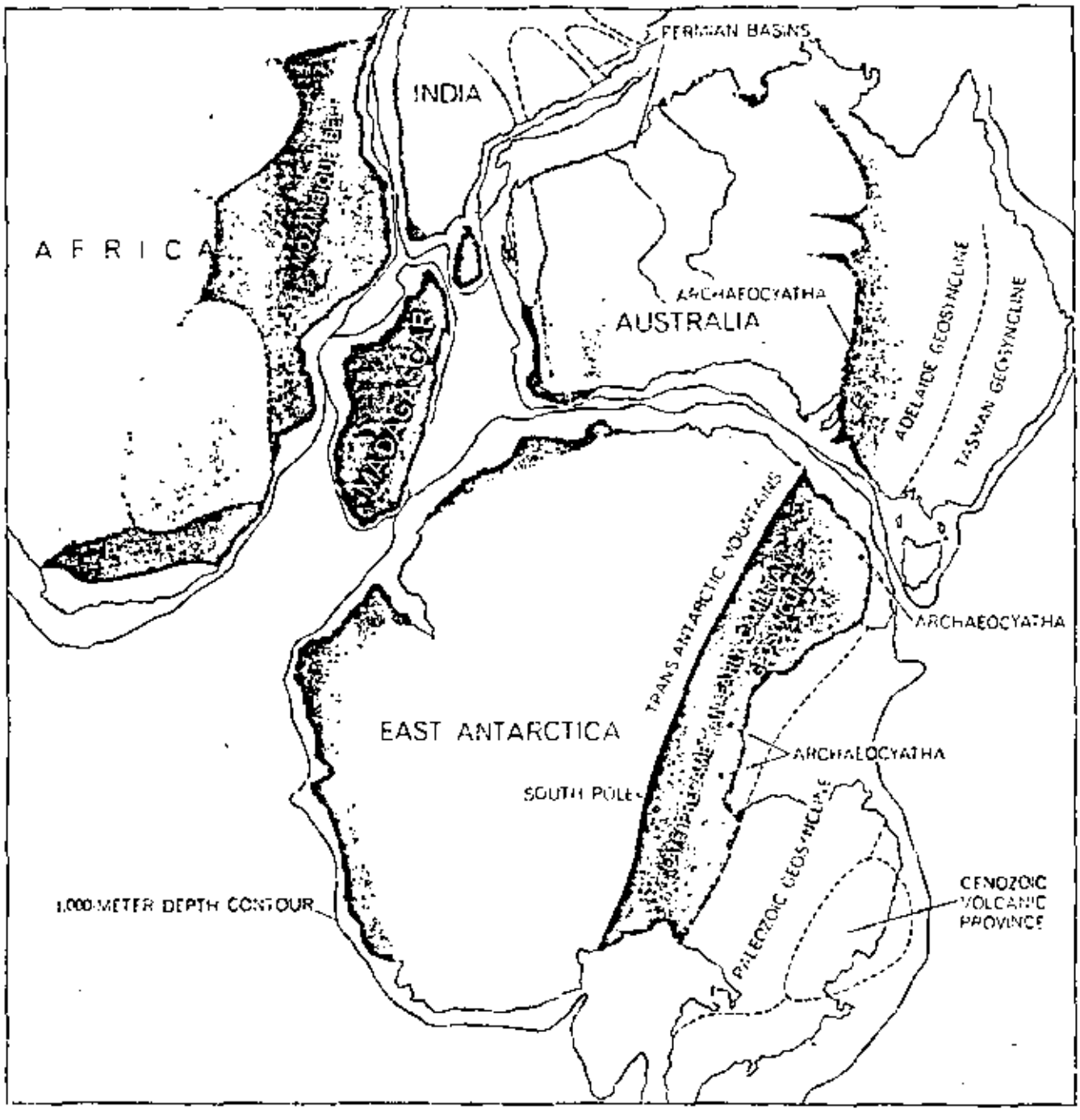

PART OF GONDWANALAND, tentatively reconstructed, brings together East Antarctica, Africa, Australia, Madagascar, India. The fit is at the 1,000-meter depth contour of the continental slope. Late Precambrian and Paleozoic geosynclines, or sediment-filled troughs, in eastern Australia are correlated in age and location with similar troughs along the Transantarctic Mountains. The deep Permian basins of northwest Australia match those of India. Glacial deposits, fauna and metal ores provide other correlations.

eters has been found to transmit seismic waves more slowly than the layers above and below it and to absorb seismic energy more strongly. This low-velocity zone is generally thought to consist of a material whose strength is reduced because a small amount of it is molten or because its temperature is approaching the melting point. The surface of the earth may therefore move around on this low-strength layer like the skin of an onion. It is believed the earth loses heat partly by conduction outward and partly by convection currents in the relatively thin layer above the weak zone. These currents, as they have been depicted by Walter M. Elsasser of Princeton and Egon Orowan of M.I.T., form rather flat convection cells.

A hypothesis that is currently popular is that the mechanism of spreading at the oceanic ridges involves the intrusion of hot material into ruptures near the surface. This material is the same as that in the low-velocity zone, lubricated by partly molten rock. A small proportion of the intruded material actually loses some of its melted fraction upward, giving rise to volcanoes and creating a thin layer (about five kilometers thick) of volcanic rock at the surface. The masses of intruded material cool as they move sideways from the central ridge, which is overlain by the thin layer of volcanic rock. This results in the observed distribution of seismic velocities at various depths, helps to explain why the flow of heat to the surface decreases with distance from the ridge and accounts for the pattern of magnetic reversals. At the sinking end of the convection cell this relatively rigid block of mantle material with its thin cover of basalt (plus a thin cover of new sediment) moves downward on an inclined plane.

It is clear where these concepts will lead. If folded mountain belts are the "bow waves" of continents plowing their way through ocean floors and ramming into other continents, we can use them to show us the relative directions of motion prior to the last great drift episode. If we look at the pre-drift Paleozoic mountain belts, such as the Appalachian belt of North America, the Hercynian of Europe and the Ural of Asia, we find that they are located *internally* in the great continental masses of Gondwanaland and Laurasia. This suggests that these pre-drift supercontinents had been formed by the inward motion of several separate blocks, which came together before they broke apart. Geologists have a new game of chess to play, using a spherical board and strange new rules.

15

THE SAN ANDREAS FAULT

DON L. ANDERSON

November 1971

The San Fernando earthquake that occurred at sunrise on February 9, 1971, jolted many southern Californians into acute awareness that California is earthquake country. Although it was only a moderate earthquake (6.6 on the Richter scale), it was felt in Mexico, Arizona, Nevada and as far north as Yosemite National Park, more than 250 miles from San Fernando. It was recorded at seismic stations around the world. In spite of its relatively small size the San Fernando earthquake was extremely significant because it happened near a major metropolis and because its effects were recorded on a wide variety of seismic instruments. Within hours the affected region was awarm with geologists mapping faults and seismologists installing portable instruments to monitor aftershocks and the deformation of the ground. It was immediately clear from data telemetered to the Seismological Laboratory of the California Institute of Technology in Pasadena from the Caltech Seismic Network that the earthquake was not centered on the much feared San Andreas fault or, for that matter, on any fault geologists had labeled as active. The faults in the area, however, are all part of the San Andreas fault system that covers much of California.

The San Andreas fault system (and its attendant earthquakes) is part of a global grid of faults, chains of volcanoes and mountains, rifts in the ocean floor and deep oceanic trenches that represent the boundaries between the huge shifting plates that make up the earth's lithosphere. The concept of moving plates is now fundamental to the theory of continental drift, which was long disputed but is now generally accepted in modified form on the basis of voluminous geological, geophysical and geochemical evidence. The theory had received strong support from the discovery that the floors of the oceans have a central rise or ridge, often with a rift along the axis, that can be traced around the globe. Within the rift new crustal material is continuously being injected from the plastic mantle below, forming a rise or ridge on each side of the rift. The newly formed crustal material slides away from the ridge axis. Since the magnetic field of the earth periodically reverses polarity, the newly injected material "freezes" in stripes parallel to the ridge axis, whose north-south polarity likewise alternates. By dating these stripes one can estimate the rate of seafloor spreading.

The San Andreas fault system forms the boundary between the North American plate and the North Pacific plate and separates the southwestern part of California from the rest of North America. In general the Pacific Ocean and that part of California to the west of the San Andreas fault are moving northwest with respect to the rest of the continent, although the continent inland at least as far as Utah feels the effects of the interactions of these plates.

The relative motion between North America and the North Pacific has been estimated in a variety of ways. Seismic techniques yield values between 1½ and 2½ inches per year. The ages of the magnetic stripes on the ocean floor indicate a rate of about 2½ inches per year. Geodetic measurements in California give rates between two and three inches per year. The ages of the magnetic anomalies off the coast of California indicate that the oceanic rise came to intersect the continent at least 30 million years ago. Geologists and geophysicists at a number of institutions (notably the University of Cambridge, Princeton University and the Scripps Institution of Oceanography) have proposed that geologic processes on a continent are profoundly affected when a continental plate is intersected by an oceanic rise. At the rates given above the total displacement along the San Andreas fault amounts to at least 720 miles if motion started when the rise hit the continent and if all the relative motion was taken up on the fault. Displacements this large have not been proposed by geologists, but the critical tests would involve correlation of geology in northern California with geology on the west coast of Baja California, an area that has only recently been studied in detail. One can visualize how the west coast of North America may have looked 32 million years ago by closing up the Gulf of California and moving central and northern California back along the San Andreas fault to fit into the pocket formed by the coastline of the northern half of Baja California. This places all of California west of the San Andreas fault south of

DISPLACEMENT ALONG SAN ANDREAS FAULT is clearly visible in this aerial photograph of a region a few miles north of Frazier Park, Calif., itself 65 miles northwest of Pasadena, where the fault runs almost due east and west. This east-west section of the San Andreas fault is part of the "big bend" where the fault appears to be locked. The photograph is reproduced with north at the right. The hilly region to the left (south) of the fault line is moving upward (westward) with respect to the flat terrain at the right, causing clearly visible offsets in the two largest watercourses as they flow onto the alluvial plain.

29

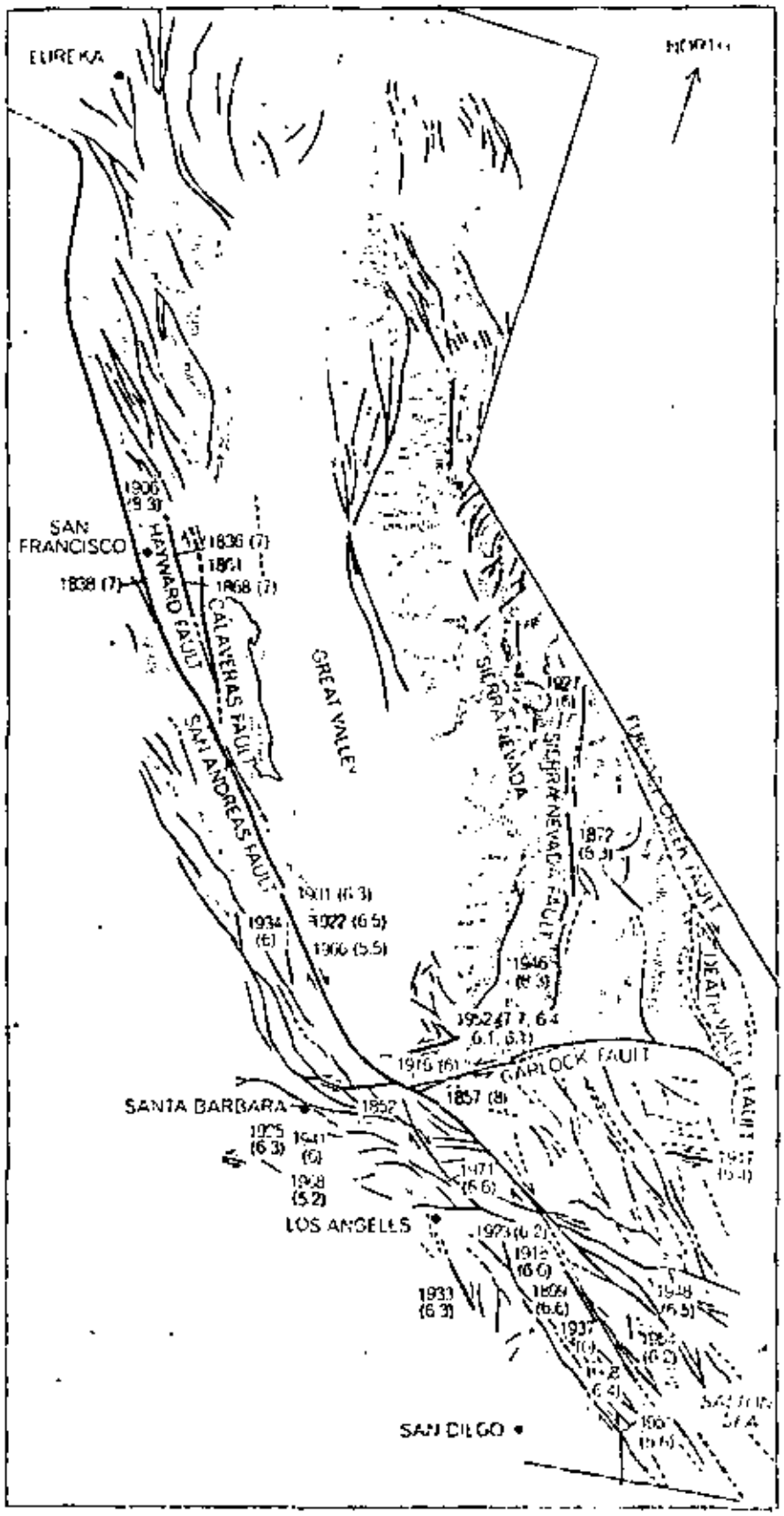

SIMPLIFIED FAULT MAP of California identifies in heavy black lines the faults that have given rise to major earthquakes since 1836. The magnitude of all but two of the earthquakes is given in parentheses next to the year of occurrence. For events that predated the introduction of seismological instruments the magnitudes are estimated from historical accounts. For two major events, the earthquakes of 1852 and 1861, information is too sparse to allow a magnitude estimate. Arrows parallel to the faults show relative motion.

the present Mexican border [*see illustration on page 150*].

California is riddled with faults, most of which trend roughly northwest-southeast, like most of the other tectonic and geologic features of California (such as the Sierra Nevada and the Coast Ranges). The prominent exceptions are the east-west-trending transverse ranges and faults that make up a band some 100 miles wide extending inland from between Los Angeles and Santa Barbara. The San Gabriel Mountains, which form the rugged backdrop to Los Angeles, are part of this complex geologic region, and it was here that the San Fernando earthquake struck. The northeast-trending Garlock fault and the Tehachapi Mountains, which separate the Sierra Nevada and the Mojave Desert, also cut across the general grain of California. The area to the west of most of the northwest-trending faults is moving northwest with respect to the eastern side. This is called *right-lateral motion*. If one looks across the fault from either side, the other side is moving to the right.

Motion on the Garlock fault is left-lateral, which, combined with the right-lateral motion on the San Andreas fault, means that the Mojave Desert is moving eastward with respect to the rest of California. Parts of the faults that have been observed or inferred to move as a result of earthquakes in historic times are shown in the illustration at the left. Also shown are the dates of the earthquakes and the magnitude of some of the more important ones. In general both the length of rupture and the total displacement are greater for the larger earthquakes. Horizontal displacements as great as 21 feet were observed along the San Andreas fault after the San Francisco earthquake of 1906, which had a magnitude of 8.3 on the Richter scale. (The Richter scale, devised by Charles F. Richter of Cal Tech, is logarithmic. Although each unit denotes a factor of 10 in ground amplitude, or displacement, the actual energy radiated by an earthquake is subject to various modifications.) The San Fernando earthquake produced displacements of six feet, whose direction was almost equally divided between the horizontal and the vertical.

The trend of the San Andreas fault system is roughly northwest-southeast from San Francisco to the south end of the Great Central Valley (the San Joaquin Valley) and again from the north of the Salton Sea depression to the Mexican border. The motion along the faults

in these areas is parallel to the fault and is mainly strike-slip, or horizontal. Between these two regions, from the south end of the San Bernardino Mountains to the Garlock fault, the faults bend abruptly and run nearly east and west, producing a region of overthrusting and crustal shortening [*see illustration below*]. The attempt of the southern California plate to "get around the corner" as it moves to the northwest is responsible for the complex geology in the transverse ranges, for the abrupt change in the configuration of the coastline north of Los Angeles and ultimately for the recent San Fernando earthquake. The big bend of the San Andreas fault is commonly regarded by seismologists as being locked and possibly as being the location of the next major earthquake. Much of the motion in this region, however, is being taken up by strike-slip motion along faults parallel to the San Andreas fault and by overthrusting on both sides of the fault. The displacements associated with the larger earthquakes in southern California in the vicinity of the big bend have averaged out to about 2¾ inches per year since 1800. The Kern County earthquake of 1952 (magnitude 7.7) apparently took care of most of the accumulated strain, at least at the north end of the big bend, that had built up since the Fort Tejon earthquake of 1857 (magnitude 8).

The San Andreas fault system cannot be completely understood independently of the tectonics and geology of most of the western part of North America and the northeastern part of the Pacific Ocean. This vast region is itself only a part of the global tectonic pattern, all parts of which seem to be interrelated. The earthquake, tectonic and mountain-building activities of western North America are intimately related to the relative motions of the Pacific and North American plates. Just as it is misleading to think of the San Andreas fault as an isolated mechanical system, so it is misleading to think of the entire San Andreas fault as a single system. The part of the fault that lies in northern California was activated earlier and has moved farther than the southern California section. The northern portion is less active seismically than the southern section and seems to have been created in a different way. It is also moving in a slightly different direction.

Measuring Displacements

There are several ways to measure displacements on major faults. Fairly recent displacements are reflected in offset stream channels [*see illustration on page 142*]. Many such offsets measured in thousands of feet are apparent across the San Andreas fault in central California, some of which can be directly related to earthquakes of historic times.

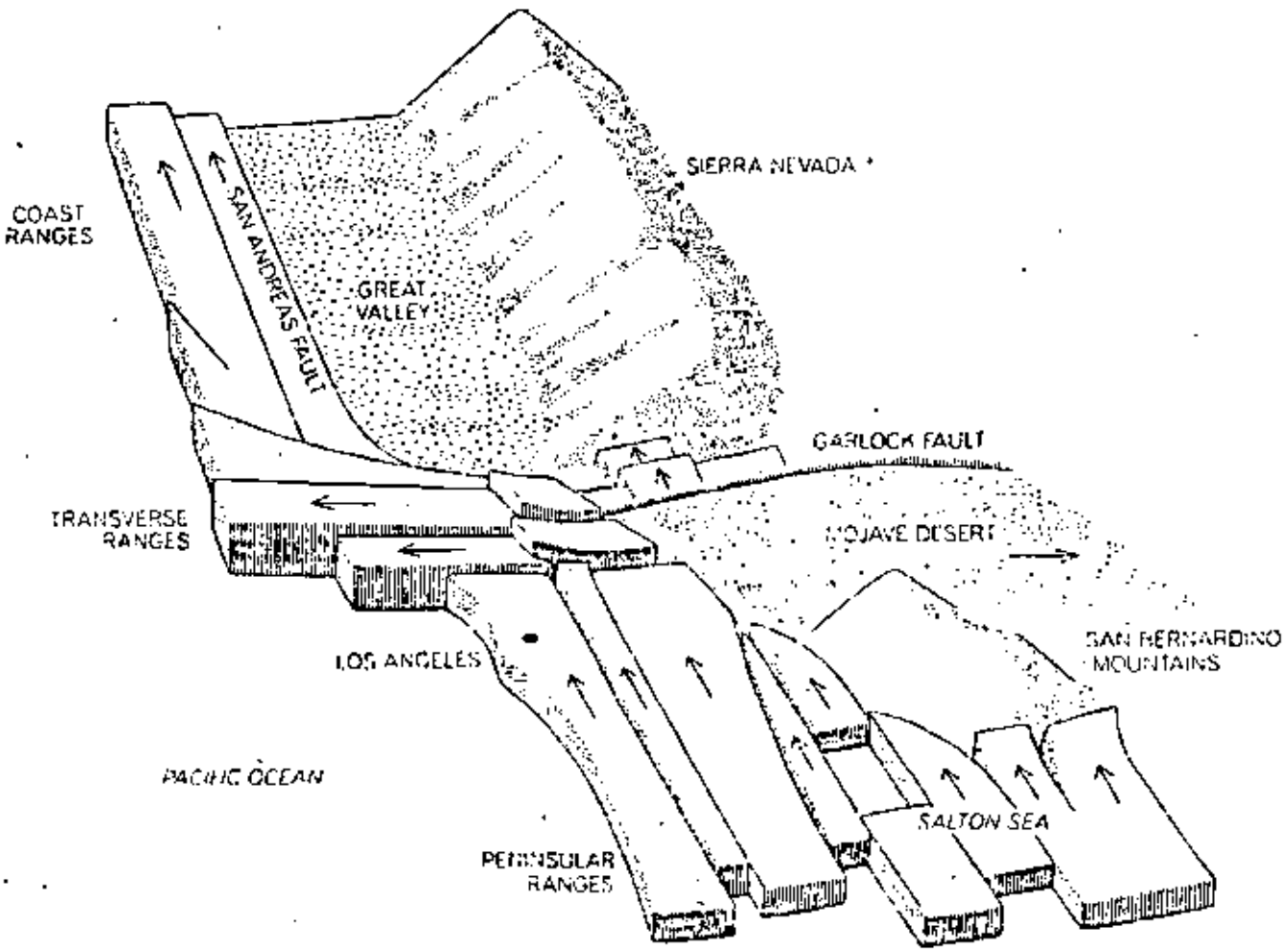

MOTION OF EARTH'S CRUST in southern California is generally northwest except where the lower group of blocks encounters the deep roots of the Sierra Nevada. At this point the blocks are diverted to the left (west), creating the transverse ranges and a big bend in the San Andreas fault system. Above the bend the blocks continue their northwesterly march, carrying the Coast Ranges with them. The Salton Sea trough at the lower right evidently represents a rift that has developed between two blocks.

31

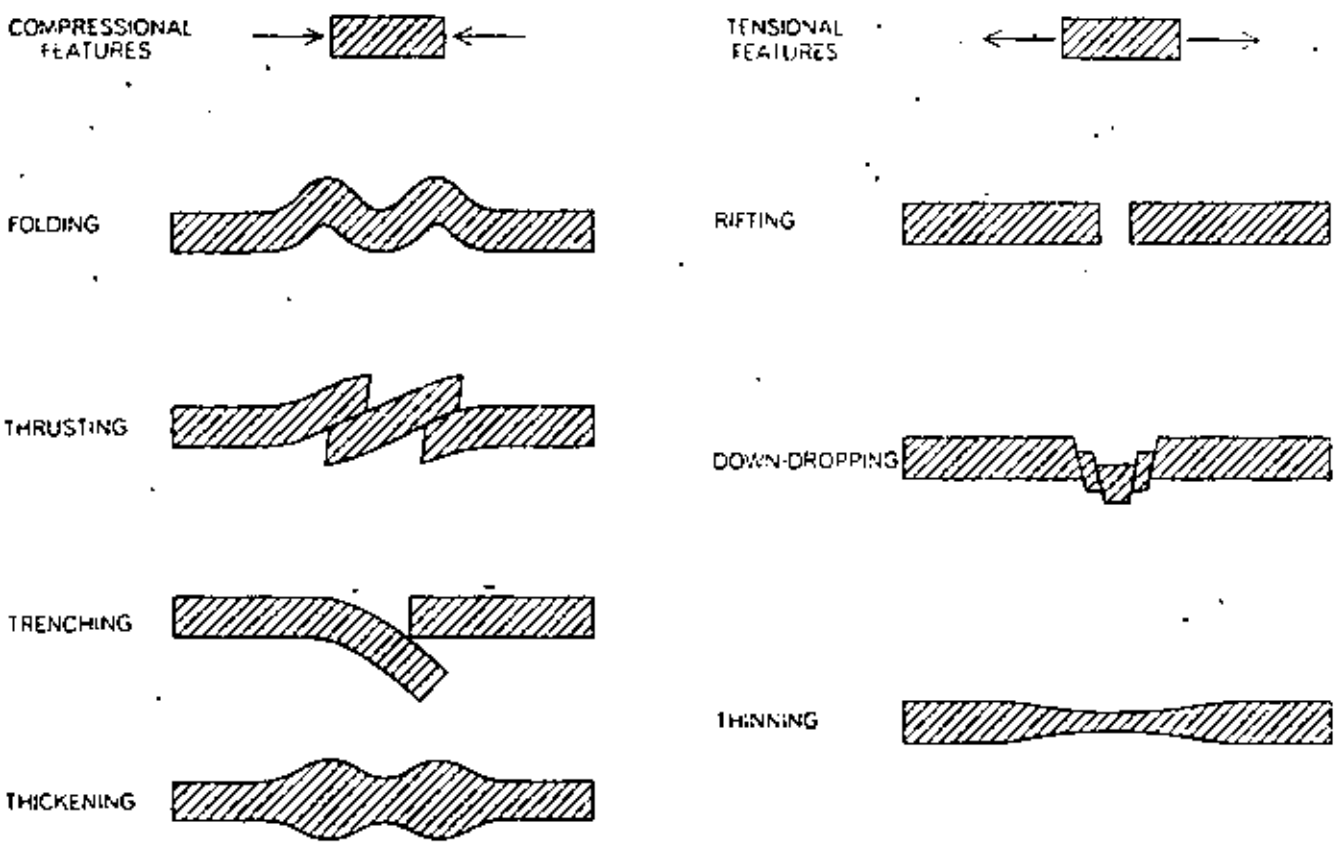

RESPONSE OF CRUSTAL PLATES to compression (*left*) and tension (*right*) accounts for most geologic features. According to the recently developed concept of plate tectonics, the earth's mantle is covered by huge, rigid plates that can be colliding, sliding past one another or rifting apart. The rifting usually occurs in the ocean floor. The San Andreas fault marks the location where two plates are sliding past each other. Plate tectonics helps to explain how the continents have drifted into their present locations.

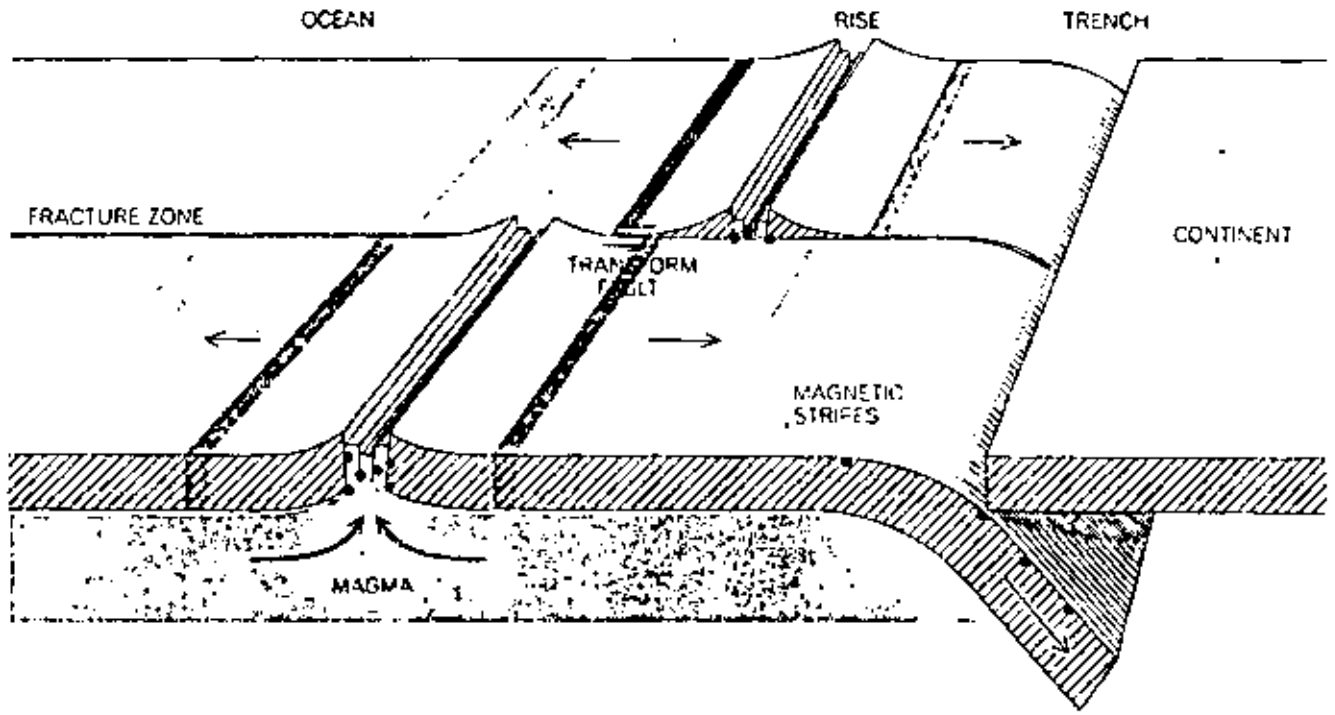

RIFT IN OCEAN FLOOR (*color*) initiates three major features of oceanic plate tectonics. The rift is bordered by a rise or ridge created by magma pushed up from the mantle below. The magma solidifies with a magnetic polarity corresponding to that of the earth. When, at long intervals, the earth's polarity reverses, the polarity of newly formed crust reverses too, resulting in a sequence of magnetic "stripes." A trench results when an oceanic plate meets a continental plate. A fracture zone and transform fault result when two plates move past each other. Earthquakes (*dots*) accompany these tectonic processes. The earthquakes in the vicinity of a rise and along a transform fault are shallow. Deep-focus earthquakes occur where a diving oceanic plate forms a trench.

Erosion destroys this kind of evidence very quickly. By matching up distinctive rock units that have been broken up and moved with respect to each other it is possible to document offsets of tens to hundreds of miles. A sedimentary basin often holds debris that could not possibly have been derived from any of the local mountains; matching up these basins with the appropriate source region on the other side of the fault can provide evidence of still larger displacements. When these various kinds of information are combined, one obtains a rate of about half an inch per year for motion on the San Andreas fault in northern and central California over the past several tens of millions of years.

This is much less than the 2½ inches per year that is inferred for the rate of separation of Baja California and mainland Mexico and the rate that is inferred from seismological studies in southern California. There are several possible explanations for the discrepancy. Northern and southern California may be moving at different rates; this seems unlikely since they are both attached to the same Pacific plate. On the other hand, part of the compression in the transverse ranges may result from a differential motion between the two parts of the state. Another possibility is that all of the relative motion between the North American plate and the Pacific plate is not being taken up by the San Andreas fault or even by the San Andreas fault system but extends well inland. The fracture zones of the Pacific seem to affect the geology of the continent for a distance of at least several hundred miles.

The Great Central Valley and the Sierra Nevada lie between two major fracture zones that abut the California coast: the Mendocino fracture zone and the Murray fracture zone. The transverse ranges, the Mojave Desert and the Garlock fault are all in line with the Murray fracture zone. Recent volcanism lines up with the extensions of the Clarion fracture zone and the Mendocino fracture zone. The basin and range geological province of the western U.S., a region of crustal tension and much volcanism, may represent a broad zone of deformation between the Pacific plate and the North American plate proper. Seismic activity is certainly spread over a large, diffuse region of the western U.S.

Although the subject has been quite controversial, most geologists are now willing to accept large horizontal displacements on the faults in California, particularly the San Andreas. Displacements as large as 450 miles of right-lat-

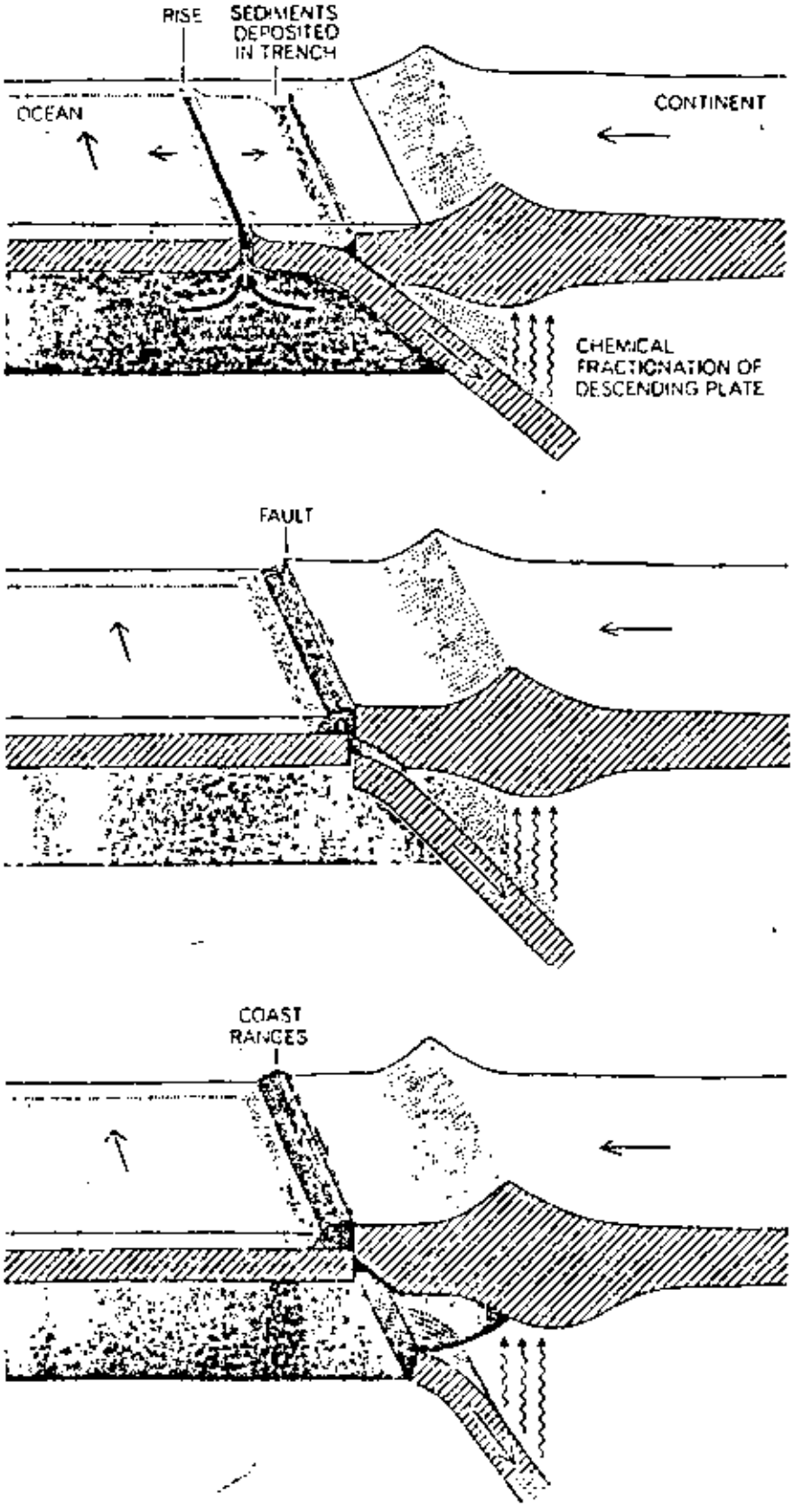

INTERACTION BETWEEN RISE AND TRENCH leads to mutual annihilation. The trench, formed as the oceanic plate dives under the continental plate, slowly fills with sediments carried by rivers and streams (*top*). Meanwhile the melting of the descending slab adds new material to the continent from below. When the axis of the rise reaches the edge of the continent, the flow of magma into the rift is cut off and trench sediments are scraped onto the western (that is, left) part of the oceanic plate (*middle*). The descending plate disappears under the continent and the sediments travel with the oceanic plate (*bottom*). The northern part of the San Andreas fault may have been formed in this way.

eral slip have been proposed for the northern segment of the fault. Displacements on the southern San Andreas fault are put at no more than 300 miles. This discrepancy has been puzzling to geologists. My own conclusion is that the part of northern and central California west of the San Andreas fault has moved northwest more than 700 miles and that the southern San Andreas fault has slipped about 300 miles, which makes the apparent discrepancy even worse. The discrepancy disappears if one drops the concept of a single San Andreas fault and admits the possibility that the two segments of the fault were initiated at different times.

The two-fault hypothesis is supported by straightforward extrapolation of the record on the ocean floor. The two San Andreas faults formed at different times, in different ways and may be moving at different rates. The record indicates that the western part of North America caught up with a section of the East Pacific rise somewhere between 25 million and 30 million years ago. Before the collision a deep oceanic trench existed off the coast such as now exists farther to the south off Central America and South America. The trench had existed for many millions of years, receiving sediments from the continent; subsequently the sediments were carried down into the mantle by the descending oceanic plate, which was diving under the continent. Based on what we know of trench areas that are active today one can assume that the plate sank to 700 kilometers and that the process was accompanied by earthquakes with shallow, intermediate and deep foci.

The Origin of Continents

Let us examine a little more closely what happens when an oceanic rise, the source of new oceanic crust, approaches a trench, which acts as a sink, or consumer of crust. Evidently the rise and the trench annihilate each other. The oceanic crust and its load of continental debris, which was formerly in the trench, rise because the crust is no longer connected to the plate that was plunging under the continent. The trench deposits are so thick they eventually rise above sea level and become part of the continent. The deposits are still attached to the oceanic plate, however, and travel with it (*see illustration on preceding page*).

In the case of the Pacific plate off California the deposits move northwest with respect to the continent. This is the stuff of coastal California north of Santa Barbara, particularly the Coast Ranges. According to this view, the northern segment of the San Andreas fault was born at the same time as northern California. The rise and the trench initially interacted near San Francisco, which then was near Ensenada in Baja California. Ensenada in turn was near the northern end of the Gulf of California, which was then closed.

The tectonics and geologic history of California, and in fact much of the western U.S., are now beginning to be understood in terms of the new ideas developed in the theories of sea-floor spreading, continental drift and plate tectonics. Many of the basic concepts were laid down by the late Harry H. Hess of Princeton and Robert S. Dietz of the Environmental Science Services Administration. Tanya Atwater of the University of California at San Diego and Warren Hamilton of the U.S. Geological Survey and their colleagues have made particularly important contributions by applying the concepts of plate tectonics to continental geology. We now know that the outer layer of the earth is immensely mobile. This layer, the lithosphere, is relatively cold and

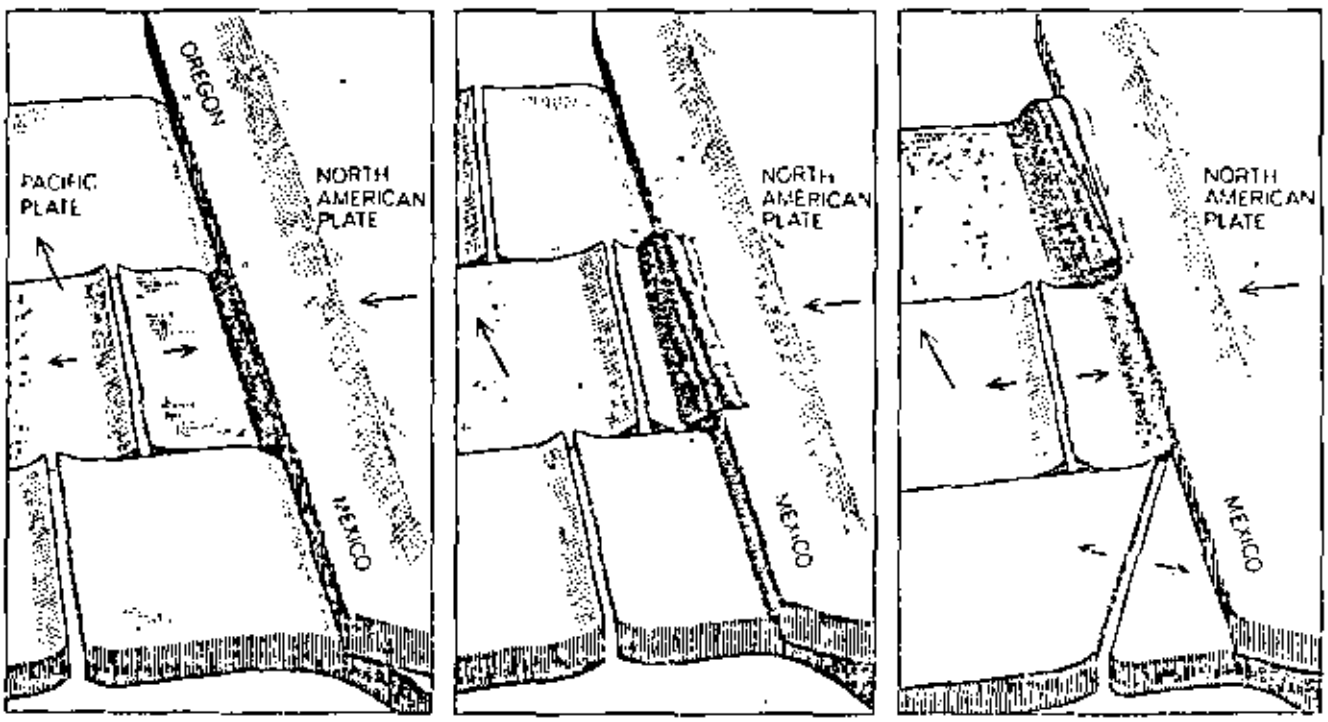

FORMATION OF SAN ANDREAS FAULT SYSTEM is depicted schematically in the six diagrams on these two pages. Some 30 million years ago (*left*) an oceanic rise system lay off the west coast of North America, which was carried by a plate moving toward the rise crests. The continental plate overrides the Pacific plate, producing a long trench. Meanwhile the entire Pacific plate is moving northwest. After a few million years (*right*) the rise nearest the continent is shut off. The trench by now has been filled with material eroded from the continent. These deposits will later become the California Coast Ranges. NORTHERN SECTION of San Andreas fault is created when the former trench deposits become attached to the northward-moving Pacific plate (*left*). The San Andreas fault lies between the two opposed arrows indicating relative plate motions. Meanwhile to the south a tilted rise crest

rigid and slides around with little resistance on the hot, partially molten asthenosphere.

Where the crust is thick, as it is in continental regions, the temperatures become high enough in the crust itself to cause certain types of crustal rocks to lose their strength and to offer little resistance to sliding. There is thus the possibility that the upper crust can slide over the lower crust and that the moving plate can be much thinner than is commonly assumed in plate-tectonic theory. The molten fraction of the asthenosphere, called magma, rises to the surface at zones of tension such as the mid-oceanic rifts to freeze and form new oceanic crust. The new crust is exposed to the same tensional forces (presumably gravitational) that caused the rift in the first place, therefore it rifts in turn and subsequently slides away from the axis of the rise. In addition to providing the magma for the formation of new crust, the melt in the asthenosphere serves to lubricate the boundary between the lithosphere and the asthenosphere and effectively decouples the two. The rise is one of the types of boundary that exist between lithospheric plates and is the site of small, shallow tensional earthquakes.

When two thin oceanic lithospheric plates collide, one tends to ride over the other, the bottom plate being pushed into the hot asthenosphere. The boundary becomes a trench. When the lower plate starts to melt, it yields a low-density magma that rises to become part of the upper plate; this magma becomes the rock andesite, which builds an island arc on what is to become the landward, or continental, side of the trench. (The rock takes its name from the Andes of South America. Mount Shasta in California is primarily andesite, as are the island arcs behind the trenches that surround the Pacific.) The thickness of the crust is essentially doubled as a result of the underthrusting. The material remaining in the lower plate is now denser than the surrounding material in the asthenosphere, both because it has lost a low-density fraction and because it is colder; thus it sinks farther into the mantle. In some parts of the world the downgoing slab can be tracked by seismic means to 700 kilometers, where it seems to bottom out. By this process new light material is added to the crust and new dense material is added to the lower mantle. A large part of what comes up stays up; a large part of what goes down stays down.

The introduction of chemical fractionation and a mechanism for "unmixing" makes the process different from the one customarily visualized, in which gigantic convection cells carry essentially the same material in a continuous cycle. The new process is able to explain in a convincing way how continents are formed and thickened. As the continent thickens and rises higher because of buoyancy, erosional forces become more effective and dump large volumes of continental sediments into the coastal trenches. A portion of the sediments is ultimately dragged under the continent to melt and form granite. The light granitic magma rises to form huge granitic batholiths such as the Sierra Nevada. A batholith is a large mass of granitic rock formed when magma cools slowly at great depth in the earth's crust. It is carried to the surface by uplifting forces and exposed by erosion.

The concept of rigid plates moving around on the earth's surface and interacting at their boundaries has been remarkably successful in explaining the evolution of oceanic geology and tectonics. The oceanic plates seem to behave rather simply. Tension results in a rise, compression results in a trench and lateral motion results in a transform fault

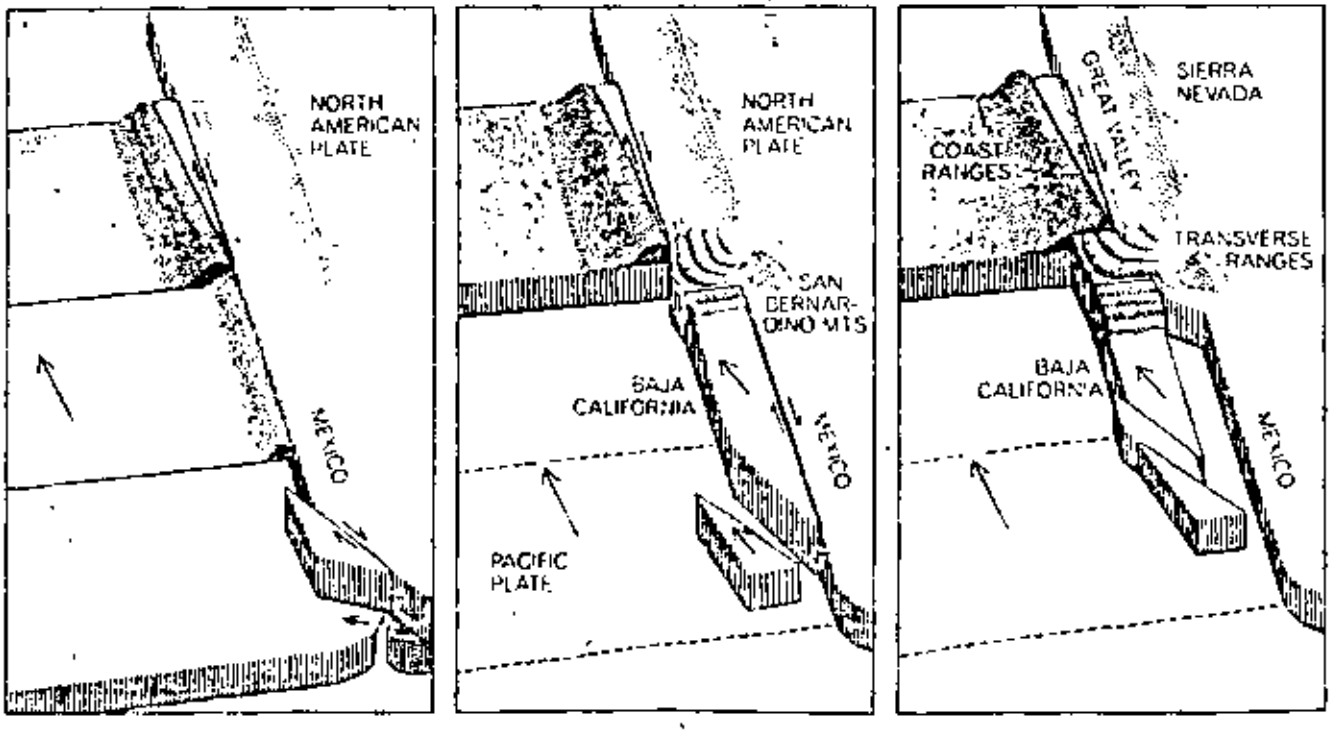

(not yet visible in the first pair of diagrams) is ready to encounter the continent end on at a break in the coastline south of Baja California. The collision (*right*) breaks off a part of the Baja California peninsula, which becomes attached to the Pacific plate and starts its journey to the northwest. SOUTHERN SECTION of San Andreas fault is now fully activated (*left*) as the Baja California block begins sliding past the North American plate and collides with deeply rooted structures to the north, the Sierra Nevada and San Bernardino Mountains, which deflect the block to the west. More of Baja California breaks loose, opening up the Gulf of California. As Baja California continues to move northwestward (*right*) the Gulf of California steadily widens. The compression at the north end of the Baja California block creates the transverse ranges, which extend inland from the vicinity of present-day Santa Barbara.

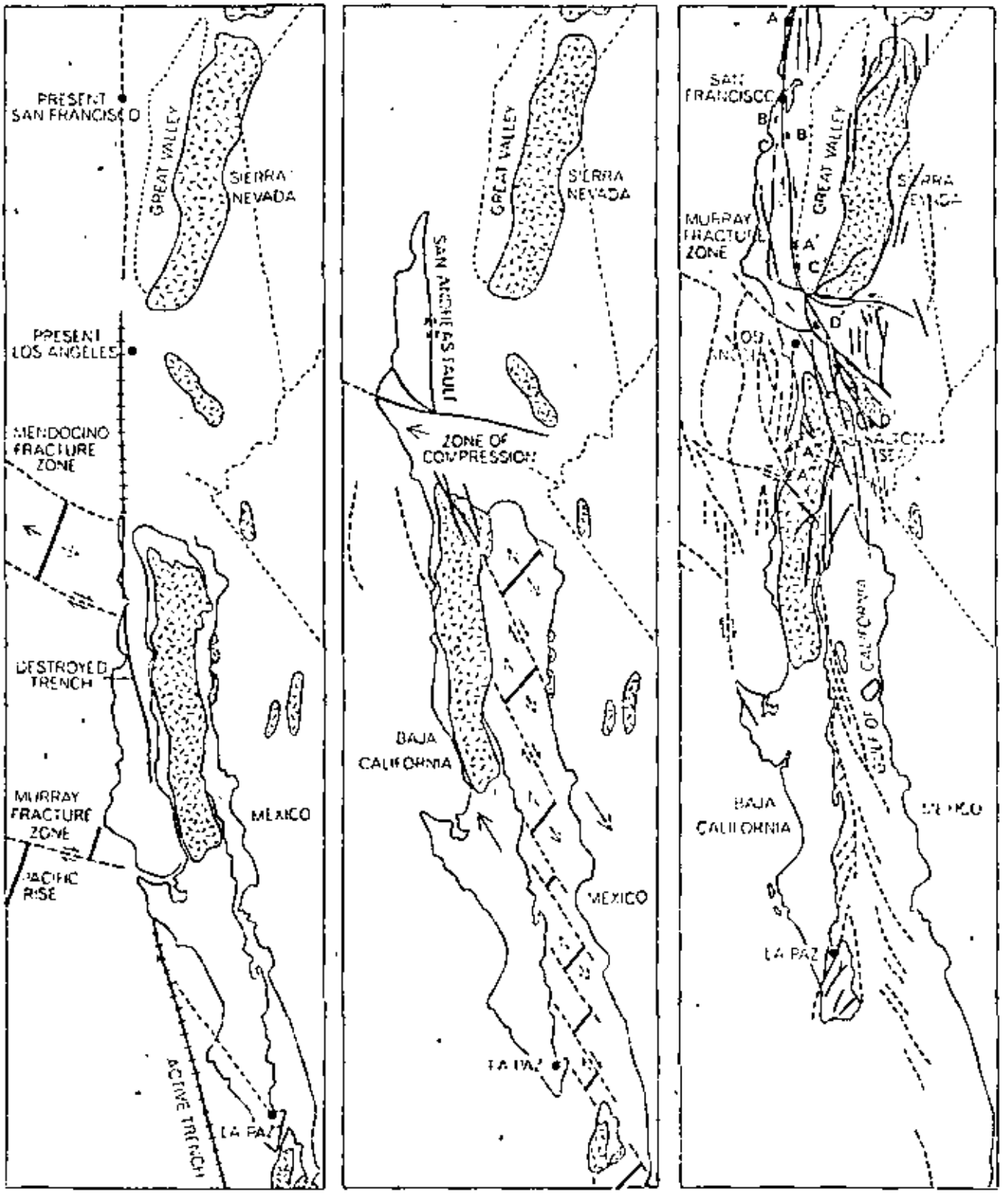

EARLY AND LATE STAGES in the history of the San Andreas fault are depicted. Twenty-five million years ago *(left)* Baja California presumably nestled against mainland Mexico. The first section of oceanic rise between the Murray fracture zone and the Pioneer fracture zone has just collided with the continent. Trench deposits are uplifted and become part of the Coast Ranges of California. The block containing the present San Francisco area *(dark color)* is about to start its long northward journey. A block immediately to the east *(light color)* becomes attached to the Pacific plate and eventually is jammed against the San Bernardino Mountains. Three million years ago *(middle)* the Gulf of California has started to open. As the peninsula moves away from mainland Mexico a series of rifts appear, fill with magma and are offset by numerous fractures. Baja California may have been torn off in one piece or in slivers. Southwest California and Baja California today *(right)* continue to slide northwest against the North American mainland. The illustration shows major fault systems and offshore fracture zones. On the basis of unique rock formations geologists infer that the Los Angeles area has moved northwest about 150 miles (*C* to *D*) in the past 20 million years or less. Other studies indicate that the Palo Alto region has been carried about 200 miles (*C* to *C'*). Coastal rocks to the north of San Francisco have been displaced at least 300 miles (*B* to *A*) and perhaps as much as 650 miles (*A'* to *A*) in the past 30 million years.

and a fracture zone [*see bottom illustration on page 146*]. The interaction of oceanic and continental plates or of two continental plates is apparently much more complicated, and this is one reason the new concepts were developed by study of the ocean bottom rather than continental geology.

The boundary between two oceanic plates can be a deep oceanic trench, an oceanic rise or a strike-slip fault depending on whether the plates are approaching, receding from or moving past each other. The forces involved are respectively compressional, tensional and shearing. When a thick continental plate is involved, compression can also result in high upthrust and folded mountain ranges. The Himalayas resulted from the collision of the subcontinent of India with Asia. I shall show that the transverse ranges in California were formed in a similar way. Tension can result in a wide zone of crustal thinning, normal faulting and volcanism; it can also create a fairly narrow rift of the kind found in the Gulf of California and the Red Sea [*see top illustration on page 148*].

The interaction of western North America with the Pacific plate has led to large horizontal motions along the San Andreas fault, to concentrated rifting as in the Salton Sea trough and the Gulf of California, to diffuse rifting and normal faulting accompanied by volcanism in the basins and range province of California, Nevada, Utah and Arizona, to large vertical uplift by overthrusting as in the transverse ranges north and west of Los Angeles, to the generation of large batholiths such as the Sierra Nevada and to the incorporation of deep-sea trench material on the edge of the continent. Ultimately the geology, tectonics and seismicity of California can be related to the collision of North America with the Pacific plate.

Most of the Pacific Ocean is bounded by trenches and island arcs. Trenches border Japan, Alaska, Central America, South America and New Zealand. Island arcs are represented by the Aleutians, the Kuriles, the Marianas, New Guinea, the Tongas and Fiji. The arcs are themselves bordered by trenches. All these areas are characterized by andesitic volcanism and deep-focus earthquakes. Western North America is lacking a trench and has only shallow earthquakes, but the geology indicates that there was once a trench off the West Coast, and in fact there was once a rise. The present absence of a rise and a trench, the absence of deep-focus earthquakes and the existence of uplifted deep-sea sediments are all related.

Tracing back the history of the interaction of the Pacific plate with the North American plate, one is forced to conclude that the northern part and the southern part of the San Andreas fault originated at different times and in different ways. The northern part was evidently formed about 30 million years ago when a portion of rise between the Mendocino fracture zone and the Murray fracture zone approached an offshore trench bordering the southern part of North America. At that time the west coast of North America resembled the present Pacific coast of South America: there was a deep trench offshore, high mountains paralleled the coastline and large underthrusting earthquakes were associated with the downgoing lithosphere.

Origin of the Fault

As the rise approached the continent both the geometry and the dynamics of interaction changed [*see illustrations on pages 148 and 149*]. Depending on the spreading rate of the new crust generated at the rise and the rate at which the rise itself approaches the continent, the relative motion between the rise and the continental plate will decrease, stop or reverse when the rise hits the trench. The forces keeping the trench in existence will therefore decrease, stop or reverse, leading to uplift of the sedimentary material that has been deposited in the trench. In classical geologic terms these are known as eugeosynclinal deposits. Although they have been exposed to only moderate temperatures, they have been subjected to great pressures, both hydrostatic (owing to their depth of burial) and directional (owing to the horizontal compressive forces between the impinging plates). Eugeosynclinal sediments are therefore strongly deformed and become even more so as they are contorted and sheared during uplift. Much of the western edge of California and Baja California is underlain by this material, called the Franciscan formation. The formation is physically attached to the Pacific plate and is therefore moving northwest with respect to the rest of North America. The present boundary is the northern part of the San Andreas fault. Today this section of the San Andreas system extends from Cape Mendocino, north of San Francisco, to somewhere south and east of Santa Barbara, near the beginning of the great bend of the San Andreas fault, where the San Andreas and the Garlock faults intersect.

Meanwhile, 30 million years ago, another section of the rise south of the Murray fracture zone was still offshore, together with an active trench. Baja California was still attached to the mainland of Mexico and the Gulf of California had not yet opened up. The southern part of the San Andreas fault had not yet been formed.

The abrupt change in the direction of the coastline south of the tip of Baja California suggests that here the rise approached the continent more end on than broadside. A sliver of existing continent was welded onto the Pacific plate and rifted away from Mexico, thus forming Baja California and the Gulf of California. Thereafter Baja California participated in the northwesterly motion of the Pacific plate, with the result that the Gulf of California widened progressively with time.

About five million years were required for northern California, which had broken off from Baja California, to be carried about 200 miles to the northwest. At the end of that time the Gulf of California and the Salton Sea trough had not yet opened. The faults that delineate the major geologic blocks in southern California had not yet been activated. The block bearing the San Gabriel fault, now north of San Fernando, occupied the future Salton Sea trough. The transverse ranges will eventually be formed from the Santa Barbara, San Gabriel and San Bernardino blocks by strong compression from the south when Baja California breaks loose from mainland Mexico. This also opens up the Gulf of California and the Salton Sea trough.

As northern California is being carried away from Baja California by the Pacific plate another segment of oceanic rise south of the Murray fracture zone approaches the southern half of Baja California, where the situation described above is repeated except that the rise crest encounters a sharp bend in the coastline and the trench hits just south of the tip of the peninsula. Now instead of approaching the continent more or less broadside the rise approaches the continent end on. Mainland Mexico is still decoupled from that part of the Pacific plate to the west of the rise by the rise and the trench. Baja California, however, is now coupled to the northwestward-moving Pacific plate and Baja California is torn away from the mainland. This happened between four and six million years ago. Magma from the upper mantle wells up into the rift, forming a new rise that works its way north into the widening gulf. Alternatively, the entire peninsula of Baja California could have broken off from the mainland at the

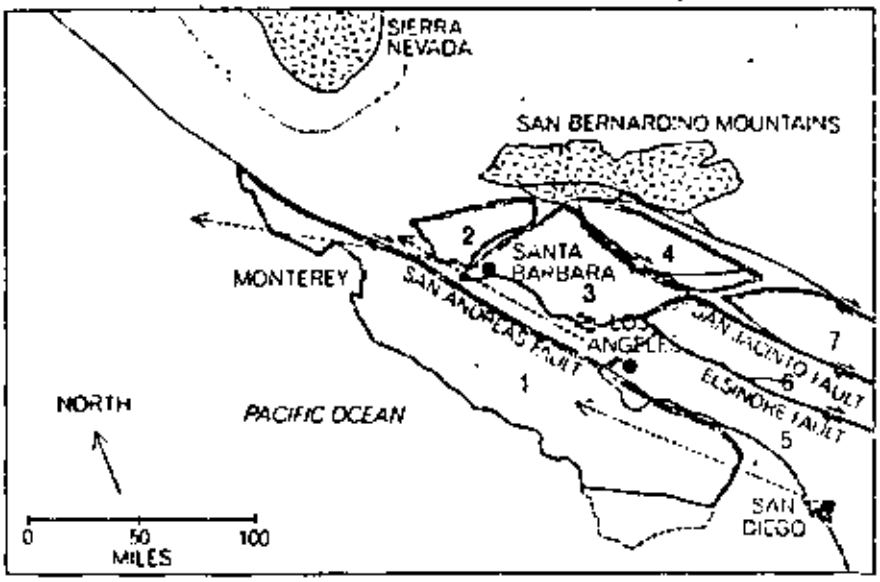

SEQUENCE OF SIMPLIFIED VIEWS shows the movement of major blocks in southern California over the past 12 million years. In the first view (above) the Gulf of California has not yet appreciably opened but the block carrying the Coast Ranges (1) has started to move rapidly northwest with activation of northern portion of San Andreas fault. Dots show origin and arrows show displacement of San Diego, Los Angeles and Santa Barbara.

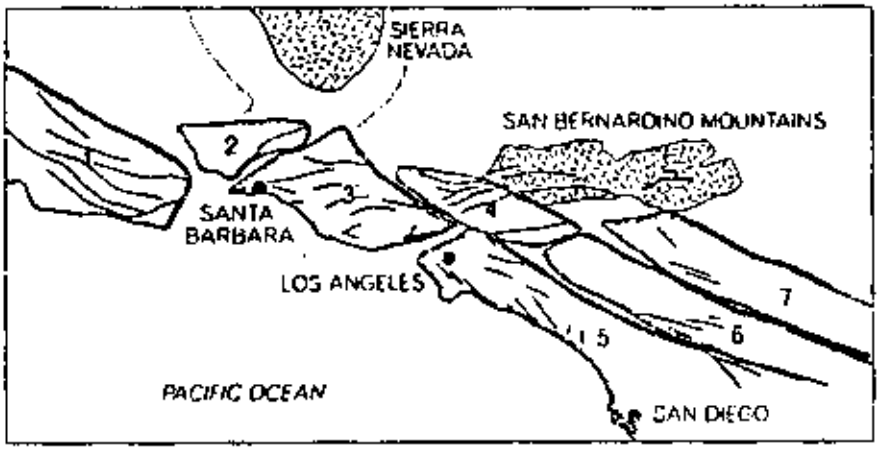

TWO MILLION YEARS AFTER ACTIVATION of the southern portion of the San Andreas fault four blocks (2, 3, 4, 7) have been forced against the deep roots of the Sierra Nevada and San Bernardino Mountains. Compressive forces create the transverse ranges. Meanwhile the block carrying the Coast Ranges (1) has been carried far to the northwest.

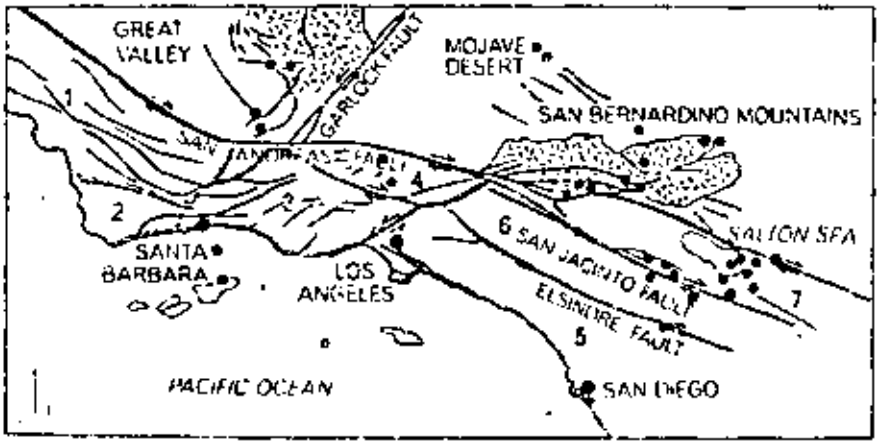

GEOLOGY OF SOUTHERN CALIFORNIA TODAY is dominated by compressive forces operating in the big bend of the San Andreas fault, which connects the southern and northern parts of the system. Colored dots show the location of earthquakes in the recent past.

same time. As the peninsula, including parts of southern California, moves north it collides with parts of the continent that are still attached to the main North American plate. This results in compression, overthrusting and shearing and the eventual formation of the transverse ranges.

The southern part of the San Andreas fault system was therefore formed by the rifting off of a piece of continent. Today it represents the boundary between two parts of the continental plate that are moving with respect to each other. This part of the San Andreas fault was formed well east, or inland, of the southward projection of the northern San Andreas.

The northerly march of southern California and Baja California seems to have been blocked when the moving plate encountered the thick continental crust to the north, particularly the massive granitic San Bernardino mountain range, which includes the 11,485-foot San Gorgonio Mountain. Since large and high mountain ranges have deep roots, the crust in this region is probably much thicker than normal, perhaps as thick as 50 kilometers. Earthquakes in this region are all shallower than 20 kilometers, which may be the thickness of the sliding plates. The blocks veer westward and are strongly overthrust as they attempt to get around the obstacle; this movement generates the big bend in the San Andreas fault system. The deflected blocks eventually join up with the northern California block.

Earthquake Country

From a social and economic point of view earthquakes are one of the most important manifestations of plate interaction. From a scientific point of view they supply a third dimension to the study of faults and the nature of the interactions between crustal blocks, including the stresses involved and the nature of the motions.

Seismologists at the University of California at Berkeley and at the Cal Tech Seismological Laboratory have been keeping track of earthquake activity in California for more than 40 years. Both groups have installed arrays of seismometers that telemeter seismic data to their laboratories for processing and dissemination to the appropriate public agencies. During the 36-year period 1934 through 1969 there were more than 7,300 earthquakes with a Richter magnitude of 4 or greater in southern California and adjacent regions [*see illustration on page 154*]. Many thousands more earthquakes of smaller magnitude are

routinely located and reported in the seismological bulletins. Although damage depends on local geological conditions and the nature of the earthquake, a rough rule of thumb is that a nearby earthquake of magnitude 3.5 or greater can cause structural damage. The average annual number of earthquakes of magnitude 3 or greater in southern California recorded since 1934 is 210; the number in any one year has varied from a low of 97 to a high of 391. The strongest earthquake in this period was the Kern County event of magnitude 7.7 in 1952. The aftershocks of that event increased the total number of events for several years thereafter.

In general the larger the earthquake, the greater the displacement across a fault and the greater the length of fault that breaks. The great earthquakes of 1906 and 1857 respectively caused large displacements across the northern and central parts of the San Andreas fault and relieved the accumulated strain in these areas. The accumulation of strain in southern California is relieved mainly by slip on a series of parallel faults and by overthrusting on faults at an angle to the main San Andreas system; that is what happened in the Kern County and San Fernando earthquakes. The major east-west-trending transverse ranges were formed in this way. In the process deep-seated ancient rocks were uplifted and exposed by erosion.

Another seismically active area associated with major faults is south of the Mojave Desert near San Bernardino, where the faults show a sudden change in direction. The central part of the Mojave Desert is also moderately active. This is consistent with the idea that the sliding lithosphere is diverted by the San Bernardino Mountains. Faults and evidence of relatively recent volcanic events abound in the area. The northern part of Baja California is also quite active. An interesting feature of seismicity maps of southern California is the alignment of earthquakes in zones that trend roughly northeast-southwest, approximately at right angles to the major trend of the San Andreas system.

The map on the next page shows that the San Andreas fault itself has played only a small role in the seismicity of southern California over the past 30-odd years. One must not forget, however, that the great earthquake of 1857 probably broke the San Andreas fault for about 180 miles northwest and southeast from the epicenter. That epicenter is thought to have been near Fort Tejon, which is close to the projected intersection of the Garlock and San Andreas

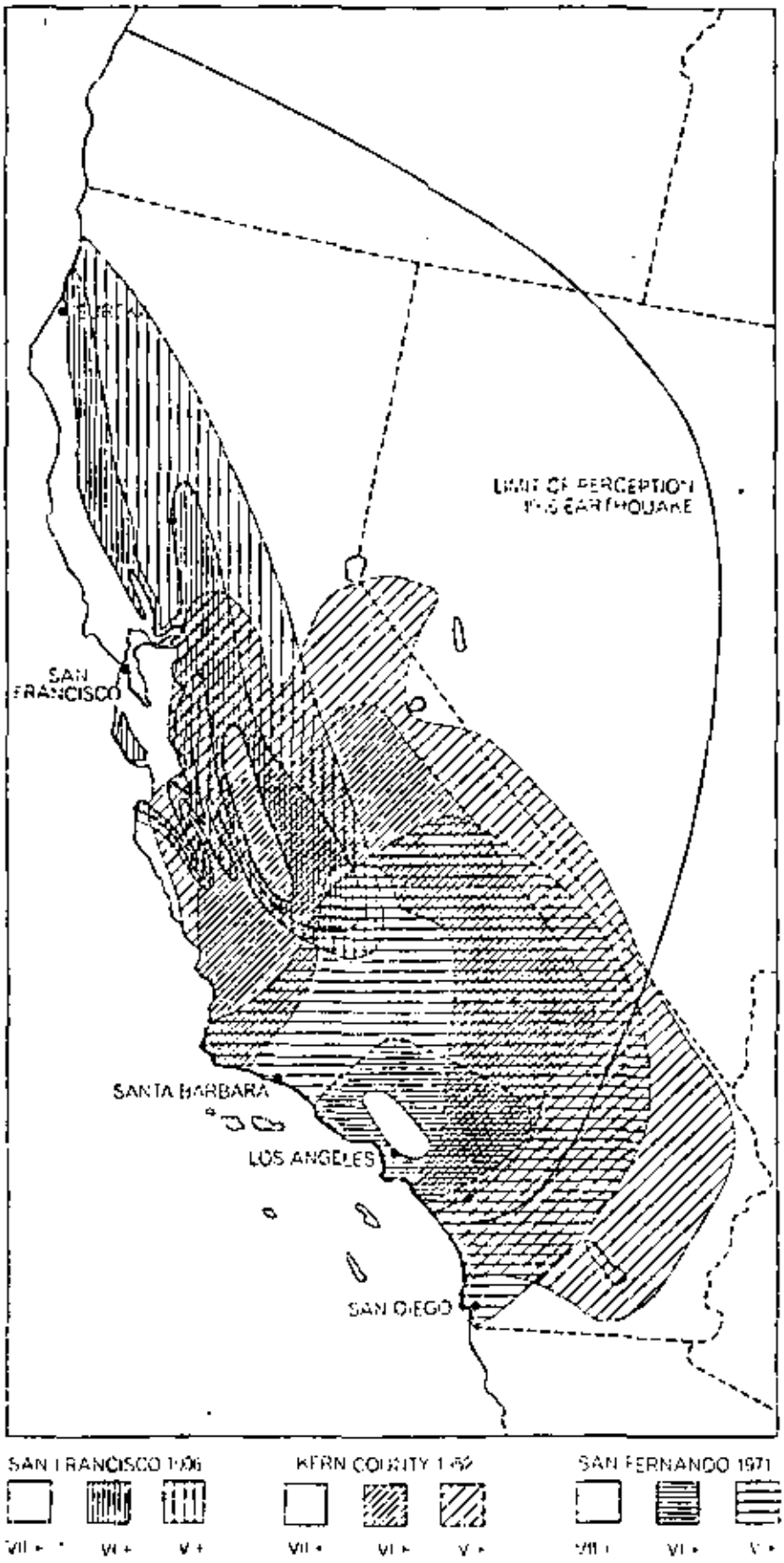

ISOSEISMAL CONTOUR MAP shows the pattern and intensity of ground-shaking produced by the 1906 San Francisco earthquake (magnitude 8.3), the 1952 Kern County earthquake of magnitude 7.7 and the 1971 San Fernando earthquake of magnitude 6.6. The Roman numerals indicate levels of perceived intensities as defined by the modified Mercalli scale. A short description of each level in the scale appears in the text on page 155.

faults; the actual location of the epicenter is uncertain by hundreds of miles because there were no seismic instruments in those days. Since that time this part of southern California has been remarkably quiet and seems to be locked, generating neither earthquakes nor creep. Activity along the San Andreas fault picks up near Cushing, which is about midway between Bakersfield and San Francisco. Alignments of earthquakes are apparent along the San Jacinto and Imperial faults in the Salton Sea trough near the Mexican border. Although these faults lie west of the main San Andreas fault, they are part of the San Andreas system. The White Wolf fault, which is northwest of and parallel to the Garlock fault, has also been quite active, particularly after the Kern County earthquake, which occurred on this fault. The White Wolf fault lines up with the Santa Barbara Channel area, which has similarly been quite active.

One way to quantify the seismicity of southern California is to count the number of earthquakes per year per 1,000 square kilometers and compare this figure for the world as a whole. For example, southern California averages one earthquake of magnitude 3 or greater per year per 1,000 square kilometers. Thus within the entire region there are about 200 such earthquakes per year. The rate for earthquakes of magnitude 6.6, the size of the San Fernando earthquake, is about one every five or six years. The actual rates, however, vary considerably from year to year and depend somewhat on the time interval of the sample. The number of earthquakes decreases rapidly with size, and the average recurrence interval is not well established for the larger earthquakes. Southern California is about 10 times more active seismically than the world as a whole, which is simply to say that California is earthquake country.

Although certain areas in southern California are relatively free of earthquakes, none is immune from their effects. One of the largest quiet areas is the western part of the Mojave Desert wedge. This is surprising because the region is bounded on the northwest and southwest by areas that are obviously under large compression, as is shown by the upthrust mountains in the transverse and Tehachapi ranges and the large overthrust earthquakes that occurred in Kern County and San Fernando. It appears that the region is being protected from the northwesterly march of the southern California–Baja California block by the San Bernardino batholith and may represent a stagnation area in the lee of the mountains. Only a small number of earthquakes are centered near San Diego, although the larger earthquakes in northern Baja California and in the mountains between San Diego and the Salton Sea are felt in San Diego. The Great Central Valley north of Bakersfield and the eastern part of the Sierra Nevada are fairly inactive, as is a large area north of Santa Barbara in the Coast Ranges.

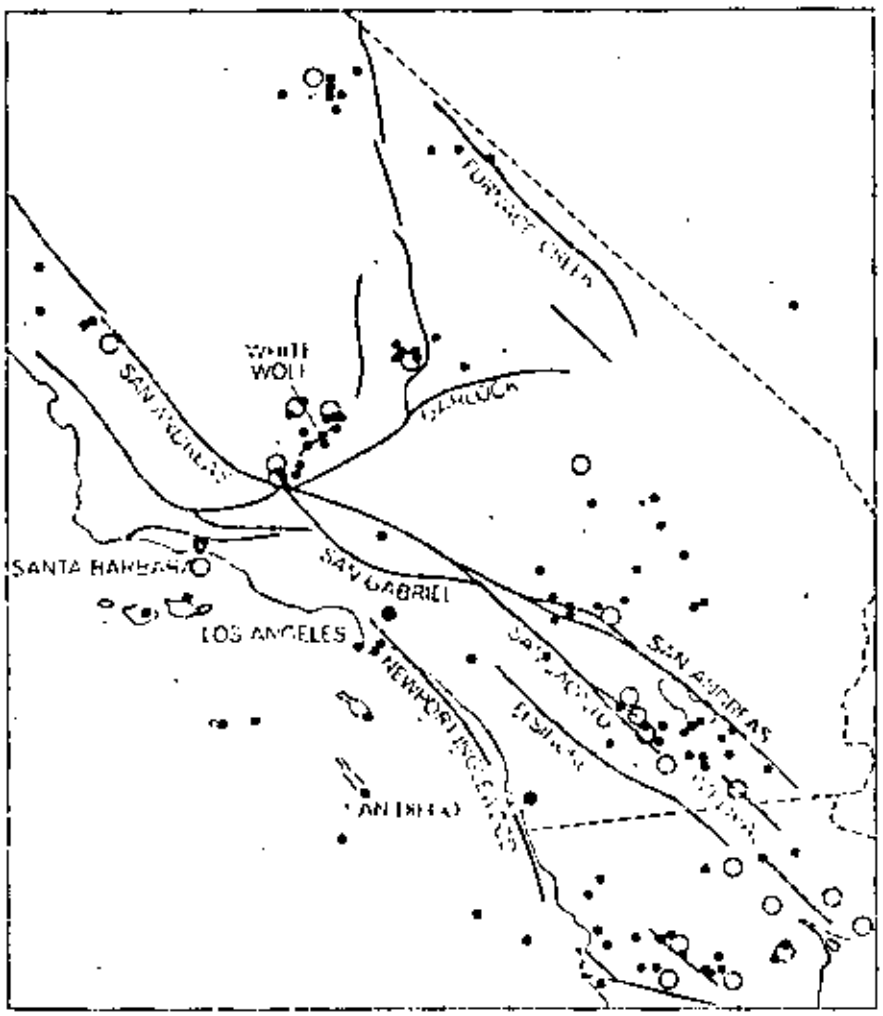

THIRTY-SIX-YEAR EARTHQUAKE RECORD shows the epicenters of all events of magnitude 3 or greater recorded in southern California and in the northern part of Baja California from 1934 through 1969. The epicenter is the point on the earth's surface above the initial break. Dots show earthquakes between 3 and 5.9 in magnitude. Open circles indicate earthquakes of magnitude 6 or greater. The hypocenter, the point of the initial break in the earth's crust, is often many miles below the surface in thrust-type earthquakes, a type frequently observed in this region. In the 36-year period southern California and adjacent regions experienced more than 7,300 earthquakes with a magnitude of 3 or more. Earthquakes are about 10 times more frequent in this area than they are in the world as a whole.

Magnitude and Intensity

It is somewhat deceptive to plot earthquakes as small points on a map. The points represent the epicenter: the point on the surface above the initial break. Once the break is started it can continue, if the earthquake is a major one, for hundreds of miles. Earthquakes of the thrust type, which result from a failure in compression, typically first break many miles below the surface; the surface break and maximum damage can be 10 miles or more from the epicenter. The distance over which strong shocks were felt during three large California earthquakes in this century (1906, 1952 and 1971) can be represented by plotting isoseismals: lines of equal intensity [*see illustration on preceding page*]. The shape of the pattern varies with the type of earthquake and with the nature of the local geology; structures on deep sedimentary basins or on unconsolidated fill get a more intense shaking than structures on bedrock. The isoseismals of the

San Francisco earthquake are long and narrow, both because of the orientation of the fault and the length of the faulting and because of the northwest-southeast trend of the valleys. The orientation of the valleys in turn is controlled by the orientation of the San Andreas fault.

The public and the news media are confused about the various measures of the size of an earthquake. There are many parameters associated with an earthquake; they are usually regarded as fault parameters. They include the length, depth and orientation of the fault, the direction of motion, the rupture velocity, the radiated energy, the causal stresses and their orientation, the stress drop (which is related to the strength or the friction along the fault), the energy spectrum, the amount of offset or displacement and the time history of the motion. Most of these parameters can be estimated from seismic records, even from signals recorded several thousand kilometers from the earthquake. To obtain high precision, however, one needs records from many well-distributed seismic stations together with field observations at the site of the earthquake.

The magnitude on the Richter scale is a number assigned to an earthquake from instrumental readings of the amplitude of the seismic waves on a standard seismometer, the Wood-Anderson torsion seismometer. The amplitude must be suitably corrected for spreading and attenuation in the earth, and for instrumental response if a non-standard instrument is used. The magnitude is closely related to the energy of the earthquake, the single most important quantity by which earthquakes can be ranked one against another. If all the corrections are adequately made, a seismologist anywhere in the world will assign the same magnitude. In practice, because of the complicated radiation pattern of earthquakes and because of the distortion of the waves traveling through the earth, the initial magnitude assigned by various observatories may differ slightly. The magnitude scale is logarithmic and is open-ended at both ends. It is not a scale with a maximum value of 10, as is often reported in the press, and negative magnitudes are routinely measured by seismologists working on microearthquakes.

The intensity scale was developed for engineering purposes and is a qualitative measure of the intensity of ground vibration and structural damage. These qualitative assessments are assigned Roman numerals from I to XII. Unlike the magnitude of an earthquake, the intensity varies with distance and depends on the nature of the local ground. In general alluvial valleys, soft sediments and areas of uncompacted fill will magnify ground shaking and will register higher intensities than adjacent areas on solid rock.

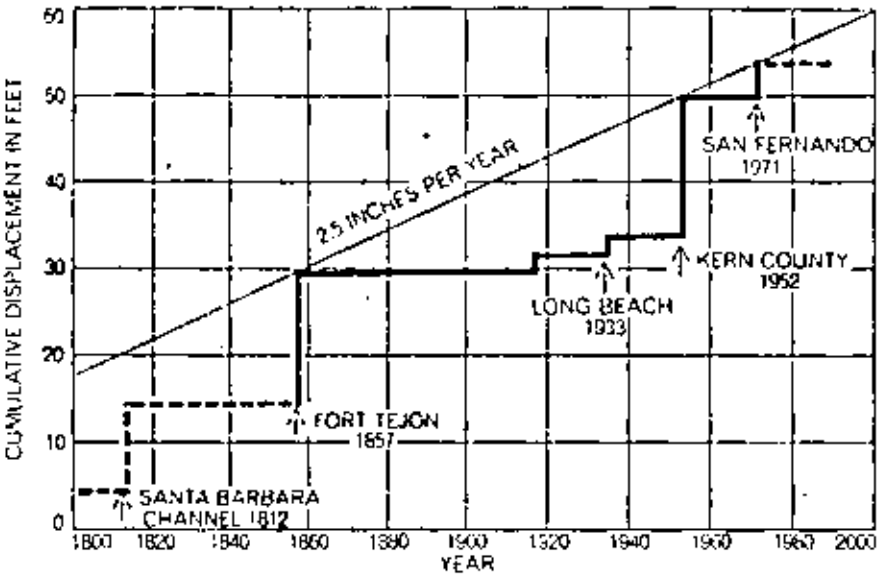

CUMULATIVE DISPLACEMENTS directly related to earthquakes indicate that southern California west of the San Andreas fault system is sliding northwestward at an average rate of 2½ inches per year. Major earthquakes relieve stresses that have built up over decades.

The intensity scale in common usage today is the Modified Mercalli Intensity Scale. The following characterizations of intensity, abridged from longer descriptions, indicate the kind of observations on which the Mercalli scale is based:

I. Not felt except by a very few under special circumstances. Birds and animals are uneasy, trees sway; doors and chandeliers may swing slowly.

II. Felt only by a few persons at rest, particularly on the upper floors of buildings.

III. Felt indoors, but many people do not recognize as an earthquake. Vibrations like the passing of light trucks. Duration of the shaking can be estimated.

IV. Windows, dishes and doors rattle. Walls make creaking sounds. Sensation like the passing of heavy trucks. Felt indoors by many, outdoors by few.

V. Felt by nearly everyone, many awakened. Small unstable objects are displaced or upset; plaster may crack.

VI. Felt by all; many are frightened and run outdoors. Some heavy furniture is moved; books are knocked off shelves and pictures off walls. Small church and school bells ring. Occasional damage to chimneys, otherwise structural damage is slight.

VII. Most people run outdoors. Difficult to stand up. Noticed by drivers of automobiles. Damage is negligible in buildings of good design and construction, slight to moderate in well-built ordinary structures, considerable in poorly built or badly designed structures. Waves on ponds and pools.

Intensity VII corresponds to the general experience within five or 10 miles of the surface faults associated with the San Fernando earthquake of last February. The following intensity levels were experienced in a small area of the northern San Fernando Valley and would be widely experienced in more severe earthquakes.

VIII. Steering of automobiles affected. Frame houses move on foundations if not bolted down; loose panel walls are thrown out. Some masonry walls fall. Chimneys twist or fall. Damage is slight in specially designed structures, great in poorly constructed buildings. Heavy furniture is overturned.

IX. General panic. Damage is considerable in specially designed structures; partial collapse of substantial buildings. Serious damage to reservoirs and underground pipes. Conspicuous cracks in the ground.

X. Most masonry and frame structures are destroyed with their foundations. Some well built wooden structures are destroyed. Rails are bent slightly. Large landslides.

XI. Few, if any, masonry structures remain standing. Bridges are destroyed. Broad fissures in the ground. Rails are bent severely.

XII. Damage is nearly total. Objects are thrown into the air.

It is clear that the Mercalli intensity scale is people oriented, and one can as

41

timate the intensity from his own experience during an earthquake. The National Oceanic and Atmospheric Administration compiles information on intensities by mailing out questionnaires to a sample of the population living in an area that has experienced a sizable earthquake.

In order to obtain more exact information about the ground motions involved in earthquakes engineers have developed strong-motion accelerometers that automatically trigger and start to record when shaken severely. Most of these instruments are installed in the seismic areas of the U.S., with a particularly heavy concentration in and around Los Angeles. The instruments are expensive and must be located very close to an earthquake to provide useful data. More than 250 of the instruments were triggered during the San Fernando earthquake, and a wealth of engineering data will be provided by these records.

A strong-motion instrument records ground acceleration as a function of time. Accelerations are commonly reported as fractions of a g, the acceleration due to gravity at the earth's surface. One g is roughly 10 meters per second per second. In designing a building to withstand moderate earthquakes, engineers are concerned chiefly with the maximum accelerations, the period or frequency of shaking and the duration of shaking. Buildings in earthquake-hazard regions with stringent building codes are usually designed to withstand at least .1 g of acceleration; this corresponds to an intensity of about VII on the Mercalli scale.

Although there is no direct correlation between intensity and magnitude, the zone of destruction increases as the magnitude increases for shallow-focus earthquakes. In general the larger the magnitude of an earthquake, the longer the fault length, the larger the displacement across the fault and the longer the duration of shaking. The longer fault length alone accounts for much of the increased area of destruction. For example, the San Francisco earthquake of 1906 had an intensity of VII or greater out to a distance of 500 miles from the epicenter, and this may not have been the largest California earthquake in historic times. The San Francisco earthquake had a magnitude of 8.3. The 1952 Kern County earthquake (magnitude 7.7) had an intensity of VII or greater out to 50 miles. The recent San Fernando earthquake (magnitude 6.6) damaged older structures out to 25 miles. An earthquake of magnitude 5.5, the Parkfield earthquake of 1966, produced comparable damage to a distance of 10 miles.

The February Earthquake

The San Fernando earthquake occurred in the San Gabriel Mountains just north of the San Fernando Valley, a densely populated northern suburb of Los Angeles. The San Gabriel Mountains are part of the structural province of the transverse ranges: the band of east-west-trending mountains, valleys and faults that is characterized by strong and geologically recent tectonic deformation. Geologists recognize that the region is one of recent crustal shortening caused by north-south compression. The mountains, produced by buckling and thrusting, are one result of this crustal shortening. They have been thrusting over the valleys to the south for at least five million years along fault planes that dip to the north or northeast.

Although many faults are known to have been active in this area in the past several thousand years, the San Fernando earthquake produced the first historic example of surface faulting. The San Gabriel Mountains rise abruptly some 5,000 feet above the San Fernando Valley and the Los Angeles basin to the south. During the earthquake of February 9 a wedge-shaped prism of the crystalline basement rock comprising the San Gabriel Mountains was thrust over the San Fernando Valley to the southwest, thereby raising the elevation of a section of the San Gabriel Mountains and sliding it slightly to the west. The displacement is consistent with the motions that have been occurring for millions of years, as one can infer from geologic offsets and uplifts. It also agrees with the general picture presented here, namely that the transverse ranges were formed by the collision of the southern and Baja California block with the central and northern California block, and with the concept that the southern California block is being diverted to the west by the massive San Bernardino batholith. One can infer that the thickening of the crust involved in the overthrusting and uplift of the San Gabriel Mountains made this region an additional obstacle to the northwesterly march of

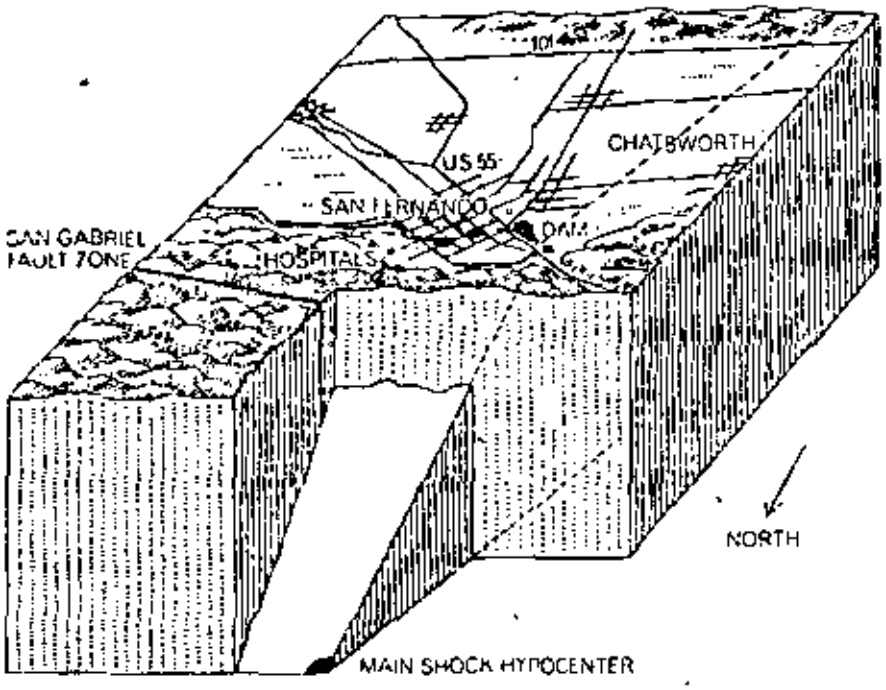

HYPOCENTER OF SAN FERNANDO EARTHQUAKE (*dark color*) of last February was 13 kilometers deep and 12 kilometers north of the area where the principal ground-shaking occurred. The earthquake collapsed sections of two hospitals in the San Fernando Valley, taking 64 lives, and so seriously weakened the earthen wall of the Van Norman Dam at the northern end of the San Fernando Valley that 80,000 people living below the dam had to leave their homes until the water level in the reservoir could be lowered. Total damage caused by the earthquake is estimated at $500 million to $1 billion. This three-dimensional view is based on a drawing prepared by two of the author's colleagues, Bernard Minster and Thomas Jordan, who worked with information supplied by geologists and geophysicists of the California Institute of Technology. The view is looking toward Los Angeles.

the southern California block. If it did, this would lend additional support to the notion that the plates in California are only 15 to 20 kilometers thick. An intriguing possibility is that the upper part of the crust is sliding with relatively little friction on a layer of rock rich in the mineral serpentine.

The hypocenter, or point of initial rupture, of the San Fernando earthquake was at a depth of 13 kilometers under the San Gabriel Mountains. The fault motion was propagated to the surface along a fault inclined northward at an angle of 45 degrees and broke the surface near the cities of San Fernando and Sylmar, at the boundary between the crystalline rocks of the mountains and the sediments of the valleys [*see illustration on page 156*]. Two heavily damaged hospitals were between the epicenter and the surface break and were thus on the upthrust, or elevated, block. The hundreds of aftershocks following the earthquake covered an area of approximately 300 square kilometers, the total volume of rock lifted up was about 2,500 cubic kilometers.

Even though the elevation difference between the peaks of the San Gabriel Mountains, such as Mount Wilson and Mount Baldy, and the floors of the adjacent valleys is impressive, it does not represent the total uplift. Erosion removes material from the mountains and deposits it in the valleys. The total amount of differential vertical motion probably exceeds two and a half miles, and horizontal displacements in the transverse ranges probably exceed 25 miles. Many thousands of earthquakes of the San Fernando type must have occurred in the area over the past several million years.

Seismic surveillance of the region with instruments dates back only four decades. In this period the northern San Fernando Valley was less active seismically than many other parts of the greater Los Angeles area, although it was comparable to the average for all southern California. On the basis of the seismic data there was no reason to believe the San Fernando area was any more or less likely than any other region of recent mountain-building in southern California to experience a large earthquake. On the other hand, the thrusting and bending associated with the geologic processes in the region, and the tilting that was associated with the earthquake and its aftershocks, suggest that a dense network of tiltmeters could provide a warning of the next large earthquake here.